For Reference

NOT TO BE TAKEN FROM THIS ROOM

For Reference

NOT TO BE TAKEN FROM THIS ROOM

Ex libris
universitatis
albertensis

QUAECUMQUE VERA

University of Alberta
Printing Department

THE UNIVERSITY OF ALBERTA

POSITIONING SERVOS WITH PRINTED MOTORS

by

Ⓒ JAMES DUNSMOOR

A THESIS
SUBMITTED TO THE FACULTY OF GRADUATE STUDIES
IN PARTIAL FULFILLMENT OF THE REQUIREMENTS FOR THE DEGREE OF
MASTER OF SCIENCE

DEPARTMENT OF ELECTRICAL ENGINEERING

EDMONTON, ALBERTA
JUNE, 1967

[illegible]

[illegible]

BY

[illegible] ©

[illegible]

[illegible]

[illegible]

[illegible]

[illegible]

[illegible]

[illegible]

UNIVERSITY OF ALBERTA

FACULTY OF GRADUATE STUDIES

The undersigned certify that they have read, and recommend to the Faculty of Graduate Studies for acceptance, a thesis entitled "Positioning Servos With Printed Motors", submitted by James Dunsmoor in partial fulfillment of the requirements for the degree of Master of Science.

ABSTRACT

The project described in this thesis deals with the performance of a printed circuit direct current servo motor in a high-speed, high-accuracy positional control system.

A detailed analysis of the basic motor relationships is first given. The steady-state relationships are then used to experimentally determine the motor parameters.

The methods used to provide a tachometer or rate signal suitable for velocity damping are then introduced. A small D.C. tachometer-generator winding which was devised and mounted on the shaft inside the motor is subsequently shown to yield satisfactory results. The changes in various motor constants due to this modification are described.

The basic linear second-order control system is investigated and is shown to be insufficiently accurate. The remainder of the thesis deals with the achievement of speed and accuracy by non-linear means: error-limiting and the utilization of maximum acceleration. Performance of the system employing derivative or phase-advance control is investigated and near-optimal response is ultimately realized by operating the system as closely as possible to an on-off or switched system.

ACKNOWLEDGMENTS

The author wishes to express his sincere appreciation to the staff members and graduate students of the Department of Electrical Engineering for their co-operation during the course of this work.

The author particularly wishes to acknowledge the advice and assistance of Professor Y. J. Kingma under whose supervision the project was carried out.

The financial assistance provided by the National Research Council and the University of Alberta is very gratefully acknowledged by the author.

TABLE OF CONTENTS

Page

CHAPTER 1: INTRODUCTION

1.1 Description of Printed Circuit Motor 1

1.2 Objectives and Methods of Analysis 3

CHAPTER 2: DERIVATION OF BASIC MOTOR RELATIONSHIPS

2.1 Simplified Equivalent Circuit of Armature 6

2.2 Inherent Frictional Torques 8

2.3 Equation of Motion and Velocity Response 10

2.4 Velocity Transfer Function 10

2.5 Velocity Transfer Characteristic 11

2.6 Effect of Brush Contact Resistance and Voltage Drop 12

2.7 A Volt-Amp Characteristic 15

2.8 Positional Transfer Function 16

2.9 Representation as a Tachometer Feedback System 17

2.10 Effect of Armature Inductance 18

2.11 An Electromechanical Circuit Analogy 19

2.12 Summary 22

CHAPTER 3: EXPERIMENTAL DETERMINATION OF MOTOR PARAMETERS

3.1 Introduction 23

3.2 Generator Open-Circuit Characteristic 24

3.3 Generator Load Characteristics 25

3.4 Brush Contact Resistance and Voltage Drop 27

3.5 Frictional Torques and Losses 29

3.6 Velocity Transfer Characteristic: Dead Zone 33

3.7 Motor Volt-Amp Characteristic 35

3.8 Summary 37

CHAPTER 4: DERIVATION OF A RATE SIGNAL

4.1 Introduction 39

4.2 The Subtraction Method 40

4.3 An A.C. Speedometer 44

4.4 A D.C. Tachometer-Generator 46

CHAPTER 5: BASIC LINEAR POSITIONAL CONTROL SYSTEM

5.1 Introduction 52

5.2 Transient Analysis 52

5.3 Effect of Non-Viscous Frictional Torque 53

5.4 Effect of Brush Contact Voltage Drop 59

5.5 Description of the Physical System 63

5.6 Experimental Results and Conclusions 66

CHAPTER 6: COMPENSATION TECHNIQUES TO IMPROVE THE BASIC SYSTEM

6.1 Introduction 70

6.2 Dither Compensation For Static Frictional Torque 70

6.3 Compensation for Coulomb Frictional Torque 73

6.4 Dither Plus Comparator Compensation 75

6.5 Compensation for Brush Contact Voltage Drop 77

6.6 Summary 78

CHAPTER 7: LIMITING OF POSITIONAL ERROR

7.1 Introduction 79

7.2 Phase Plane Analysis 81

7.3 A Graphical Analysis of Transient Response 85

7.4 Experimental Results and Summary 95

CHAPTER 8: DERIVATIVE OF ERROR CONTROL

8.1 Introduction 101

8.2 Linear Analysis of Transient Response 101

8.3 Experimental Results 103

8.4 Summary 104

CHAPTER 9: USE OF CONDITIONAL DAMPING

9.1 Introduction 107

9.2 Phase Plane Analysis 108

9.3 Experimental Results and Summary 113

CHAPTER 10: LIMITING OF CONTROL SIGNAL

10.1 Introduction 115

10.2 Phase Plane Analysis 115

10.3 Optimizing the Physical System 120

10.4 Experimental Results and Summary 122

CHAPTER 11: LIMITING OF POSITION ERROR PLUS CONTROL SIGNAL

11.1 Introduction 125

11.2 Phase Plane Analysis 125

11.3 Optimizing the Physical System 130

11.4 Experimental Results and Summary 133

CHAPTER 12: PHASE ADVANCE STABILIZATION

12.1 Introduction 137

12.2 Transient Analysis in Linear Region 138

12.3 Phase Plane Analysis 139

12.4 Optimizing the Physical System 141

12.5 Experimental Results and Summary 143

CHAPTER 13: REALIZATION OF OPTIMAL RESPONSE

13.1 Introduction 146

13.2 Phase Plane Analysis of Optimal Response 147

13.3 The "V-Mod-V" System 148

13.4 The S.E.R.M.E. System 149

13.5 Optimal Response Times of the Physical Systems 150

CONCLUSIONS 152

BIBLIOGRAPHY 153

APPENDIX 1: MOTOR PERFORMANCE SPECIFICATIONS 154

APPENDIX 2: POWER AMPLIFIER 157

APPENDIX 3: POWER SUPPLY 160

APPENDIX 4: CIRCUIT SCHEMATIC DIAGRAMS 162

LIST OF FIGURES

FIGURE	TITLE	PAGE
1.1	Exploded View of Printed Motor	4
1.2	Design of Printed Circuit Armature	5
2.1	Simplified Equivalent Circuit of Armature	6
2.2	Constant Torque Characteristics	8
2.3	Frictional Torque Characteristics	8
2.4	Velocity Transfer Characteristic	11
2.5	Brush Contact Drop	12
2.6	Motor Resistances	13
2.7	Modified Equivalent Circuit	14
2.8	Modified Velocity Characteristic	14
2.9	Theoretical Volt-Amp Characteristic	15
2.10	Motor Block Diagram	16
2.11	Representation as a Tachometer Feedback System	17
2.12	Electro-Mechanical Analog	20
3.1	Experimental Generator Open Circuit Characteristics	24
3.2	Ideal Generator Load Characteristics	25
3.3	Experimental Generator Load Characteristics	26
3.4	Measurement of $V_c(I_a)$	28
3.5	Brush Contact Drop	28
3.6	Frictional Torques For Motor Plus Load	29
3.7	Determination of Frictional Torques	30
3.8	Power Input to Modified Motor	32
3.9	Calculated Frictional Torques	32
3.10	Dead-Zone of Unmodified Motor	34
3.11	Dead-Zone of Modified Motor	34
3.12	No-Load Velocity Transfer Characteristics	34
3.13	Measurement of Volt-Amp Characteristic	35
3.14	Motor Volt-Amp Characteristics	36

4.1 Derivation of a Rate Signal by Subtraction Method 41

4.2 Error in Subtraction Method 42

4.3 Subtraction Method Static Characteristic 42

4.4 Step Response by Subtraction Method 43

4.5 Radial Magnetic Field 45

4.6 A.C. Speedometer Winding 45

4.7 Wave Winding For Utilization of Radial Field 46

4.8 Construction Principle of D.C. Tachometer 47

4.9 Tachometer-Generator Equivalent Circuit 48

4.10 D.C. Tachometer-Generator Winding 49

4.11 Cross Section of Modified Motor 49

4.12 Step Response of Modified Motor 50

5.1 Block Diagram of Basic Linear Positional System 51

5.2 Effect of Frictional Torque on Overdamped Response 54

5.3 Example Showing Effect of Frictional Torque 55

5.4 Simplified Block Diagram 56

5.5 Phase Plane Trajectories for $\Theta_f = .05, \xi = .20$ 58

5.6 Frictional Error Zone 58

5.7 Assumed Brush-Contact Drop 59

5.8 System Transient Functions 61

5.9 Representative Block Diagram Showing Inherent Non-Linearities 62

5.10 Basic Linear System 1 65

5.11 Basic Linear System 2 65

5.12 Comparison of Two Rate Methods 66

5.13-20 Experimental Responses for Basic Systems 68-69

6.1-6.3 Effect of Dither Compensation 72

6.4 Velocity Comparator Characteristic 73

6.5 Linearized Velocity Transfer Characteristic 74

6.6 Basic System Compensated for Coulomb Friction 75

6.7 Transfer Characteristic-Friction Compensated 75

6.8 Comparator Output and Uncompensated Response 76
6.9 Comparator Output and Compensated Response 76
6.10 Overdamped Responses of System with Friction Compensation 76
6.11 Underdamped Responses of System With Friction Compensation 76
6.12 Modification of Subtraction Method 78
7.1 Error Detector D.C. Characteristic 80
7.2 Limiting of Positional Error 80
7.3 Phase Plane Diagram of Linear System 84
7.4 Effect of Velocity Limiting 84
7.5 Phase Trajectories for $\xi = 0.8 \quad G_1 = 4.34$ 84
7.6 Times Spent in Limited Regions - Unmodified Motor 87
7.7 Times Spent in Limited Regions - Modified Motor 87
7.8 Velocity at Time of Exit From Limited Region - Unmod. Motor 89
7.9 Velocity at Time of Exit From Limited Region - Mod. Motor 89
7.10 Approximation of Time Spent in Limited Region 90
7.11 Optimization Chart for Minimizing Peak Times 94
7.12-24 Experimental Responses of Position Error Limited System 96-100
8.1 Derivative of Error Control System 101
8.2-6 Experimental Responses of Derivative Control System 105-106
9.1 Conditional Tachometer Feedback 107
9.2 Phase Plane Analysis 108
9.3 Time And Velocity at End of Limited Region - Unmod. Motor 111
9.4 Time and Velocity at End of Limited Region - Mod. Motor 111
9.5 Phase Trajectories of Conditionally Damped System 112
9.6 Physical System Using Conditional Derivative Control 113
9.7 Limited Error and Derivative 114
9.8 Experimental Responses Using Conditional Derivative Damping 114
10.1 Control Signal Limiting 115
10.2 Linear Region 116
10.3 Approximate Normalized Phase Plane Boundaries 117

10.4 Phase Trajectory of Underdamped "On-Off" System 119

10.5 Chart for Determination of Overshoot 120

10.7 Non-Optimized Trajectories 121

10.8 Experimental System 122

10.9-10 Experimental Responses 123

10.11-13 Phase Plane Trajectories 124

11.1 Limiting of Error and Control Signal 125

11.2 Boundaries of Linear Regions 126

11.3 Approximate Phase Trajectories 129

11.4 Critical Boundary 131

11.5-12 Experimental Responses 134-136

12.1 Derivative Controller and Ideal Lead Network 137

12.2 Phase Advance Stabilization 138

12.3 Approximate Normalized Phase Plane Boundaries 140

12.4-5 Experimental Responses of Phase Lead Control System 145

13.1 Optimal Trajectories 147

13.2 "V-Mod-V" System 148

13.3 The S.E.R.M.E. Controller 149

13.4 Idealized and Actual Optimal Response Functions 150

A1.1 Motor Performance Curves (24 VDC Input) 155

A1.2 Motor Speed Torque Characteristics 155

A1.3 Motor Pulse Characteristics 155

A2.1 Power Amplifier Simplified Schematic 158

A2.2 Power Amplifier Frequency Response 159

A2.3 Power Amplifier Phase Shift 159

A3.1 Dual Power Supply Schematic 160

A3.2 Power Supply Voltage Regulation Curves 161

A4.1-10 Schematic Diagrams of Circuits Used 162-164

LIST OF SYMBOLS

SYMBOL	MEANING
E	Amplitude of voltage increment
E_c	Control signal
E_d	Dead-zone half-width
E_ε	Error voltage signal
E_f	Equivalent opposing voltage due to non-viscous friction
E_g	Generated back e.m.f.
E_o	Power amplifier output voltage
E_t	Armature terminal voltage
$G(s)$	General block transfer function
G_1	Gain of error-detector block
G_2	Gain of power amplifier block
$G_\omega(s)$	Velocity transfer function
$G_\theta(s)$	Positional transfer function
I_a	Armature current
J_a	Armature moment of inertia
J_t	Total inertia of armature and load
K	Gain constant of motor block
K_d	Motor damping constant
K_g	Motor (generator) voltage constant
K_m	Motor regulation
K_t	System tachometer constant
K_t'	Differentiator constant
K_T	Motor torque constant
K_ω	Tachometer voltage constant
L_a	Armature inductance
p	Normalized Laplace operator
P	Power
P_L	Power loss

R_a	Motor terminal resistance
R_b	Brush resistance
R_c	Contact resistance
R_s	Series resistance
R_t	Total amplifier load resistance
R_w	Armature winding resistance
s	Laplace operator
t	Real time
t_1, t_2	Time spent in limited region
t_L	Time spent in linear region
t_n	Normalized time
t_p	Time at which maximum value is first reached
t_s	Settling time
T	Torque generated
T_c	Coulomb frictional torque
T_f	Total non-viscous frictional torque
T_s	Static frictional torque
T_v	Viscous frictional torque
$u(t)$	Unit step function
V_c	Brush-contact voltage drop
V_s	Error detector voltage limit
V_t	Tachometer generated e.m.f.
w	Width of linear region
θ	Output angular position
θ_ε	Positional error
θ_f	Equivalent opposing input due to non-viscous friction
θ_i	Reference angular input
θ_p	Amplitude of first output overshoot

ξ	Damping ratio
ω, Ω	Shaft angular velocity
ω_ε, Ω_ε	Error signal velocity
ω_n	System undamped natural frequency
ω_d	System damped frequency of oscillation
ω_f	Final velocity of shaft
ν_ε	Normalized error velocity
τ	System time constant
τ_a	Motor electrical time constant
τ_d	Time constant of phase advance network
τ_m	Motor electromechanical time constant
τ_m'	Motor mechanical time constant
ϕ	Phase angle by which position lags velocity

Other symbols used are defined in the text.

CHAPTER ONE

INTRODUCTION

1.1 DESCRIPTION OF PRINTED CIRCUIT MOTOR

The motor used in this work is a Model 488 direct drive servo motor made by Printed Motors, Inc. of Glen Cove, New York. Its ratings are 24 volts D.C., 3300 rpm, 7.5 amps and 100 watts. The following outstanding features of the motor owe their existence to the novel construction of the printed armature:

(1) very low moment of inertia, hence high torque-inertia ratio;

(2) very low armature inductance, hence negligible electrical time constant;

(3) low mechanical time constant, hence rapid response;

(4) good cooling properties, hence high-temperature operation possible;

(5) no magnetic attraction between rotating and stationary parts, hence bearings are lightly loaded and little frame conducted noise is generated;

(6) no "cogging" (preferential angular position), hence theoretically no limit on angular accuracy to which shaft can be positioned;

(7) high pulse torque capability;

(8) no rotating iron to vary permeability of magnetic path, hence very smooth torque at constant current.

A physical description of the motor is simplest by reference to Figure 1.1. The eight-pole permanent magnet structure is shown in (a). Poles are alternately magnetized North and South. Figure 1.1(b) shows the front face of the printed armature. The aluminum disc to which it is secured is part of the shaft. The low drop silver-graphite brushes bear directly on the armature on the annular ring around this disc. The spoke-like structure on the back of the armature (d) provides a certain amount of eddy current damping as well as added rigidity.

The flux return plate (e) is of soft iron and is thinly impregnated with a non-conducting material. This prevents the possibility of arcing at high currents due to the close proximity of the printed armature. The flux return plate acts as a keeper against magnetization loss. The magnetizing windings are therefore normally cemented in place and left there after assembly and magnetizing.

The four brush holders are rigidly mounted in a disc which is shown together with the face plate in (f). The brush "pig-tails" are soldered to the face plate on which a printed circuit connects diametrically opposite brushes together and to one of the terminals. Coil springs of very fine wire hold the brushes lightly but firmly against the armature when assembled.

The printed armature is shown in Figure 1.2. It is manufactured by modern printed circuit techniques on a substrate of mylar, epoxy-glass or high alumina ceramic. The result is a very lightweight continuous winding giving the motor its advantageous properties. One "turn" of the eight-pole wave winding is shown. Each side of the winding is identical in appearance having 121 segments. Connections from side to side are made by plated-through holes.(3) Since the field in the annular region of these segments is axial and reverses each 45°, rotation results when a direct current flows by applying a voltage to the armature terminals. Only one pair of brushes is actually required but since they must be 45° (or 135°) apart, two pairs eliminate mechanical unbalance and decrease total brush resistance, but also double the brush friction.

A list of the reported motor specifications is given in Appendix 1.

Figure 4.5 shows the internal radial magnetic field.

Figure 4.11 shows a cross section of the motor.

1.2 OBJECTIVES AND METHODS OF ANALYSIS

Since the printed motor is intentionally a low-inertia device, it is natural to consider only applications in which low-inertia loads are to be positioned. Experimental results will be confined to a constant load of almost negligible inertia.

Although the reference input to a control system might be any desired function of time, in many practical applications, such as incrementing, only the step function response is of interest. Step input magnitudes ranging from zero to π radians will be considered while a practical range from approximately 5° to 175° will be used.

Specifications for positional control systems are, in general, based on desired response time and desired accuracy. In particular, for this work, optimization of response will be for minimum steady-state error and either near-zero overshoot with a minimum peak time, or zero overshoot with a minimum rise time or settling time.

Laplace transforms will be used for real-time transient analysis of linear behavior. A normalized phase plane analysis of non-linear responses will be employed. Certain approximations will be made in some of the latter cases to facilitate the optimization procedure.

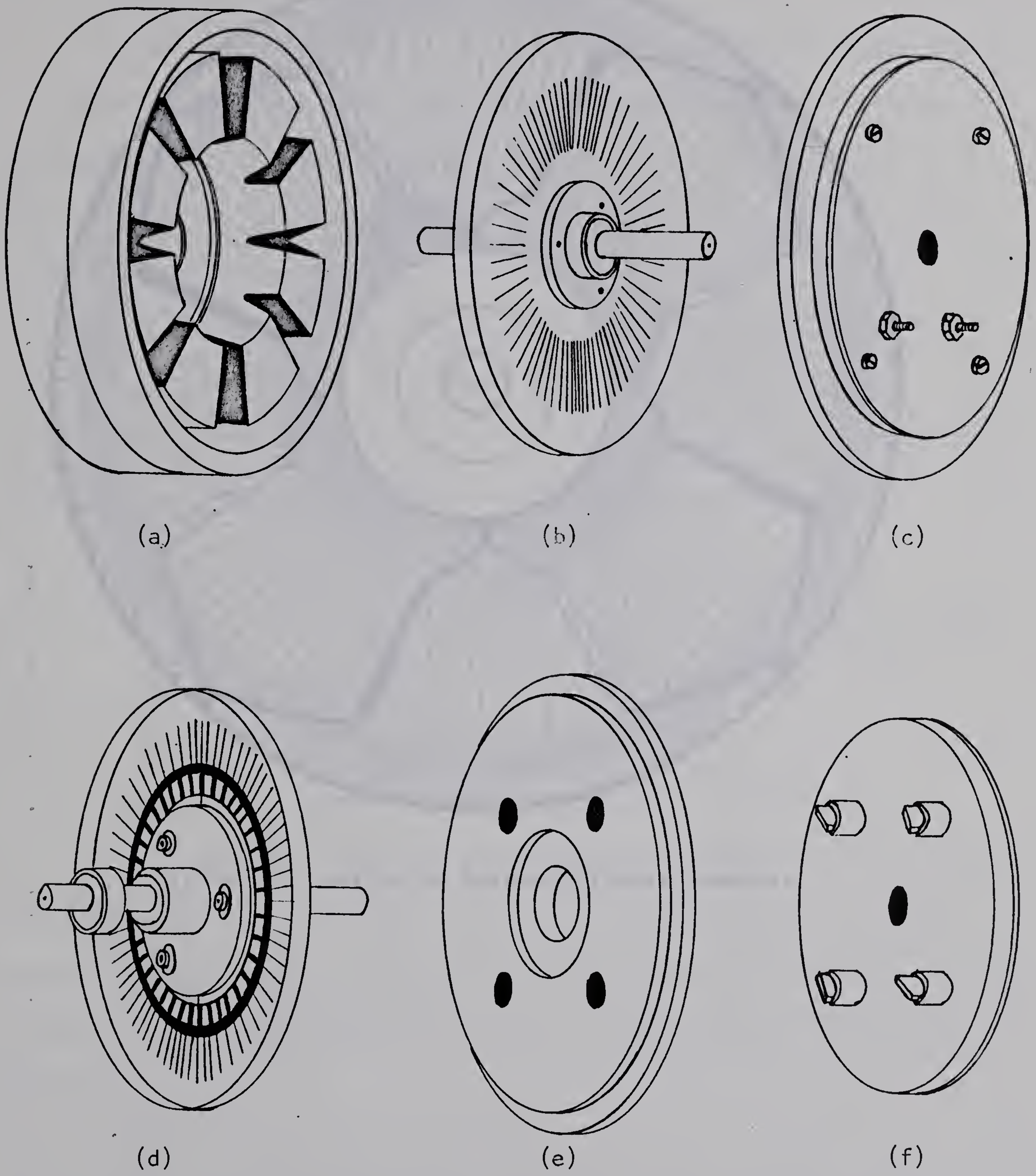

Figure 1.1 Exploded View of Printed Motor

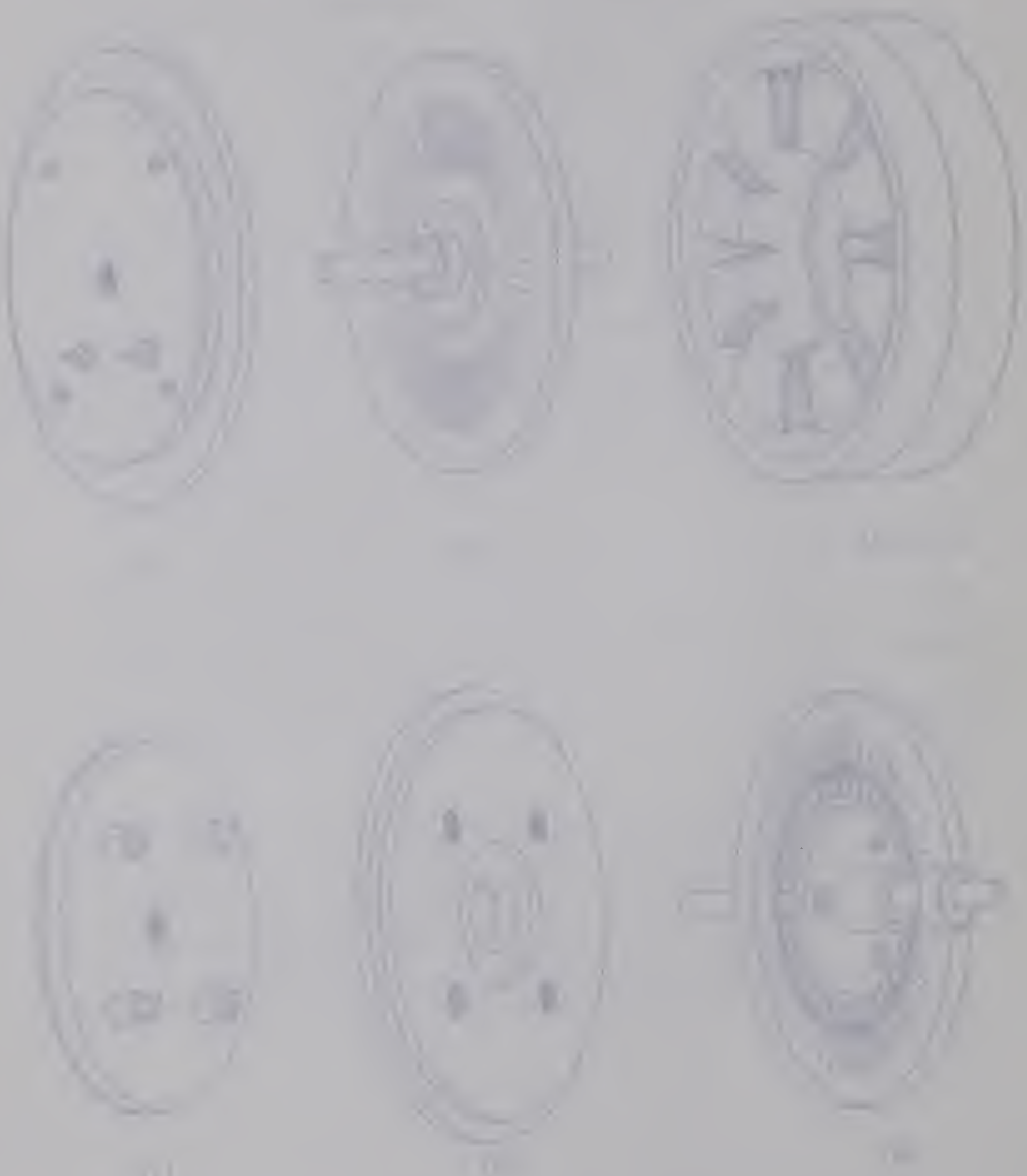

[illegible]

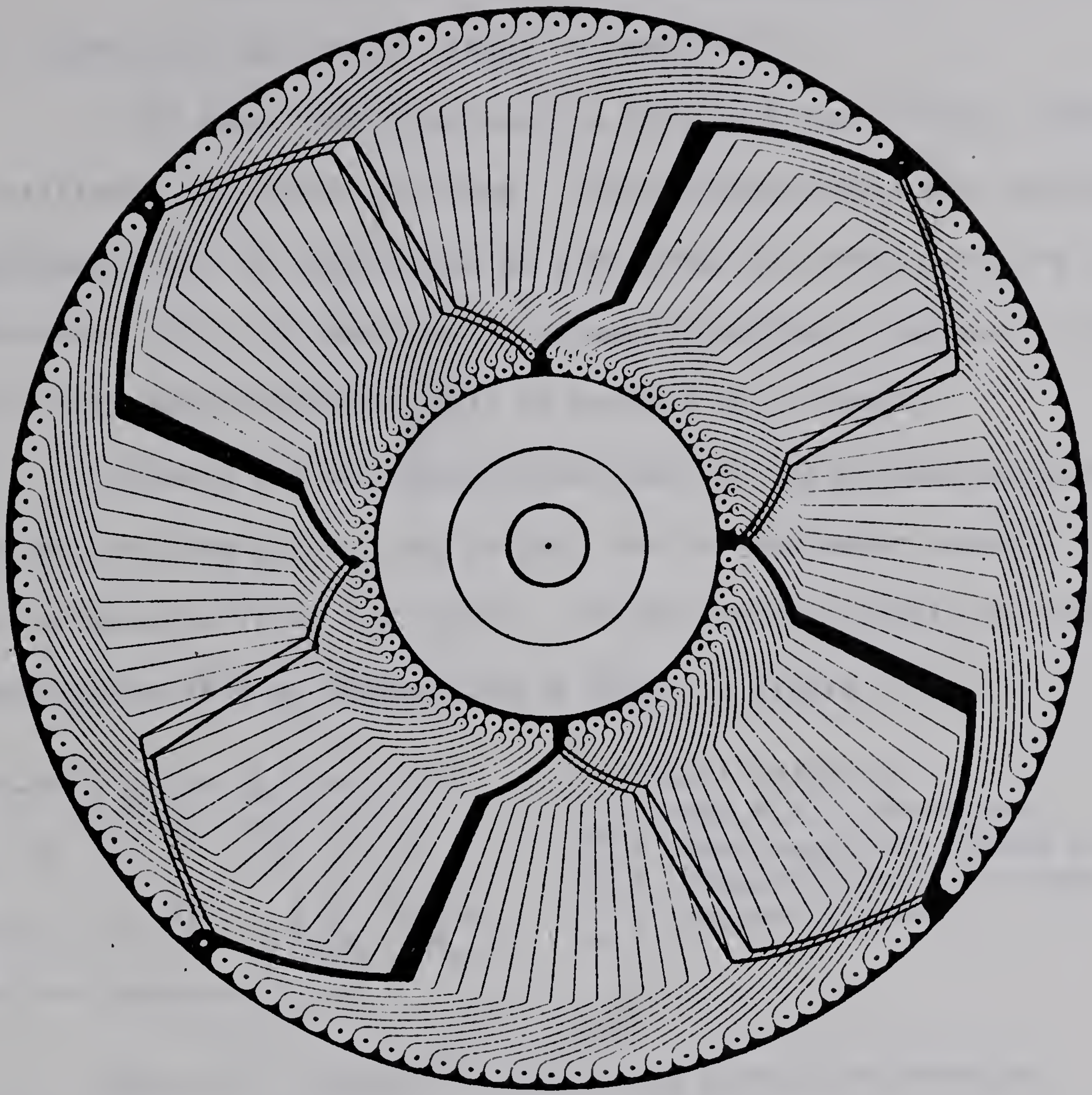

Figure 1.2 Design of Printed Circuit Armature

CHAPTER TWO

DERIVATION OF BASIC MOTOR RELATIONSHIPS

2.1 SIMPLIFIED EQUIVALENT CIRCUIT OF ARMATURE

The power amplifier used in this work must not be loaded by a resistance less than 1.04 ohms. Since the printed motor terminal resistance (R_a) is reported to be 0.60 ohms, a current limiting resistance ($R_s \simeq 0.5$ ohms) will be used in series. Subsequently the motor plus series resistor will be treated as a "block".

Due to the negligible inductance of the printed armature and the very uniform current and torque, the printed motor closely approximates an ideal D.C. motor. The equivalent circuit of the printed armature can thus be represented as shown in Figure 2.1.

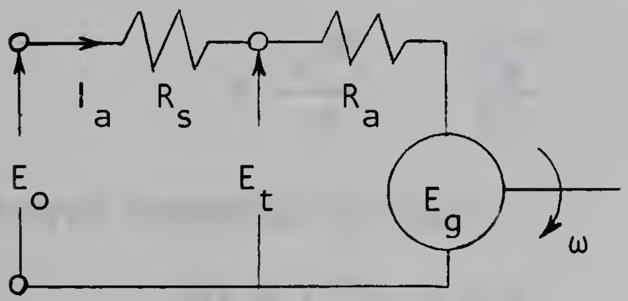

ω = shaft velocity
E_g = back e.m.f. generated
E_o = power amplifier output voltage
E_t = armature terminal voltage
I_a = armature current

Figure 2.1 Simplified Equivalent Circuit of Armature

It was noted that the flat conductors contain no iron. Their rotation, therefore, negligibly modulates the magnetic flux. Since armature reaction is also negligible, the back e.m.f. generated is simply proportional to shaft speed. The motor voltage constant may thus be defined:

$$E_g = K_g \omega \tag{2.1}$$

For the equivalent circuit, the loop equation is

$$E_o = E_g + I_a(R_a + R_s) \tag{2.2}$$

Let $$R_t = R_a + R_s \tag{2.3}$$

then $$E_o = K_g \omega + I_a R_t \tag{2.4}$$

The torque developed by the motor is proportional to armature current. The motor torque constant is thus defined by

$$T = K_T I_a \tag{2.5}$$

As a point of interest, it can be shown that the two constants, in consistent units, are equal. Assume that the armature rotates at constant velocity through unit angular displacement.

Total time taken = $1/\omega$ sec (2.6)

Total electrical energy consumed

$$W = \frac{E_t I_a}{\omega} \tag{2.7}$$

$$= \frac{(I_a R_a + E_g) I_a}{\omega} \tag{2.8}$$

$$= \frac{I_a{}^2 R_a}{\omega} + \frac{K_g T}{K_T} \tag{2.9}$$

Energy converted to heat

$$W_1 = I_a{}^2 R_a \times 1/\omega \tag{2.10}$$

Energy converted to motion

$$W_2 = T \tag{2.11}$$

Now $W = W_1 + W_2$ (2.12)

thus $\dfrac{I_a{}^2 R_a}{\omega} + \dfrac{K_g T}{K_T} = \dfrac{I_a{}^2 R_a}{\omega} + T$ (2.13)

and $K_g = K_T$ (2.14)

2.2 INHERENT FRICTIONAL TORQUES

At constant velocity, the transfer characteristic is found from equation 2.4

$$\omega = \frac{E_o - I_a R_t}{K_g} \tag{2.15}$$

$$= \frac{E_o}{K_g} - \frac{T R_t}{K_T K_g} \tag{2.16}$$

If T_1, T_2, etc. were constant external frictional torque loads, a set of curves related to the torque-speed curves results as shown in figure 2.2.

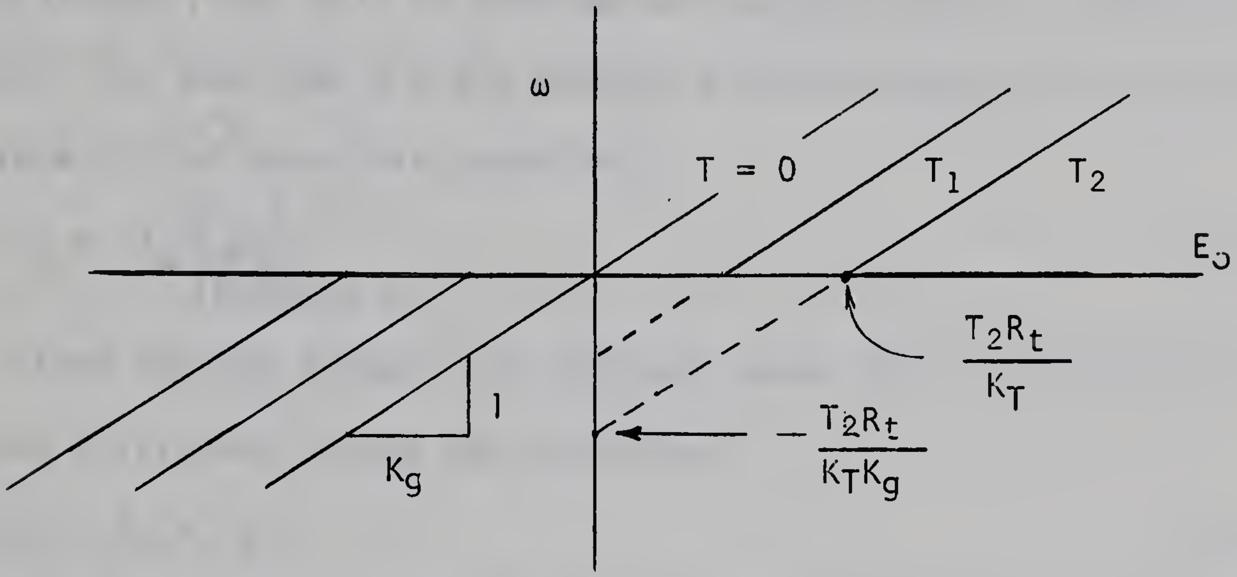

Figure 2.2 Constant Torque Characteristics

The curve for T=0 implies that even the smallest applied voltage will cause a finite velocity of rotation, that is, that the useable torque is $K_T I_a$. This, of course, is not the case. Three types of opposing torques must be considered: static friction ("stiction"), Coulomb friction, and viscous friction. The first two may be combined and represented by the characteristic shown in figure 2.3.

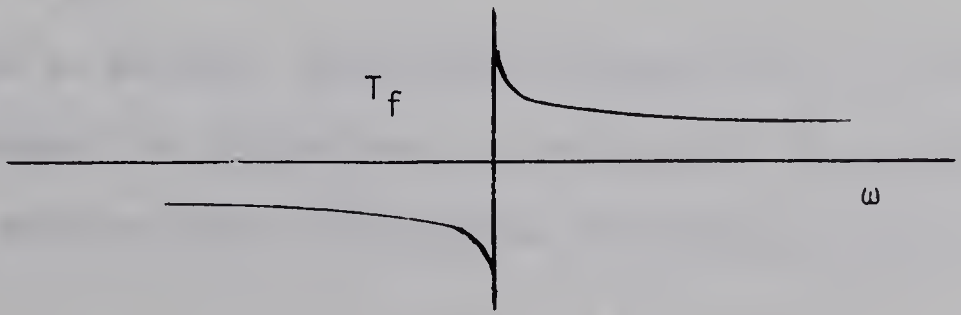

Figure 2.3 Frictional Torque Characteristic

Since the exact shape of this characteristic would be difficult to determine accurately, it is more reasonable to treat stiction and Coulomb friction separately. Coulomb frictional torque may generally be assumed constant (particularly at any reasonable velocity) although it may decrease slightly with speed. It is of primary interest since it causes much of the "dead zone" problem.

Define $T_c \equiv |T_c| \left(\frac{\omega}{|\omega|}\right)_{\omega \neq 0}$ (2.17)

The value of the torque due to stiction, that is, the "starting torque", may well be considerably greater than T_c depending on how "sticky" the bearings are and how the brushes happen to be placed on the armature in the rotor rest position.

Define $T_s \equiv |T_s| \left(\frac{E_o}{|E_o|}\right)_{\omega = 0}$ (2.18)

Since the two torques, as defined, never occur simultaneously, an opposing frictional torque can be defined

$$T_f \equiv T_c + T_s \tag{2.19}$$

The third opposing torque is that due to viscous friction or viscous damping, often called "windage" in conventional machines. In certain applications a higher viscous damping torque is desireable and is easily accomplished in printed circuit machines by replacing the insulated core of the armature winding by a conductive one, such as aluminum.(3) Eddy current then provides a braking torque proportional to speed. The motor damping constant may thus be defined

$$T_v \equiv K_d \omega \tag{2.20}$$

Since an external load might introduce any or all of these opposing frictional torques, for convenience, T_f and K_d will be assumed to include load friction. An external load will thus be considered as purely inertial.

2.3 EQUATION OF MOTION AND VELOCITY RESPONSE

In any state of motion, the torque developed by the motor minus the opposing frictional torques must equal the angular acceleration times the total moment of inertia (rotor plus load), that is:

$$J_t\dot{\omega} + K_d\omega + T_f = T \tag{2.21}$$

This is the equation of motion. Its solution for a step input is of interest. From equations 2.4 and 2.5

$$T = \frac{K_T(E_o - K_g\omega)}{R_t} \tag{2.22}$$

Substituting into equation 2.21 and rearranging,

$$\dot{\omega} + \frac{R_tK_d + K_TK_g}{J_tR_t}\omega + \frac{T_f}{J_t} = \frac{K_TE_o}{J_tR_t} \tag{2.23}$$

Assuming $E_o = Eu(t)$, $T_f = T_fu(t)$ and $\omega(0) = \dot{\omega}(0) = 0$

$$\dot{\omega} + \frac{R_tK_d + K_TK_g}{J_tR_t}\omega = \frac{K_TE - T_fR_t}{J_tR_t}u(t) \tag{2.24}$$

For which the solution is

$$\omega(t) = \omega_f\left(1 - e^{-t/\tau_m}\right) \tag{2.25}$$

where

$$\omega_f = \frac{K_TE - T_fR_t}{R_tK_d + K_TK_g} \tag{2.26}$$

and

$$\tau_m = \frac{J_tR_t}{R_tK_d + K_TK_g} \tag{2.27}$$

2.4 VELOCITY TRANSFER FUNCTION

It will be shown in Chapter Six how the effects of friction can be eliminated. In equation 2.23, let $T_f = 0$ and $\omega(0) = \dot{\omega}(0) = 0$. Taking the Laplace transform

$$s\Omega(s) + \frac{1}{\tau_m}\Omega(s) = \frac{K_T}{J_tR_t}E_o(s) \tag{2.28}$$

The motor gain constant can now be defined

$$K \equiv \frac{K_T}{J_t R_t} \tag{2.29}$$

Thus the velocity transfer function is given by

$$G_\omega(s) = \frac{\Omega(s)}{E_o(s)} = \frac{K}{s + 1/\tau_m} \tag{2.30}$$

2.5 VELOCITY TRANSFER CHARACTERISTIC

For zero acceleration, the equation of motion becomes

$$K_d\omega + T_f = T \tag{2.31}$$

$$K_d\omega + T_c + T_s = \frac{K_T(E_o - K_g\omega)}{R_t} \tag{2.32}$$

Substituting from equations 2.17 and 2.18 and rearranging,

$$\omega\left(K_d + \frac{K_T K_g}{R_t}\right) = E_o\frac{K_T}{R_t} - |T_c|\left(\frac{\omega}{|\omega|}\right)_{\omega\neq 0} - |T_s|\left(\frac{E_o}{|E_o|}\right)_{\omega=0} \tag{2.33}$$

The resulting characteristic is shown in figure 2.4. Some possibilities for the multi-valued type of hysteresis are shown for the negative portion only.

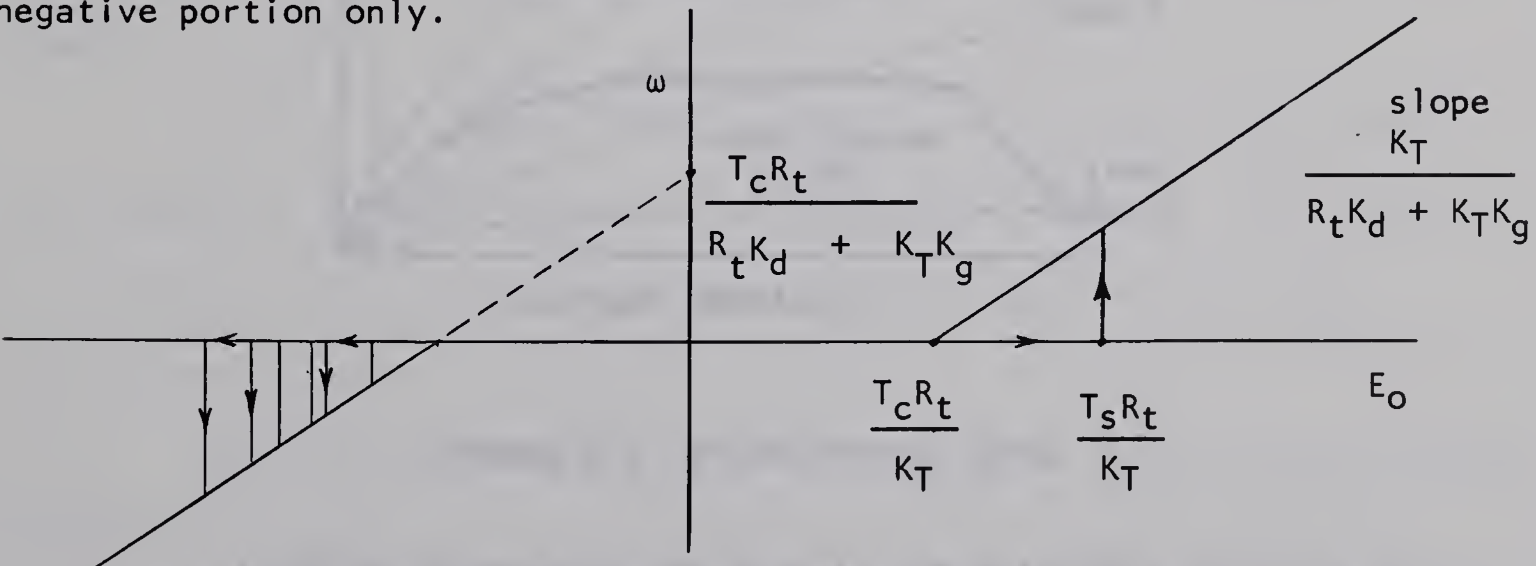
ω
$\frac{T_c R_t}{R_t K_d + K_T K_g}$
slope $\frac{K_T}{R_t K_d + K_T K_g}$
$\frac{T_c R_t}{K_T}$
$\frac{T_s R_t}{K_T}$
E_o

Figure 2.4 Velocity Transfer Characteristic

Comparing this characteristic to those of figure 2.2, viscous damping is seen to decrease the slope since the torque is not constant with speed. A reduction in final velocity is the price paid then when the motor time constant is reduced by increasing the value of K_d.

2.6 EFFECT OF BRUSH CONTACT RESISTANCE AND VOLTAGE DROP

Heretofore the armature terminal resistance has been assumed constant. In spite of the low-drop brushes used this is unfortunately not the case. The voltage drop from the motor terminal to the copper of the armature segments comprises of the drop in the brush itself, its lead and the drop across the contact which is an interface consisting of graphite film, loose particles, air space and copper-oxide film. The termperature, thickness and general condition of each of these parts control the total contact drop. The resistance of the brush itself (R_b) decreases with temperature and the temperature, in turn, depends on the current density in the various parts of the contact surface. It is impossible to make any complete analysis of these various factors, but a somewhat speculative picture is shown in figure 2.5.

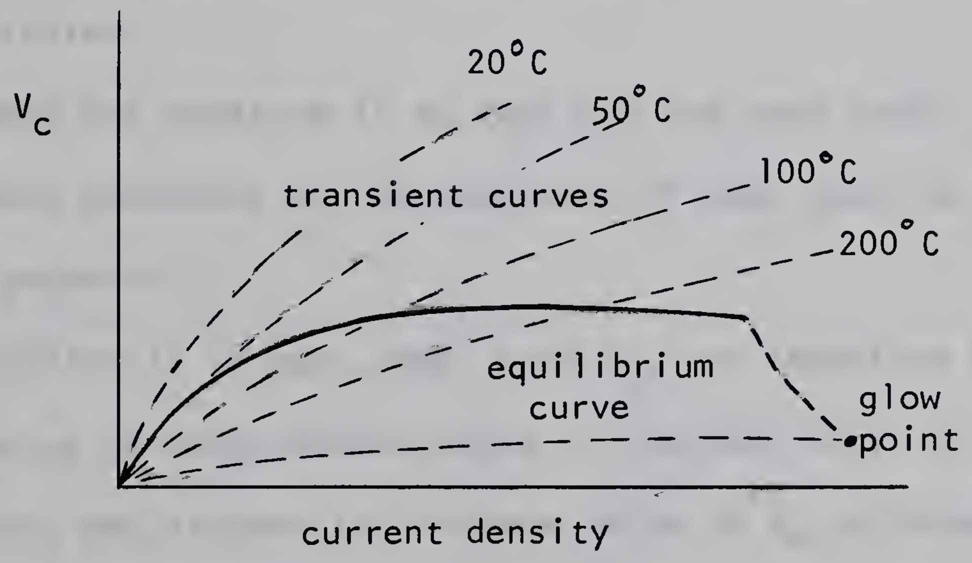

Figure 2.5 Brush Contact Drop

It can be noted that the drop is approximately constant over a wide range so that the power loss is nearly proportional to current. This means that the brush plus contact resistance varies somewhat as shown in figure 2.6 (b).

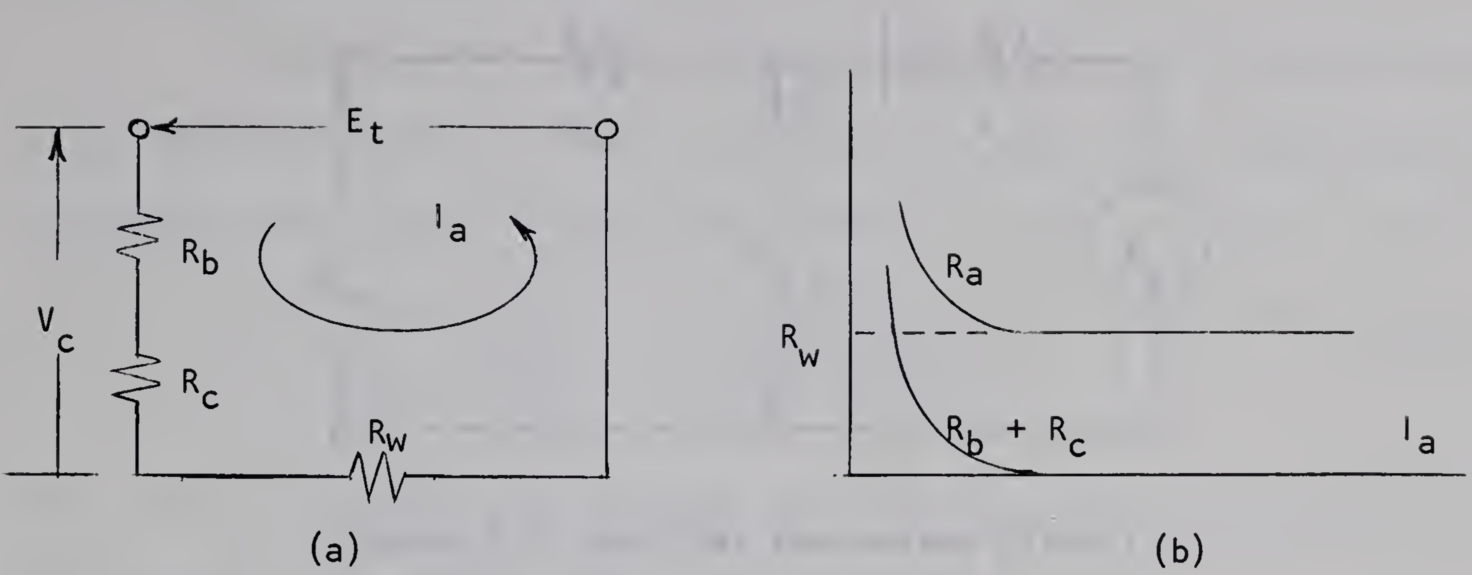

Figure 2.6 Motor Resistances

The situation is further degraded by the fact that as the armature rotates neither brush pressure nor the thickness of the interface film remain constant and minute particles of both copper and graphite may be torn away. Thus the contact resistance (R_c) may vary even at a constant speed of rotation.

When the armature is at rest (in the dead zone), the value of R_c is somewhat dependent on the placement of each brush on a particular segment or segments.

Suffice it to say, then, that R_a, and therefore R_t, is high and multi-valued up to some maximum value in the dead zone, is not constant at low speeds, and reaches its minimum value of R_w at higher speeds provided the current is not low.

Even at higher speeds where $R_c + R_b$ may be considered negligible, the contact voltage drop Vc is present and cannot be neglected in an accurate analysis. If it is considered constant, it may be included as a voltage source in the equivalent circuit as shown in figure 2.7.

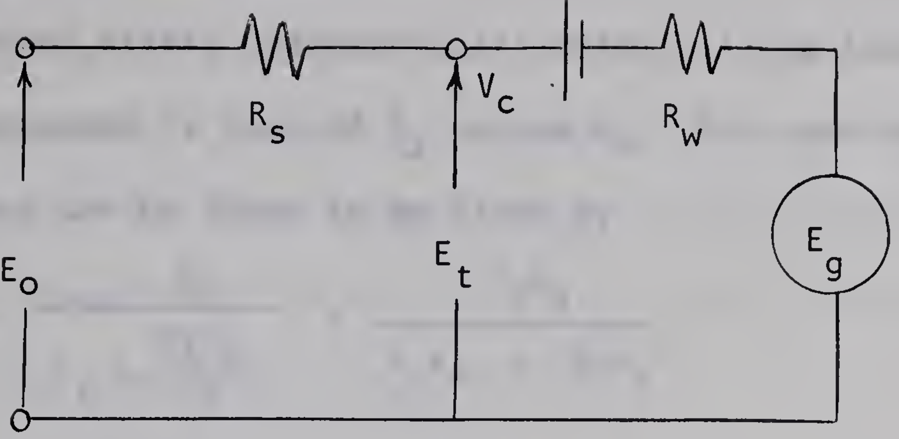

Figure 2.7 Modified Equivalent Circuit

The effect of V_c can thus be dealt with by replacing E_o by $E_o - V_c$ in all equations and realizing that R_t means $R_s + R_w$. The contact voltage may contribute significantly to the dead zone as shown in figure 2.8.

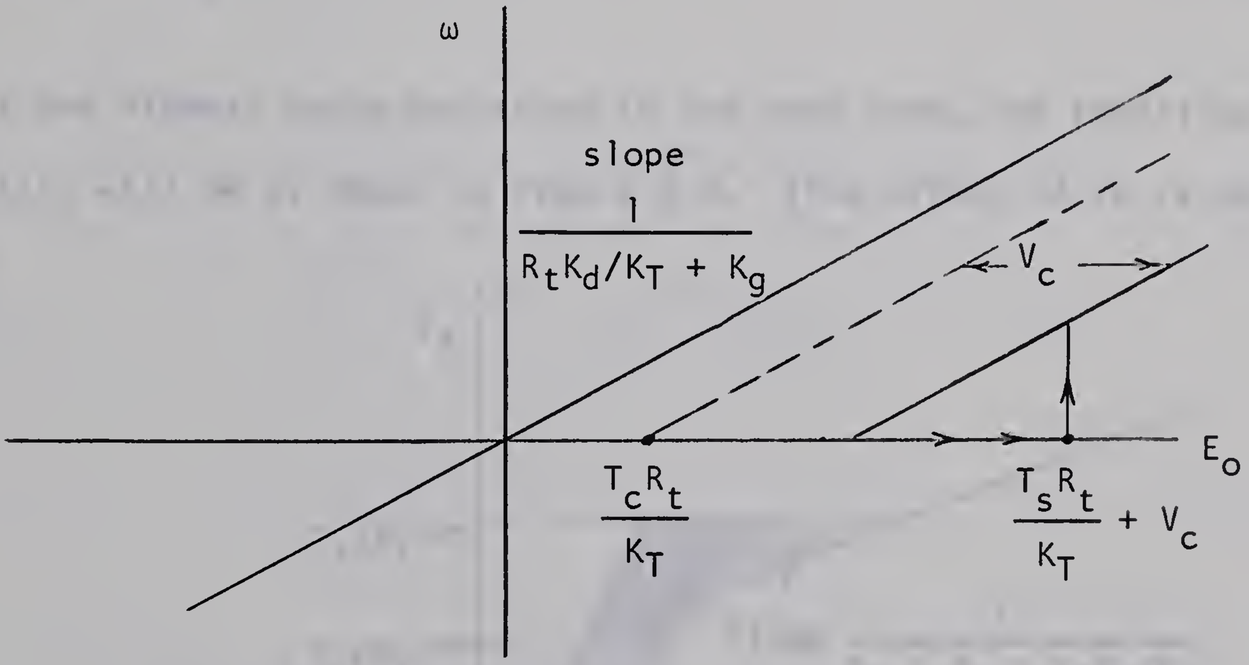

Figure 2.8 Modified Velocity Characteristic

The final velocity for a step response is thus revised:

$$\omega_f = \frac{E_o - (V_c + T_fR_t/K_T)}{K_g + K_dR_t/K_T} \tag{2.34}$$

2.7 A VOLT-AMP CHARACTERISTIC

A second static characteristic which will be informative for experimental purposes is that of I_a versus E_o. For zero acceleration, armature current can be shown to be given by

$$I_a = \frac{E_o}{R_t + \frac{K_T K_g}{K_d}} + \frac{T_f K_g}{R_t K_d + K_T K_g} \tag{2.35}$$

Thus the slope and intercept (extension to I_a-axis) are determined for the region in which $\omega \neq 0$. Now in the dead zone

$$I_a = \frac{E_o}{R_t} \tag{2.36}$$

And at the edge of the dead zone

$$E_o = \pm \frac{T_f R_t}{K_T} \tag{2.37}$$

If $R_{t_{max}}$ is the highest value occurring in the dead zone, the resulting characteristic will be as shown in figure 2.9. (The effect of Vc is not included.)

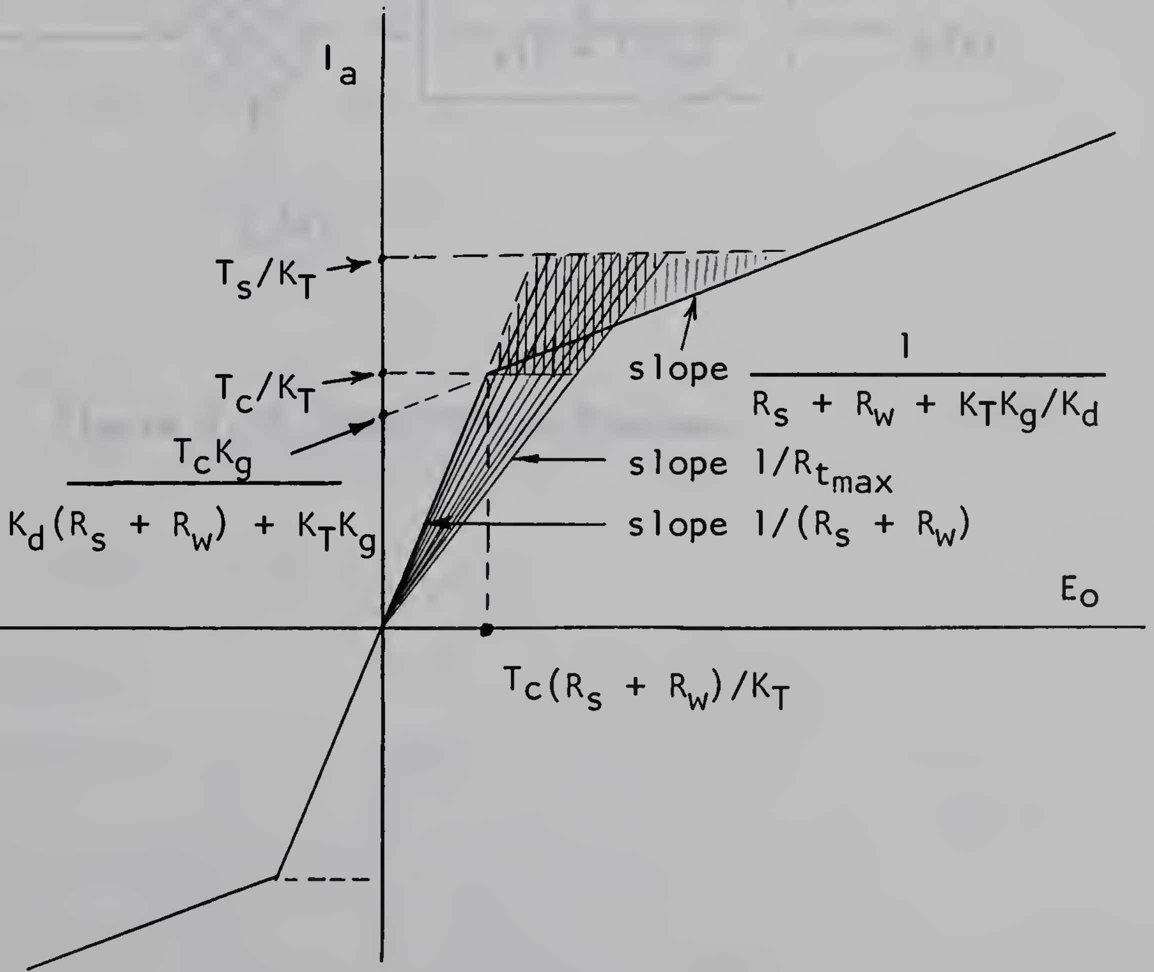
I_a
T_s/K_T
T_c/K_T
$\frac{T_c K_g}{K_d(R_s + R_w) + K_T K_g}$
slope $\frac{1}{R_s + R_w + K_T K_g/K_d}$
slope $1/R_{t_{max}}$
slope $1/(R_s + R_w)$
E_o
$T_c(R_s + R_w)/K_T$

Figure 2.9 Theoretical Volt-Amp Characteristic

2.8 POSITIONAL TRANSFER FUNCTION

The transfer function of the motor as a velocity transducer is given by equation 2.30. It must be remembered that this is only approximate since both friction and brush contact drop have been neglected. Since a positional system is the interest here, the motor positional transfer function is found directly from equation 2.30.

$$\Omega(s) = s\Theta(s) \tag{2.38}$$

thus $$G_\theta(s) = \frac{\Theta(s)}{E_o(s)} = \frac{K}{s(s + 1/\tau_m)} \tag{2.39}$$

The effect of frictional torque and brush contact drop can be shown as opposing voltage inputs to the block as shown in figure 2.10.

Let $$E_f(s) = \frac{R_t}{K_T} T_f(s) \tag{2.40}$$

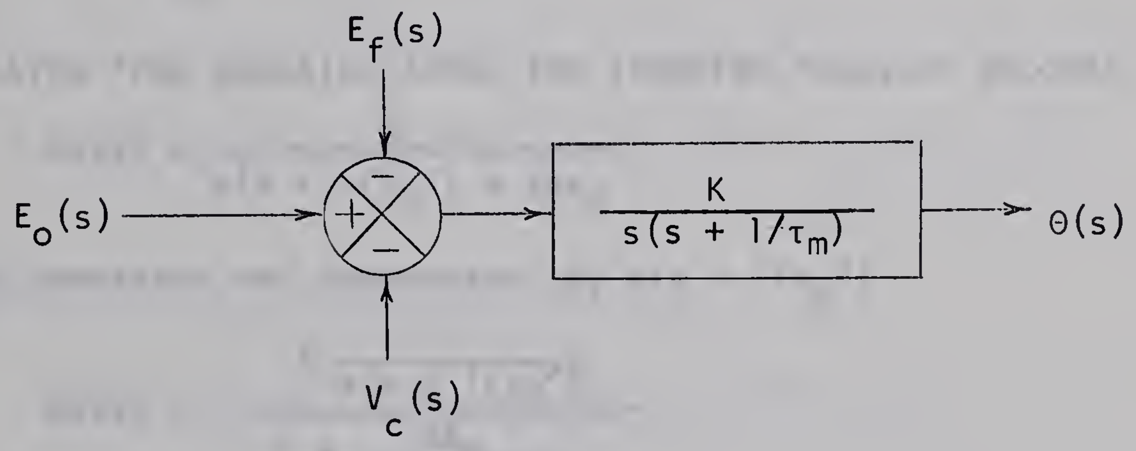

Figure 2.10 Motor Block Diagram

2.9 REPRESENTATION AS A TACHOMETER FEEDBACK SYSTEM

It is of interest to note that the motor itself may be represented as a tachometer feedback system due to the effect of the back e.m.f. If the expression for τ_m is substituted into equation 2.39, the transfer function is given by:

$$G\theta(s) = \frac{K}{s\left(s + \dfrac{R_tK_d + K_TK_g}{J_tR_t}\right)} \tag{2.41}$$

To demonstrate the above statement, this may be written as

$$G\theta(s) = \frac{K}{s(s + \frac{K_d}{J_t}) + s\,\dfrac{K_TK_g}{J_tR_t}} \tag{2.42}$$

A mechanical time constant may now be defined

$$\tau_m{}' \equiv \frac{J_t}{K_d} \tag{2.43}$$

Substituting from equation 2.29, the transfer function becomes

$$G\theta(s) = \frac{K}{s(s + 1/\tau_m{}') + sKK_g} \tag{2.44}$$

Dividing numerator and denominator by $s(s + 1/\tau_m{}')$

$$G\theta(s) = \frac{K\,\dfrac{1}{s(s + 1/\tau_m{}')}}{1 + \dfrac{KK_g}{(s + 1/\tau_m{}')}} \tag{2.45}$$

which is of the form $\dfrac{G(s)}{1 + G(s)H(s)}$

where $$G(s) = \frac{K}{s(s + 1/\tau_m{}')} \tag{2.46}$$

and $$H(s) = sK_g \tag{2.47}$$

The equivalent block diagram is shown in figure 2.11.

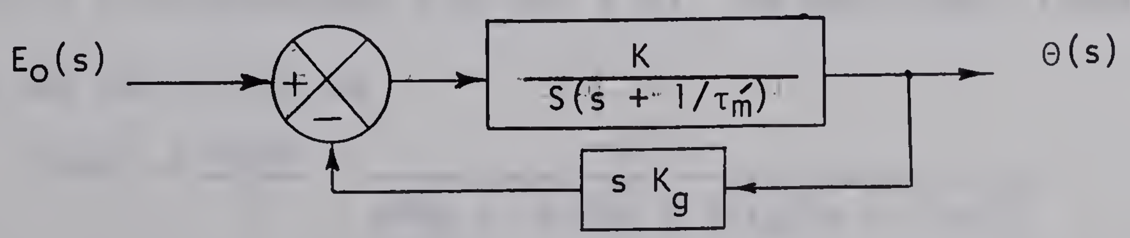

Figure 2.11 Representation as a Tachometer Feedback System

2.10 EFFECT OF ARMATURE INDUCTANCE

It was stated in Section 1.1 that the small armature inductance produces negligible electrical time constant. As such it has been neglected. A derivation including its effect will be of some interest at least for purposes of comparison of printed motors with conventional types. The only change is in the basic armature equation.

$$E_o(s) = I_a(s)\left(R_t + sL_a\right) + K_g\Omega(s) \tag{2.48}$$

thus
$$I_a(s) = \frac{E_o(s) - K_g\Omega(s)}{R_t + sL_a} \tag{2.49}$$

The equation of motion is repeated:

$$J_t\, s\Omega(s) + K_d\Omega(s) = T(s) \tag{2.50}$$

also
$$T(s) = K_T\, I_a(s) \tag{2.51}$$

thus
$$I_a(s) = \frac{J_t s\Omega(s) + K_d\Omega(s)}{K_T} \tag{2.52}$$

Equating equations 2.49 and 2.52 and rearranging,

$$E_o(s)\left[\frac{1}{R_t + sL_a}\right] = \Omega(s)\left[\frac{J_t s + K_d}{K_T} + \frac{K_g}{R_t + sL_a}\right] \tag{2.53}$$

The velocity transfer function then becomes

$$G_\omega(s) = \frac{\Omega(s)}{E_o(s)} = \frac{K_T}{K_T K_g + (R_t + sL_a)(J_t s + K_d)} \tag{2.54}$$

$$= \frac{K_T/J_t R_t}{\frac{K_T K_g}{J_t R_t} + \frac{L_a}{R_t}\left(s + \frac{R_t}{L_a}\right)\left(s + \frac{K_d}{J_t}\right)} \tag{2.55}$$

The electrical time constant is now defined.

Let
$$\tau_a \equiv \frac{L_a}{R_t} \tag{2.56}$$

Substituting from equations 2.29 and 2.43, the positional transfer function may be written as

$$G\theta(s) = \frac{G\omega(s)}{s} = \frac{K}{sKK_g + s\tau_a(s + 1/\tau_a)(s + 1/\tau_m')} \tag{2.57}$$

It can be shown that the denominator, when expanded, is

$$\tau_a s^3 + s^2\left(1 + \frac{\tau_a}{\tau_m}\right) + \frac{1}{\tau_m} s \tag{2.58}$$

This makes the characteristic equation cubic if τ_a (i.e. L_a) is significant thus leading to the possibility of instability in a positional system. With negligible inductance ($\tau_a \simeq 0$), the expression $G_\theta(s)$ reduces to equation 2.39.

2.11 AN ELECTROMECHANICAL CIRCUIT ANALOGY

A quantity which is often specified and used in system calculations(4) is called the motor regulation. It is defined as the equivalent series mechanical impedance at constant terminal voltage and is therefore expressed as angular velocity per unit torque.

$$K_m \equiv \frac{\tau_m}{J_t} = \frac{R_t}{R_t K_d + K_T K_g} \tag{2.59}$$

Since K_m is seen to be independent of both motor and load inertia, it may be used to determine overall time constant (or break frequency) if the load inertia is known, or to measure the load inertia if τ_m can be found by a step or frequency response.

The significance of K_m as a mechanical impedance will be shown by finding an electrical analog(1,2) for the complete motor. Velocity will be analagous to voltage and torque to current. The equation of the armature may be written as

$$\frac{E_o}{K_g} = T\left(\frac{R_t}{K_T K_g}\right) + \omega \tag{2.60}$$

From the equation of motion

$$T = \omega(K_d + sJ_t) + T_f \tag{2.61}$$

$$\frac{E_o}{K_g} = \left[\omega(K_d + sJ_t) + T_f\right]\frac{R_t}{K_T K_g} + \omega \tag{2.62}$$

$$= \omega\left[1 + \frac{K_d R_t + sJ_t R_t}{K_T K_g}\right] + \frac{T_f R_t}{K_T K_g} \tag{2.63}$$

Solving for the velocity

$$\omega = \frac{E_o/K_g}{1 + \dfrac{R_t(K_d + sJ_t)}{K_T K_g}} - \frac{T_f}{\dfrac{K_T K_g}{R_t} + K_d + sJ_t} \tag{2.64}$$

$$= \frac{\dfrac{E_o}{K_g}\ \dfrac{1}{K_d + sJ_t}}{\dfrac{R_t}{K_T K_g} + \dfrac{1}{K_d + sJ_t}} - \frac{T_f}{\dfrac{K_T K_g}{R_t} + K_d + sJ_t} \tag{2.65}$$

Since ω corresponds to output voltage, E_o/K_g must be the equivalent "input velocity" where $R_t/K_T K_g$ is a mechanical resistance and $1/(K_d + sJ_t)$ is a mechanical impedance consisting of $1/K_d$ in parallel with $1/sJ_t$. Since torque corresponds to current, T_f can be represented by a constant current source. Its coefficient can be represented by an impedance of $R_t/K_T K_g$, $1/K_d$ and $1/sJ_t$ all paralleled. The motor can now be represented be the electrically analagous circuit shown in figure 2.12.

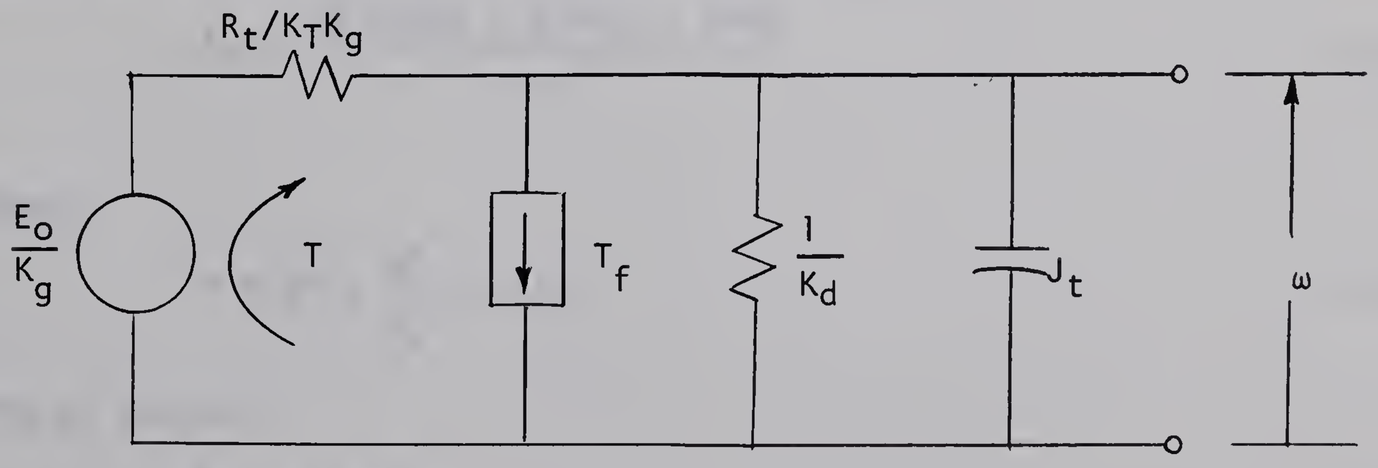

Figure 2.12 Electro-Mechanical Analog

Certain quantities of interest are readily obtainable from the analog.

The output "resistance" is seen to be

$$\frac{1}{K_d} \Big/\!\!\Big/ \frac{R_t}{K_T K_g} = \frac{R_t}{R_t K_d + K_T K_g} \qquad (2.66)$$

which is equal to motor regulation as defined.

Multiplication by the inertial "capacitor" yields the time constant as defined by equation 2.27.

The instantaneous torque produced:

$$T = \frac{E_o/K_g - \omega}{(R_t/\ K_T K_g)} \qquad (2.67)$$

Initial accelerating torque delivered:

$$T(0) = \frac{E_o K_T}{R_t} - T_f \qquad (2.68)$$

Initial acceleration:

$$\dot{\omega}(0) = \frac{T(0)}{J_t} = \frac{E_o K_T - T_f R_t}{J_t R_t} \qquad (2.69)$$

Applied voltage to achieve a desired velocity:

$$E_o = \frac{\omega_f\ (K_d R_t + K_T K_g) + T_f R_t}{K_T} \qquad (2.70)$$

Power:

$$P = \omega T = \frac{\omega^2}{K_m} = T^2 K_m \qquad (2.71)$$

Energy stored:

$$\mathcal{E}_s = \tfrac{1}{2} J_t \omega^2 \qquad (2.71)$$

2.12 SUMMARY

The basic relationships which have been derived do not uniquely apply to the printed motor. The analysis could describe any armature-controlled D.C. motor in which the field is essentially unaffected by the rotation of the armature and the inductance is negligible. The ingenious construction of the printed motor however, makes it much more nearly ideal than conventional types and as such its highly linear characteristics allow a very accurate prediction of behavior.

With the exceptions of the effects of stiction, Coulomb friction and brush contact drop, the relationships are extremely simple. It is reasonable to expect that these degrading effects will be negligible for most practical purposes since they are intentionally minimized in the manufacturing process.

CHAPTER THREE

EXPERIMENTAL DETERMINATION OF MOTOR PARAMETERS

3.1 INTRODUCTION

Up to now no quantitative description of the printed motor characteristics has been given. For verification of the basic relationships discussed and for confirmation of the reported motor specifications, some basic tests were performed from which the various motor constants could be calculated.

In order to discover the nature of the printed armature and investigate the possibilities of deriving a rate signal, the flux return plate (keeper) was removed. In adding a tachometer winding to the shaft (to be described in section 4.4), the magnetizing winding was removed to make room for two small brushes. As mentioned in section 1.1 only two brushes are necessary to supply armature current. Two were removed. The effect of these modifications on the various motor constants was determined. A description of the tests performed on both the modified and unmodified motor and the numerical results will now be given.

All mechanical constants will be given in c.g.s. units. Electrical constants will be in terms of volts, amps and ohms. Angular displacement will be measured in radians. The conversion factor from electrical to mechanical power will be used rather than letting the voltage and torque constants have the same units.

$$K_T \text{ (gm cm/amp)} = K_g\left(\frac{\text{volt}}{\text{rad/sec}}\right) \times 10.2 \times 10^3 \; \frac{\text{gm cm/sec}}{\text{watt}} \qquad (3.1)$$

Since speed was measured with a stroboscope calibrated in RPM, experimental curves are given on this basis and the constants found are converted to units of radians/second.

3.2 GENERATOR OPEN-CIRCUIT CHARACTERISTIC

If the motor shaft is rotated at speed ω, the open-circuit terminal voltage is given by equation 2.1. The voltage constant can thus be found from the slope of the generator characteristic and the torque constant may then be determined from equation 3.1.

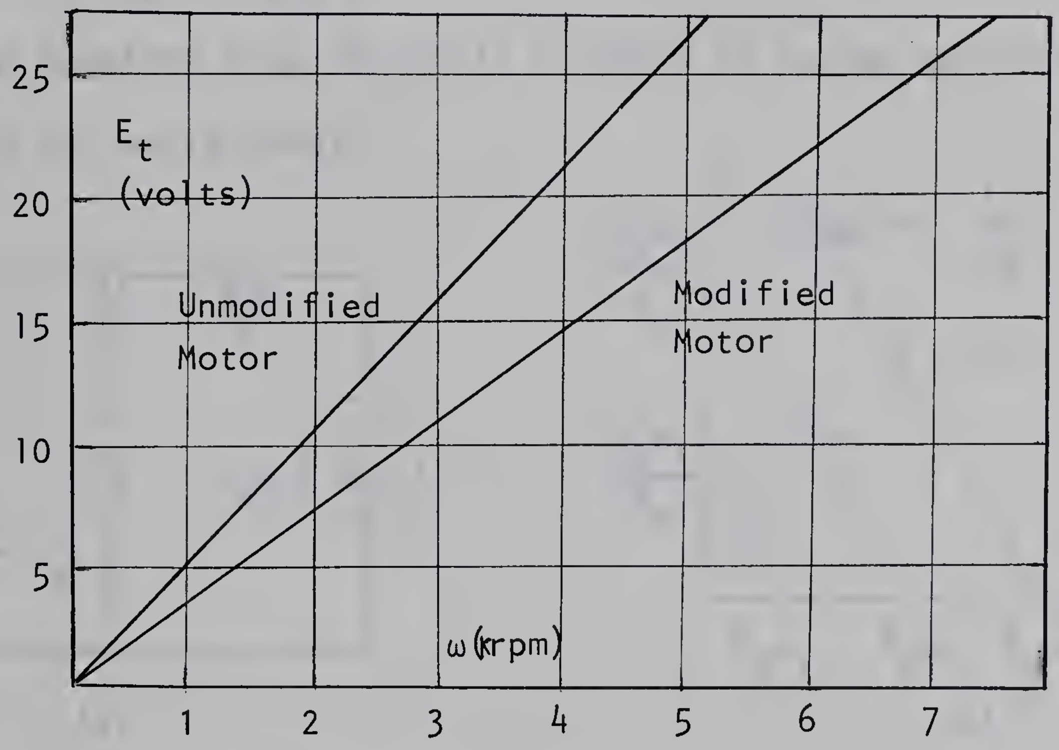

Figure 3.1 Experimental Generator Open Circuit Characteristics

Values of the experimental constants obtained from the characteristic are listed.

Unmodified motor:

K_g = 5.24 volts/Krpm = 0.050 volt sec/rad

K_T = 10.2 x 10^3 x .050 = 510 gm cm/amp

Modified motor:

K_g = 3.7 volts/Krpm = 0.035 volt sec/rad

K_T = 10.2 x 10^3 x .035 = 360 gm cm/amp

3.3 GENERATOR LOAD CHARACTERISTICS

In this test the modified motor was run as a generator at constant speed by the unmodified motor and vice versa. Loading the generator with a variable resistance results in a curve of armature (load) current versus terminal voltage having a slope which is the reciprocal of the armature terminal resistance. The curve is described by

$$E_t = K_g\omega - I_a R_a \tag{3.2}$$

If R_a were constant (i.e. $V_c = 0$), a family of curves as shown in figure 3.2 (b) would result.

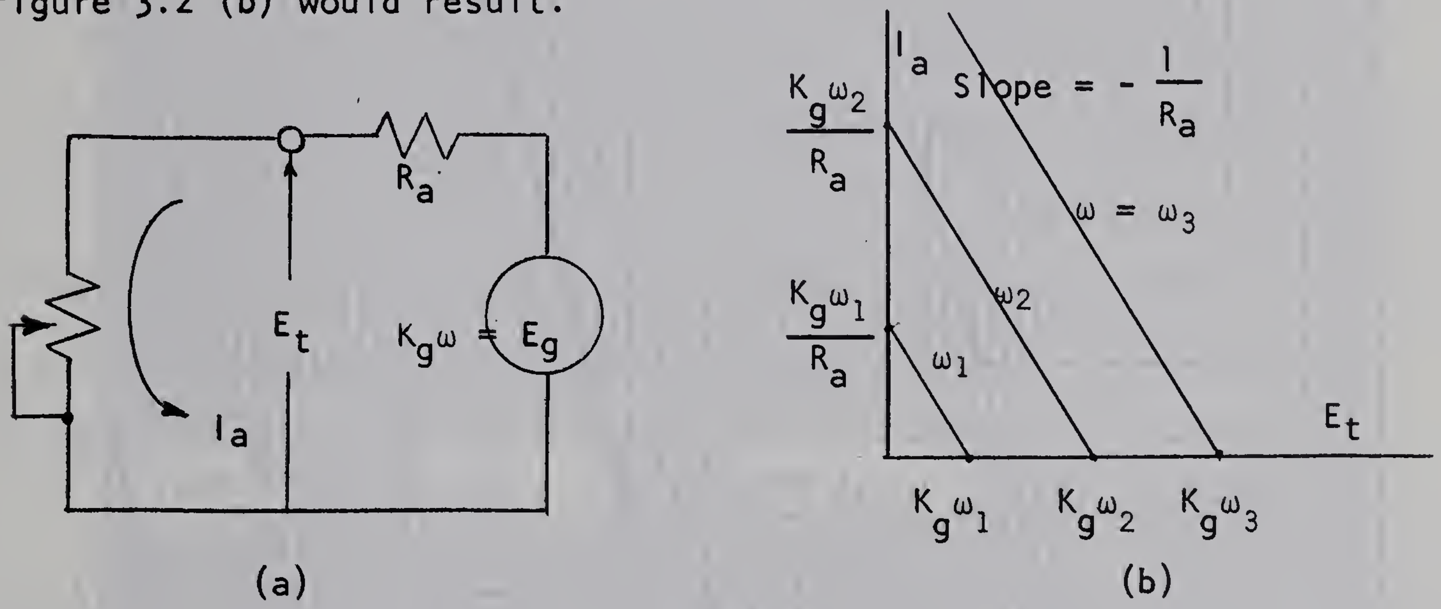

R_a
E_t
$K_g\omega = E_g$
I_a
(a)
I_a
Slope = $-\frac{1}{R_a}$
$\frac{K_g\omega_2}{R_a}$
$\frac{K_g\omega_1}{R_a}$
$\omega = \omega_3$
ω_2
ω_1
E_t
$K_g\omega_1$
$K_g\omega_2$
$K_g\omega_3$
(b)

Figure 3.2 Ideal Generator Load Characteristics

The variation of armature resistance with current is represented in figure 2.6. At low currents, the slope of the load characteristic is determined by the sum of the winding, brush and contact resistances which may be extremely large. At higher currents the slope is determined only by the winding resistance. Experimentally obtained characteristics are shown in figure 3.3. From the slopes of the linear portions, the armature winding resistances were found.

Unmodified motor:

$R_w = 0.56 \pm .03$ ohms

Modified motor:

$R_w = 0.54 \pm .03$ ohms

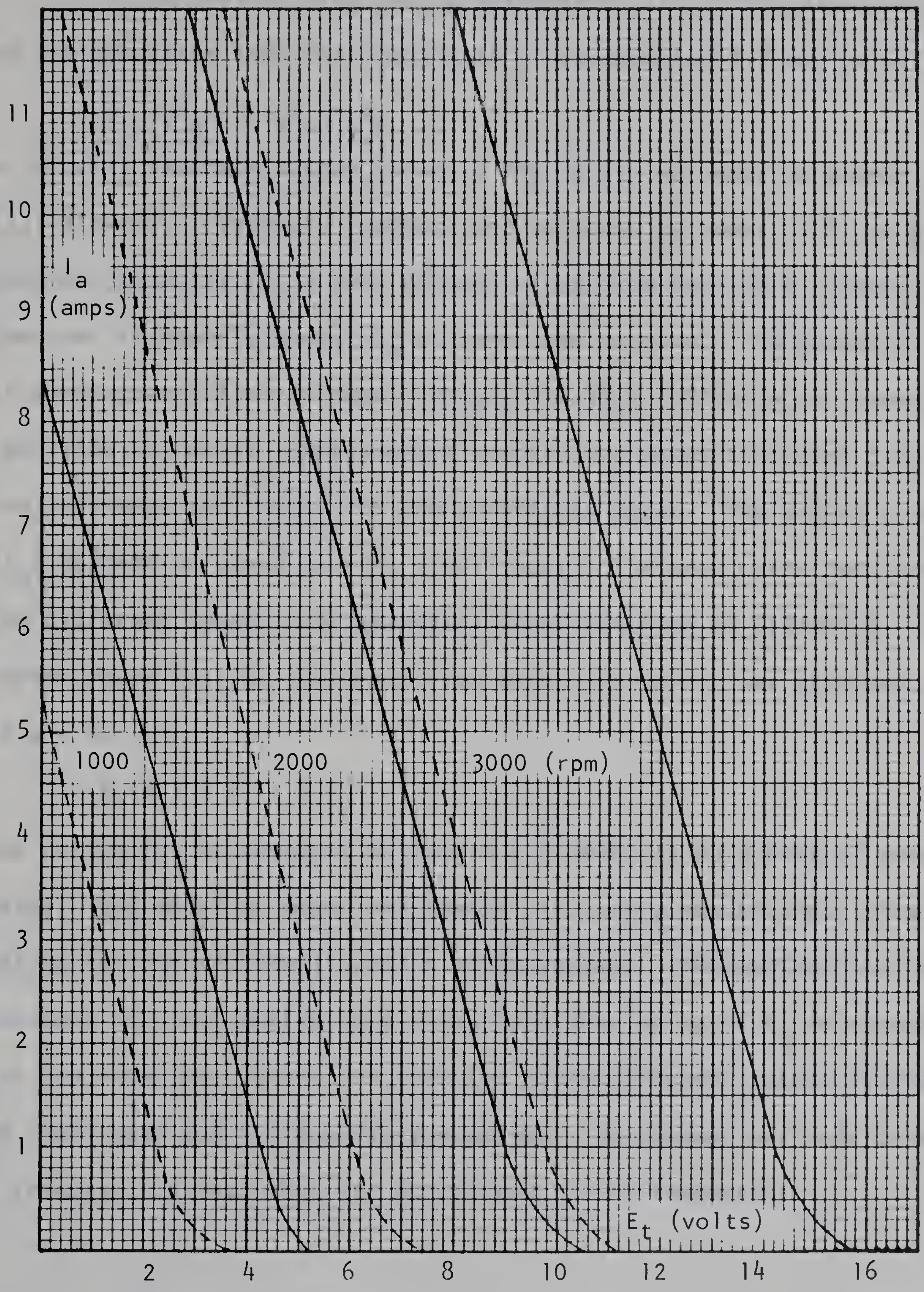

Figure 3.3 Experimental Generator Load Characteristics

——— Unmodified Motor
----- Modified Motor

3.4 BRUSH CONTACT RESISTANCE AND VOLTAGE DROP

Brush contact drop can be determined with reasonable accuracy from the generator load characteristic since equation 3.2 may be written

$$E_t = K_g\omega - I_a R_w - V_c \tag{3.3}$$

The velocity feedback system shown in figure 3.4 was used to obtain $V_c(I_a)$ directly. Velocity feedback was adjusted by means of P_1 to give a constant velocity for a load current range from zero to six amps. P_2 was set to exactly cancel E_g at zero load current. The output of the last summing amplifier is equal to $I_a R_w + V_c(I_a)$. Since R_w is known, V_c can thus be found. Experimental results are shown in figure 3.5. Curve (a) shows the result for the unmodified motor. The extent to which $V_c(I_a)$ depends on speed is also significant. The same curve resulted for three different speeds. At standstill the situation is different. From a locked rotor test on the unmodified motor, curve (b) was obtained. With $\omega = 0$

$$V_c(I_a) = E_t - I_a R_w \tag{3.4}$$

These curves may be compared to figure 2.5 which is on a base of current density. The modified motor was tested using only two brushes, thus doubling the current density for a given current. The contact-plus-brush resistance is also doubled so a slightly higher value of V_c is expected. Again the curve was almost the same for three different speeds [curve (c)]. Note that these are all equilibrium curves. No attempt was made to measure the transient curves, that is, at constant brush temperature.

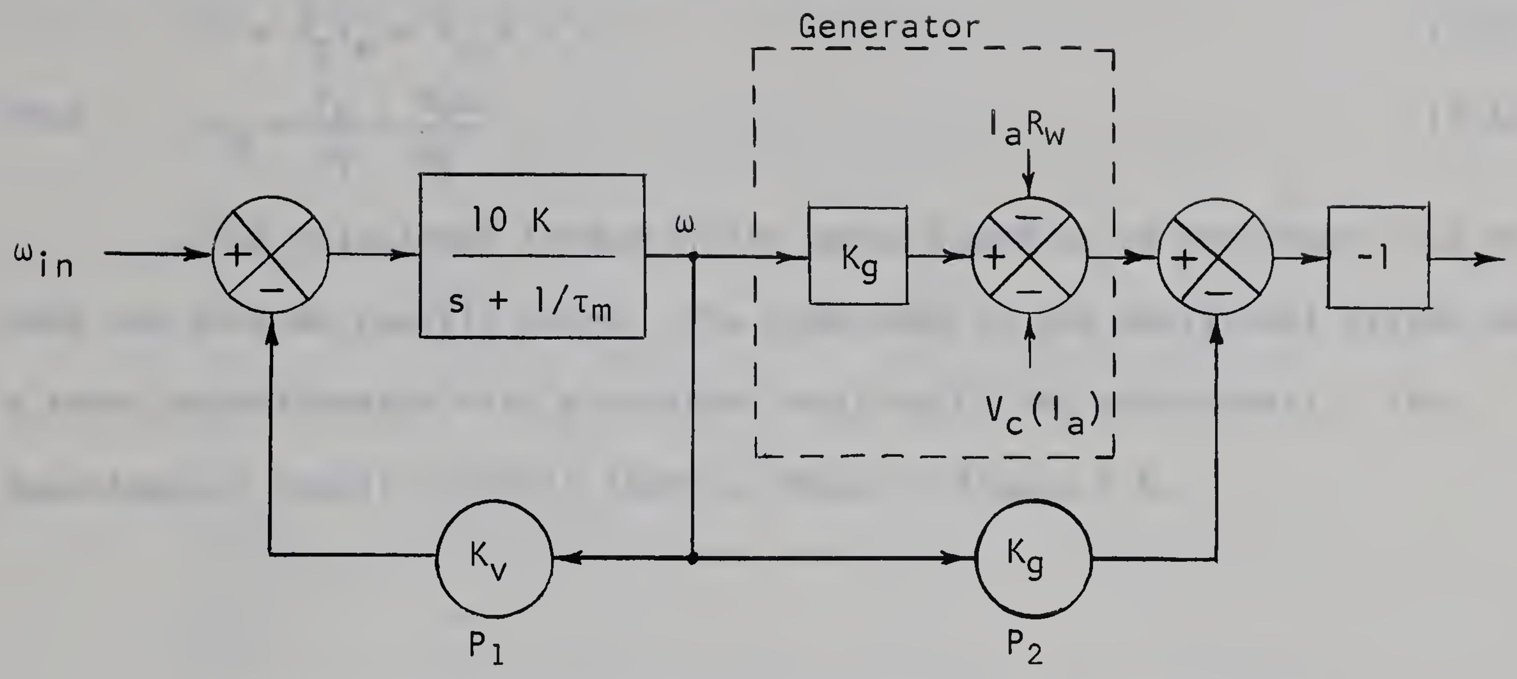
ω in
+
−
10 K
s + 1/τm
ω
Generator
Kg
IaRw
+
−
−
Vc(Ia)
+
−
-1
Kv
P1
Kg
P2

Figure 3.4 Measurement of $V_c(I_a)$

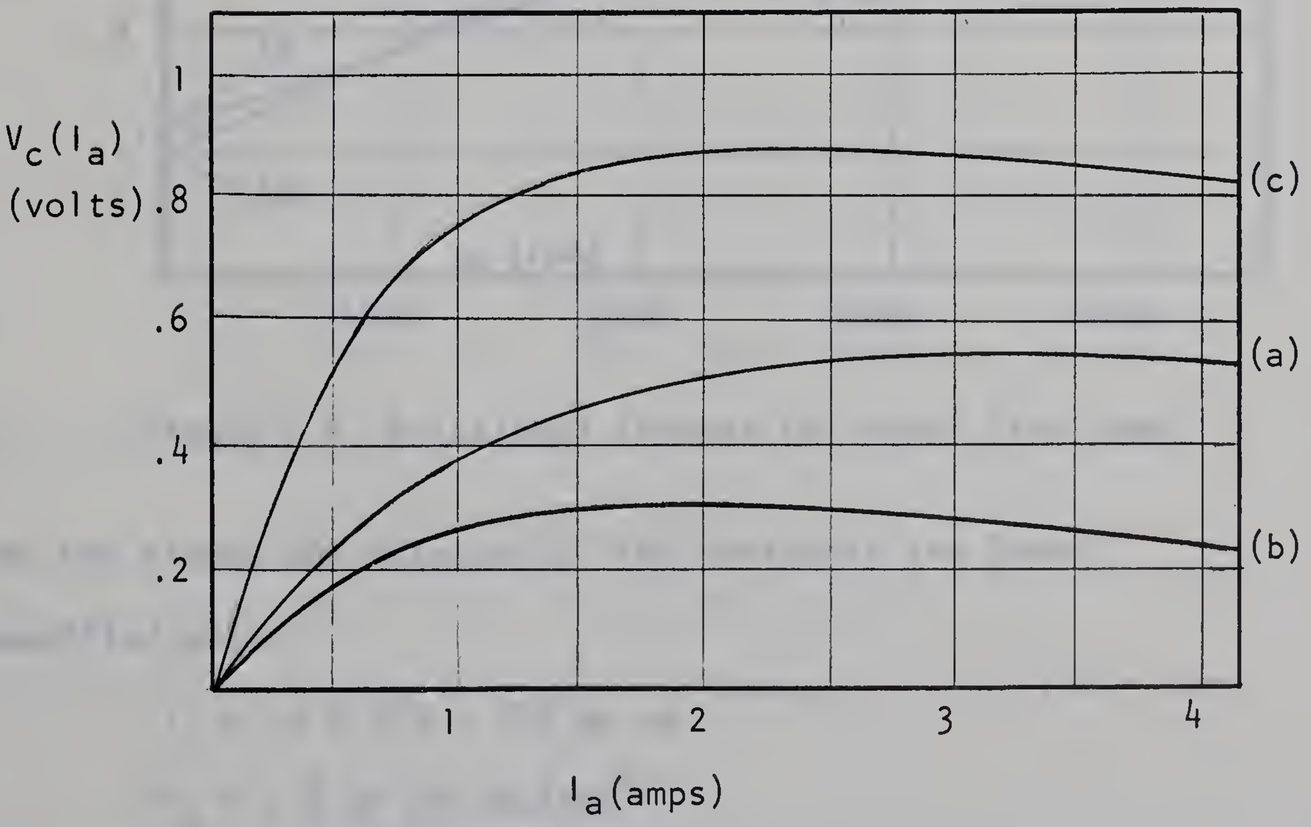

Figure 3.5 Brush Contact Drop

[illegible]

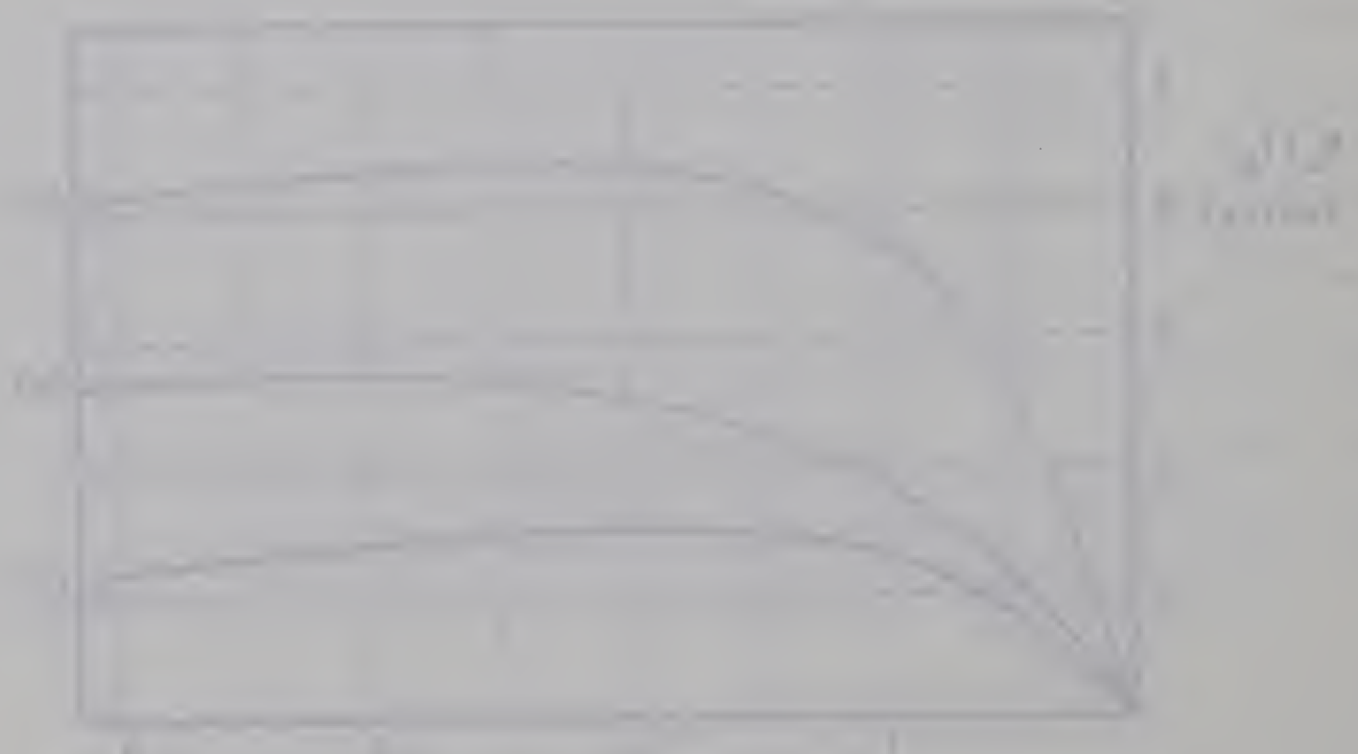

[illegible]

[illegible]

3.5 FRICTIONAL TORQUES AND LOSSES

It is a simple matter to determine both T_c and K_d provided that K_T is accurately known. At constant velocities:

$$T = K_T I_a = T_c + T_v \tag{3.5}$$

thus

$$I_a = \frac{T_c}{K_T} + \frac{K_d \omega}{K_T} \tag{3.6}$$

The frictional torque of the motor alone or of the motor plus any load can thus be readily found. The load used in the positional system was a servo potentiometer with a bellows coupling to the motor shaft. The experimental result for this load is shown in figure 3.6.

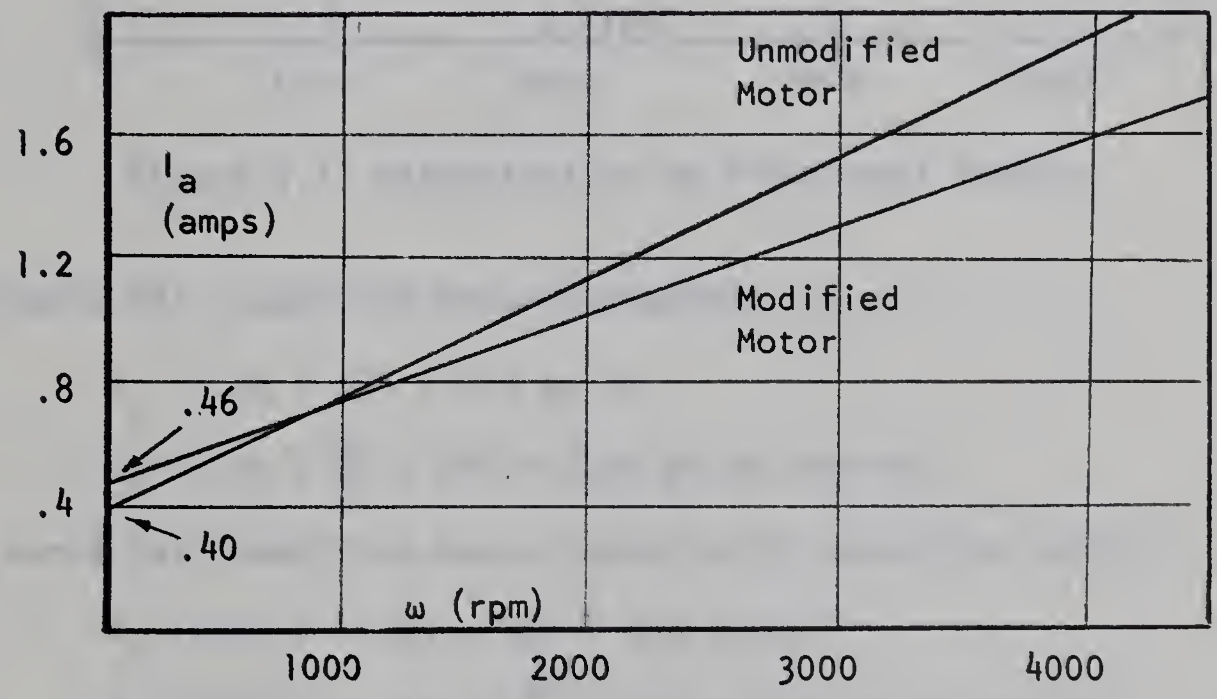

Figure 3.6 Frictional Torques For Motor Plus Load

From the slopes and intercepts, the constants are found.

Unmodified motor:

T_c = .4 x 510 = 220 gm cm

K_d = 1.8 gm cm sec/rad

Modified motor:

T_c = .46 x 360 = 165 gm cm

K_d = 1.0 gm cm sec/rad

The frictional torques and damping constants were also determined by using one motor as the load of the other. Subtraction of the constants found from a no-load test yields the frictional torque and damping constant of the load. Experimental results are shown in figure 3.7.

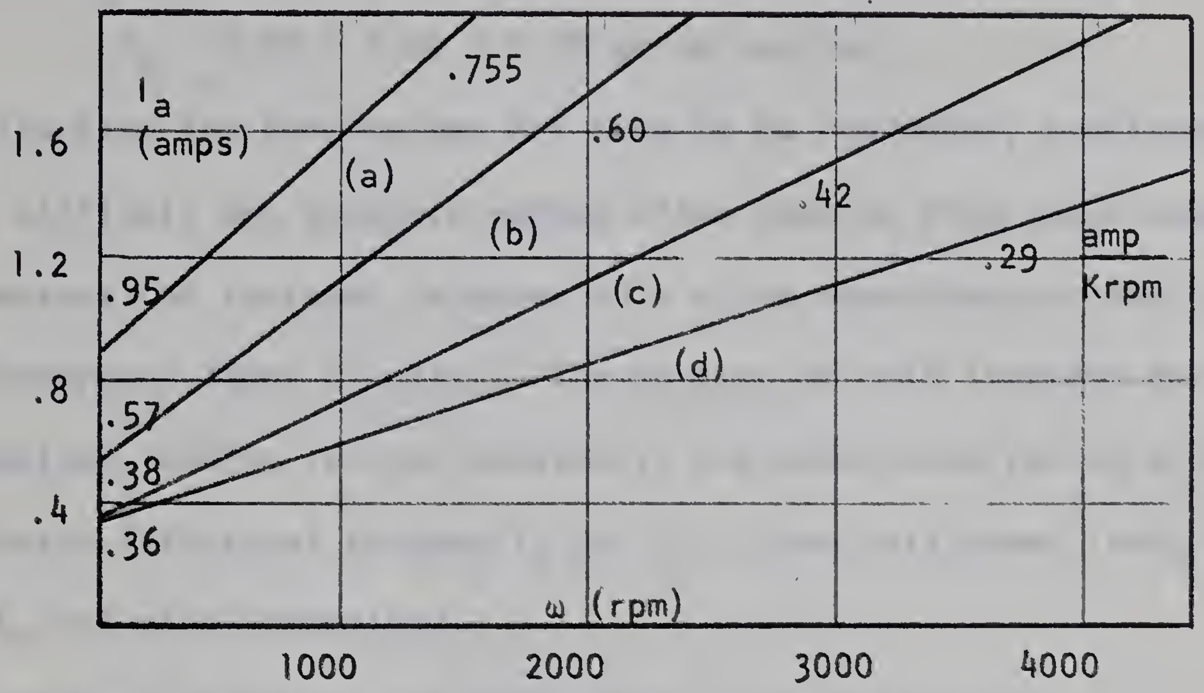

Figure 3.7 Determination of Frictional Torques

From curve (d), (modified motor unloaded):

$$T_c \simeq .36 \times 360 = 129 \text{ gm cm}$$

$$K_d \simeq .29 \times \frac{30}{\pi} \times 360 = 0.99 \text{ gm cm sec/rad}$$

From curve (a), (modified motor loaded with unmodified motor):

$$T_c \text{ (total)} \simeq .93 \times 360 = 335 \text{ gm cm}$$

$$K_d \text{ (total)} \simeq .745 \times \frac{30}{\pi} \times 360 = 2.56 \text{ gm cm sec/rad}$$

Thus, for the unmodified motor:

$$T_c \simeq 335 - 129 = 206 \text{ gm cm}$$

$$K_d \simeq 2.56 - 0.99 = 1.57 \text{ gm cm sec/rad}$$

From curve (c), (unmodified motor unloaded):

$$T_c \simeq .38 \times 510 = 194 \text{ gm cm}$$

$$K_d \simeq .42 \times \frac{30}{\pi} \times 510 = 2.04 \text{ gm cm sec/rad}$$

From curve (b), (unmodified motor loaded with modified motor):

$$T_c \text{ (total)} \simeq .57 \times 510 = 291 \text{ gm cm}$$

$$K_d \text{ (total)} \simeq .60 \times \frac{30}{\pi} \times 510 = 2.92 \text{ gm cm sec/rad}$$

Thus, for the modified motor:

$$T_c \simeq 291 - 194 = 97 \text{ gm cm}$$

$$K_d \simeq 2.92 - 2.04 = 0.88 \text{ gm cm sec/rad}$$

Results from the four curves are seen to be reasonably consistent. A more difficult but standard method often used to find these values is to measure the increase in power to a prime mover due to loading with the generator (open circuit). The portion of this increase due to mechanical loading is then equated to the power required to produce the generator frictional torques T_c and T_v. From this power loss, both T_c and K_d are then determined.

At constant velocity, the motor power loss is given by

$$P_L(\omega) = \omega(T_c + K_d\omega) + I_a{}^2R_w + I_a V_c \tag{3.7}$$

The power loss of the open-circuited generator is simply

$$P_L(\omega) = \omega(T_c + K_d\omega) \tag{3.8}$$

Let the input power to the unloaded motor be given by

$$P_1 = E_{t_1} I_{a_1} \tag{3.9}$$

With the generator coupled, the input power is

$$P_2 = E_{t_2} I_{a_2} \tag{3.10}$$

Let the increase in electrical losses be given by

$$P_{12} = (I_{a_2}{}^2 - I_{a_1}{}^2)R_w + (I_{a_2} - I_{a_1})V_c \tag{3.11}$$

Then the power loss due to generator frictional torques is

$$P_L(\omega) = P_2 - (P_1 + P_{12}) \tag{3.12}$$

For experimental purposes then, from equation 3.8

$$P_L(\omega)/\omega \times 30/\pi \times 10.2 \times 10^3 = T_c + K_d\omega \tag{3.13}$$

$P_L(\omega)$ is in watts, T_c is in gm cm, and ω is in rpm.

The losses for the loaded and unloaded cases using the modified motor as prime mover are shown in figure 3.8. The experimental determination of equation 3.13 for both "generators" is shown in figure 3.9.

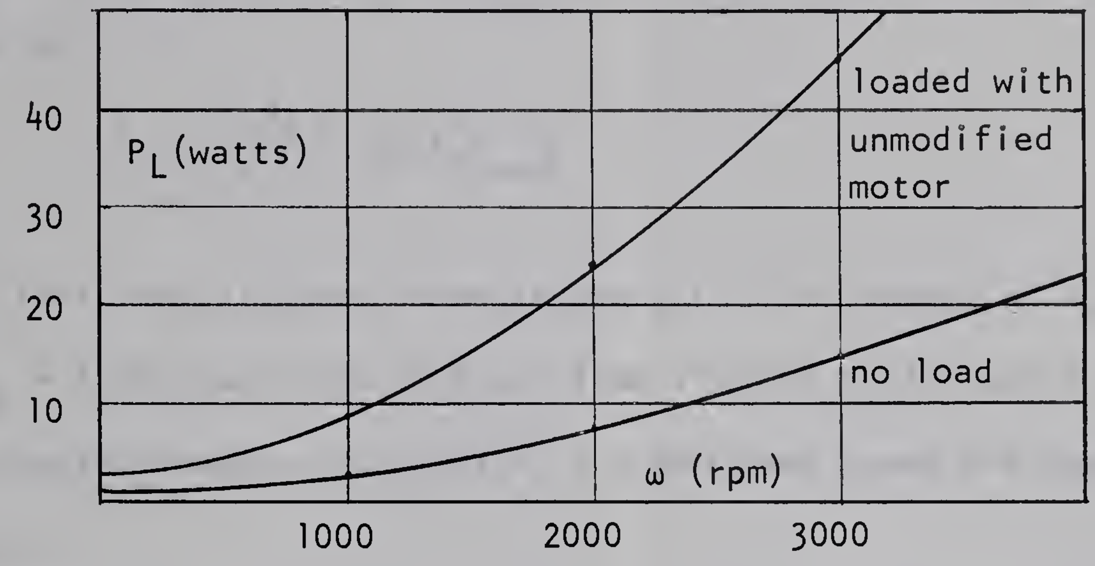

Figure 3.8 Power Input to Modified Motor

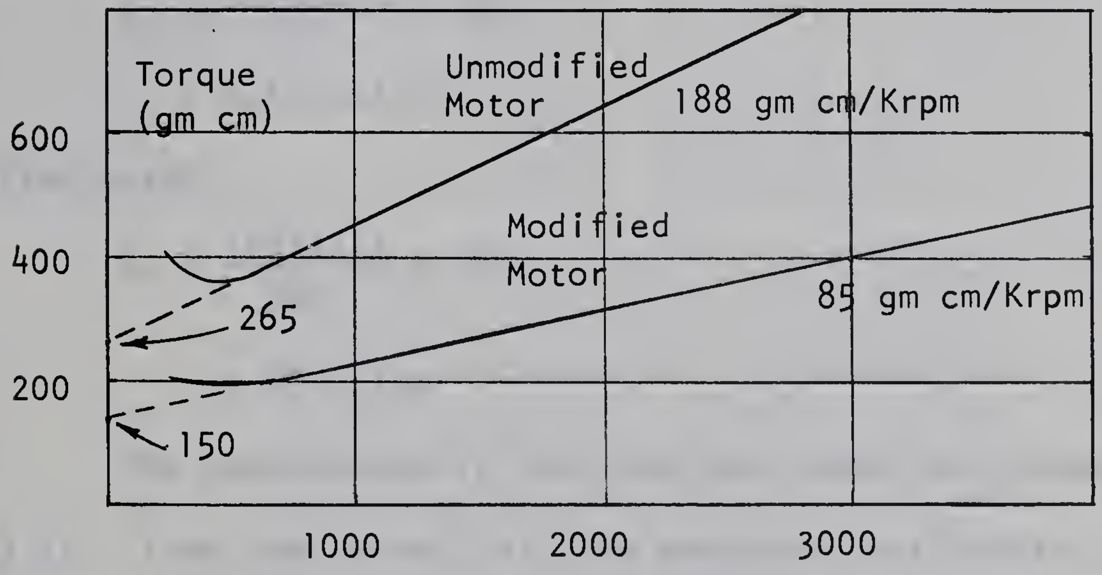

Figure 3.9 Calculated Frictional Torques

The constants are found directly from the slopes and intercepts of the two curves in figure 3.9.

Unmodified motor:

T_c = 265 gm cm

K_d = 1.80 gm cm sec/rad

Modified motor:

T_c = 150 gm cm

K_d = 0.80 gm cm sec/rad

3.6 VELOCITY TRANSFER CHARACTERISTIC: DEAD ZONE

Since the nature of $V_c(E_o)$ is unknown, the exact shape of the motor velocity characteristic cannot be predicted. Assuming V_c to be constant, it is as shown in figure 2.8. The half-width of the dead zone is given by

$$E_d = \frac{T_c R_t}{K_T} + V_c(I_a)_{\omega=0^+} \tag{3.14}$$

The first term is found from figure 3.6. The values of V_c corresponding to $I_a = T_c/K_T$ may then be found from figures 3.5(a) and 3.5(c). Using the servo potentiometer load and $R_s = 0.56\Omega$ dead zones are found for the two motors.

Unmodified motor:

$$E_d \simeq \frac{200(1.1)}{510} + .20$$

$$\simeq 0.63 \text{ volts}$$

Modified motor:

$$E_d \simeq \frac{165(1.1)}{360} + .48$$

$$\simeq 0.98 \text{ volts}$$

The experimentally obtained dead zones are shown in figures 3.10 and 3.11. From the curves (a), the dead-zone half-widths are 0.60 volts and 0.98 volts for the unmodified and modified motors respectively. This excellent agreement indicates a very reliable set of constants. However, it should be noted that the apparent linearity of the dead zone characteristics is attributable to the linearity of the $V_c(I_a)$ curves in the region $I_a < .46$ amps.

The motor velocity transfer characteristics were obtained experimentally and are shown in figure 3.12. The slopes of the two curves are now compared to those expected using the formerly determined values of motor constants.

Figure 3.10 Dead-Zone of Unmodified Motor

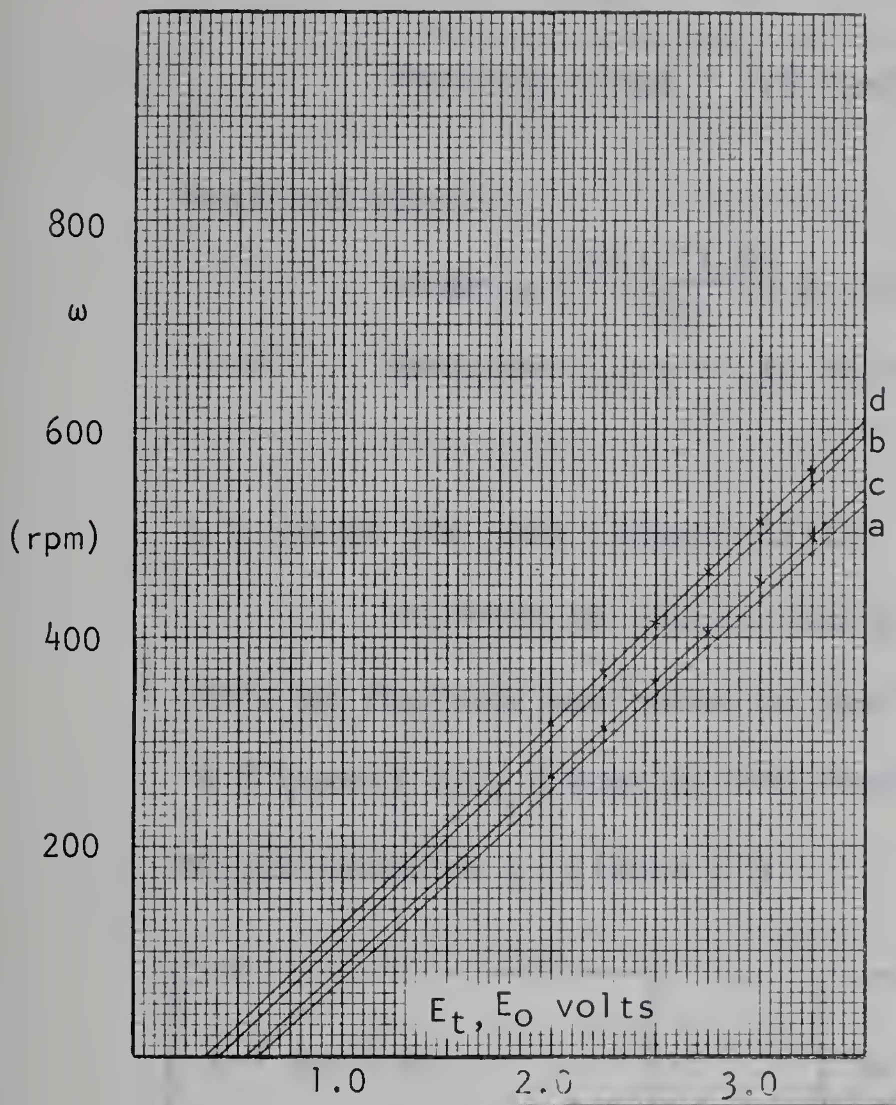

Figure 3.11 Dead-Zone of Modified Motor

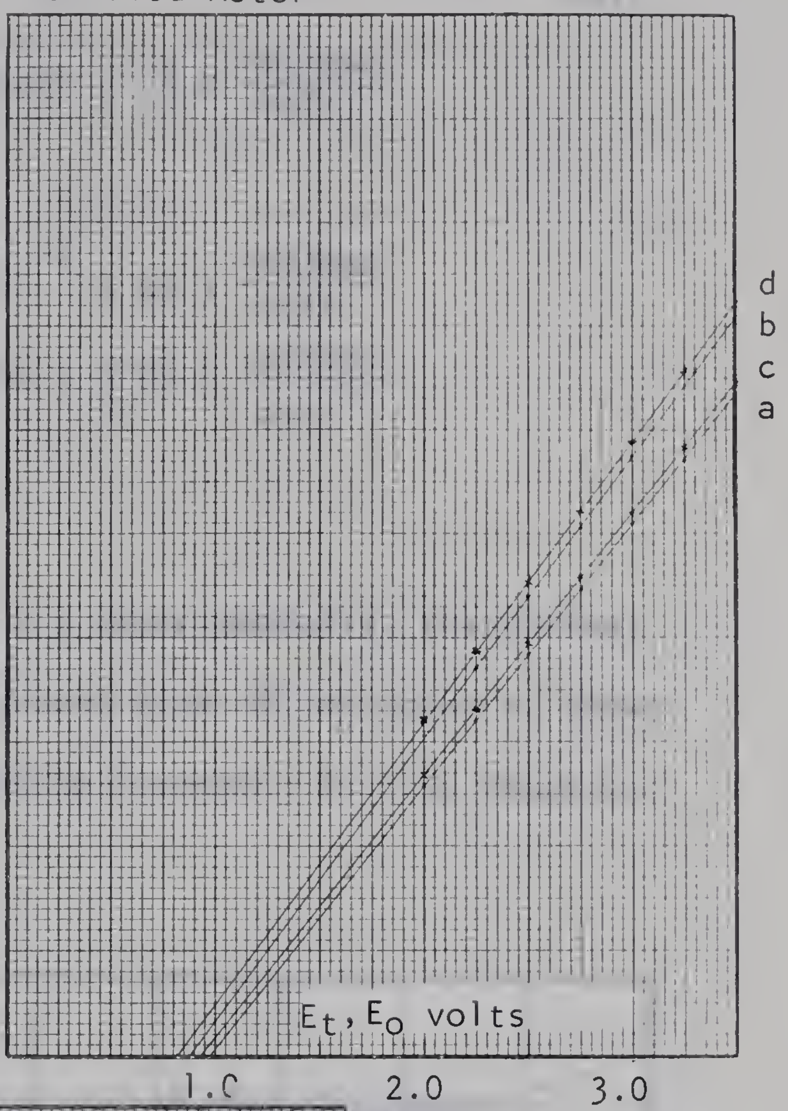

a: $\omega(E_o)$ loaded

b: $\omega(E_t)$ loaded

c: $\omega(E_o)$ no-load

d: $\omega(E_t)$ no-load

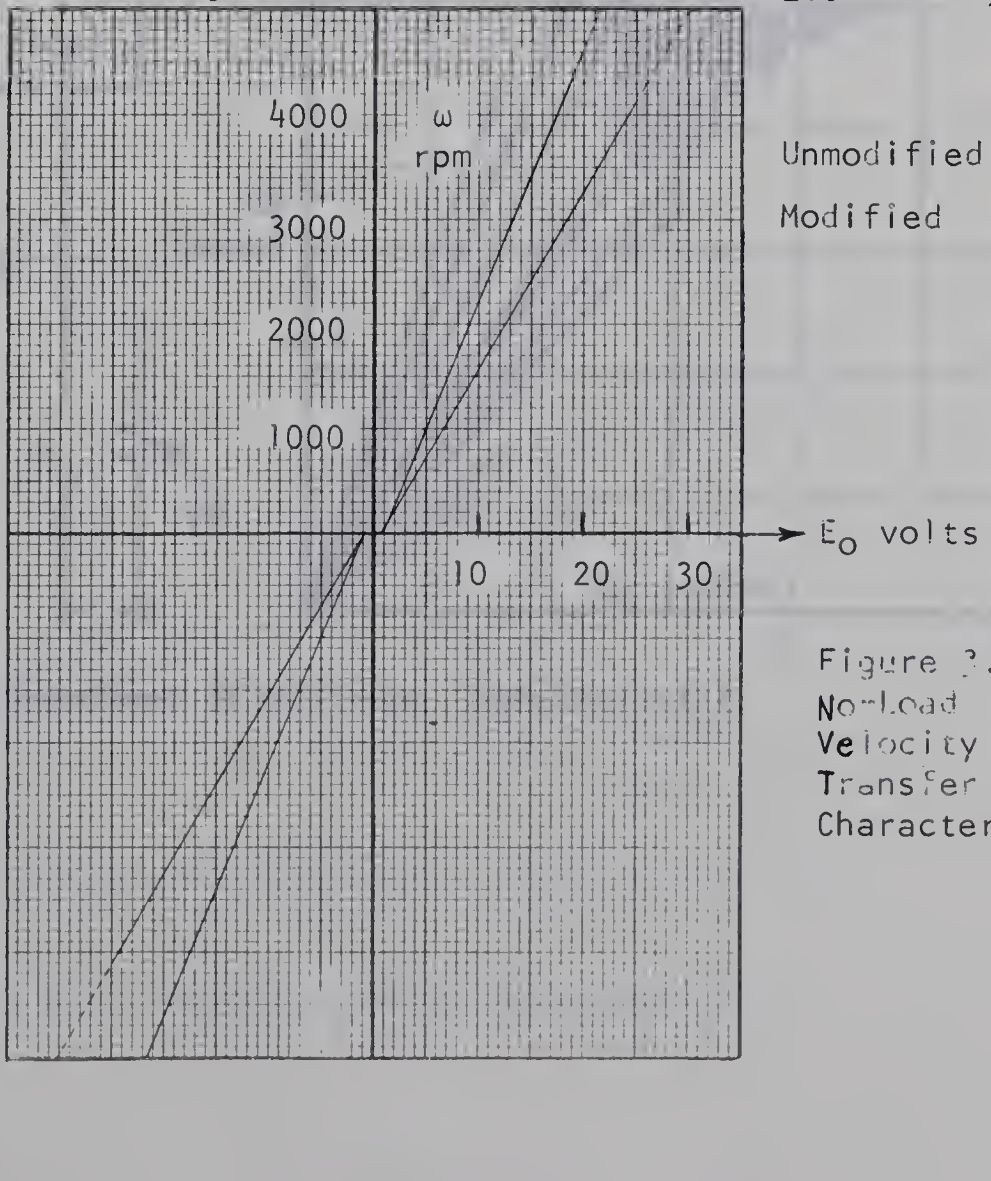

Figure 3.12 No-Load Velocity Transfer Characteristics

Unmodified motor:

$$\text{Slope} = \left(\frac{R_t K_d}{K_T} + K_g\right)^{-1} \simeq \left(\frac{(1.1)(1.8)}{510} + .05\right)^{-1} = 18.5\ \frac{\text{rad/sec}}{\text{volt}}$$

$$\text{Measured slope} \approx 173\ \text{rpm/volt} = 18.0\ \frac{\text{rad/sec}}{\text{volt}}$$

Modified motor:

$$\text{Slope} \approx \left(\frac{(1.1)(1.0)}{360} + .035\right)^{-1} = 26.3\ \frac{\text{rad/sec}}{\text{volt}}$$

$$\text{Measured slope} \approx 239\ \text{rpm/volt} = 25.1\ \frac{\text{rad/sec}}{\text{volt}}$$

3.7 MOTOR VOLT-AMP CHARACTERISTIC

In order to obtain figure 2.9 experimentally, the current limiting resistor was moved to the ground side of the motor as shown in figure 3.13. A copy of the resulting recording is also shown and may be compared to figure 2.9.

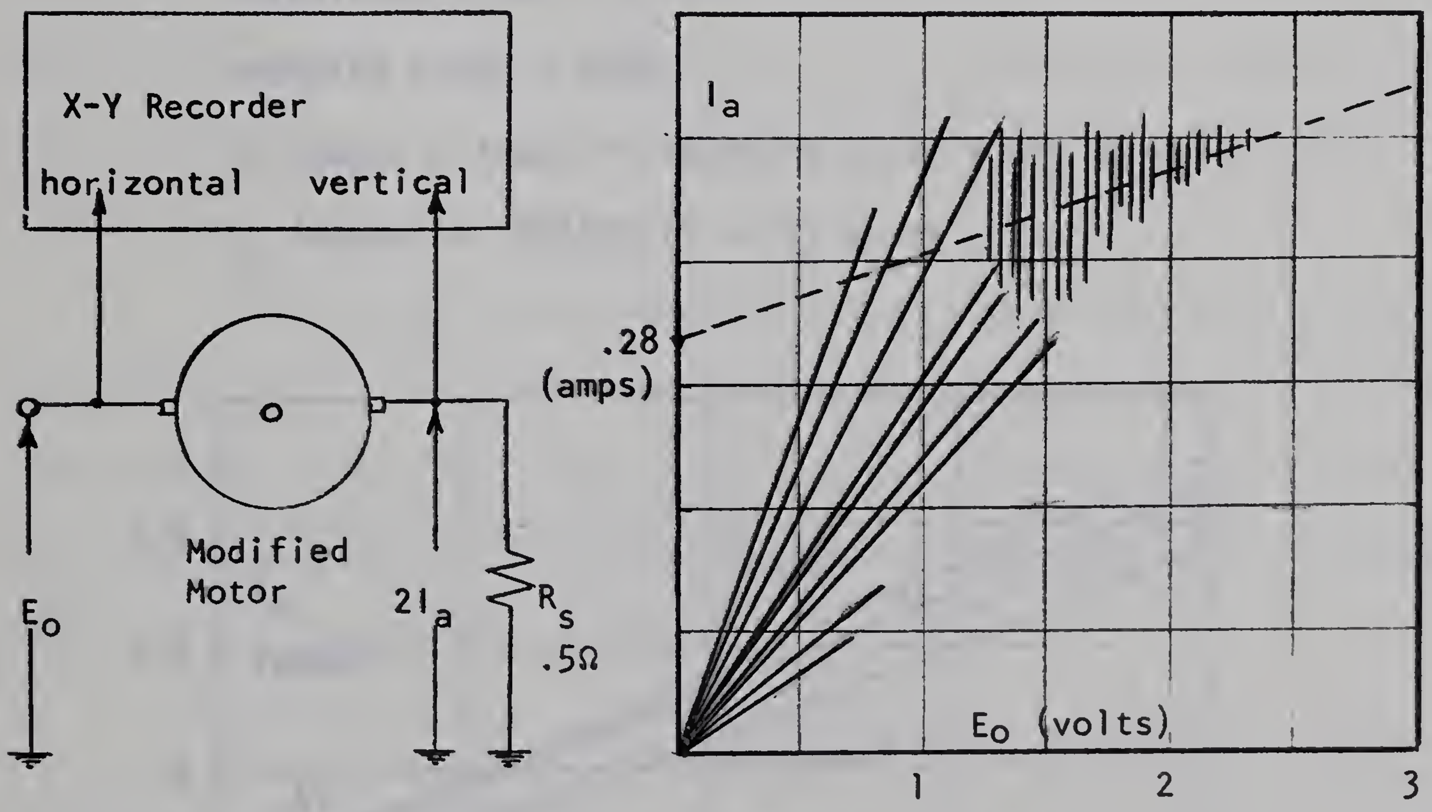
X-Y Recorder
horizontal
vertical
Modified Motor
E_o
$2I_a$
R_s
.5Ω
I_a
.28
(amps)
E_o (volts)
1
2
3

Figure 3.13 Measurement of Volt-Amp Characteristic

The volt-amp characteristics were also measured using an ammeter and voltmeter. Results are shown in figure 3.14. The theoretical current-axis intercept and slope are given by equation 2.35. These are now checked against those obtained experimentally using the formerly-determined values of motor constants. The Coulomb frictional torque is found from the intercept.

Unmodified motor:

$$\text{Calculated slope} = \left(R_t + \frac{K_T K_g}{K_d}\right)^{-1} = 0.0655$$

Measured slope = 0.064

T_c (motor + load) ≃ .42(510 + 38.1) = 230 gm cm

T_c (motor) ≃ .28(548.1) = 154 gm cm

Modified motor:

Calculated slope ≃ 0.072

Measured slope ≃ 0.067

T_c (motor + load) ≃ .42(360 + 29.1) = 164 gm cm

T_c (motor) ≃ .28(389.1) = 109 gm cm

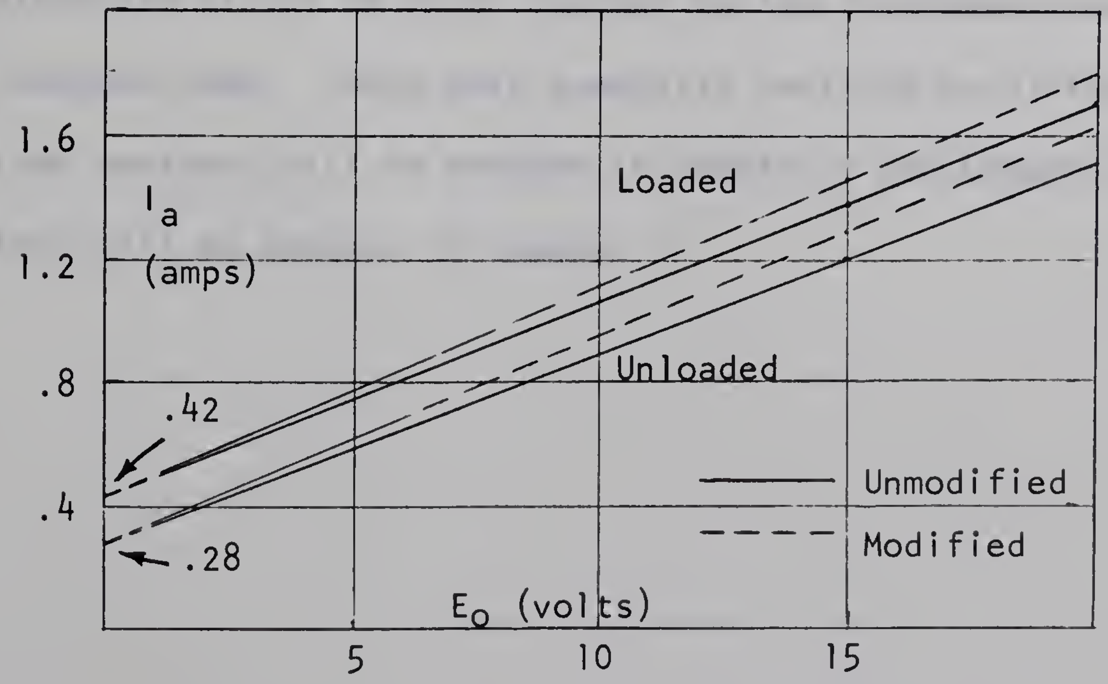

Figure 3.14 Motor Volt-Amp Characteristics

3.8 SUMMARY

The values of both obtained and derived constants are listed in the table on page 38. They are based on the use of the servo potentiometer load and series resistance of 0.56 ohms (reason to be given in Section 4.2). The armature inertia given in the motor specifications is 1.29 gm cm sec^2. A somewhat larger value is assumed to account for load and coupling inertia and that of the added winding in the case of the modified motor.

The relatively large reduction in K_g (or K_T) caused by the removal of the flux return plate (for a period of several weeks) is the most serious effect of the modification. Since K_g is proportional to field strength, the permanent magnet structure of the modified motor was reduced to about 70% of its former strength. The most detrimental results of this may be seen in equations 2.27 and 2.29. The motor time constant is nearly proportional to K_g^{-2} so it has become approximately twice its original value. The motor gain constant is also decreased to 70% of its original value.

The values of the constants listed are of course only accurate to within the limits of error imposed by the instruments and the graphical methods used. These were generally verified by different tests. The time constant will be checked in Chapter 4 and Chapter 7; the gain constant will be checked in Chapter 7.

Table of Experimental Constants

CONSTANT	UNITS	UNMODIFIED MOTOR	MODIFIED MOTOR
K_g	volt sec/rad	.05	.035
K_T	gm cm/amp	510	360
R_t	ohms	1.12	1.10
K_d	gm cm sec/rad	1.8	1.0
T_c	gm cm	220	165
E_f	volts	.43	.50
K_m	rad/gm cm sec	.04	.076
J_t	gm cm sec^2	≃1.5	≃1.6
τ_m	sec	≃.06	≃.12
K	rad/volt sec^2	≃300	≃200

CHAPTER FOUR

DERIVATION OF A RATE SIGNAL

4.1 INTRODUCTION

The improvement in performance of a positional system by using velocity or rate feedback is well-known. The difficulty in obtaining a rate signal suitable for damping, however, is equally well-known; hence, the so-called tachometer problem. Its solution, by simple means, is the main intention of this work.

An A.C. drag-cup tachometer-generator geared to the shaft and operating on a 400 Hz., 115 VAC input is commonly used in servo systems since it has very low inertia and friction. Rectification is provided by a synchronized chopper-rectifier. System performance is degraded by the friction of the gears and the phase shift of the required filter. The necessity of providing the external supply is also quite undesireable.

In systems where motor speed control is the requirement, optical tachometers yielding digital outputs often prove to be the most accurate. Such a type is used in the S-1 Servo System (4) in which the pick-off device is mounted as an integral part of the printed motor. The expense of the lamp, lens, grating, pick-off device and reference oscillator is a practical disadvantage and the necessary indication of direction is not directly available.

Differentiating circuits are occasionally used to provide a rate signal. Most practical circuits however, are far from ideal differentiators and are generally subject to noise. This will be seen in Chapters 8 and 12.

4.2 THE SUBTRACTION METHOD

The back e.m.f. developed by the windings of the printed armature is equal to K_g times the rotor velocity. When the shaft is physically rotated, this generated voltage is seen to be a high quality D.C. with very low ripple content. It was originally hoped to somehow add two brushes to the motor and pick off this voltage, or a fraction of it to use as a rate feedback signal. On dissembling the motor and discovering the nature of the printed armature (figure 1.2), this proved to be impossible due to the always-present drop in the armature resistance. The possibility of external subtraction of this drop has led to what will be called the subtraction method.

For any D.C. motor, a small series resistor may be used without too seriously degrading the performance. From the basic equations then, (Section 2.1)

$$E_o = I_a(R_a + R_s) + K_g\omega \tag{4.1}$$

$$E_t = I_aR_a + K_g\omega \tag{4.2}$$

Eliminating I_a,

$$K_g\omega = \frac{R_a + R_s}{R_s} E_t - \frac{R_a}{R_s} E_o \tag{4.3}$$

If a tachometer-generator constant is defined as

$$K_\omega = K_g \frac{R_s}{R_a} \tag{4.4}$$

then a "tachometer" output can be expressed as

$$K_\omega\ \omega = \frac{R_a + R_s}{R_a} E_t - E_o \tag{4.5}$$

This voltage may be derived simply as shown in figure 4.1 providing the coefficient of E_t can be accurately set.

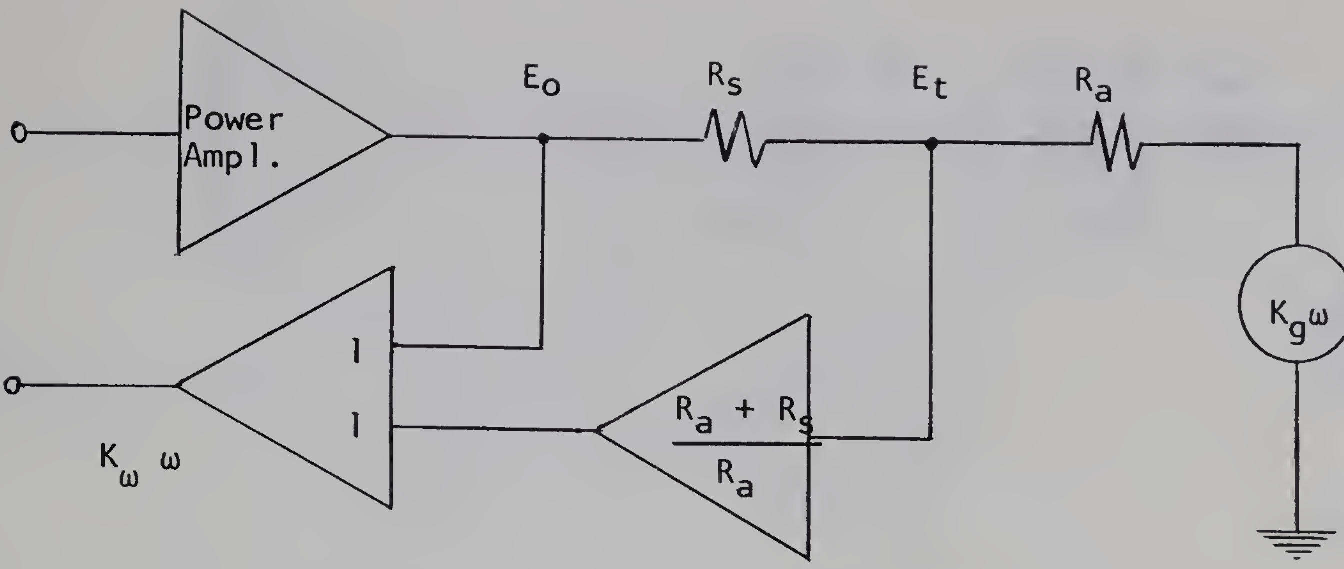

Figure 4.1 Derivation of a Rate Signal by Subtraction Method

For this work the subtraction method will be used for the unmodified motor. Its armature resistance was determined as 0.56 ohms in Section 3.3. Since the power amplifier cannot be loaded with less than 1.04 ohms it is fortunately a simple matter to let $R_s = R_a = 0.56$ ohms. For this case, equation 4.5 becomes

$$K_\omega \omega = 2 E_t - E_o \tag{4.6}$$

This selection of convenience explains why the value of $R_s = .56$ was used throughout the experimental tests. It must be remembered that use of a series resistance higher than necessary vastly degrades overall performance by increasing the block's time constant, and decreasing its gain constant. It would actually be most desireable to use a value of .48Ω.

The major problem with the subtraction method is that a truly linear characteristic cannot be obtained due to the brush contact voltage drop and its somewhat unreliable dependence on armature current. Consider the network shown in figure 4.2.

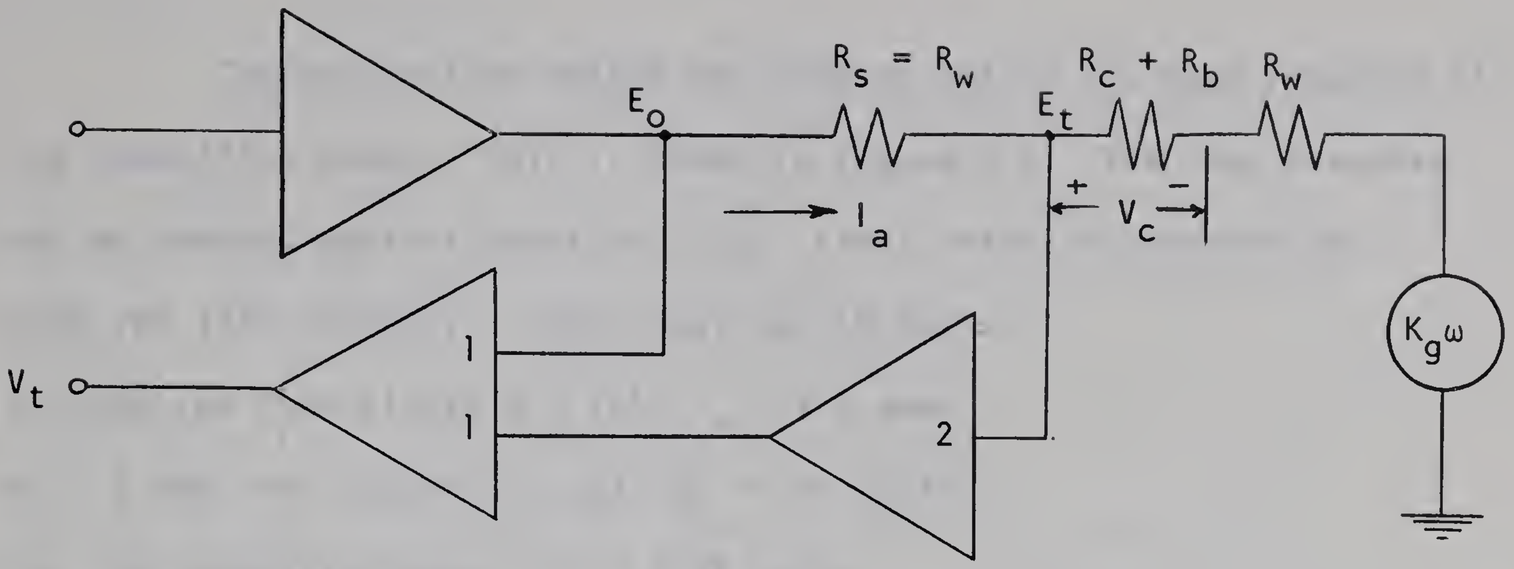

Figure 4.2 Error in Subtraction Method

The actual output is given by

$$V_t = K_g\omega + V_c(I_a) \tag{4.7}$$

Based on the curves of figure 3.5, the actual characteristic for the subtraction method - for static values of speed - is as shown in figure 4.3.

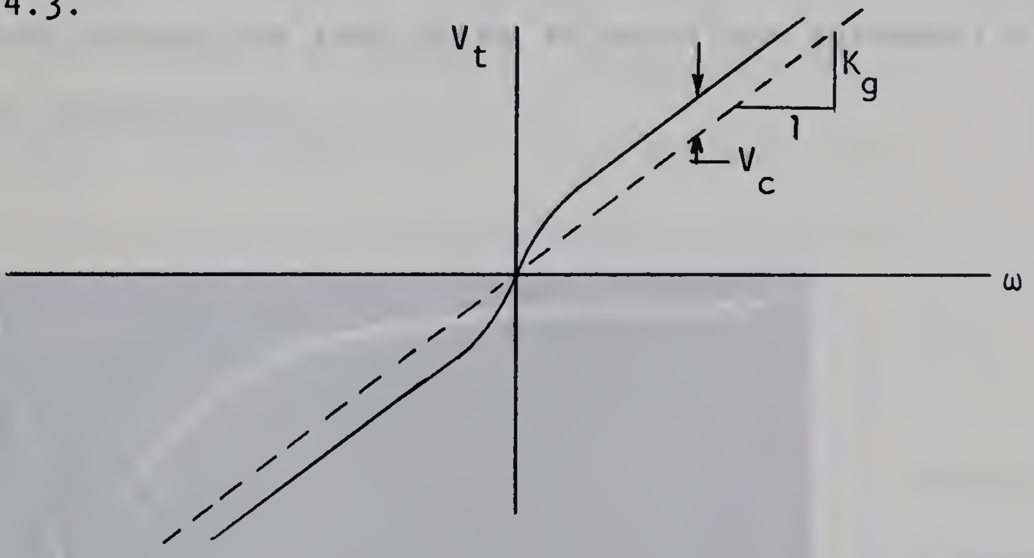

Figure 4.3 Subtraction Method Static Characteristic

This problem becomes a most serious one when it is realized that current is proportional to instantaneous torque - inertial and frictional - so that in cases of rapid current changes, the "transient" curves $V_c(I_a)$ of figure 2.5 would be followed. In underdamped step responses, it will be shown in Chapter 5 that current and velocity may be of different sign at different times thus further degenerating the situation. One possible method of compensating for $V_c(I_a)$ will be suggested in Chapter 6.

The subtraction method was used to obtain the step response of the unmodified motor. This is shown in figure 4.4. The step response can be checked against equation 2.34. Final velocity measured was 3000 rpm (314 rad/sec). Step input was 18 volts.

At 3000 rpm from figure 3.7 (c), $I_a \simeq 1.5$ amps

At 1.5 amp from figure 3.5 (a), $V_c \simeq .47$ volts

For the unmodified motor, $E_f \simeq 0.43$ volts.

Substituting these values

$$\omega_f = \frac{E - (V_c + E_f)}{K_g + K_d R_t / K_T} = 18.55\ (18 - .9) = 317 \text{ rad/sec}$$

From figure 4.4,

$$\tau_m \simeq 55 \text{ msec} \pm 5 \text{ msec}$$

The observed values are seen to be in excellent agreement with those determined theoretically.

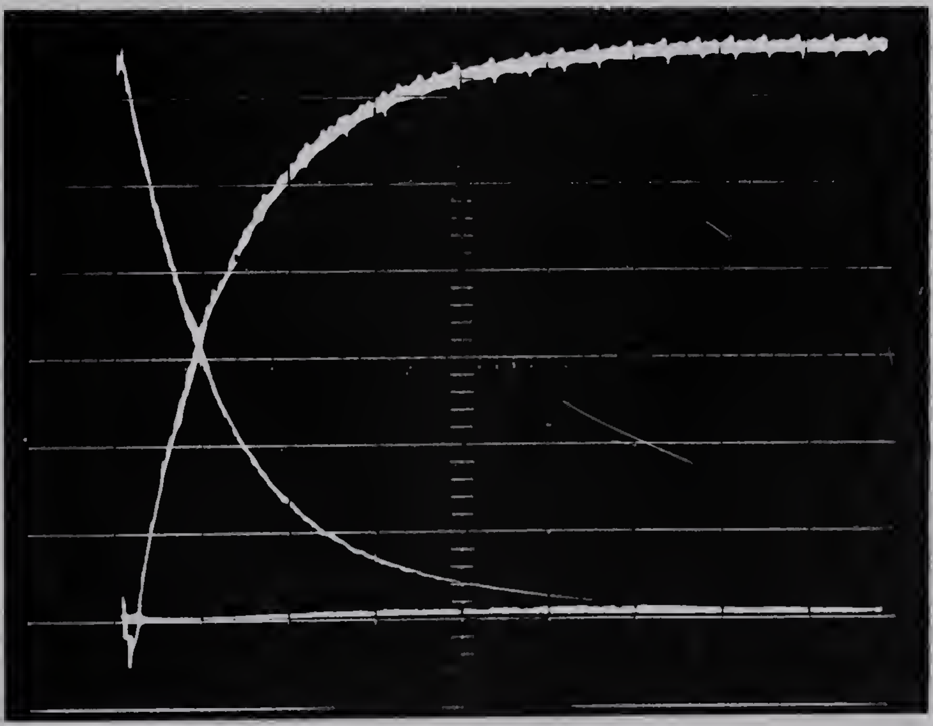

1 volt/div. vertical

50 msec./div. horiz.

Figure 4.4 Step Response by Subtraction Method

4.3 AN A.C. SPEEDOMETER

The quality of the D.C. voltage generated by the printed motor suggests that the same principles could be used if it were possible to add a second winding similar to the printed armature itself. It would not be possible to add a disc-like winding in the longitudinal field which turns the printed armature since the gap between the pole faces and the flux return plate is very narrow (intentionally) as can be seen in figure 4.11. There is, however, sufficient room to add a coil in the radial field, that is, within the magnet structure. As a prelude to describing the winding which was ultimately used, a description of a simple A.C. winding using this field will be given.

Figure 4.6 shows the construction of the winding. Both the amplitude and frequency of the A.C. voltage generated are proportional to shaft speed. Its operation is very straightforward. If one imagines each vertical section of the winding in front of a magnet pole, it is easy to see that the radial components of the magnetic field induce currents in these sectors upward and downward alternately each 45°. An alternating current thus flows throughout the winding and is brought out of the motor via brushes connected as in 4.6(c). For any such winding the frequency is four cycles per revolution or 66.67 Hz. per Krpm.

The amplitude of the derived voltage is of course only proportional to speed and cannot be rectified in any manner to provide an indication of direction. The particular winding tested yielded 175 mv. per Krpm. Although of no use for rate feedback in the positional system, it did show the feasibility of using the radial field for an added tachometer-generator.

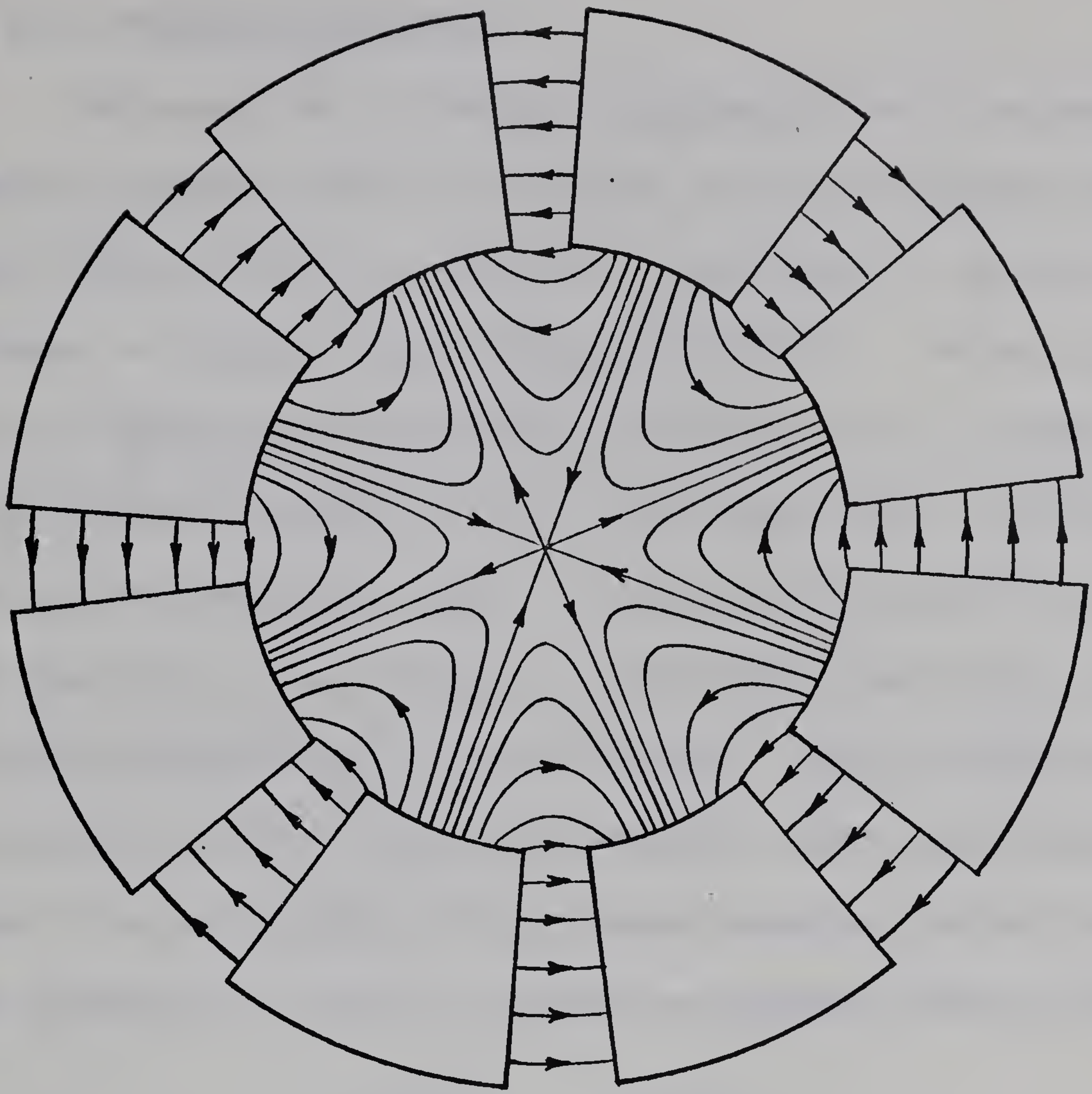

Figure 4.5 Radial Magnetic Field

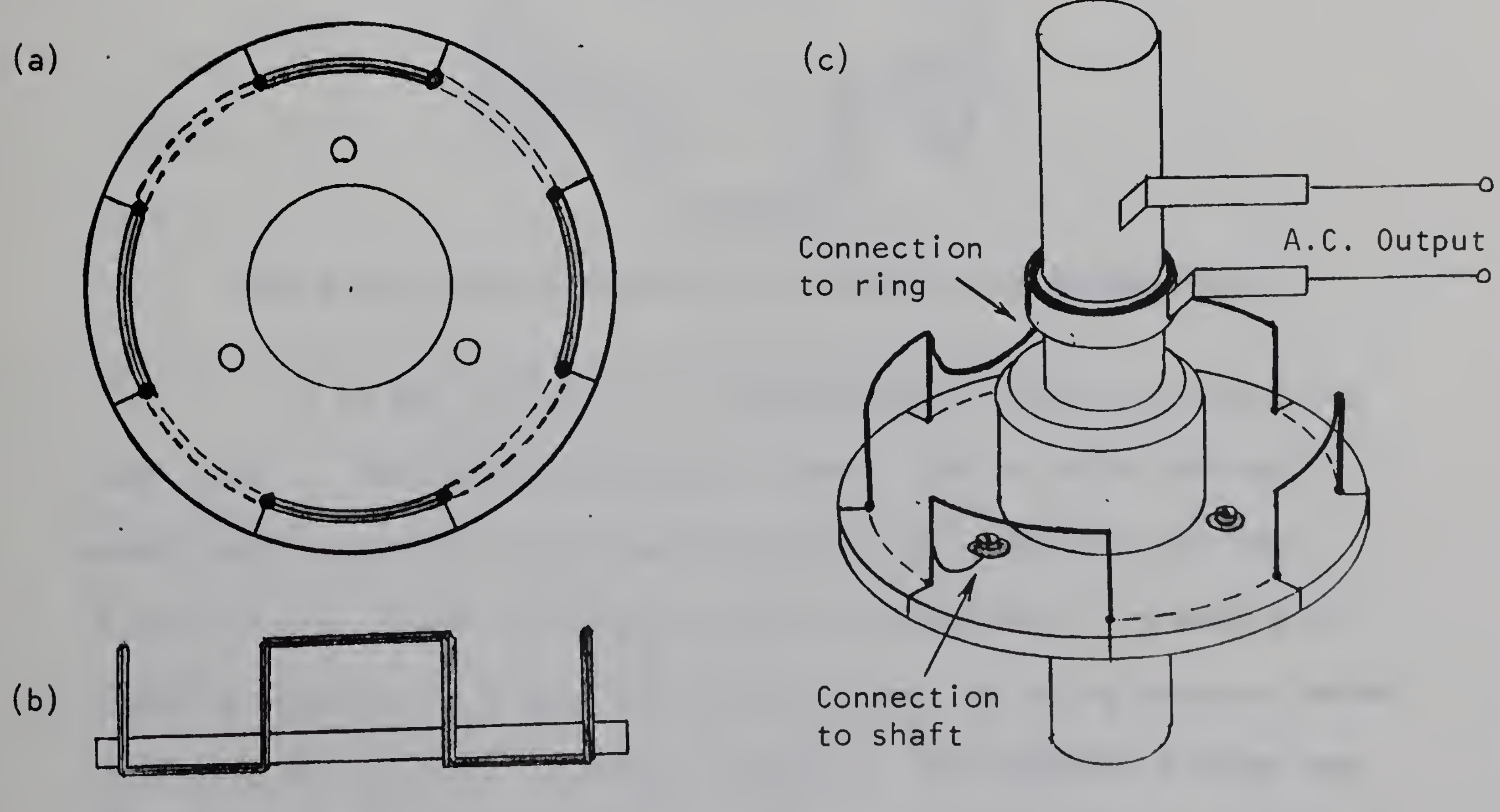
(a)
(b)
(c)
Connection to ring
A.C. Output
Connection to shaft

Figure 4.6 A.C. Speedometer Winding

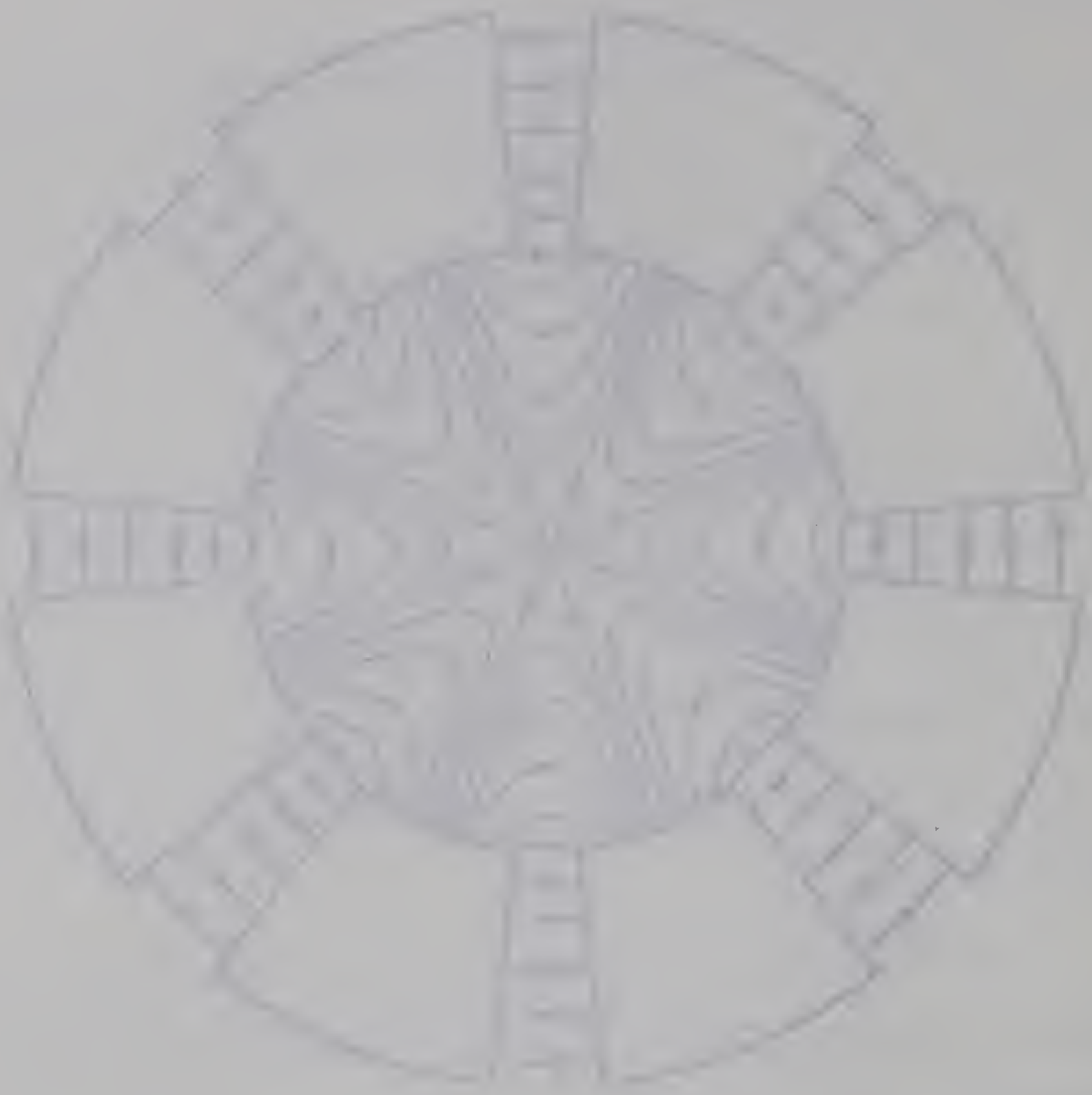

[illegible]

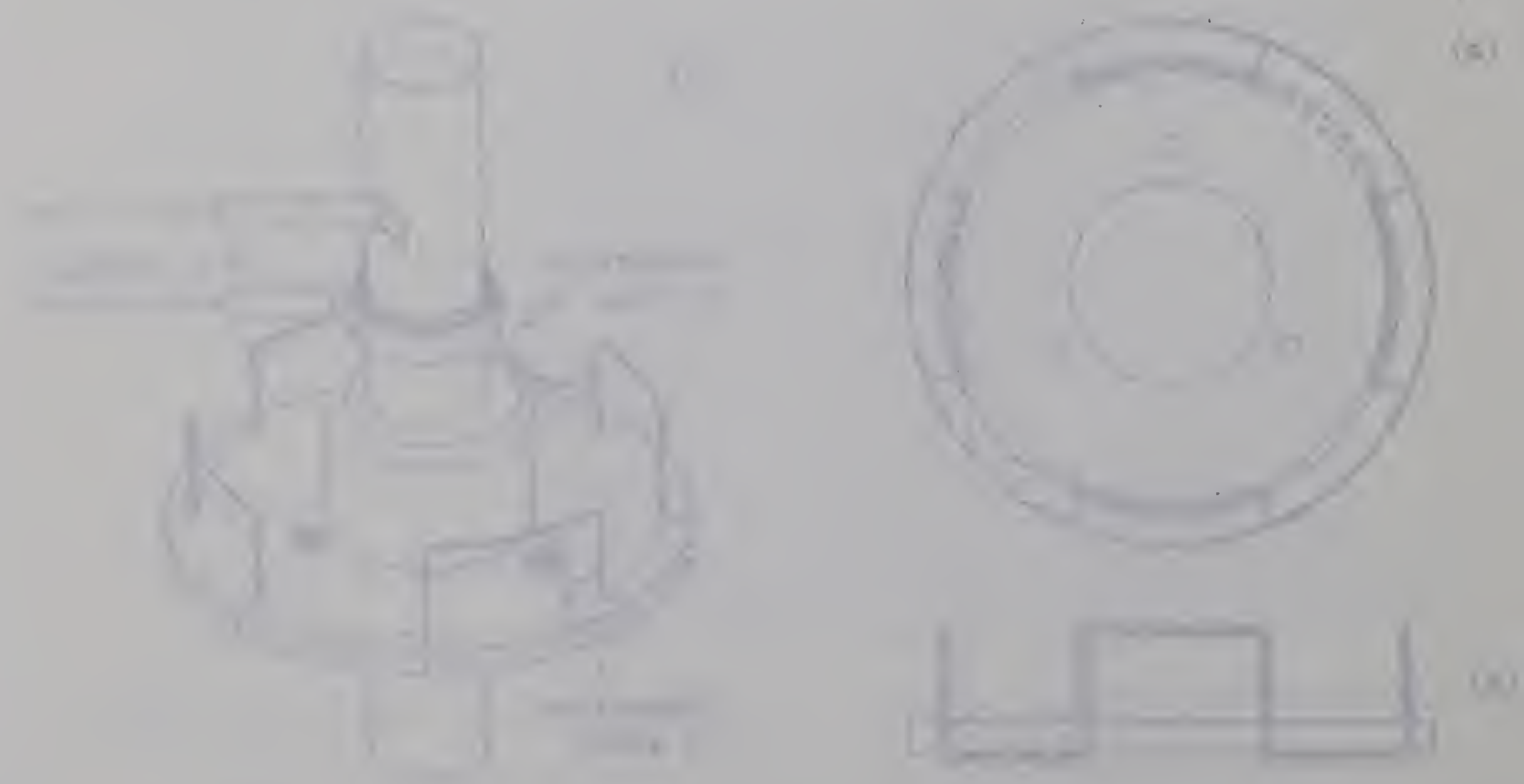
(a)
(b)

[illegible]

4.4 A D.C. TACHOMETER-GENERATOR

The basic idea of the A.C. speedometer may be extended. If the vertical sectors could be shifted by one wire thickness each complete revolution until a cylinder of two layers of vertical sectors were formed, a complete wave winding would result. The ends could be brought out by two brushes as before to provide an A.C. voltage, or could be connected together to form a continuous coil. Two brushes bearing against the outer layer, if placed at 45° or 135° in the main axis of the field (i.e. in front of a pole face) would then yield a D.C. voltage proportional to shaft velocity. The principle would then be exactly that of the printed armature itself when acting as a generator. As in the case of the printed armature, the coil acts as its own commutator. Figure 4.7 shows two complete turns of such a coil.

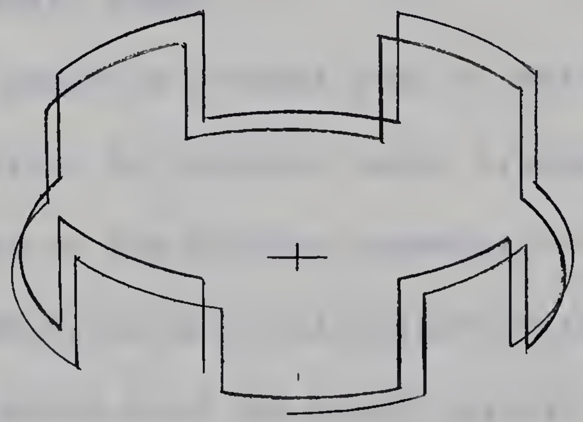

Figure 4.7 Wave Winding For Utilization of Radial Field

It is not difficult to imagine the problem of constructing such a coil. Only two windings are shown. Two or three hundred would vastly clutter the top and bottom of the resulting cylinder. A much simpler scheme of construction was conceived. The same principle is used but in a less efficient manner. By using angular rather than vertical sectors, no clutter results. The pick-off brushes may then be placed between the magnet poles. One turn of such a coil is shown in figure 4.8.

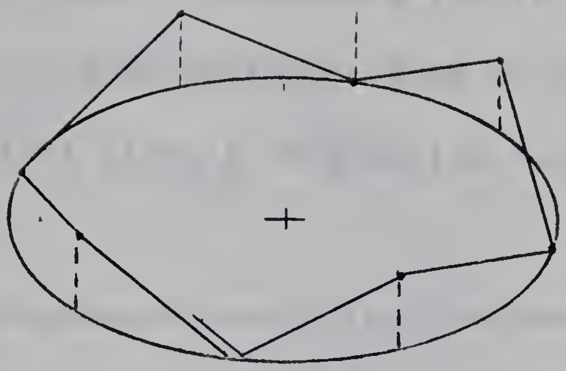

Figure 4.8 Construction Principle of D.C. Tachometer

The design and construction details of the added winding D.C. tachometer-generator which was used is shown in figure 4.10. The wave winding has about four hundred segments angled at about 45° to the shaft axis. It was hand-wound on a thin lightweight polystyrene cylinder. The windings were impregnated with an insulating varnish and the outer surface was smoothed and exposed by high-speed polishing with very fine emery paper.

The small graphite brushes bear directly on the outer surface in a manner similar to the main motor brushes. They are similarly set at the same angle as the winding segments for most efficient "commutation". Brush friction is minimized by the use of very fine compression springs which hold the brush against the coil. Brush holders are of brass insulated with heat-shrinkable tubing and epoxy cemented in place 45° apart (between two magnet poles).

The disc on which the coil is mounted is also of polystyrene and is shaped to fit the hyperboloidical interior of the coil. It is drilled and bolted to the back of the aluminum disc which secures the printed armature as shown in figure 4.11.

The coil is of #24 copper wire. Its weight is 22.5 gms. The moment of inertia is an almost insignificant addition to total rotor inertia. Electrical resistance was measured as 10.5 ohms.

When installed it was found to produce a fairly low-ripple, highly reliable D.C. output of 0.96 volts per Krpm or 91.4×10^{-4} volts per rad/sec. Its equivalent circuit (neglecting inductive effects) is as shown in figure 4.9.

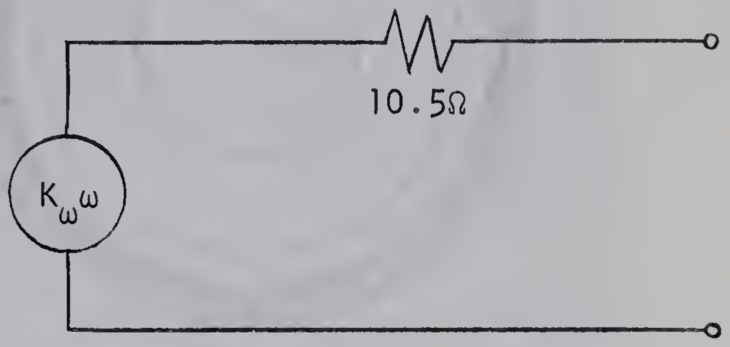

Figure 4.9 Tachometer-Generator Equivalent Circuit

The tachometer-generator was used to measure the motor frequency response. The corner frequency was determined as 1.25 Hz. ± 0.20 Hz. The time constant can thus be found ($R_s = .50\Omega$)

$$\tau_m = (2\pi \times 1.25)^{-1} = 0.127 \text{ sec} \pm .02 \text{ sec}$$

The velocity step response was also observed using the tachometer output and is shown in figure 4.12.

The result can be checked against equation 2.34.

Final velocity measured was 4620 rpm (485 rad/sec).

Step input was 19.7 volts.

At 4620 rpm from figure 3.7 (d), $I_a \simeq 1.6$ amps

At 1.6 amps from figure 3.5 (c), $V_c \simeq .85$ volts

For the modified motor (loaded), $E_f \simeq .50$ volts

thus $$\omega_f = \frac{E - (V_c + E_f)}{K_g + \frac{K_d R_t}{K_T}} = 26.3(18.4) \simeq 485 \text{ rad/sec}$$

From figure 4.12, $\tau_m \simeq .13$ sec ± .01 sec

Agreement between predicted and observed values is excellent.

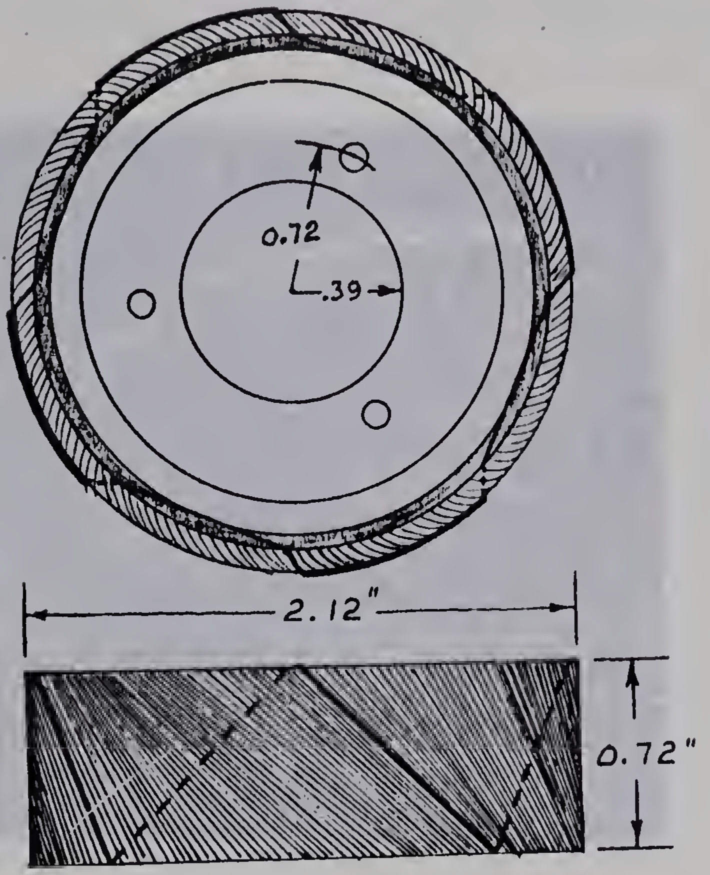
0.72
.39
2.12"
0.72"

Figure 4.10 D.C. Tachometer-Generator Winding

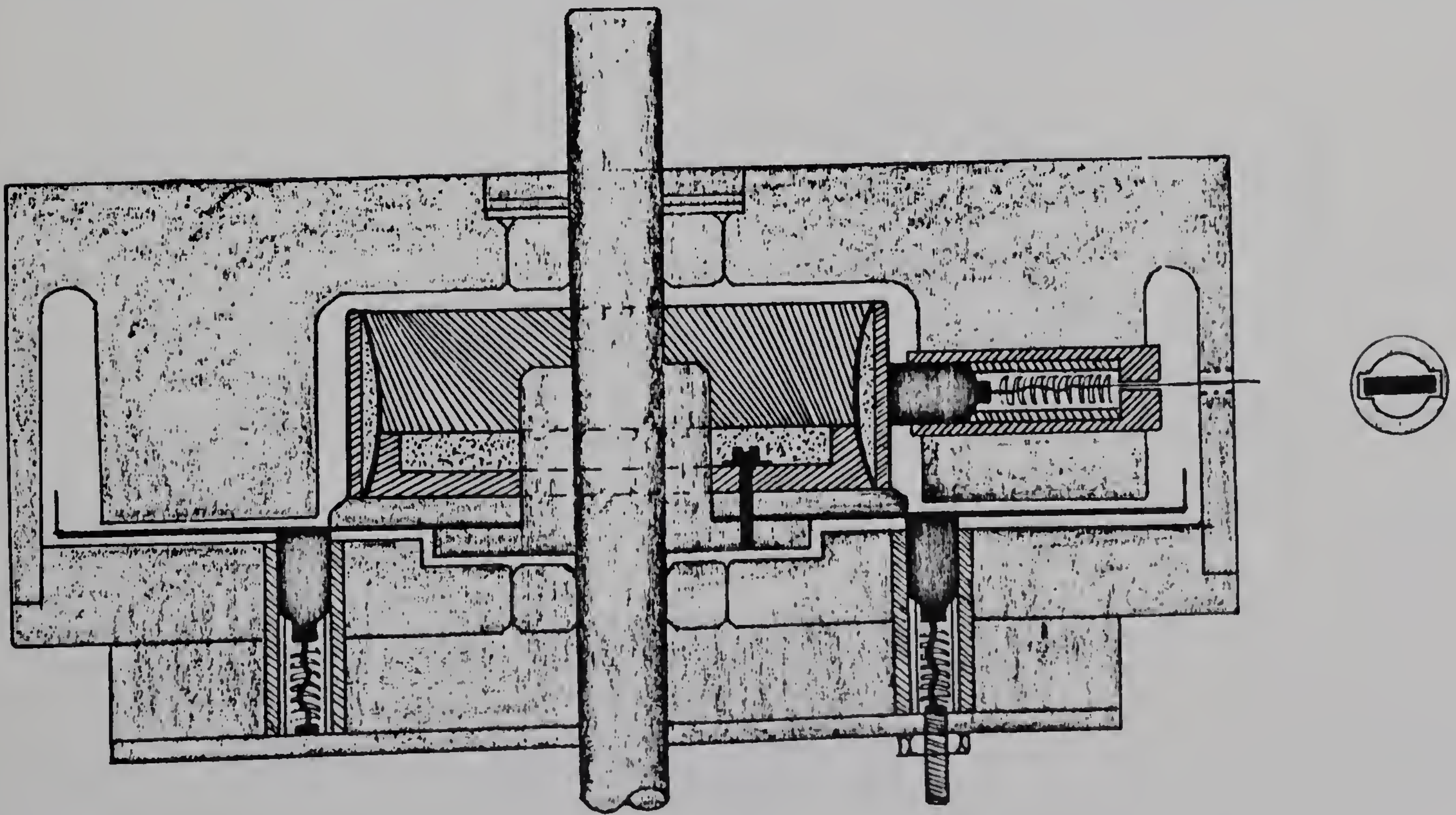

Figure 4.11 Cross Section of Modified Motor

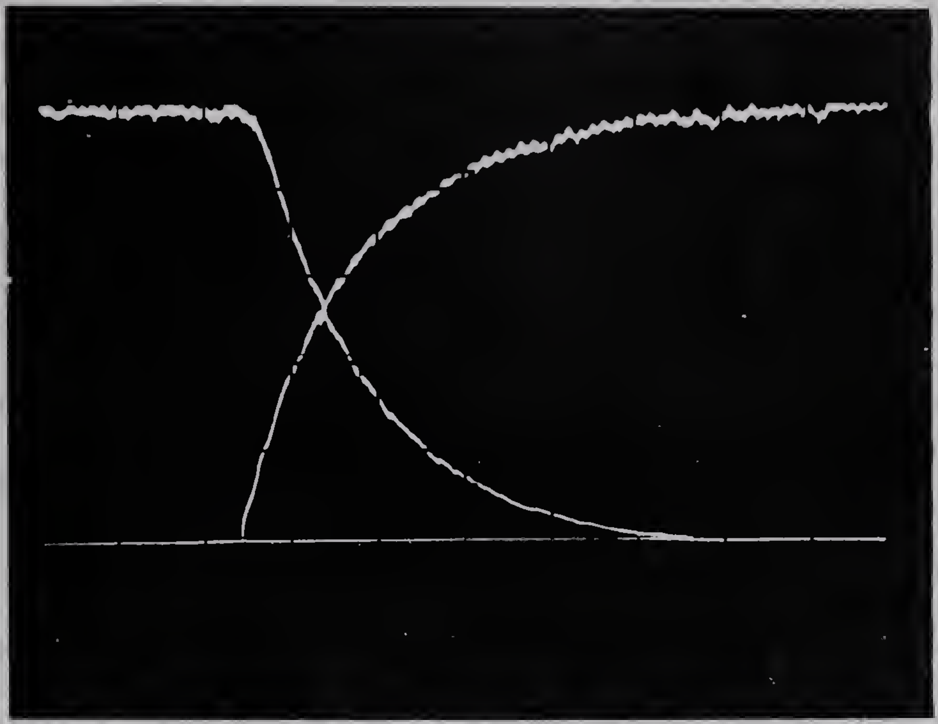

.1 volt/div. vertical

.1 sec./div. horizontal

Figure 4.12 Step Response of Modified Motor Using Tachometer-Generator Output

[illegible]

[illegible]

[illegible]

[illegible]

CHAPTER FIVE

BASIC LINEAR POSITIONAL CONTROL SYSTEM

5.1 INTRODUCTION

Now that the motor constants are known and a rate signal is available, the operation of a basic linear positional control system will be investigated. The system is called linear in the respect that the amplifiers will not be allowed to undergo saturation or limiting over the desired range of increments. The dead-zone non-linearity will be considered.

Normalization of time will be introduced to facilitate the phase-plane method of analysis which will be used in following sections. The block diagram of the basic system is shown in figure 5.1.

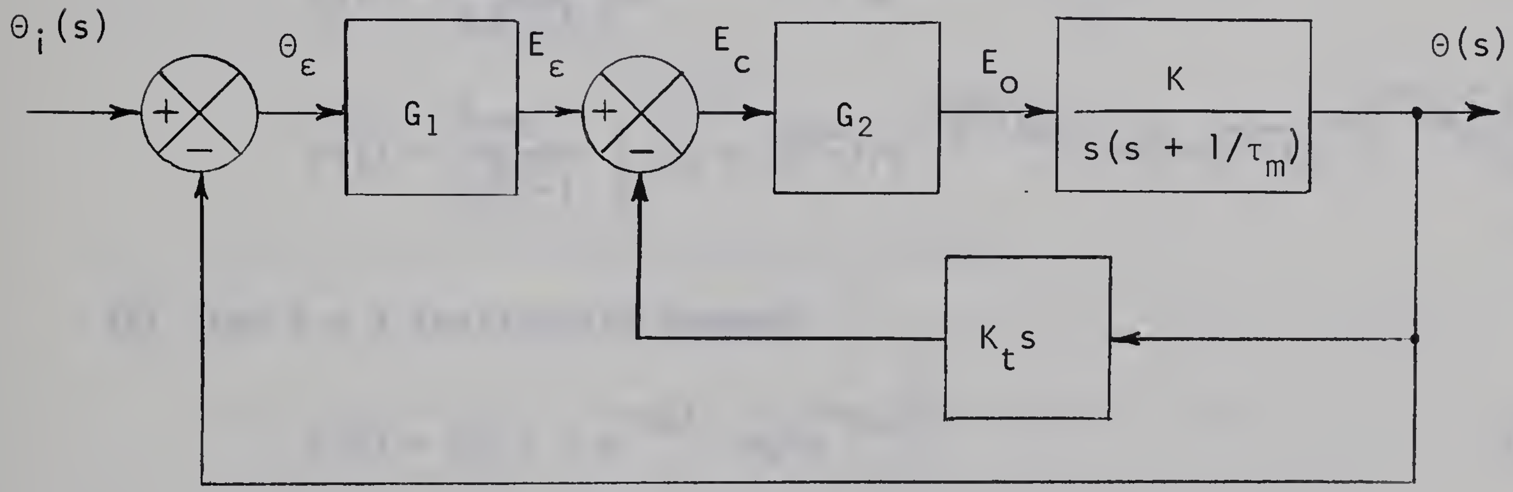

Figure 5.1 Block Diagram of Basic Linear Positional System

5.2 TRANSIENT ANALYSIS

The transfer function for the familiar system is

$$\frac{\Theta(s)}{\Theta_i(s)} = \frac{KG_1G_2}{s^2 + s(1/\tau_m + KK_tG_2) + KG_1G_2} \tag{5.1}$$

which is of the form

$$G(s) = \frac{\omega_n^2}{s^2 + 2\xi\omega_n s + \omega_n^2} \tag{5.2}$$

where:

$$\omega_n = \sqrt{\frac{K_T G_1 G_2}{J_t R_t}} \tag{5.3}$$

and

$$\xi = \frac{R_t K_d + K_T(K_t G_2 + K_g)}{2\sqrt{J_t R_t K_t G_1 G_2}} \tag{5.4}$$

The step response is found by letting

$$\Theta_i(s) = \Theta_i/s \tag{5.5}$$

then

$$\Theta(s) = \frac{\omega_n{}^2\Theta_i}{s(s^2 + 2\xi\omega_n s + \omega_n{}^2)} \tag{5.6}$$

Solutions are found from the inverse Laplace Transform

(a) For $\xi>1$ (overdamped)

$$\Theta(t) = \Theta_i + \frac{\Theta_i}{2\sqrt{\xi^2-1}}\left[\frac{e^{-(\xi + \sqrt{\xi^2-1})\omega_n t}}{\xi + \sqrt{\xi^2-1}} - \frac{e^{-(\xi - \sqrt{\xi^2-1})\omega_n t}}{\xi - \sqrt{\xi^2-1}}\right] \tag{5.7}$$

$$\dot{\Theta}(t) = \frac{\Theta_i\omega_n}{2\sqrt{\xi^2-1}}\left[e^{\sqrt{\xi^2-1}\,\omega_n t} - e^{-\sqrt{\xi^2-1}\,\omega_n t}\right]e^{-\xi\omega_n t} \tag{5.8}$$

$$\ddot{\Theta}(t) = \frac{\Theta_i\omega_n{}^2}{2\sqrt{\xi^2-1}}\left[(\xi + \sqrt{\xi^2-1})e^{-\sqrt{\xi^2-1}\,\omega_n t} - (\xi^2 - \sqrt{\xi^2-1})e^{\sqrt{\xi^2-1}\,\omega_n t}\right]e^{-\xi\omega_n t} \tag{5.9}$$

(b) For $\xi = 1$ (critically damped)

$$\Theta(t) = \Theta_i\left[1 - e^{-\omega_n t} - \omega_n t e^{-\omega_n t}\right] \tag{5.10}$$

$$\dot{\Theta}(t) = \Theta_i\omega_n{}^2 e^{-\omega_n t}t \tag{5.11}$$

$$\ddot{\Theta}(t) = \Theta_i\omega_n{}^2 e^{-\omega_n t}(1 - \omega_n t) \tag{5.12}$$

(c) $\xi<1$ (underdamped)

$$\Theta(t) = \Theta_i - \frac{\Theta_i e^{-\xi\omega_n t}}{\sqrt{1-\xi^2}}\,\mathrm{SIN}(\omega_n\sqrt{1-\xi^2}\,t + \phi) \tag{5.13}$$

where $\phi = \mathrm{COS}^{-1}\,\xi$ (5.14)

$$\dot{\Theta}(t) = \frac{\Theta_i\omega_n}{\sqrt{1-\xi^2}}\, e^{-\xi\omega_n t}\ \mathrm{SIN}(\omega_n\sqrt{1-\xi^2}\,t) \tag{5.15}$$

$$\ddot{\Theta}(t) = -\Theta_i\ \frac{\omega_n{}^2}{\sqrt{1-\xi^2}}\, e^{-\xi\omega_n t}\ \mathrm{SIN}(\omega_n\sqrt{1-\xi^2}\,t - \phi) \tag{5.16}$$

The underdamped response of equation 5.13 is generally of more interest since a few small damped oscillations are generally preferable to a sluggish overdamped response. Some quantities of interest for this case can be found.

Damped frequency of oscillation:

$$\omega_d = \omega_n\sqrt{1-\xi^2} \tag{5.17}$$

Peak time (time to peak of first overshoot):

$$t_p = \frac{\pi}{\omega_n\sqrt{1-\xi^2}} \tag{5.18}$$

Amplitude of first overshoot:

$$\Theta_p = \Theta_i\left[1 + e^{-\frac{\xi\pi}{\sqrt{1-\xi^2}}}\right] \tag{5.19}$$

5.3 EFFECT OF NON-VISCOUS FRICTIONAL TORQUE

To obtain a more complete picture of the system response, frictional torque must be considered. As shown in figure 2.10, it may be represented as a voltage input to the motor block diagram.

$$\Theta(s) = \frac{\omega_n{}^2\left[\Theta_i(s) - \dfrac{E_f(s)}{G_1G_2}\right]}{s^2 + 2\xi\omega_n s + \omega_n{}^2} \tag{5.20}$$

The steady-state output is given by

$$\Theta(t)_{ss} = \lim_{s\to 0} s\left[\Theta_i(s) - \frac{E_f(s)}{G_1G_2}\right] \tag{5.21}$$

It can be seen that if the second term is significant, a large steady-state error may result. Voltage restraints on the product G_1G_2 will be

seen to eliminate the possibility of reducing this error by increasing the forward path gain of the basic system if linear operation is to be maintained. To analyze the system response with frictional torque included, an equivalent frictional input may be defined

$$\Theta_f(s) = \frac{E_f(s)}{G_1G_2} = \frac{T_f(s)R_t}{K_TG_1G_2} = \frac{T_f(s)}{KJ_tG_1G_2} = \frac{T_f(s)}{J_t\omega_n^2} \tag{5.22}$$

Recall that frictional torque was given by

$$T_f = |T_c|\left(\frac{\dot{\Theta}}{|\dot{\Theta}|}\right)_{\dot{\Theta}\neq 0} + |T_s|\left(\frac{E_o}{|E_o|}\right)_{\dot{\Theta}=0} \tag{5.23}$$

For the overdamped and critically damped cases, T_f does not change sign and may be considered constant. It can be assumed that

$$T_f(s) = T_c/s \tag{5.24}$$

The net equivalent step input is

$$\Theta_{i_{eq.}}(s) = \Theta_i(s) - \Theta_f(s) = \frac{\Theta_i - \Theta_f}{s} \tag{5.25}$$

In equations 5.7 and 5.10, Θ_i may be replaced by $\Theta_{i_{eq.}}$ The resulting response is shown in figure 5.2 (b).

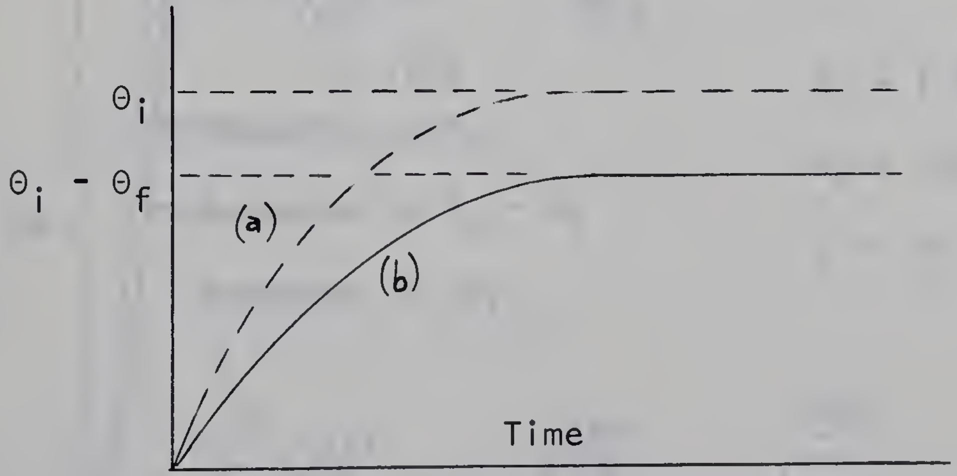

Figure 5.2 Effect of Frictional Torque on Overdamped Response

For values of ξ near unity, the steady-state error will be given by $\Theta_\varepsilon(s.s.) = T_cR_t/K_TG_1G_2$ (5.26)

For highly overdamped cases, however, where the velocity becomes very low as the final position is approached, the magnitude of the error may be somewhat greater.

For the underdamped case, the change in sign of T_c at each successive peak makes analysis a bit more difficult. The effect may be shown by considering the equivalent input as

$$\Theta_{i_{eq.}} = \frac{\Theta_i}{s} - \Theta_f\left(\frac{1}{s} - \frac{2}{s}e^{-st_p} + \frac{2}{s}e^{-2st_p} - \frac{2}{s}e^{-3st_p} + \cdots\right) \qquad (5.27)$$

The resulting time response may be found by finding the responses to $\Theta_i(s)$ and $-\Theta_f(s)$ separately, then adding, or by finding the actual equivalent input at times 0, t_p, $2t_p$, $3t_p$, etc. sequentially. The results are shown for a particular example in figure 5.3.

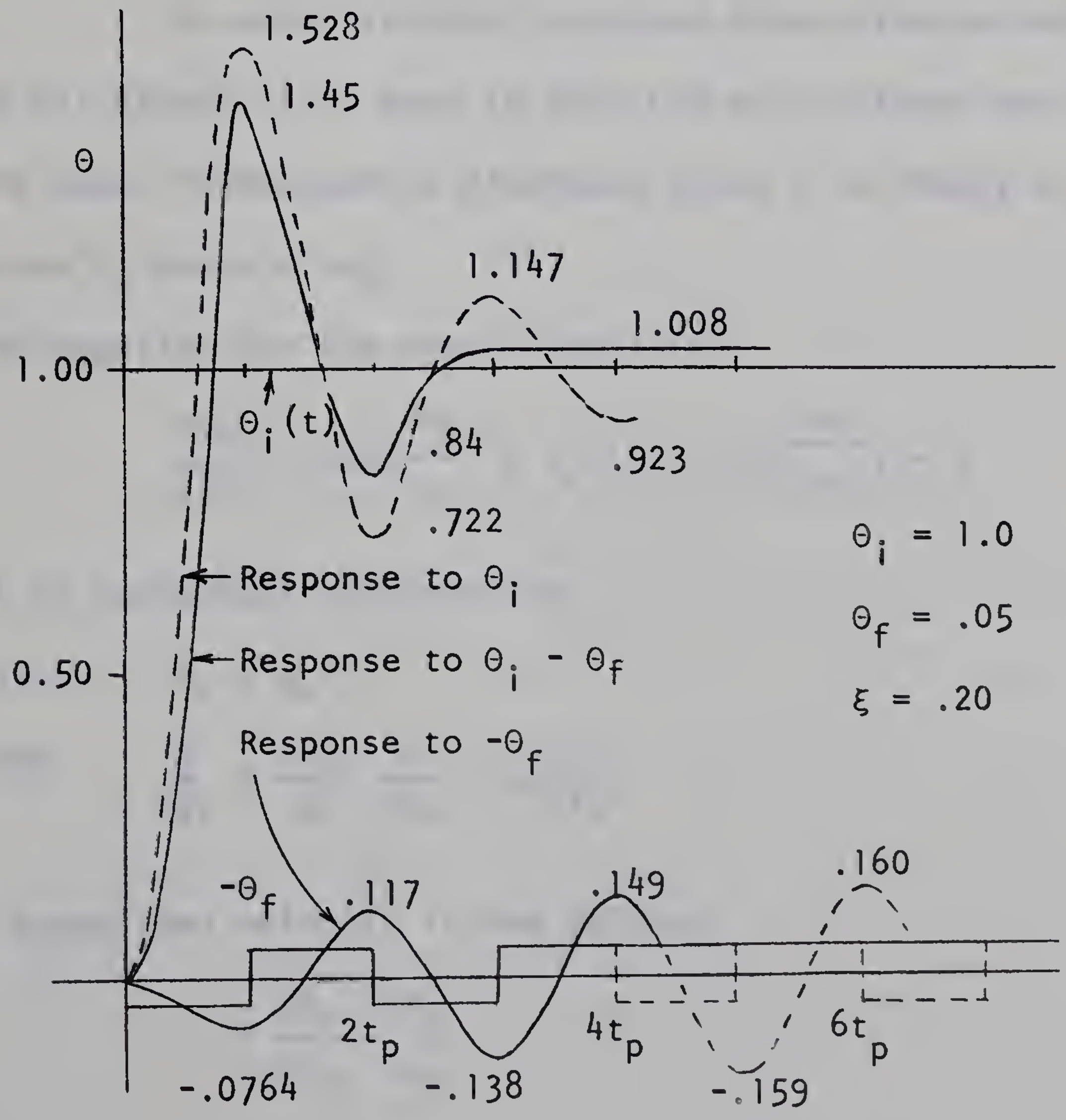

Figure 5.3 Example Showing Effect of Frictional Torque

Further insight can be gained by investigating the phase plane trajectory of the response to a step. The system may be simplified as shown in figure 5.4.

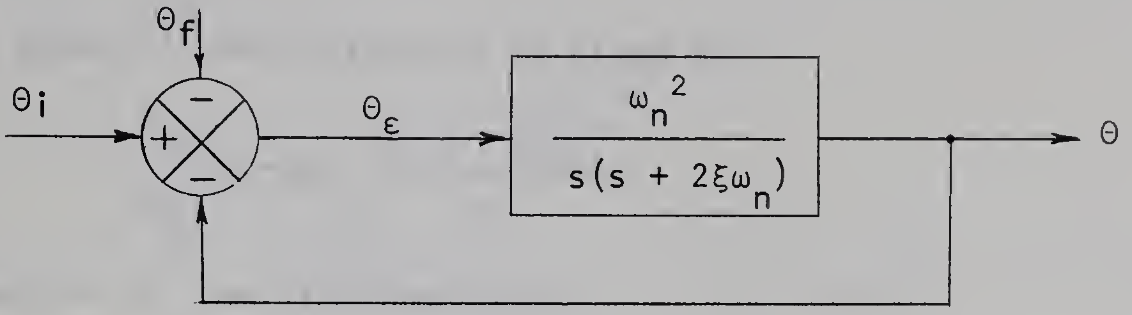

Figure 5.4 Simplified Block Diagram

The system equation is

$$\frac{d^2\Theta}{dt^2} + 2\xi\omega_n \frac{d\Theta}{dt} + \omega_n^2\Theta = \omega_n^2\left(\Theta_i - \Theta_f\left(\frac{\omega}{|\omega|}\right)\right) \qquad (5.28)$$

In order to make the phase plane diagram useful for increments of all sizes, it is best to plot the error signal and its derivative. The same information is displayed since Θ is simply a constant. (Θ_i) minus Θ_ε and $\omega = -\omega_\varepsilon$.

The equation for the error signal is

$$\frac{d^2\Theta_\varepsilon}{dt^2} + 2\xi\omega_n\frac{d\Theta_\varepsilon}{dt} + \omega_n^2\left(\Theta_\varepsilon + \Theta_f\left(\frac{\omega_\varepsilon}{|\omega_\varepsilon|}\right)\right) = 0 \qquad (5.29)$$

It is convenient to normalize.

Let $t_n = \omega_n t$ (5.30)

thus $\frac{d}{dt} = \frac{dt_n}{dt}\,\frac{d}{dt_n} = \omega_n\frac{d}{dt_n}$ (5.31)

A normalized velocity is now defined

$$\nu_\varepsilon = \frac{d\Theta_\varepsilon}{dt_n} = \frac{\omega_\varepsilon}{\omega_n} \qquad (5.32)$$

The normalized system equation becomes

$$\frac{d\nu_\varepsilon}{dt_n} + 2\,\xi\,\frac{d\Theta_\varepsilon}{dt_n} + \Theta_\varepsilon + \Theta_f\frac{\nu_\varepsilon}{|\nu_\varepsilon|} = 0 \tag{5.33}$$

The slope of the trajectory is given by

$$\frac{d\nu_\varepsilon}{d\Theta_\varepsilon} = -2\xi - \frac{\Theta_\varepsilon + \Theta_f\frac{\nu_\varepsilon}{|\nu_\varepsilon|}}{\nu_\varepsilon} \tag{5.34}$$

Equations of the isoclines are

$$\nu_\varepsilon = -\frac{\Theta_\varepsilon + \Theta_f\,\frac{\nu_\varepsilon}{|\nu_\varepsilon|}}{2\xi + \frac{d\nu_\varepsilon}{d\Theta_\varepsilon}} \tag{5.35}$$

The phase plane diagram is shown in figure 5.5 for $\xi = .2$, $\Theta_f = .05$. Trajectory slopes are indicated on the isoclines. The outer trajectory ($\Theta_i = 1.0$) is that of the former example and shows how T_f greatly reduces overshoots although this particular steady-state error is small. The trajectories for two smaller steps show how an error of up to $\pm\Theta_f$ can occur. Whenever the magnitude of Θ_ε is less than Θ_f and the velocity goes to zero (at a peak or minimum), then the torque developed by the motor is insufficient to overcome the static frictional torque and no further motion is possible. The minimum width of this friction zone is $\dfrac{2T_cR_t}{K_TG_1G_2}$ but since T_s is usually greater than T_c, the maximum width may be considerably greater. The curves of figure 5.6 illustrate the effect of varying the damping ratio.

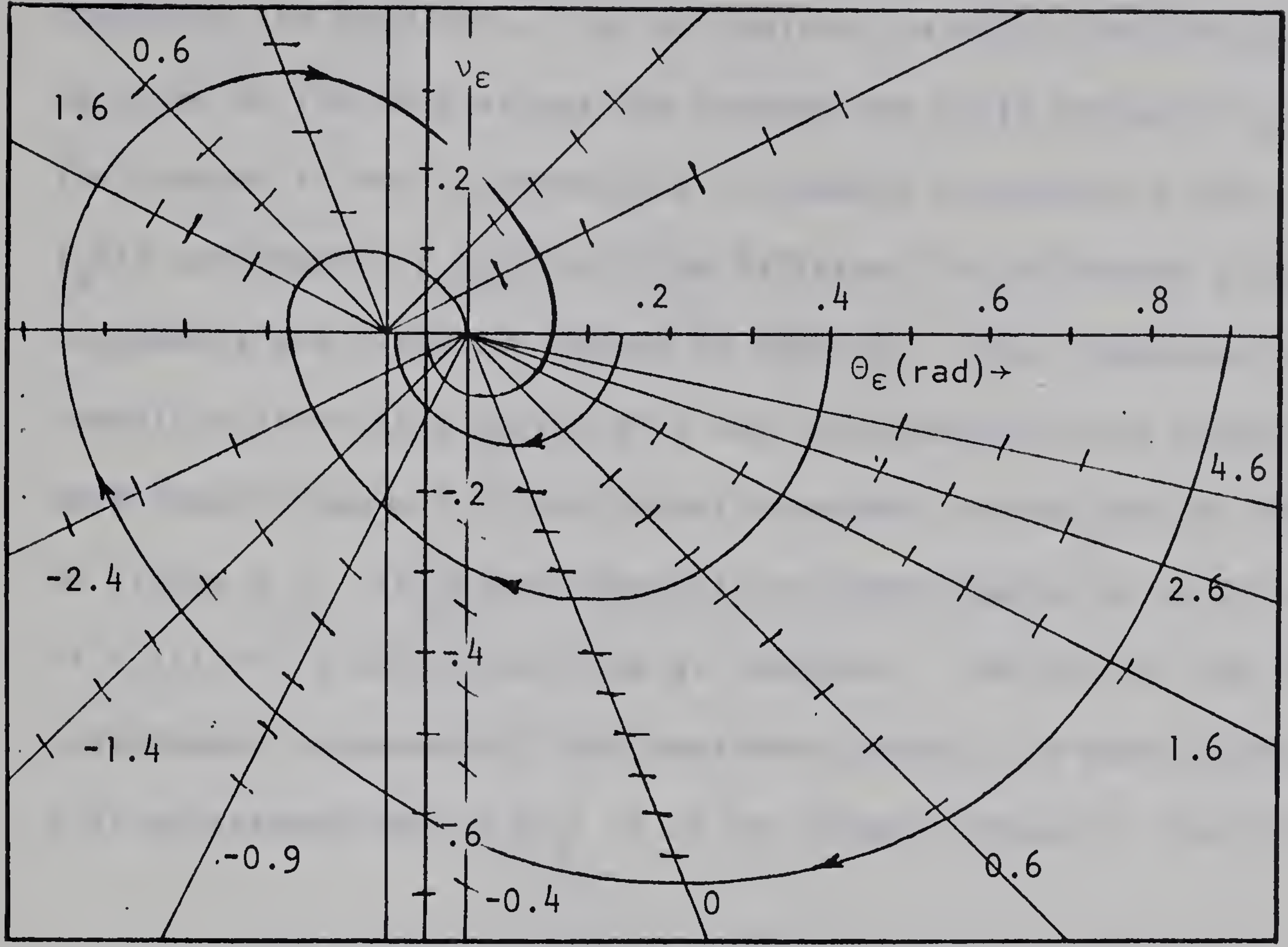

Figure 5.5 Phase Plane Trajectories For $\Theta_f = .05$ $\xi = .20$

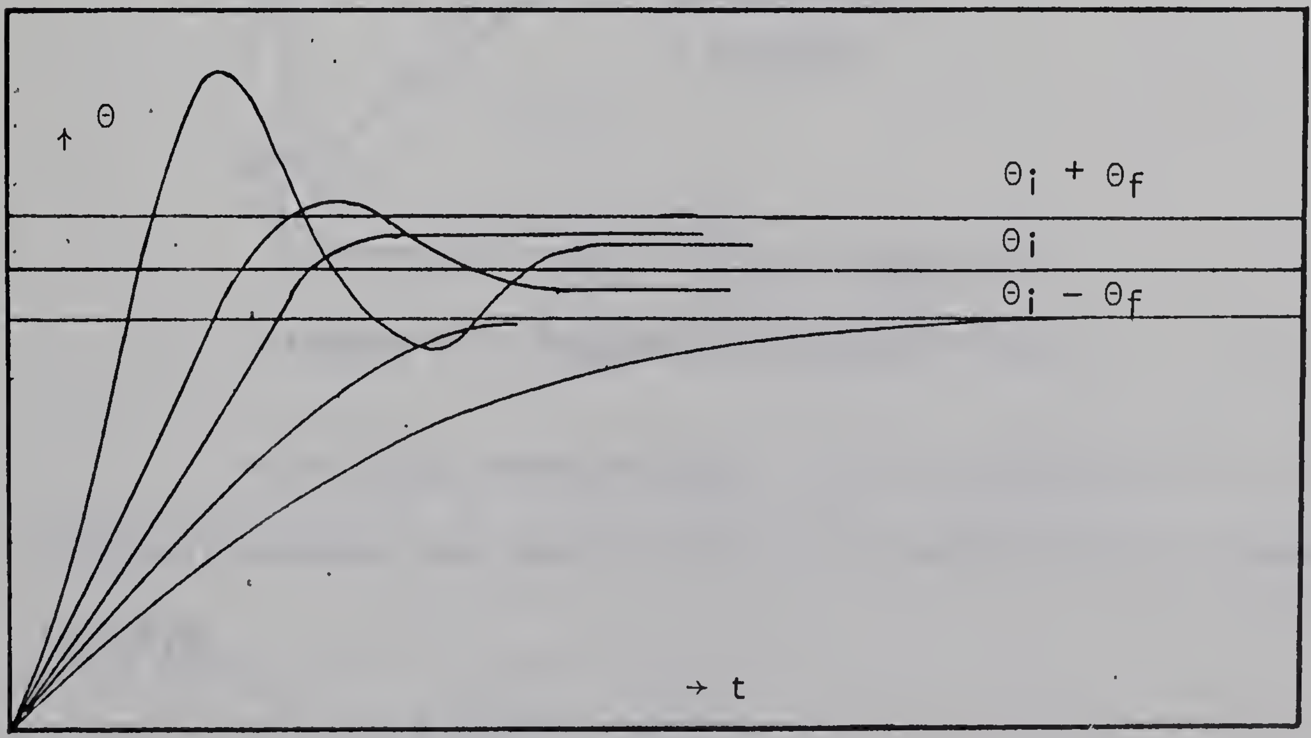

Figure 5.6 Frictional Error Zone

5.4 EFFECT OF BRUSH CONTACT VOLTAGE DROP

The inclusion of E_f accounts for less than half the error caused by the dead zone. For a complete analysis, consideration must be given to the drop across the brushes and brush contacts $V_c(I_a)$. The problem is nearly impossible to analyze accurately since $I_a(t)$ and therefore $V_c(t)$ will be different for different sizes of increments and different values of damping. Since responses are usually quite rapid, $V_c(I_a)$ will not follow equilibrium curves as were found (figure 3.5) but rather transient curves such as those of figure 2.5. It is only possible to make a guess as to the nature of $V_c(t)$ for a particular type of response. The case of the slightly underdamped response will be considered since it is most useful. It will be assumed that $V_c(I_a)$ is of the general shape of figure 5.7.

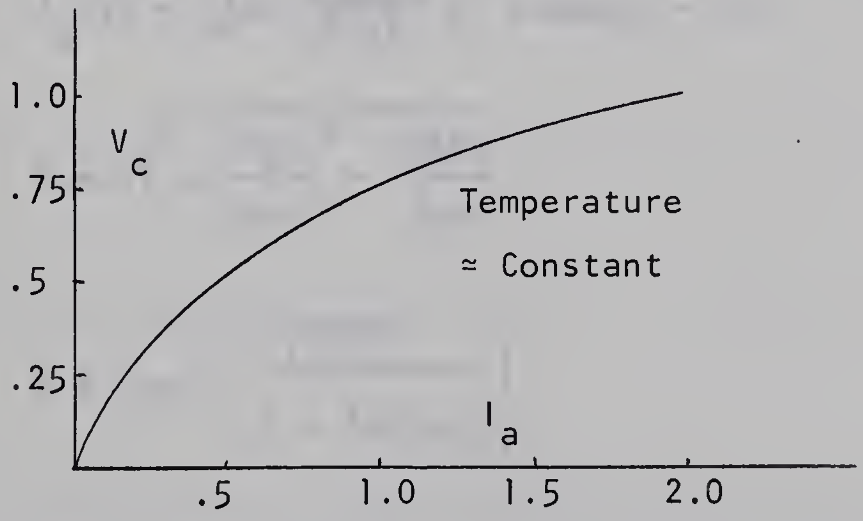

Figure 5.7 Assumed Brush-Contact Drop

First $I_a(t)$ must be found. This is possible if it is initially assumed that both E_f and V_c are negligible with respect to $\Theta_i G_1 G_2$

$$I_a(t) = \frac{1}{K_T}\left[J_t\ddot{\Theta} + K_d\dot{\Theta}\right] \tag{5.36}$$

Substituting from expressions 5.15 and 5.16

$$I_a(t) = \frac{J_t}{K_T}\left(-\frac{\Theta_i \omega_n^2}{\sqrt{1-\xi^2}} e^{-\xi\omega_n t} \mathrm{SIN}(\omega_d t - \phi)\right) + \frac{K_d}{K_T}\left(\frac{\Theta_i \omega_n}{\sqrt{1-\xi^2}} e^{-\xi\omega_n t} \mathrm{SIN}\omega_d t\right) \tag{5.37}$$

$$I_a(t) = \frac{\Theta_i J_t \omega_n^2}{K_T} \cdot \frac{e^{-\xi\omega_n t}}{\sqrt{1-\xi^2}} \cdot \left(\frac{K_d}{J_t \omega_n} \mathrm{SIN}\ \omega_d t - \mathrm{SIN}(\omega_d t - \phi)\right) \tag{5.38}$$

The first term is equal to $I_a(0)$ (by setting $t = 0$ in the expression). This can be checked in the actual system:

$$I_a(0) = \frac{E_o(0)}{R_t} = \frac{\Theta_i G_1 G_2}{R_t} = \frac{\Theta_i \omega_n^2}{K R_t} = \frac{\Theta_i J_t \omega_n^2}{K_T} \tag{5.39}$$

The expression in parentheses can be simplified further and the final expression becomes

$$I_a(t) = I_a(0) \frac{e^{-\xi\omega_n t}}{\sqrt{1-\xi^2}} B \quad \mathrm{SIN}(\omega_d t - \psi) \tag{5.40}$$

where

$$B = -\sqrt{1 + \left(\frac{K_d}{J_t \omega_n}\right)^2 - \frac{2\xi K_d}{J_t \omega_n}} \tag{5.41}$$

and

$$\psi = \mathrm{TAN}^{-1}\left(\frac{\sqrt{1-\xi^2}}{\xi - K_d/J_t\omega_n}\right) \tag{5.42}$$

The zero-crossings of $I_a(t)$ are of interest since $V_c(t)$ changes sign at these points. This will also be important when the effect of $V_c(t)$ on the subtraction method is investigated.

It is unnecessary to evaluate the zero-crossings exactly if we notice that with the values to be used, the term $K_d/J_t\omega_n << 1$, such that

$$B \simeq -1 \tag{5.43}$$

and for any practical damping ratios, say $.5 < \xi < .95$

$$\psi \simeq \mathrm{TAN}^{-1}\left(\frac{\sqrt{1-\xi^2}}{\xi}\right) = \phi \tag{5.44}$$

It is shown then, and should be intuitively obvious that the current is nearly proportional to acceleration.

$$I_a(t) \simeq -I(0)\,\frac{e^{-\xi\omega_n t}}{\sqrt{1-\xi^2}}\,\mathrm{SIN}(\omega_d t - \phi) \tag{5.45}$$

$$\simeq \frac{J_t}{K_T}\ddot{\Theta} \tag{5.46}$$

Figure 5.8 shows an estimation of $V_c(t)$ for an underdamped response. For comparison purposes, $E_f(t)$ is also shown.

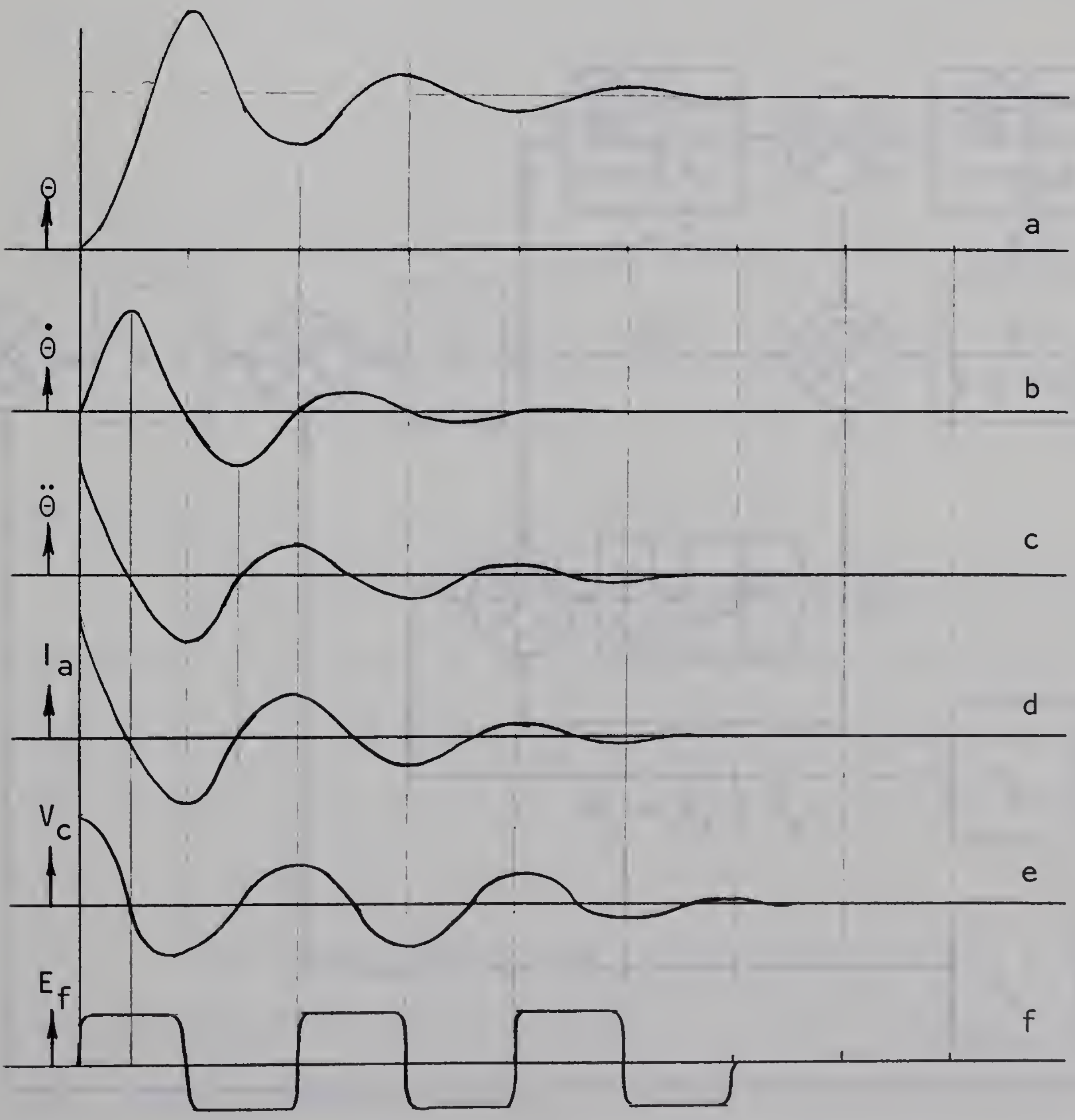

Figure 5.8 System Transient Functions

Since the magnitude of V_c depends so drastically on the size of the increment, its effect cannot be analyzed so neatly as that of E_f. Suffice it to say, that in designing for high accuracy, its existence must at least be realized.

The net equivalent opposing input during the response is the sum of V_c and E_f in figure 5.8. The problem with V_c can be essentially eliminated providing G_1G_2 can be made high enough. If the steady-state (error) value of E_o is sufficiently low, then the error current causes no appreciable V_c drop.

The effects of friction and brush contact drop may be represented as shown in the equivalent block diagram of figure 5.9.

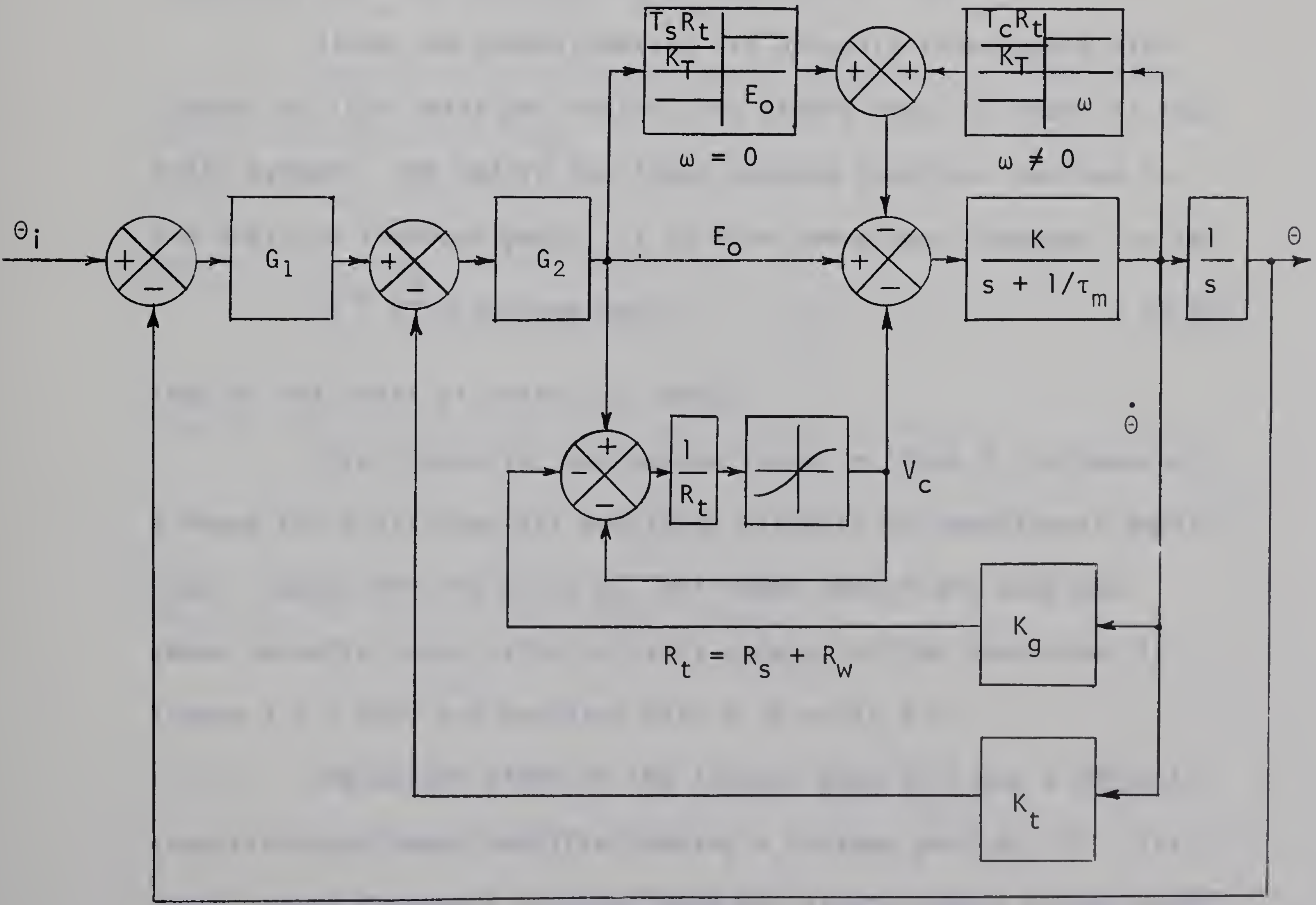
Θ_i
G_1
G_2
E_o
$\frac{T_sR_t}{K_T}$
E_o
$\omega = 0$
$\frac{T_cR_t}{K_T}$
ω
$\omega \neq 0$
$\frac{K}{s + 1/\tau_m}$
$\frac{1}{s}$
Θ
$\dot{\Theta}$
$\frac{1}{R_t}$
V_c
K_g
K_t
$R_t = R_s + R_W$
+
−

Figure 5.9 Representative Block Diagram Showing Inherent Non-Linearities

5.5 DESCRIPTION OF THE PHYSICAL SYSTEM

Two basic systems were tested:

(1) the modified motor using the added winding tachometer-generator for rate feedback;

(2) the unmodified motor using the subtraction method.

The input positional increment was set by a potentiometer of 20 KΩ while the output position was measured by a precision wire-wound servo potentiometer of 20 KΩ ± 5% with specified linearity of ± .15%. The ends of both were at either ± 15 volts D.C. such that the voltage at the wiper was 15/π volts per radian or 15/180 = 1/12 volt per degree of displacement from zero. The finite resolution of the two devices contributes slightly to system inaccuracy but this will be neglected in the analyses.

Since the potentiometers are actually transducers with "gains" of 15/π volts per radian, two blocks could be shown in the basic system: one before the input summing junction, and one in the position feedback path. It is more convenient, however, to let

$$G_1 = \frac{15}{\pi} \times \text{Voltage gain} \tag{5.47}$$

Thus G_1 has units of volts per radian.

Error detection was accomplished in block G_1 by means of a Nexus FSL-6 differential amplifier wired as an operational amplifier. Except for the block G_2, all other amplifiers used and shown hereafter were either of this type or of the type shown in figure A 4.1.They are supplied with ± 15 volts D.C.

The second block in the forward path (G_2) was a 600-watt transistorized power amplifier having a voltage gain of -10. Its upper corner frequency of 1KHz. does not significantly affect operation. A brief description of the power amplifier is given in

Appendix 2. It is fed by a ± 30-volt D.C. supply which is described in Appendix 3.

The output voltage E_o, of the power amplifier is limited by saturation to approximately ± 25 volts. Since $G_2 = -10$, if the system is to be linear over the entire range of step increments $(0 < |\Theta_i| < \pi)$, then the magnitude of the output of G_1 must be less than 2.5 volts. The maximum input voltage to the first amplifier is ± 15 so that its maximum voltage gain is 2.5/15 or 0.167. For the basic linear system, then, the transfer function of the first block is

$$G_1 = -\frac{15}{\pi} \times \frac{2.5}{15} = -.797\ \frac{\text{volts}}{\text{rad.}} \tag{5.48}$$

The physical configurations of the two basic systems tested are shown in figures 5.10 and 5.11.

Based on the values obtained in Chapter 3, system parameters are now calculated.

System 1 (modified motor):

Natural frequency of oscillation

$$\omega_n = \sqrt{KG_1G_2} \simeq \sqrt{200(7.97)} \simeq 40\ \frac{\text{rad}}{\text{sec}} \simeq 6.4\ \text{Hz.} \tag{5.49}$$

Possible steady-state error due to Coulomb friction

$$\Theta_\varepsilon(\text{s.s.}) = \frac{E_f}{G_1G_2} \simeq \pm\ \frac{.5}{7.97}\ \pm .063\ \text{rad} = \pm 3.6^\circ \tag{5.50}$$

Peak time for highly underdamped response

$$t_p = \frac{\pi}{\omega_n\sqrt{1-\xi^2}} \simeq \frac{\pi}{\omega_n} \simeq \frac{\pi}{40} \simeq 78.5\ \text{msec} \tag{5.51}$$

System 2 (unmodified motor):

$$\omega_n \simeq 50\ \text{rad/sec} \simeq 7.8\ \text{Hz.} \tag{5.52}$$

$$\Theta_\varepsilon(\text{s.s.}) \simeq \pm .054\ \text{rad} \simeq \pm 3.1^\circ \tag{5.53}$$

$$t_p \simeq \pi/50 = 63\ \text{msec} \tag{5.54}$$

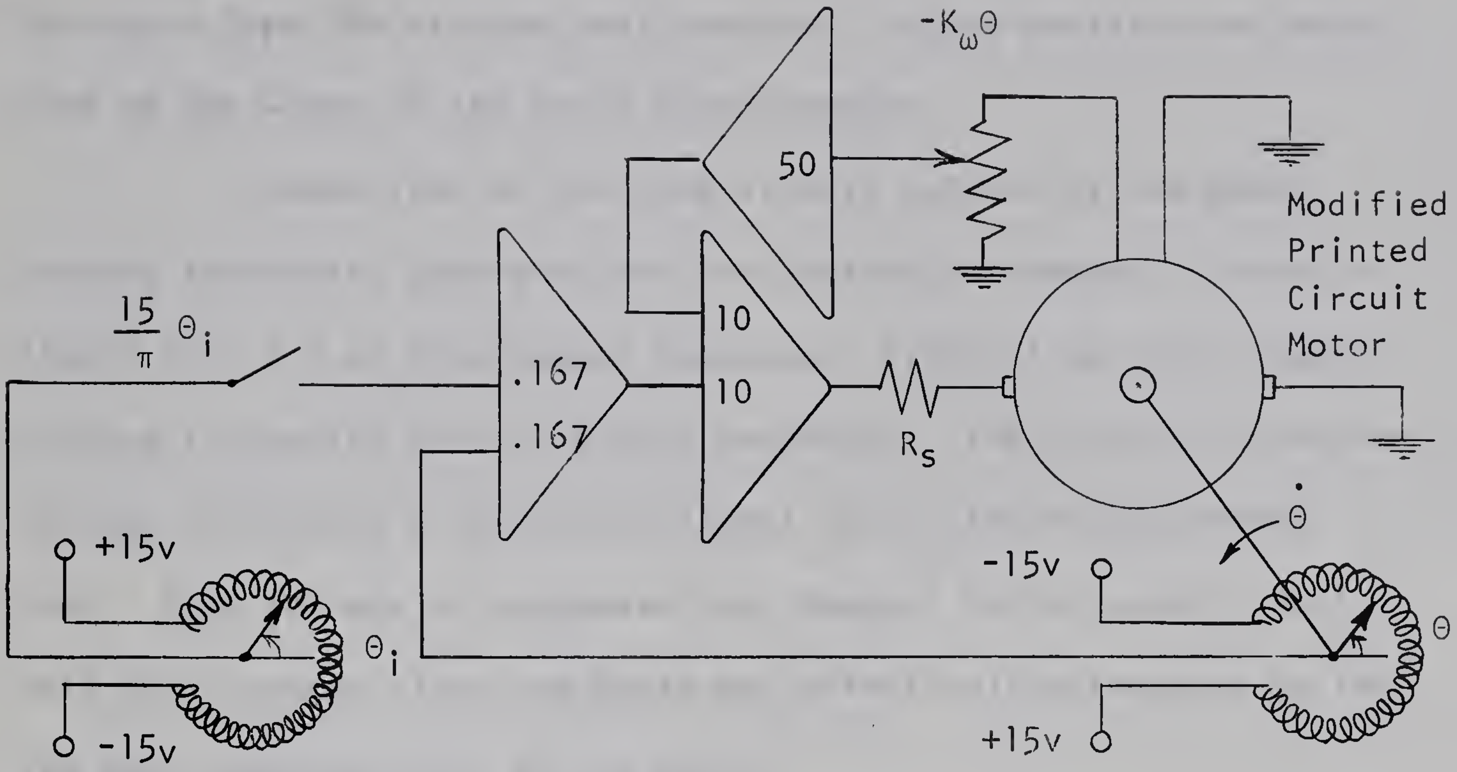

$-K_\omega\dot{\Theta}$
50
Modified
Printed
Circuit
Motor
$\frac{15}{\pi}\Theta_i$
10
10
.167
.167
R_s
$\dot{\Theta}$
+15v
-15v
Θ_i
-15v
+15v
Θ

Figure 5.10 Basic Linear System 1

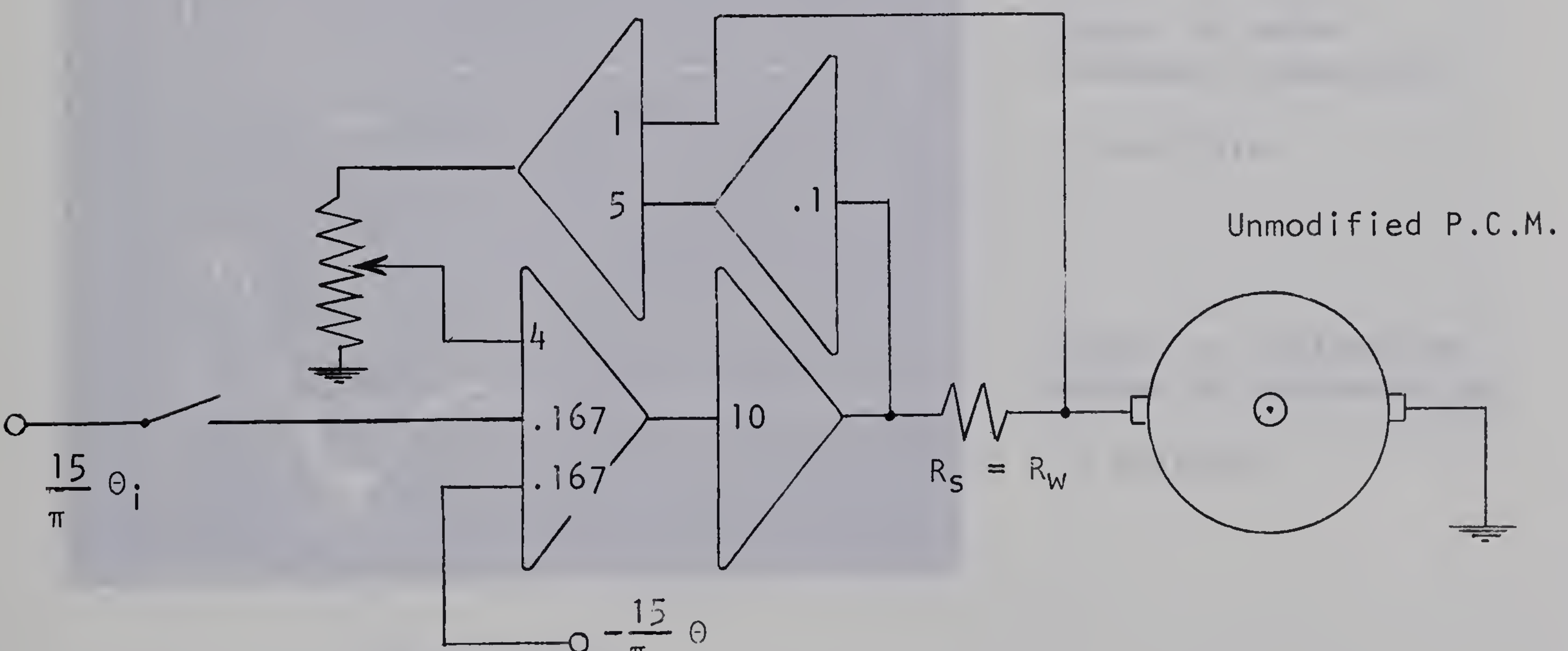

1
5
.1
Unmodified P.C.M.
4
.167
.167
10
$R_s = R_W$
$\frac{15}{\pi}\Theta_i$
$-\frac{15}{\pi}\Theta$

Figure 5.11 Basic Linear System 2
(potentiometers not shown)

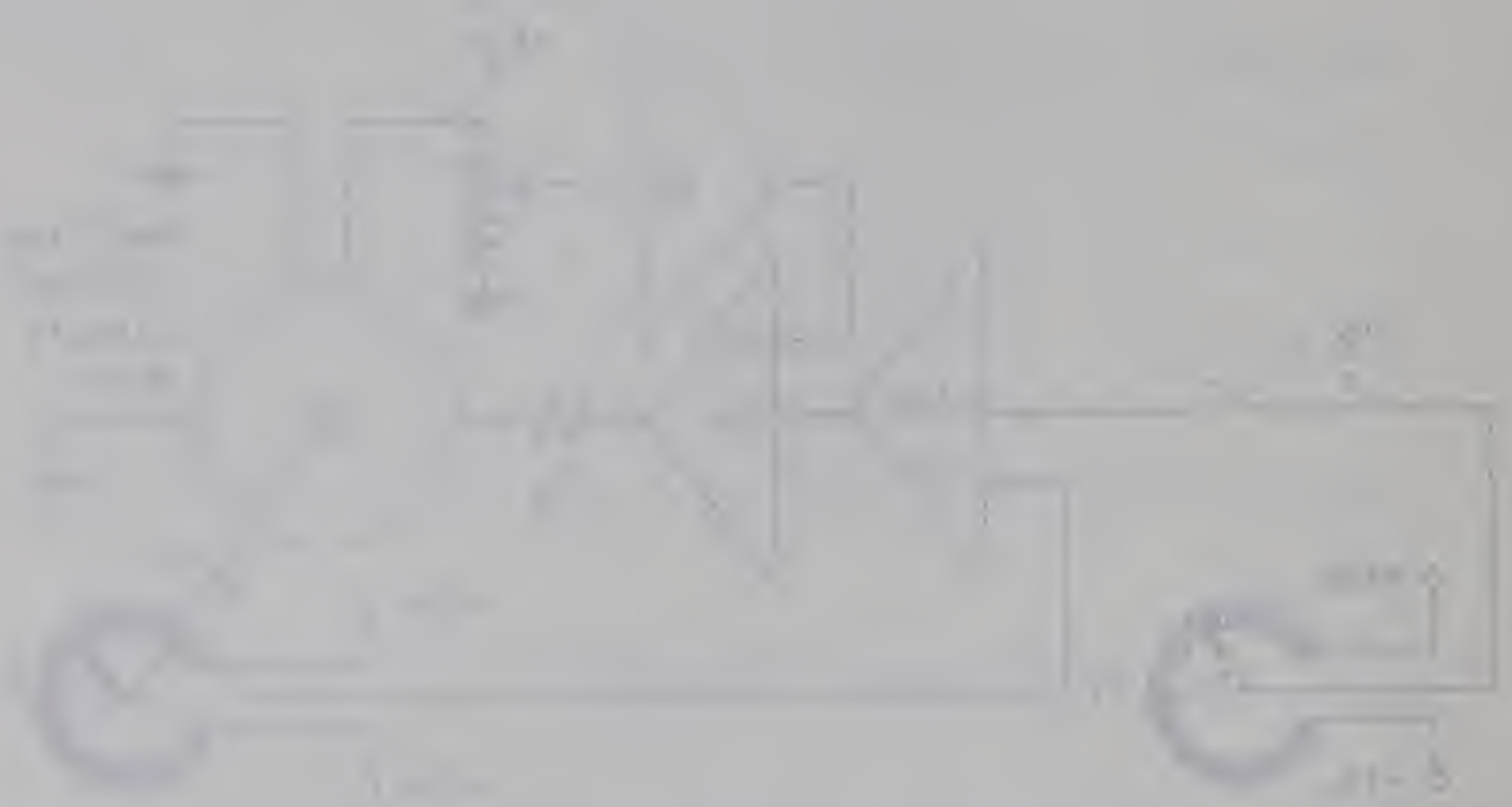

[illegible]

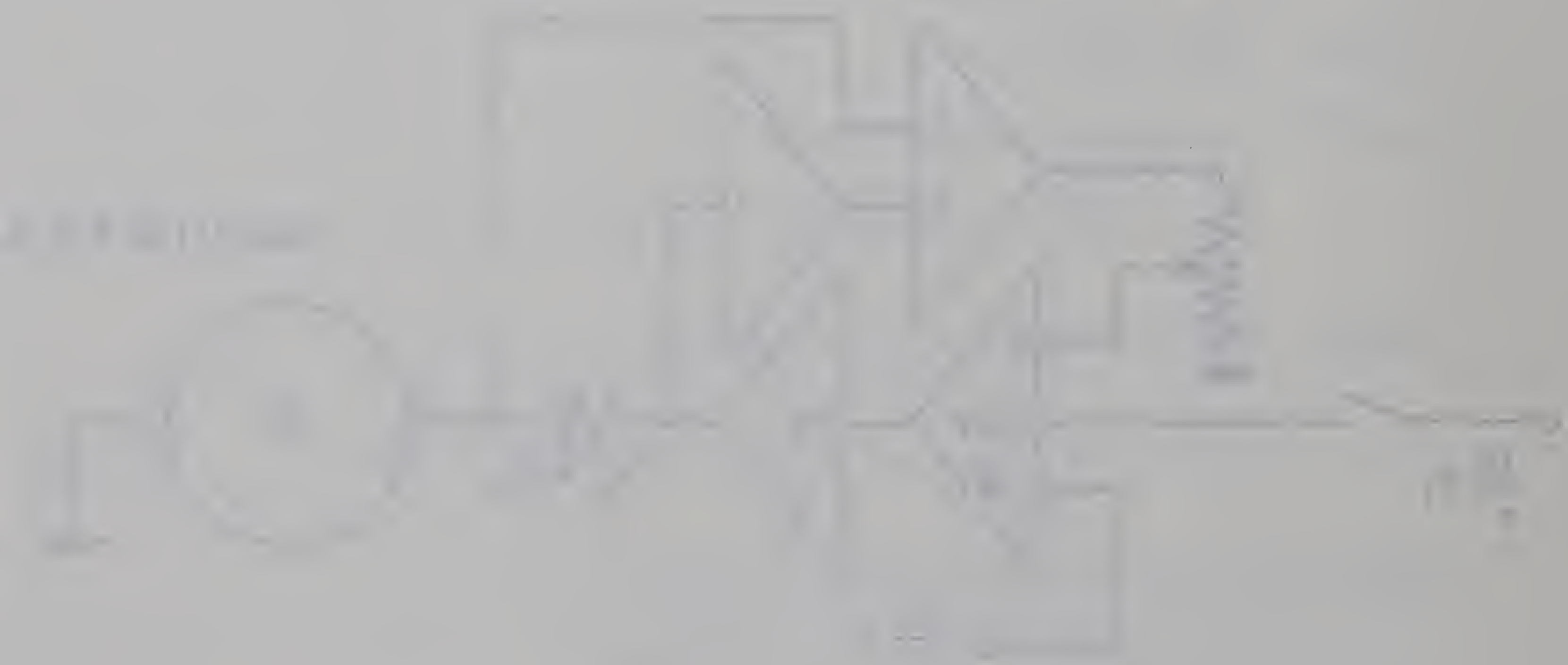

[illegible]

[illegible]

5.6 EXPERIMENTAL RESULTS AND CONCLUSIONS

The step responses of both systems were monitored using a Tektronix Type 564 storage oscilloscope. Output position was measured at the wiper of the servo potentiometer.

A comparison of the rate signals derived by the added winding tachometer generator and the subtraction method is shown in figure 5.12 for an underdamped response. System 1 was used (added winding tachometer providing rate feedback). The subtraction method is seen to produce a very noisy signal due to the brush contact drop. Both methods of tachometering, however worked equally well in this basic system since the noise was effectively attenuated by the low pass characteristic of the motor.

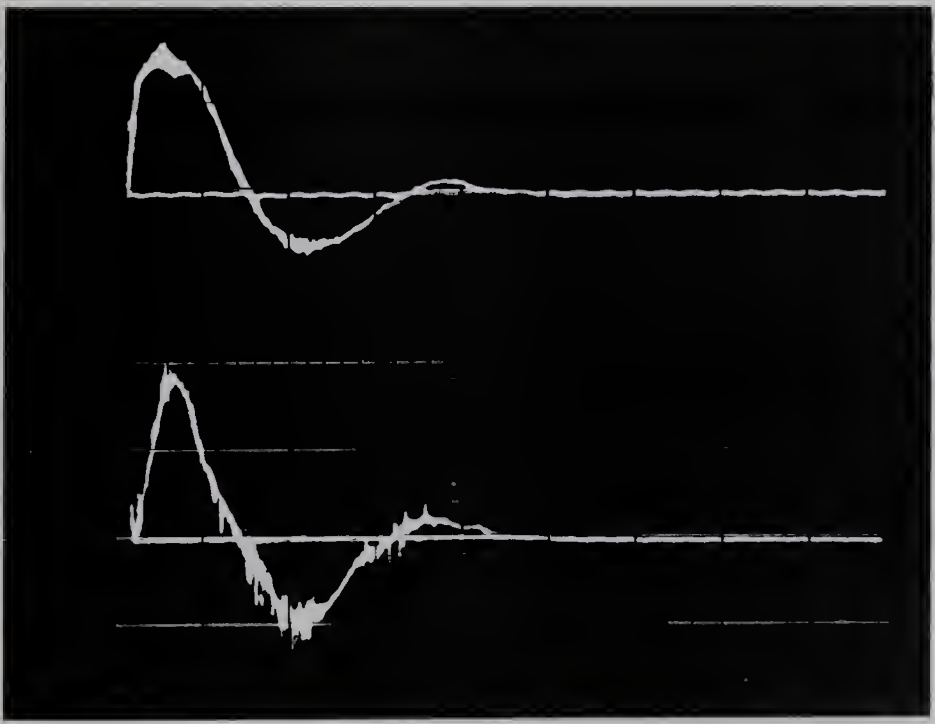

Output of added
tachometer-generator

.1 volt/div.

Output of subtraction
Method of tachometering

.5 volt/div.

50 msec./div.

Figure 5.12 Comparison of Two Rate Methods

Responses for various sizes of input increments and different damping ratios were photographed. Results for System 1 are shown in figures 5.13 to 5.16. Those for System 2 are shown in figures 5.17 to 5.20. To gain the significance of the vertical scales, recall that one volt corresponds to $\pi/15$ radians (12°). The derived rate signals are also shown for an overdamped and underdamped response for the two systems.

Although responses for both systems are reasonably fast, the steady-state errors which may occur make the basic systems unsatisfactory for applications in which any degree of accuracy is required. It must also be mentioned, that with the low values of gain used, the basic systems have inadequate stiffness. The relatively low restoring torque would permit a physical displacement of the shaft of about 20° simply by twisting it with the fingers.

From the highly underdamped responses, the observed system parameters are listed and compared to the theoretically predicted values of equations 5.49 to 5.54.

System 1:

$\omega_n \simeq 39$ rad/sec $\simeq 6.3$ Hz.	(6.4 Hz.)
$2\Theta_\varepsilon(\text{s.s.}) \simeq .14$ rad	(.126 rad)
$t_p \simeq 80$ msec.	(78.5 msec.)

System 2:

$\omega_n \simeq 54$ rad/sec $\simeq 8.6$ Hz.	(7.8 Hz.)
$2\Theta_\varepsilon(\text{s.s.}) \simeq .07$ rad	(.11 rad)
$t_p \simeq 55$ msec.	(63 msec.)

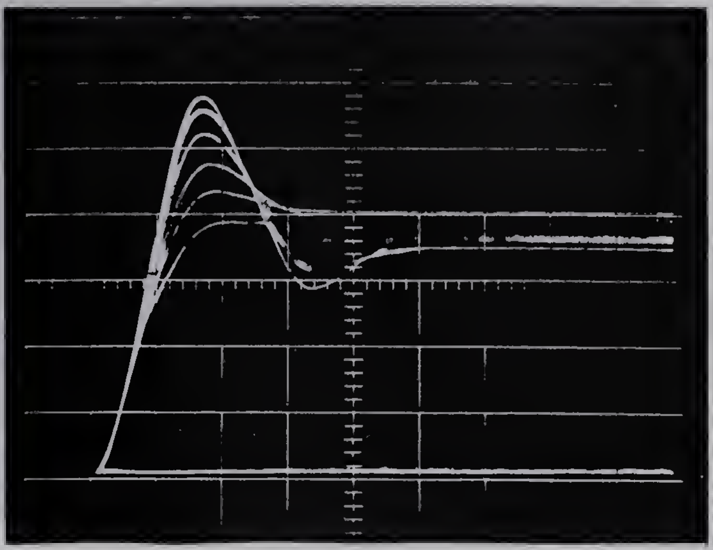

Figure 5.13

1 volt/div. vertical

50 msec./ div. horiz.

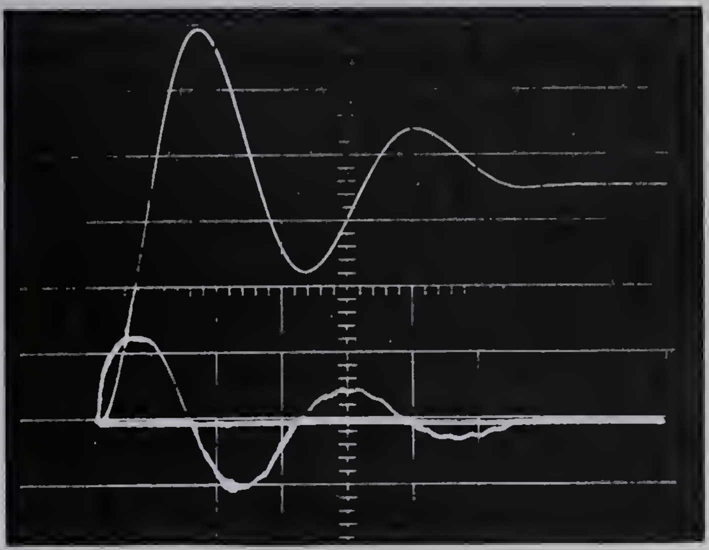

Figure 5.14

Position : 2 volt/div.

Velocity : .1 volt/div.

50 msec./div. horizontal

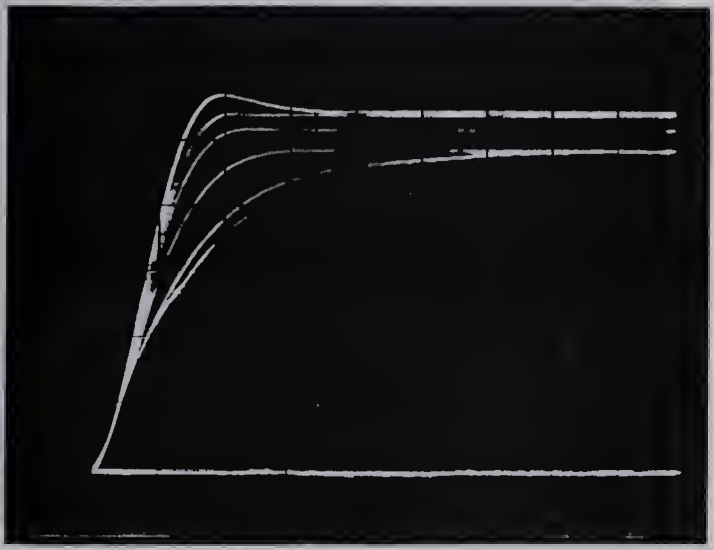

Figure 5.15

1 volt/div. vertical

50 msec./div. horiz.

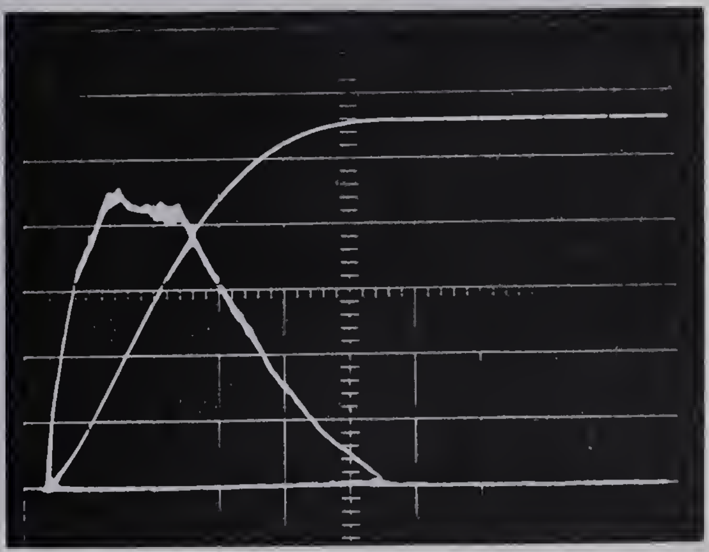

Figure 5.16

Position : 2 volts/div.

Velocity : .2 volts/div.

20 msec./div. horizontal

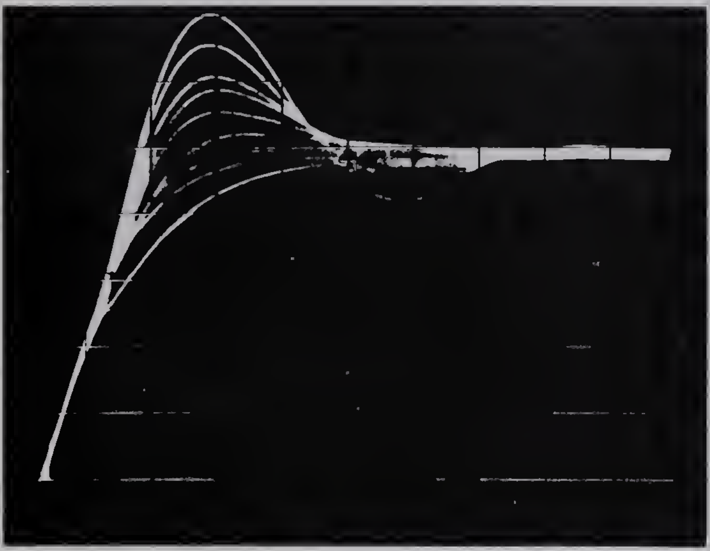

Figure 5.17

2 volts/div. vertical

20 msec./div. horiz.

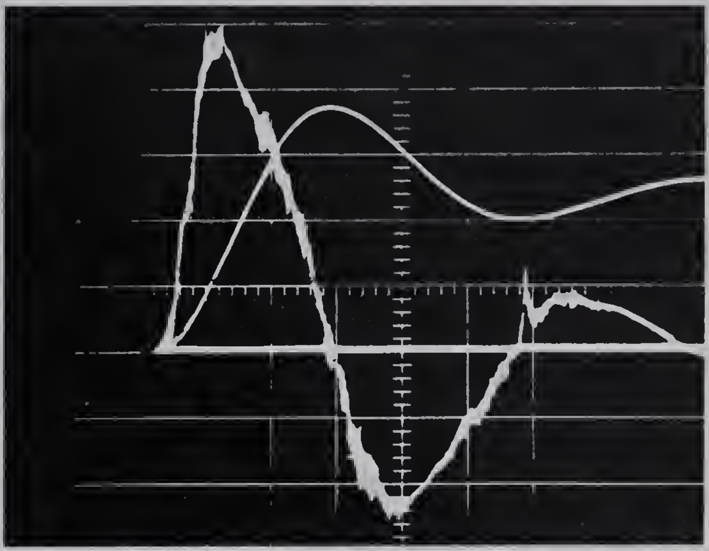

Figure 5.18

Position : 2 volts/div.

Velocity : .2 volts/div.

20 msec./div. horizontal

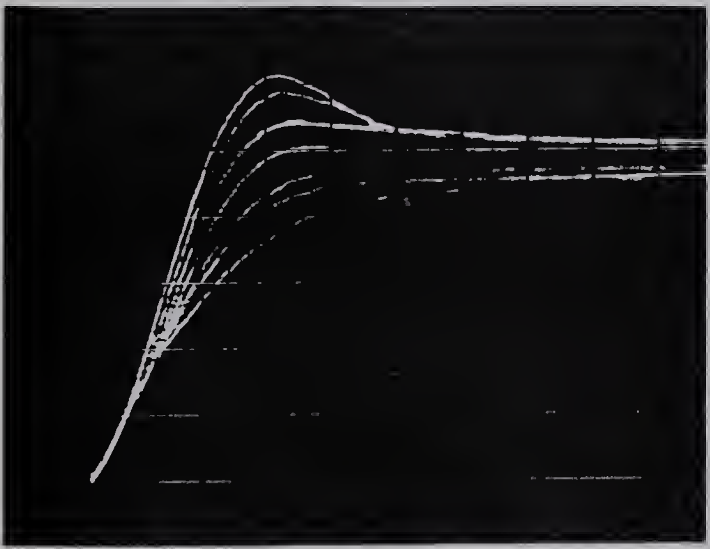

Figure 5.19

.5 volt/div. vertical

20 msec./div. horiz.

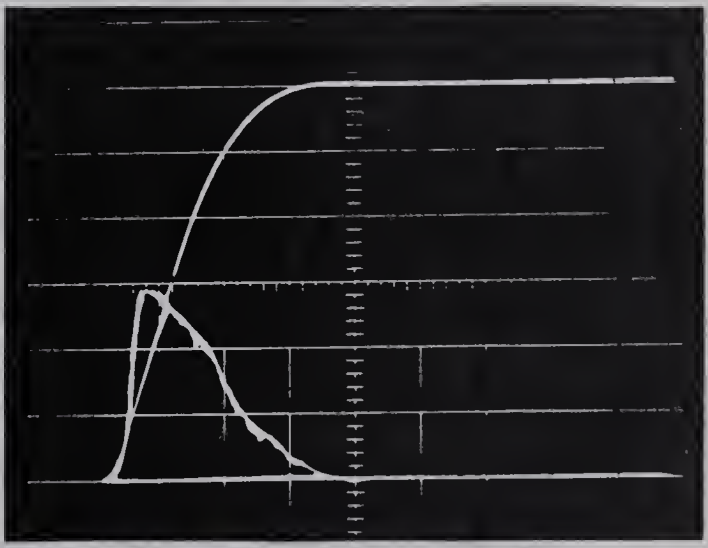

Figure 5.20

Position : 2 volts/div.

Velocity : .5 volt/div.

20 msec./div. horizontal

[illegible]
[illegible]
[illegible]
[illegible]

[illegible]
[illegible]
[illegible]

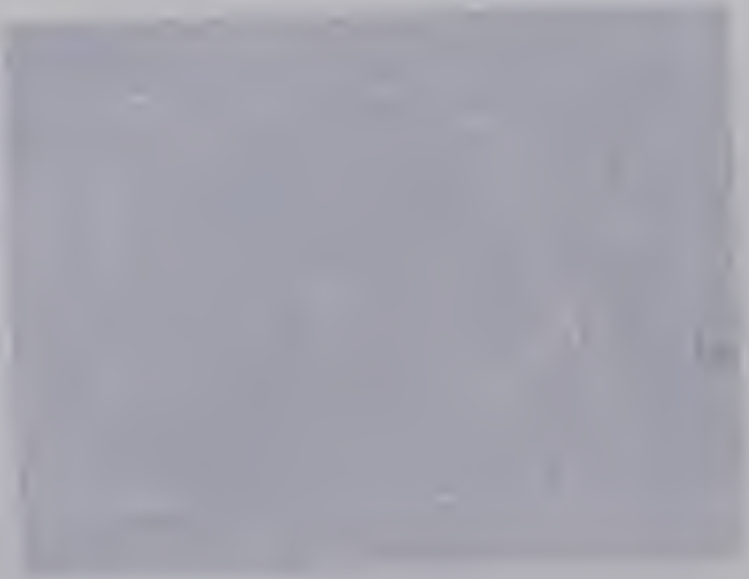

[illegible]
[illegible]
[illegible]
[illegible]

[illegible]
[illegible]
[illegible]

CHAPTER 6

COMPENSATION TECHNIQUES TO IMPROVE THE BASIC SYSTEM

6.1 INTRODUCTION

It was stated in Section 2.8 that the derived transfer function of the motor neglected the effects of static and Coulomb friction and brush contact drop, that is, the dead zone. Methods for compensating for these effects in order to actually "linearize" the motor and reduce the steady-state error will now be described.

6.2 DITHER COMPENSATION FOR STATIC FRICTIONAL TORQUE

One method for overcoming the effects of static friction is the use of dither. Dither is a relatively high-frequency, low-amplitude voltage superimposed on the D.C. input to the motor. It causes a slight vibration of the armature thus allowing the D.C. component to eventually move the armature to a position of close to zero steady-state error.

The choice of frequency and amplitude must be made simultaneously since their individual effects are not independent. A very high frequency requires much too large an amplitude to actually vibrate the armature, however the D.C. value of the part of the total input (error signal plus dither) which is greater than E_f plus V_c will actually cause movement thus effectively reducing the width of the dead zone. This means the amplitude must be slightly greater than half the maximum dead zone width in order to effectively reduce the dead zone to zero. Such amplitudes cause considerable heating of the armature, plus a noticeable whine, thus making the method somewhat impractical.

If lower frequencies are used, such that the motor will actually respond, then the dead zone width may be reduced to its minimum value (that determined by Coulomb friction), provided this

dither is present during the entire response. In this case a much lower amplitude square wave may be used. The amplitude and frequency must by chosen such that the effect on the output position (i.e. ripple) is not significant.

The effectiveness of this type of dither may be attributed to the fact that the velocity does not become exactly zero at the peaks and minimums (of an underdamped response). The vibrating effect of the dither therefore does not allow the static frictional torque to take hold at such instances.

The effect of dither was investigated using a square-wave oscillator feeding into the input amplifier of basic system 1. It was found that frequencies from 60 to 80 Hz. would reduce the steady-state error to a near-zero value. Figure 6.1 shows the steady-state errors resulting for a step of about 47°. Figure 6.2 shows the same size of increment but with 70 Hz. dither applied.

In order to cut out the dither application after a step (and thus eliminate motor hum), a dither duration circuit was built in combination with an astable square-wave dither generator (figures A4.4 and A4.3. The results of use of this circuit are shown in figure 6.3 for an overdamped and underdamped step of approximately 12° using system 2. The two inner traces are with dither applied.

In spite of the great improvement in accuracy, the time required to effect it is much too large (in the order of 300 msec.) to say that performance is satisfactory.

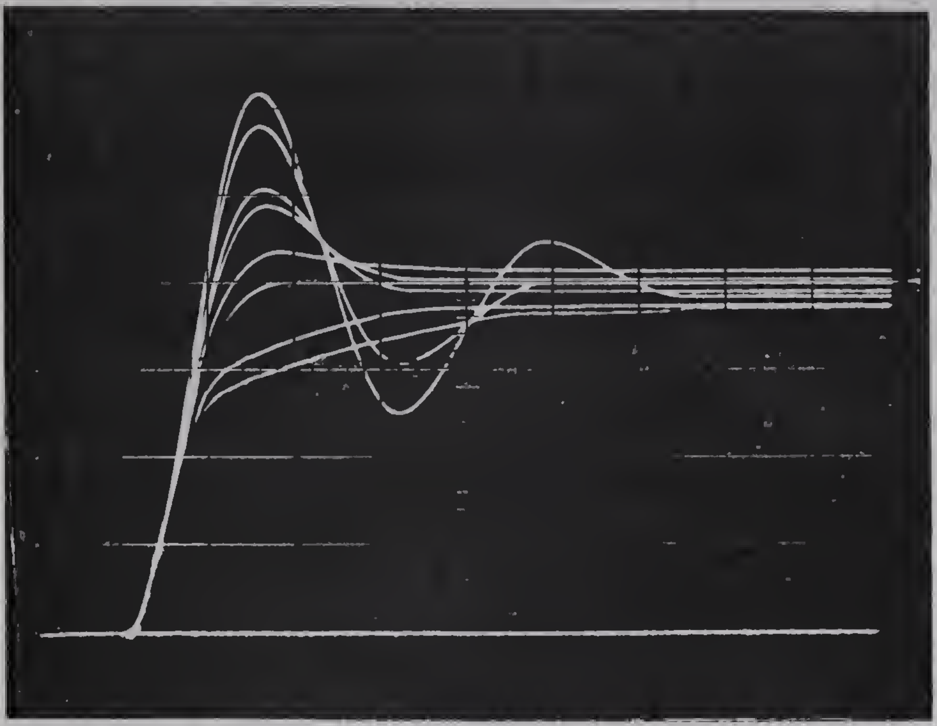

Figure 6.1

1 volt/div. vertical

50 msec./div. horiz.

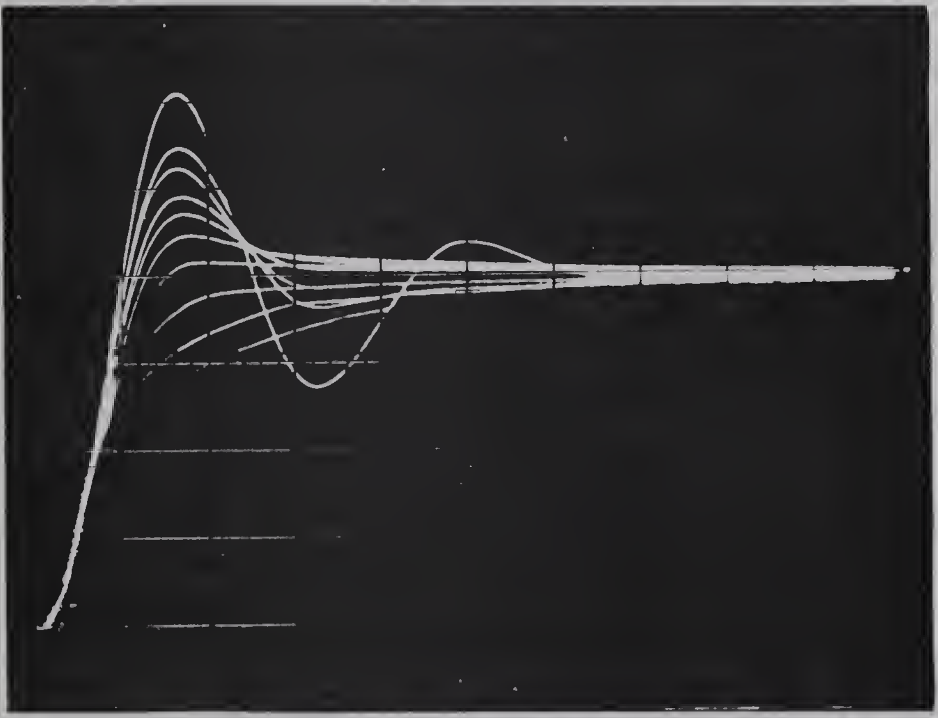

Figure 6.2

1 volt/div. vertical

50 msec./div. horiz.

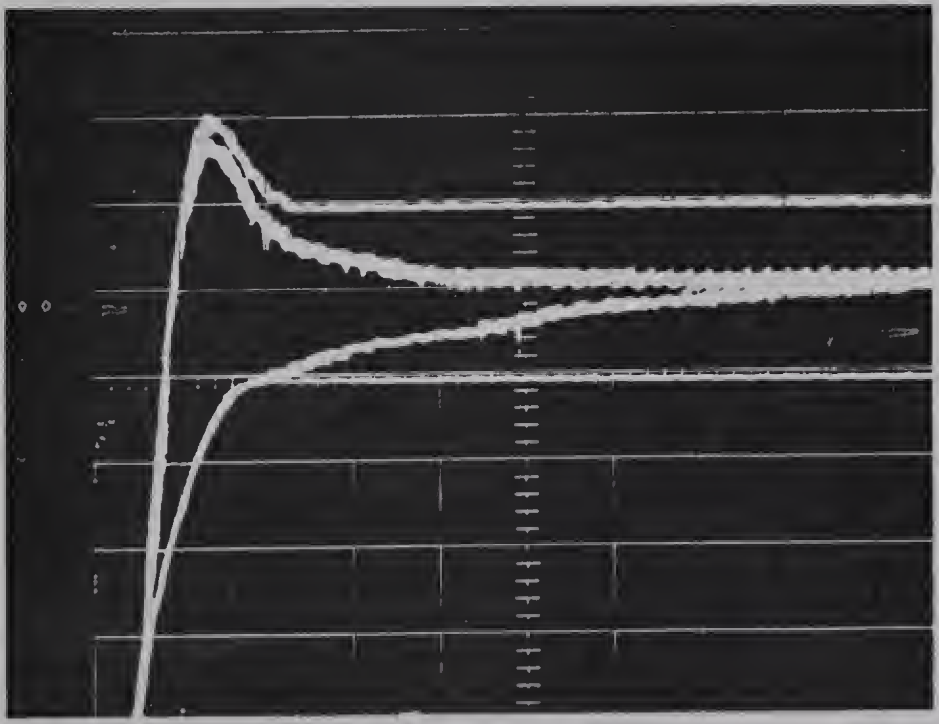

Figure 6.3

.2 volt/div. vertical

50 msec./div. horiz.

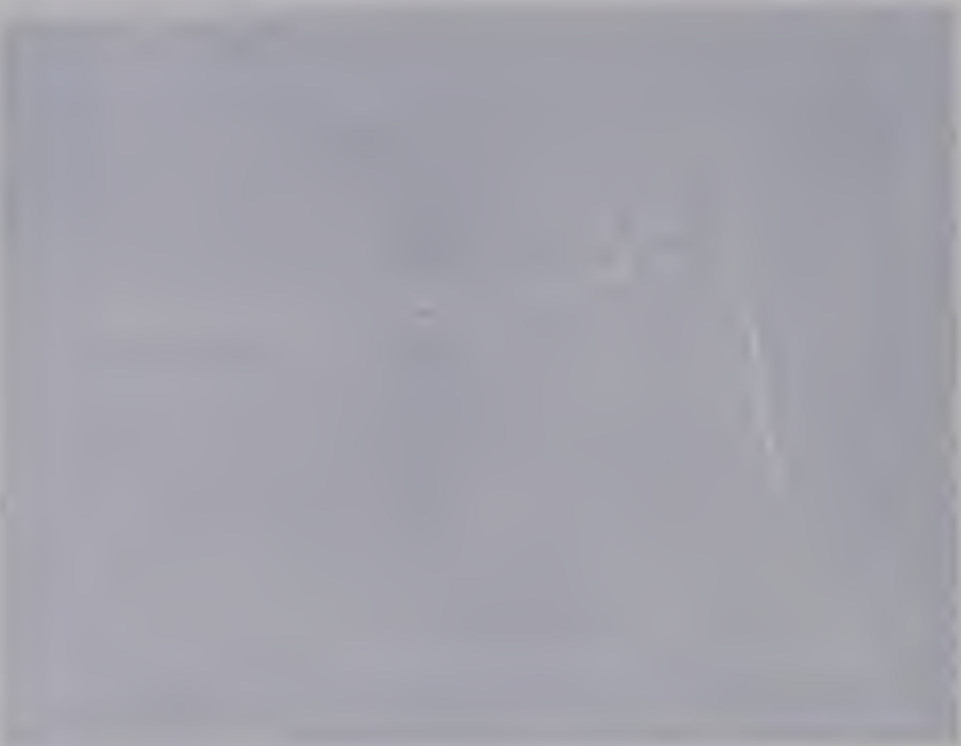

[illegible]

[illegible]

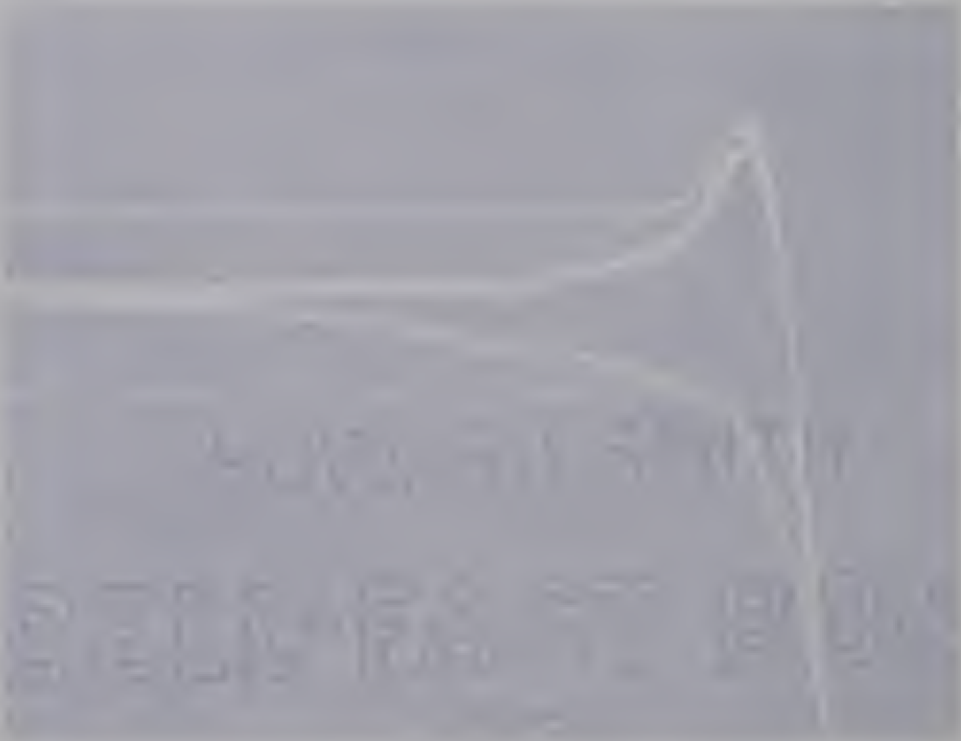

[illegible]

6.3 COMPENSATION FOR COULOMB FRICTIONAL TORQUE

The effect of Coulomb frictional torque was represented by an equivalent opposing voltage input, that is

$$E_f(s) = \frac{R_t}{K_T} T_c(s) \tag{6.1}$$

In a highly underdamped response, the overshoots and undershoots are vastly reduced by even small amounts of Coulomb friction as was shown in figure 5.3. From this example it should be apparent that if a voltage $-E_f(t)$ could be generated from the velocity signal, it could be used to exactly cancel the opposing voltage due to T_c and thus make the motor behave as a frictionless device during a response. Such linearization would render the derived motor transfer function more nearly accurate.

In an underdamped response more oscillations - of correspondingly higher amplitudes - and a reduction in rise time would occur. Damping could then be increased with a resulting improvement in performance. Overdamped responses would similarly be improved as can be seen in figure 5.2. With this type of compensation then, system transient response becomes much more predictable.

In order to generate the signal $-E_f(t)$ the relay characteristics shown in figure 6.4 is most useful. The small dead zone is necessary so that the signal is applied only when the armature is moving. The small hysteresis prevents the possibility of "chattering".

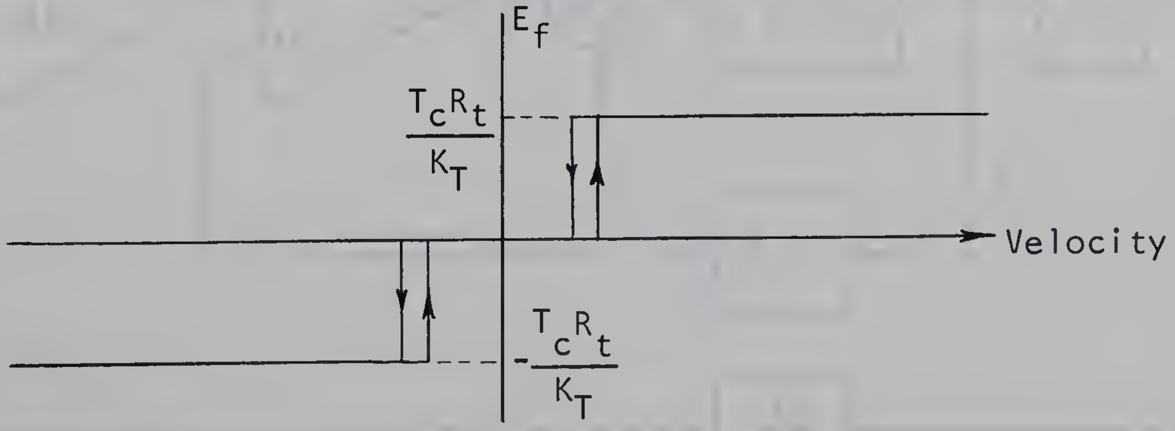

Figure 6.4 Velocity Comparator Characteristic

The desired characteristic was obtained using the comparator circuit shown in figure A 4.5. Using its output as an input to the power amplifier, the effect of Coulomb friction was completely eliminated. The resulting quasi-linear transfer characteristic is shown in figure 6.5 (the effect of V_c is neglected).

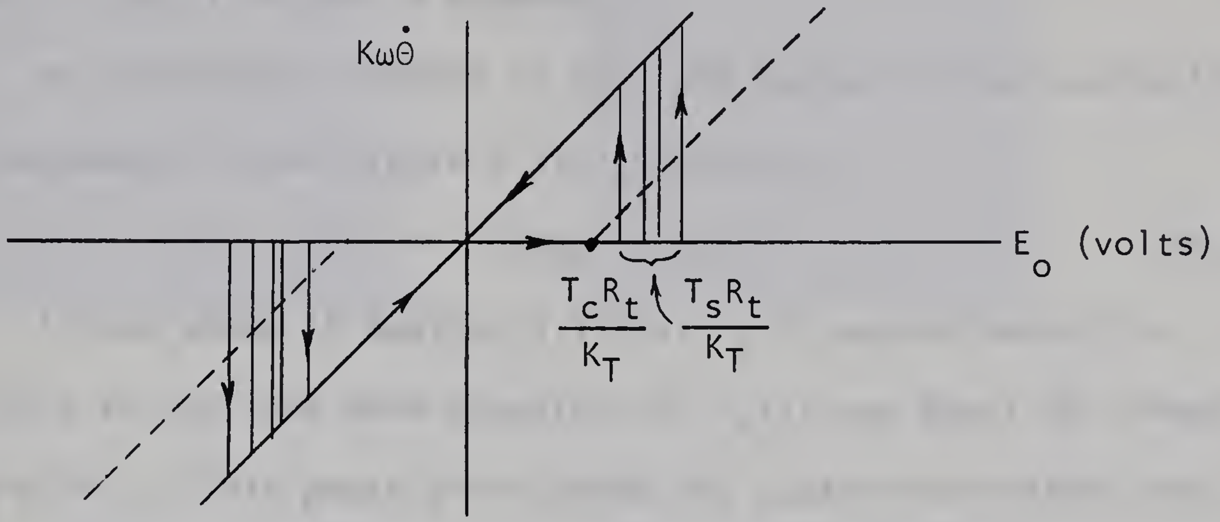

Figure 6.5 Linearized Velocity Transfer Characteristic

The compensated system is shown in figure 6.6. The comparator potentiometers were adjusted at both positive and negative velocities until the characteristic of figure 6.5 was obtained (using the X-Y recorder).

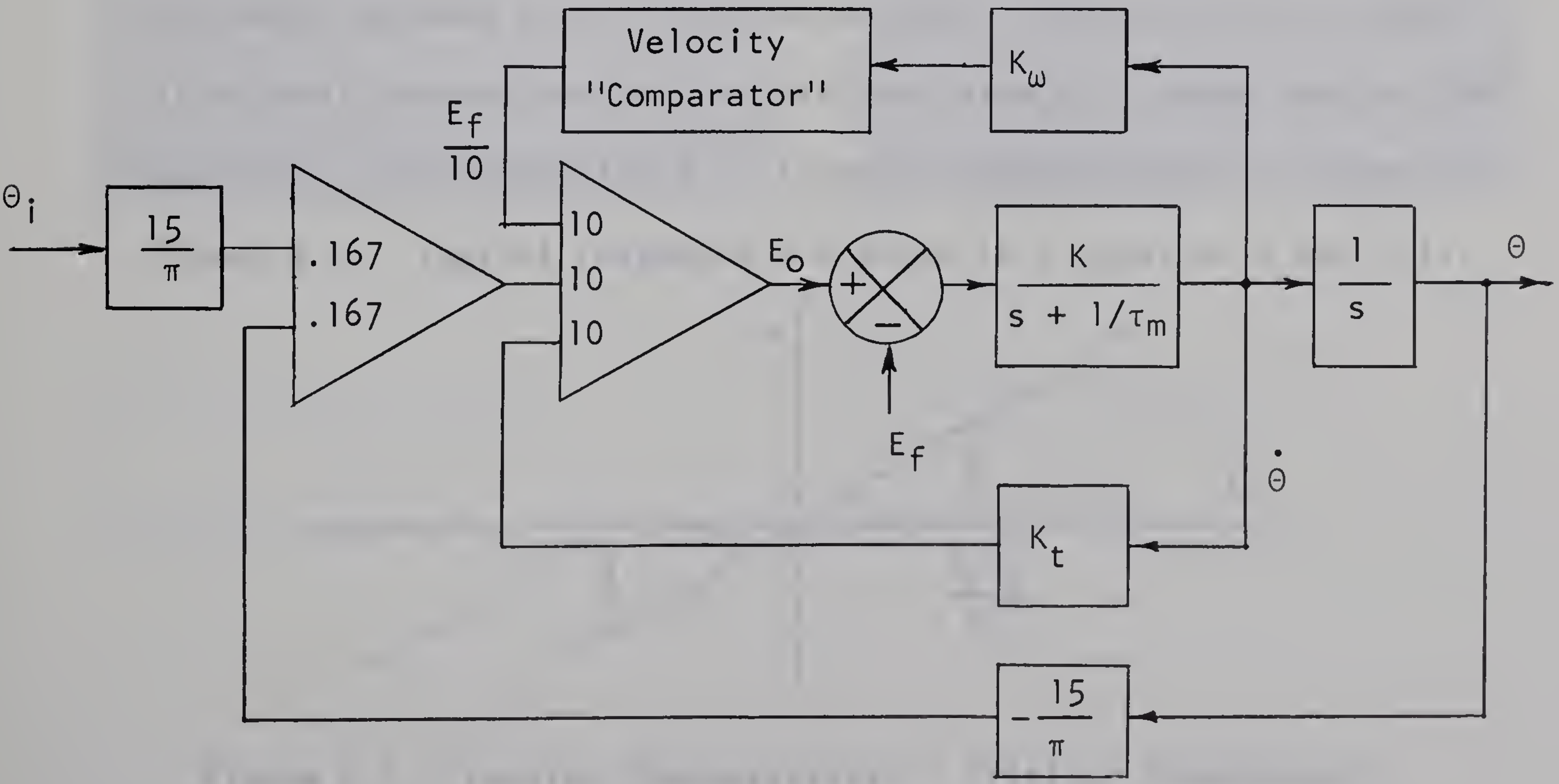
Velocity "Comparator"
K_ω
$\frac{E_f}{10}$
Θ_i
$\frac{15}{\pi}$
.167
.167
10
10
10
E_o
+
−
E_f
$\frac{K}{s + 1/\tau_m}$
$\frac{1}{s}$
Θ
$\dot{\Theta}$
K_t
$-\frac{15}{\pi}$

Figure 6.6 Basic System Compensated For Coulomb Friction

Results were obtained for the undamped response ($K_t = 0$). Figure 6.8 shows the comparator output when the system is uncompensated. The step is approximately 90°. Figure 6.9 shows the response when the comparator is used to compensate for E_f. The increase in amplitude and number of oscillations is apparent.

An unfortunate problem is that the output of the subtraction-method "tachometer" (see figure 5.11) is given by

$$V_t = -5(E_o - 2E_t) = -.5\left(K_g\omega + V_c(I_a)\right) \tag{6.2}$$

It was shown in Section 5.4 that V_c is approximately in phase with $\dot{\omega}$ so that the zero-crossings of $V_c(t)$ are about 90° ahead of those of $K_g\omega$. This phase error makes the subtraction-method rate signal too inaccurate to use as an input to the velocity comparator. For this reason no attempt was made to compensate system 2 for Coulomb friction.

6.4 DITHER PLUS COMPARATOR COMPENSATION

The results of Sections 6.2 and 6.3 may now be combined. If dither is used in conjunction with the velocity comparator then the motor behaves as a linear device when in motion and the static frictional torque observes its minimum value of T_c when leaving the dead zone. The resulting D.C. transfer characteristic is shown in figure 6.7. Typical responses are shown in figures 6.10 and 6.11.

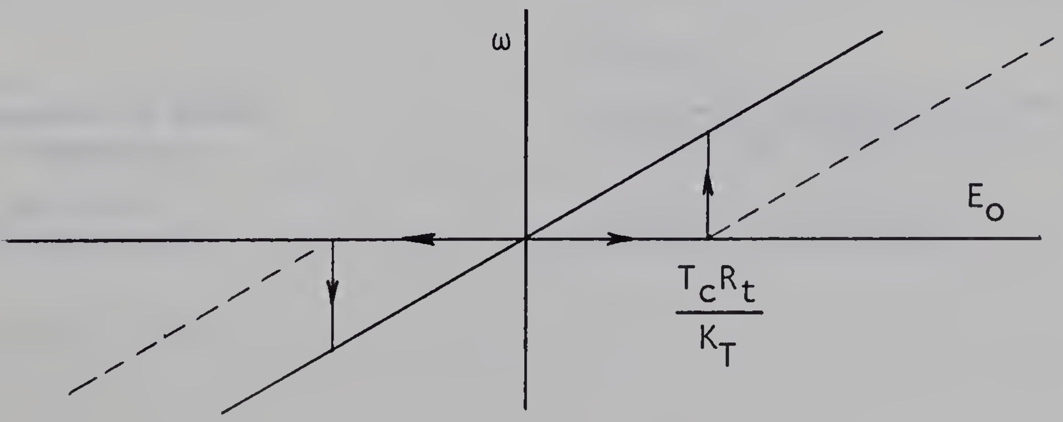

Figure 6.7 Transfer Characteristic - Friction Compensated

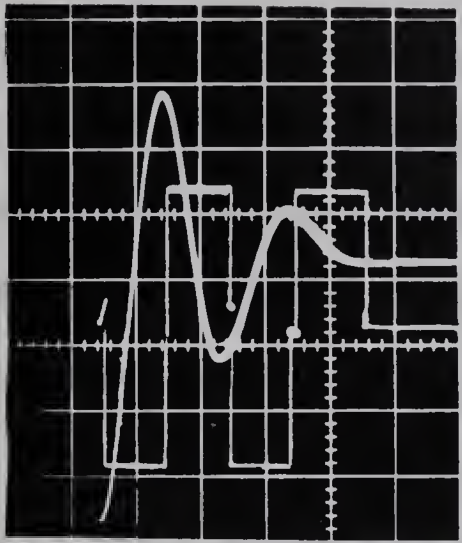

Figure 6.8

Comparator Output & Response of the Uncompensated System

100 msec./div. horizontal

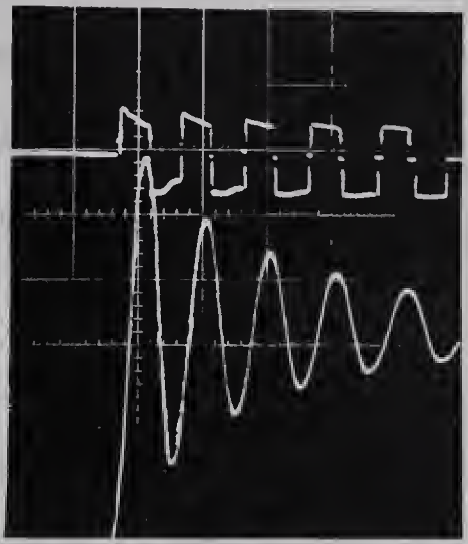

Figure 6.9

Comparator Output & Response of the Compensated System

200 msec./div. horizontal

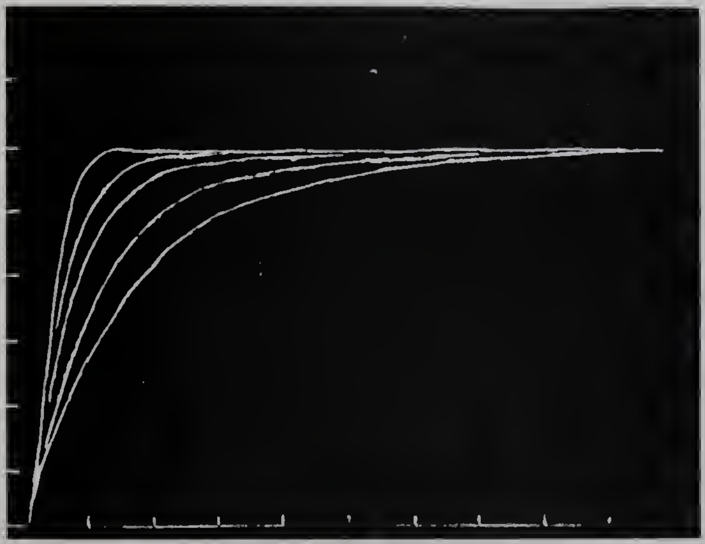

Figure 6.10

Overdamped Responses of System with Friction Compensation

2 volts/div. vertical
100 msec./div. horizontal

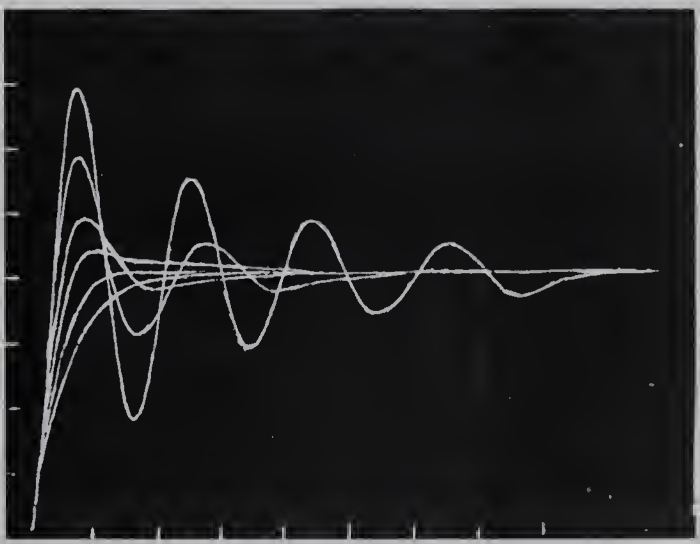

Figure 6.11

Underdamped Responses of System with Friction Compensation

2 volts/div. vertical
100 msec./div. horizontal

[illegible]

[illegible]

[illegible]

[illegible]

6.5 COMPENSATION FOR BRUSH CONTACT VOLTAGE DROP

While in motion, the motor behaves as if it has a dead zone due to $V_c(t)$. However, since this voltage depends on $I_a(t)$ it might be said that this non-linearity is itself non-linear. If it could be compensated for in a manner similar to that used for Coulomb friction, the system operation could be truly linearized.

In the case of system 2, operation is further degraded since the output of the subtraction-method tachometer contains $V_c(t)$. If $K_g\omega$ is small at the same instant $I_a(t)$ is large, for example at $t = 0^+$, then the rate feedback signal is very inaccurate.

It is necessary then, to generate a signal to oppose that of figure 5.9 (e). If the dynamic curve of figure 5.7 is assumed to give $V_c(I_a)$, then it is possible to use a type of current comparator to generate the required voltage. It is noticed that this curve bears striking resemblance to a diode characteristic. Since the input to this generator must be a voltage proportional to current which may rise to 25 amps, the generator output must be limited. Thus an operational amplifier having diodes in the feedback path is a natural solution. The circuit used is shown in figure A 4.6.

Using a system which is basically shown in figure 6.12, it was found to be possible to modify the signal produced by the subtraction-method such that it was exactly the same as the rate signal produced by the added winding tachometer-generator.

No success was obtained in attempts at further linearization of the motor using the current comparator. Since positional error attributable to V_c is very small this is not a significant point.

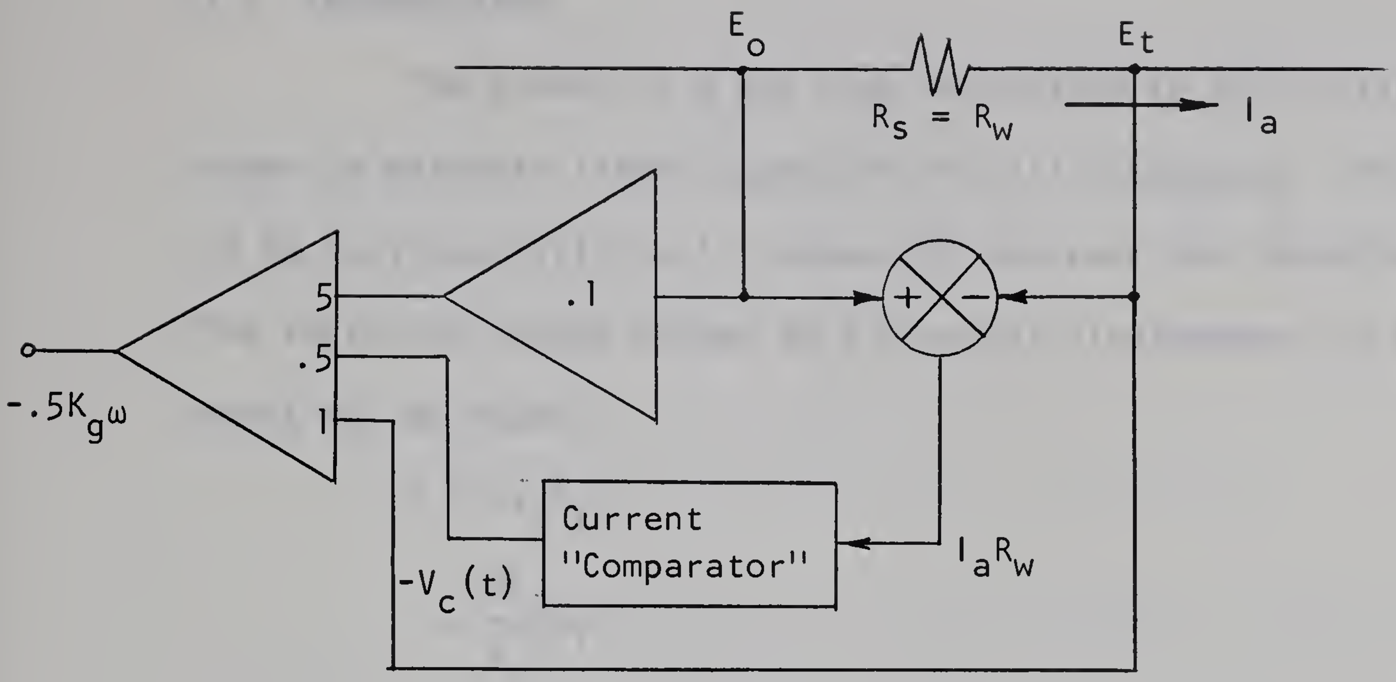

Figure 6.12 Modification of Subtraction Method To Compensate for Brush Contact Drop

6.6 SUMMARY

The methods of compensation suggested in this chapter do not solve the problem of the low restoring torque produced by a physical displacement of the shaft, that is the "stiffness" of the system. It must be remembered that the restriction to linear operation (i.e. low forward gain) would create the only situation in which such compensation would be necessary. The methods are of academic interest and might be used if an "ultra-refinement" in system accuracy were required.

CHAPTER 7

LIMITING OF POSITIONAL ERROR

7.1 INTRODUCTION

The product G_1G_2 has been restrained to 7.97 volts/rad. in order to maintain linear operation for all increments. This was seen to be very unsatisfying in respect to accuracy and restoring torque. The restoring torque caused by a physical displacement $\Delta\Theta$ of the shaft can be found:

$$T = \Delta I_a K_T \tag{7.1}$$

$$= \frac{\Delta E_o}{R_t} K_T \tag{7.2}$$

$$= \frac{G_1 G_2 \Delta\Theta\, K_T}{R_t} \tag{7.3}$$

The possible steady-state error was found to be

$$\Theta_\varepsilon(s.s.) = \pm \frac{\dfrac{T_f R_t}{K_T} + V_c(s.s.)}{G_1 G_2} \tag{7.4}$$

It is also noticed that the peak time for a step response from equations 5.3 and 5.18 is

$$t_p = \frac{\Pi}{\sqrt{KG_1G_2(1-\xi^2)}} \tag{7.5}$$

For these three reasons it is very desireable to increase G_1G_2 to as high a value as possible. Linear operation could be maintained in applications where only small increments were applied, however in this chapter non-linear operation will be investigated. The positional error (output of G_1) will be limited such that the power amplifier is not allowed to saturate (for protection). The circuit used is shown in figure A 4.7 and its D.C. transfer characteristic is shown in figure 7.1.

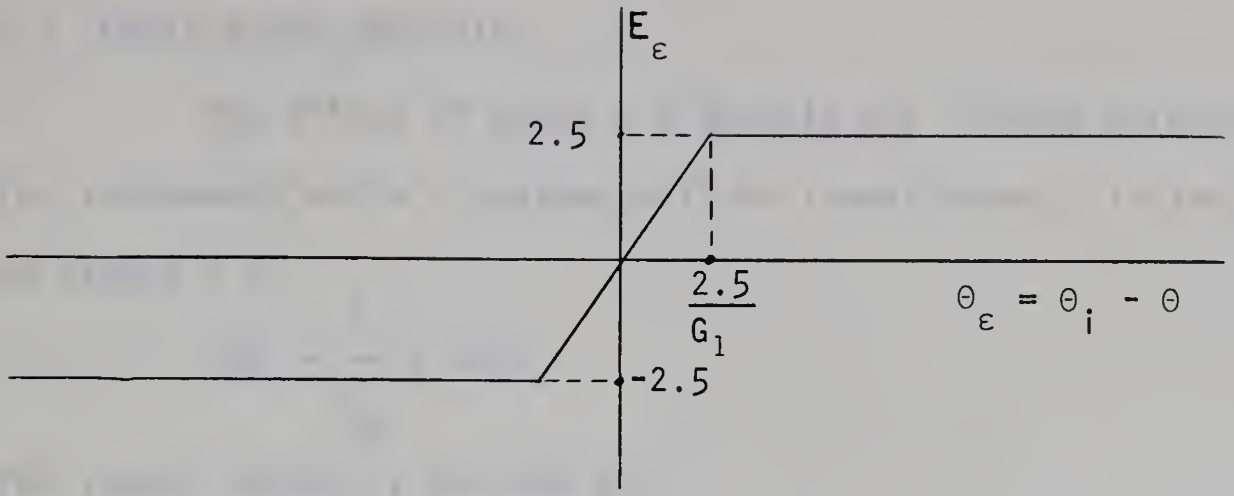

Figure 7.1 Error Detector D.C. Characteristic

If G_1 is increased sufficiently, then for most practical purposes, the steady-state error given by 7.4 may be entirely neglected. If the applied step is small enough such that the response is kept within the linear region of operation, then the values of ξ and ω_d provide a means of checking the constants τ_m and K. If A_1 and A_2 are the first two overshoots it can be shown that if $K_t = 0$

$$K = \frac{\omega_d^2}{G_1 G_2} \left\{ 1 + \left[\frac{\log A_1/A_2}{2\pi} \right]^2 \right\} \tag{7.6}$$

and

$$\tau_m = \frac{\pi}{\omega_d \log A_1/A_2} \tag{7.7}$$

The expense of the improvement in steady-state error and restoring torque will be shown to be a slight increase in response times due the occurrence of velocity limiting caused by the non-linearity. The system may be simplified as shown in figure 7.2.

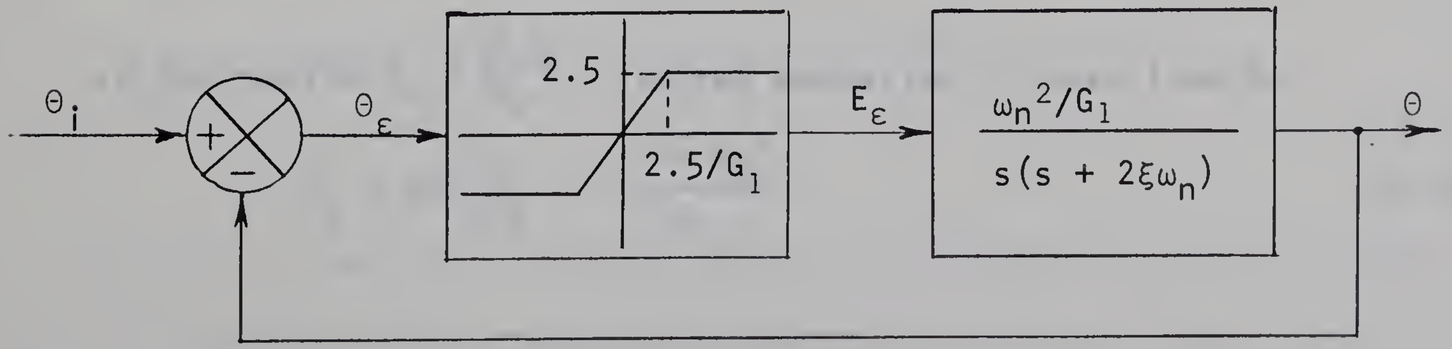

Figure 7.2 Limiting of Positional Error

7.2 PHASE PLANE ANALYSIS

The effect of using a high-gain but limited error detector for increments up to π radians will be investigated. In the system of figure 7.2

$$2\xi\omega_n = \frac{1}{\tau_m} + KG_2K_t \tag{7.8}$$

The linear region is defined by

$$-(\Theta_i - \frac{2.5}{G_1}) < \Theta < (\Theta_i - \frac{2.5}{G_1}) \tag{7.9}$$

As in Section 5.3, the error and its derivative will be plotted in the phase plane. The linear region therefore will not depend on the size of the increment.

$$-\frac{2.5}{G_1} < \Theta_\varepsilon < \frac{2.5}{G_1} \tag{7.10}$$

The system equation in the linear region is

$$\omega_n^2\Theta_\varepsilon = s(s + 2\xi\omega_n)(\Theta_i - \Theta_\varepsilon) \tag{7.11}$$

or

$$\ddot{\Theta}_\varepsilon + 2\xi\omega_n\dot{\Theta}_\varepsilon + \omega_n^2\Theta_\varepsilon = 0 \tag{7.12}$$

Normalizing as before (Equations 5.31 and 5.32)

$$\frac{d^2\Theta_\varepsilon}{dt_n^2} + 2\xi\frac{d\Theta_\varepsilon}{dt_n} + \Theta_\varepsilon = 0 \tag{7.13}$$

Isoclines in the linear region are given by

$$\nu_\varepsilon = -\frac{\Theta_\varepsilon}{2\xi + \frac{d\nu_\varepsilon}{d\Theta_\varepsilon}} \tag{7.14}$$

In the region $\Theta_\varepsilon > \frac{2.5}{G_1}$, limited operation is described by

$$\ddot{\Theta}_\varepsilon + 2\xi\omega_n\dot{\Theta}_\varepsilon = -\frac{2.5\ \omega_n^2}{G_1} \tag{7.15}$$

The normalized equation becomes

$$\frac{d\nu_\varepsilon}{d\Theta_\varepsilon} + 2\xi = -\frac{2.5}{G_1\nu_\varepsilon} \tag{7.16}$$

for which the solution is

$$\nu_\varepsilon + \frac{2.5}{2\xi G_1} = (\nu_{\varepsilon o} + \frac{2.5}{2\xi G_1})e^{-2\xi(\Theta_\varepsilon - \Theta_{\varepsilon o})} \tag{7.17}$$

where $(\Theta_{\varepsilon o}, \nu_{\varepsilon o})$ is the initial point.

Similarly, in the limited region $\Theta_\varepsilon < -\frac{2.5}{G_1}$ (7.18)

$$\frac{d\nu_\varepsilon}{d\Theta_\varepsilon} + 2\xi = \frac{2.5}{G_1\nu_\varepsilon} \tag{7.19}$$

and the solution is

$$\nu_\varepsilon - \frac{2.5}{2\xi G_1} = (\nu_{\varepsilon o} - \frac{2.5}{2\xi G_1})e^{-2\xi(\Theta_\varepsilon - \Theta_{\varepsilon o})} \tag{7.20}$$

In equations 7.16 and 7.19 it can be seen that the isoclines in the limited regions are horizontal straight lines. It is noticed that the maximum velocity (normalized) occurs at a trajectory slope of zero

$$|\nu_\varepsilon|_{max} = \frac{2.5}{2\xi G_1} \tag{7.21}$$

The system is thus said to be velocity limited. When this limit is reached, the position becomes proportional to time and very long response times may result when the limit is low.

Since the linear region is enclosed by

$$\Theta_\varepsilon = \pm\frac{2.5}{G_1} \tag{7.22}$$

it can be seen that for a fixed value of damping ratio, the shape of the phase plane diagram is independent of the gain G_1. Also for $\xi = 0.5$ the normalized velocity limit has the same value as the

the linear region extremity. This case is shown in figure 7.3 for a gain $G_1 = 2.5$. The response of the same system without limiting is shown in figure 7.4 for comparison.

The phase trajectories were obtained using an analog computer simulation of the system. Note that some of the outer trajectories would not be realizable in the physical systems since Θ_ε cannot exceed π radians.

The isocline method, though somewhat tedious, will now be used to obtain the phase trajectory of a practical case. With $\xi = 0.8$ and $G_1 = 4.34$ ($R_f/R_i = 2$ in figure A 4.7), the linear region is defined by

$$- .577 < \Theta_\varepsilon < .577 \tag{7.23}$$

The limiting velocity (normalized) is given by

$$|\nu_\varepsilon|_{max} = \frac{.577}{2(.8)} = .36 \tag{7.24}$$

In the linear region

$$-\frac{\Theta_\varepsilon}{\nu_\varepsilon} = \frac{d\nu_\varepsilon}{d\Theta_\varepsilon} + 1.6 \tag{7.25}$$

For $\Theta_\varepsilon > .577$

$$\frac{d\nu_\varepsilon}{d\Theta_\varepsilon} + 1.6 = -\frac{.577}{\nu_\varepsilon} \tag{7.26}$$

Isoclines are shown in the two regions with trajectory slopes indicated and the phase trajectories are sketched for various inputs in figure 7.5.

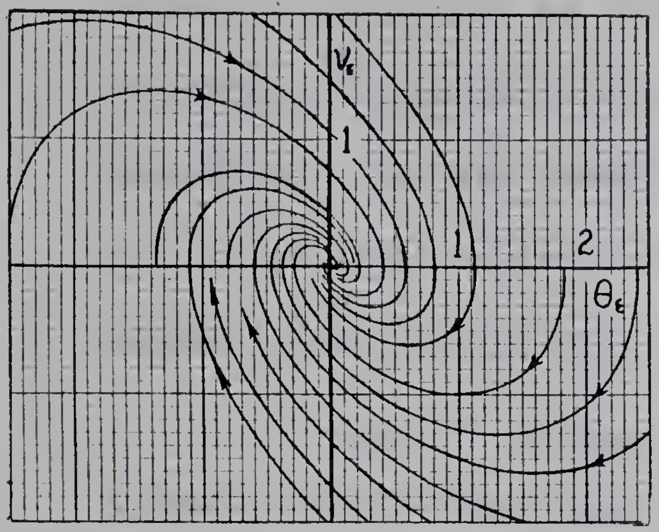

Figure 7.3 Phase Plane Diagram of Linear System

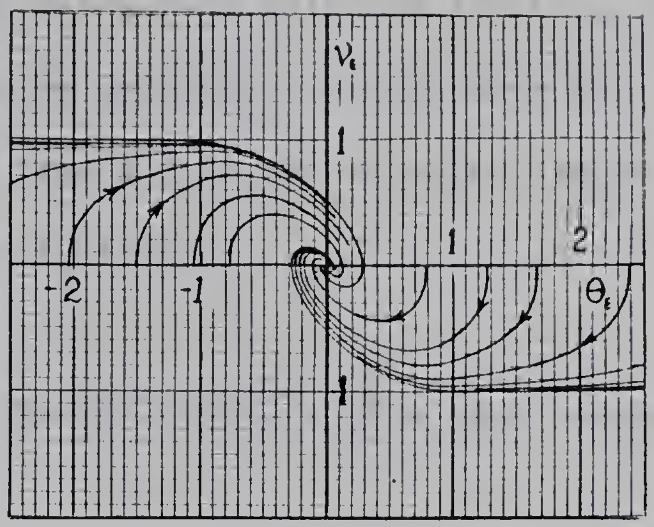

Figure 7.4 Effect of Velocity Limiting

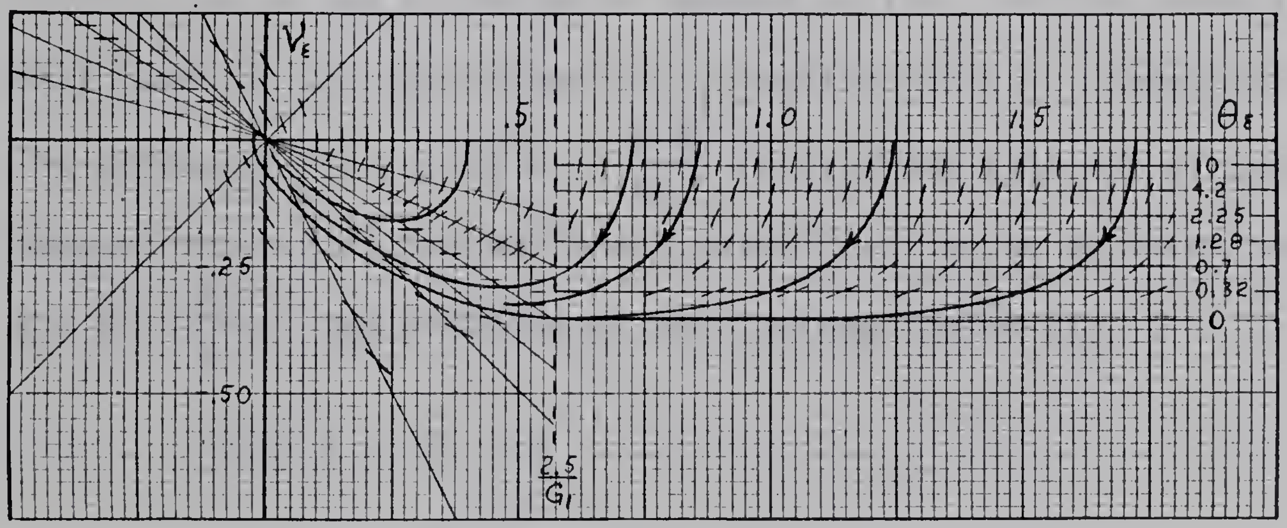

Figure 7.5 Phase Trajectories for $\xi = 0.8$, $G_1 = 4.34$

7.3 A GRAPHICAL ANALYSIS OF TRANSIENT RESPONSE

Although excellent improvement in steady-state error and restoring torque can be obtained using high gain and limiting, the increase in response time caused by velocity limiting must be considered. For the example of figure 7.5, the velocity limits for the physical systems are easily found.

System 1 (modified motor):

$$|\omega_{max}| = \omega_n|\nu_{\varepsilon max}| = .36\sqrt{10 \times 200 \times 4.34} = 33.6 \text{ rad/sec} \quad (7.27)$$

System 2 (unmodified motor):

$$|\omega_{max}| = .36\sqrt{10 \times 300 \times 4.34} = 50.5 \text{ rad/sec} \quad (7.28)$$

Let t_1 be the time spent in the limited region. The relatively low values of velocity imposed by the limiting characteristic will cause quite high values of t_1, particularly for large increments. The variation of t_1 with $\Theta_i - \frac{2.5}{G_1}$ for various settings of gain and damping ratio will now be investigated for the two physical systems.

For $\Theta_i > \frac{2.5}{G_1}$, the velocity in the limited region is

$$\omega(t) = \omega_f \, (1 - e^{-t/\tau}) \quad (7.29)$$

where $\tau = (2\xi\omega_n)^{-1} = (2\xi\sqrt{G_1}\,\sqrt{10K})^{-1}$ (7.30)

and $\omega_f = 25K\tau = \dfrac{1.25\sqrt{10K}}{\xi\sqrt{G_1}}$ (7.31)

It is reasonable then to use the factor $\xi\sqrt{G_1}$ as a parameter in the analysis.

Let $\eta = \xi\sqrt{G_1}$ (7.32)

For the unmodified motor ($\tau_m \simeq 0.06$)

$$\eta_{min} = \frac{1}{2\tau_m\sqrt{10K}} = 0.152 \quad (7.33)$$

$$\tau(\eta) = \frac{1}{2\sqrt{10K}\,\eta} = (109.6\ \eta)^{-1} \quad (7.34)$$

$$\omega_f(\eta) = \frac{1.25\sqrt{10K}}{\eta} = \frac{68.5}{\eta} \tag{7.35}$$

$$\omega_{f_{max}} = \frac{68.5}{\eta_{min}} = 450 \frac{rad}{sec} \tag{7.36}$$

For the modified motor ($\tau_m \simeq .12$)

$$\eta_{min} = 0.0933 \tag{7.37}$$

$$\tau(\eta) = (89.4\eta)^{-1} \tag{7.38}$$

$$\omega_f(\eta) = \frac{55.9}{\eta} \tag{7.39}$$

$$\omega_{f_{max}} = 600\frac{rad}{sec} \tag{7.40}$$

The angular distance travelled in time t_1 is

$$\Theta_i - \frac{2.5}{G_1} = \int_o^{t_1} \omega_f \; (1 - e^{-t/\tau}) \; dt \tag{7.41}$$

$$= \omega_f(t_1 + \tau e^{-t_1/\tau} - \tau) \tag{7.42}$$

Rearranging and substituting, the following expressions result for the unmodified and modified motors respectively:

$$109.6\eta t_1 + e^{-109.6\eta t_1} = 1 + 1.6\eta^2(\Theta_i - \frac{2.5}{G_1}) \tag{7.43}$$

$$89.4\eta t_1 + e^{-89.4\eta t_1} = 1 + 1.6\eta^2(\Theta_i - \frac{2.5}{G_1}) \tag{7.44}$$

Since t_1 cannot be expressed as a direct function of the term $\Theta_i - 2.5/G_1$, it was obtained graphically and is shown in figures 7.6 and 7.7 for various values of η.

It can be seen that as η is increased (or, for a particular value of ξ, as G_1 is increased), the time spent in the limited region becomes nearly proportional to the width of the limited region ($\Theta_i - 2.5/G_1$), that is, the exponential term in equation 7.42 becomes nearly insignificant.

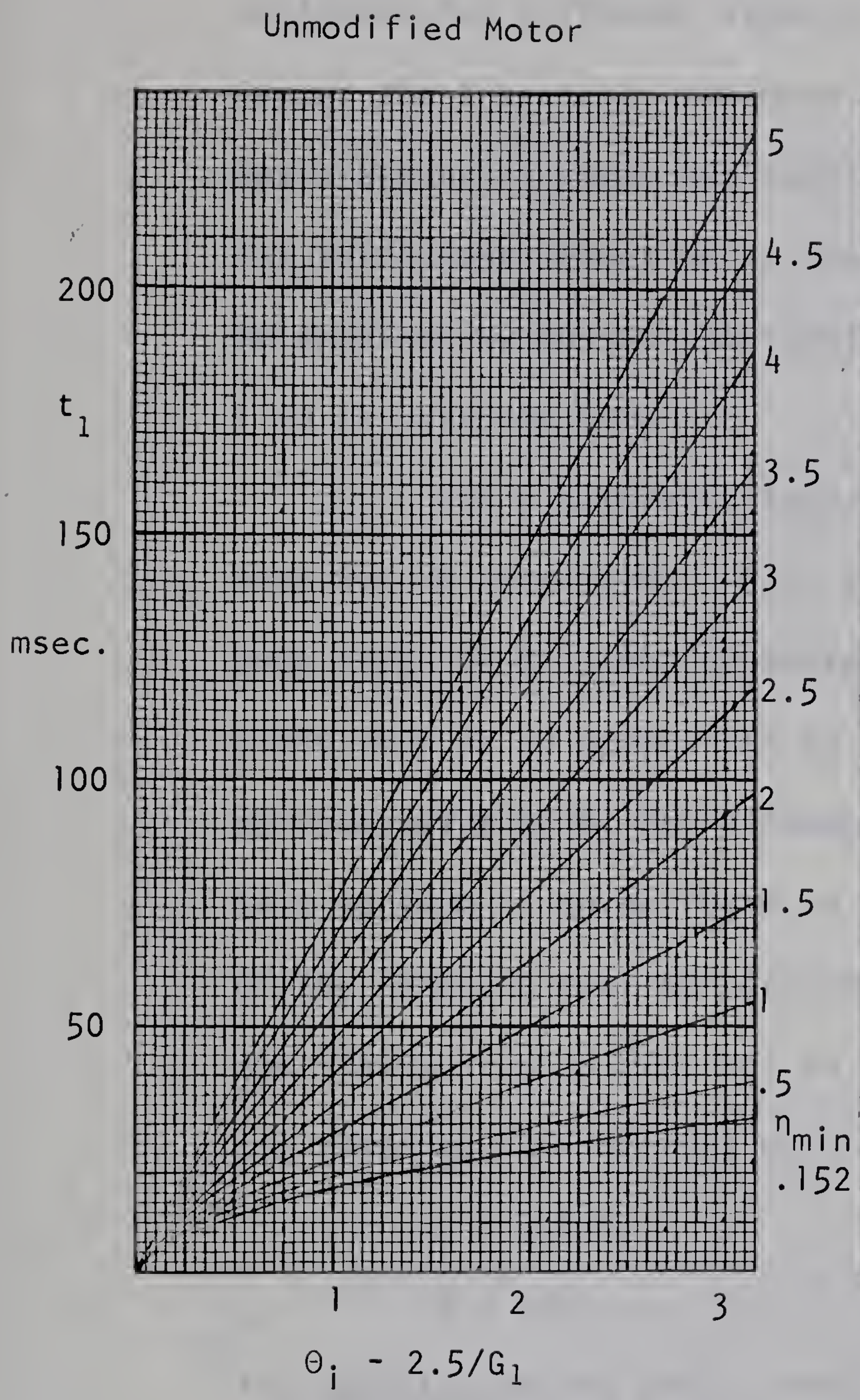

Figure 7.6

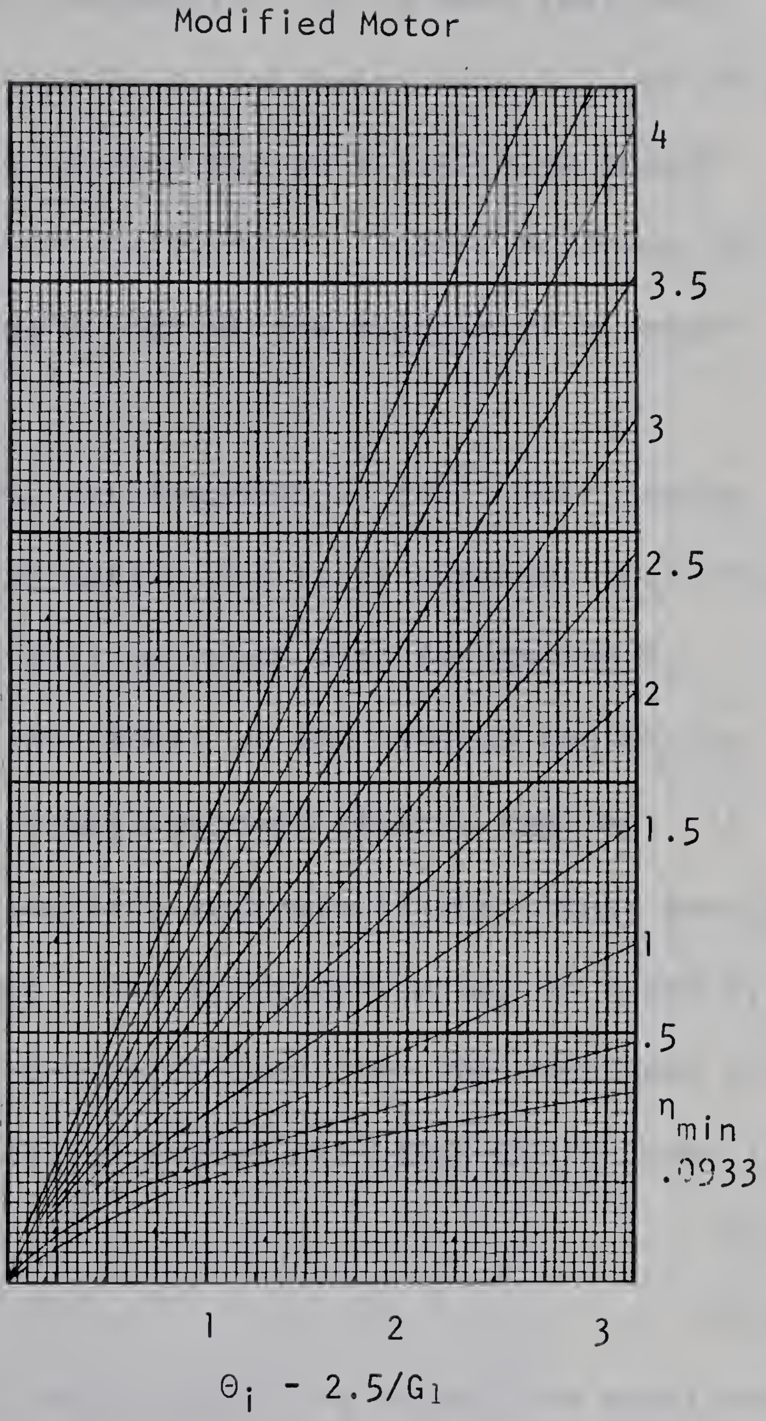

Figure 7.7

Times Spent in the Velocity Limited Regions

From these curves, the variation of t_1 with gain G_1 can be obtained. For a practical value of $\xi = 0.8$ figure 7.11 shows this variation for different sizes of increments. It is seen that the larger the increment, the more rapidly t_1 increases with G_1. On this basis alone, it seems desireable to keep the gain just high enough for sufficient reduction of steady-state error. Better accuracy can be obtained by further increasing G_1 but at the expense of a reduction in response time.

For a complete picture, the response in the linear region must now be considered. From expression 7.5 it is apparent that the peak time for a linear response will decrease with increasing G_1. Since this is in opposition to the effect in the limited region, an optimum value of G_1 for minimum total response time is implied. If this optimum is to be found, a complete analysis of the linear portion of the response must be performed. For practical values of ξ and G_1, the limited region will not be re-entered such that the remainder of the response will be that of a linear system with the initial conditions

$$\Theta = 2.5/G_1 \qquad (7.45)$$

$$\dot{\Theta} = \omega(t_1) \qquad (7.46)$$

The velocity at the end of the limited region is found from equation 7.42

$$\omega(t_1) = 25Kt_1 - \sqrt{40K}\,\eta(\Theta_i - 2.5/G_1) \qquad (7.47)$$

This velocity is plotted as a function of the width of the limited region in figures 7.8 and 7.9 again with η as a parameter.

It can be seen that for small values of η, the limiting velocity ω_f is never reached and for large values the velocity becomes constant at ω_f except for very small increments.

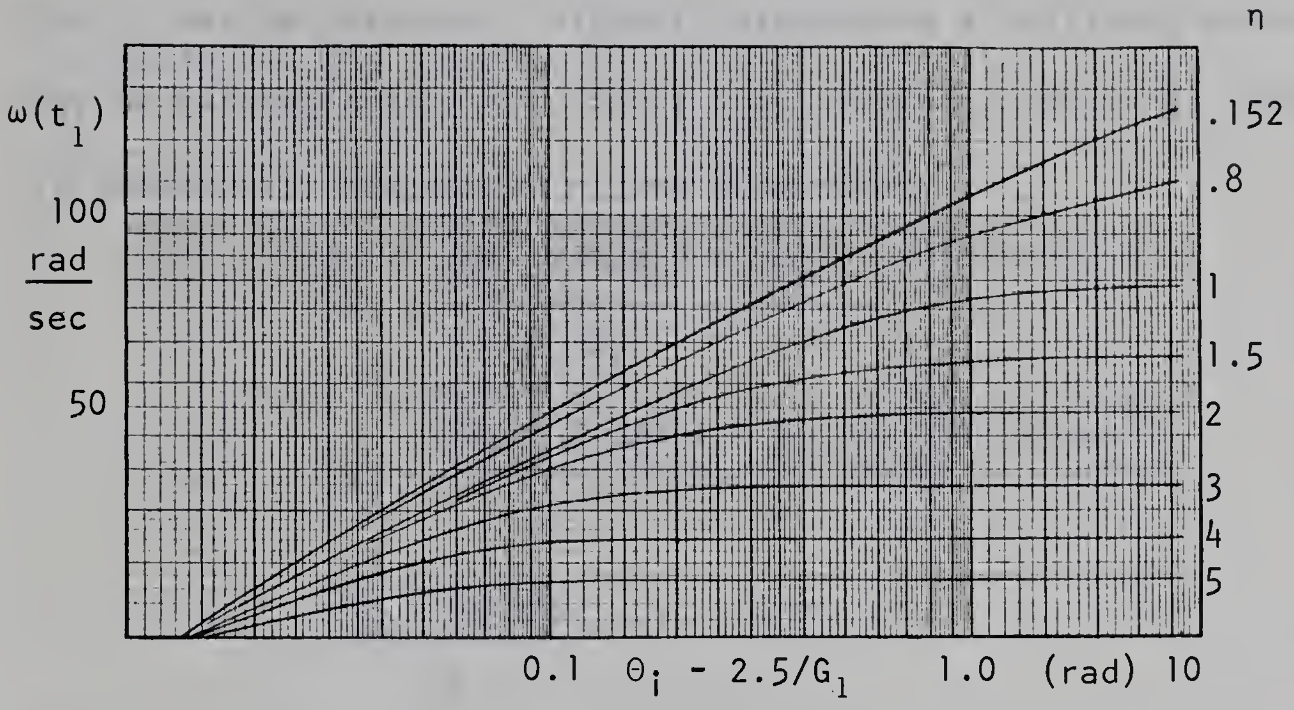

Figure 7.8 Velocity at Time of Exit From Limited Region - Unmodified Motor

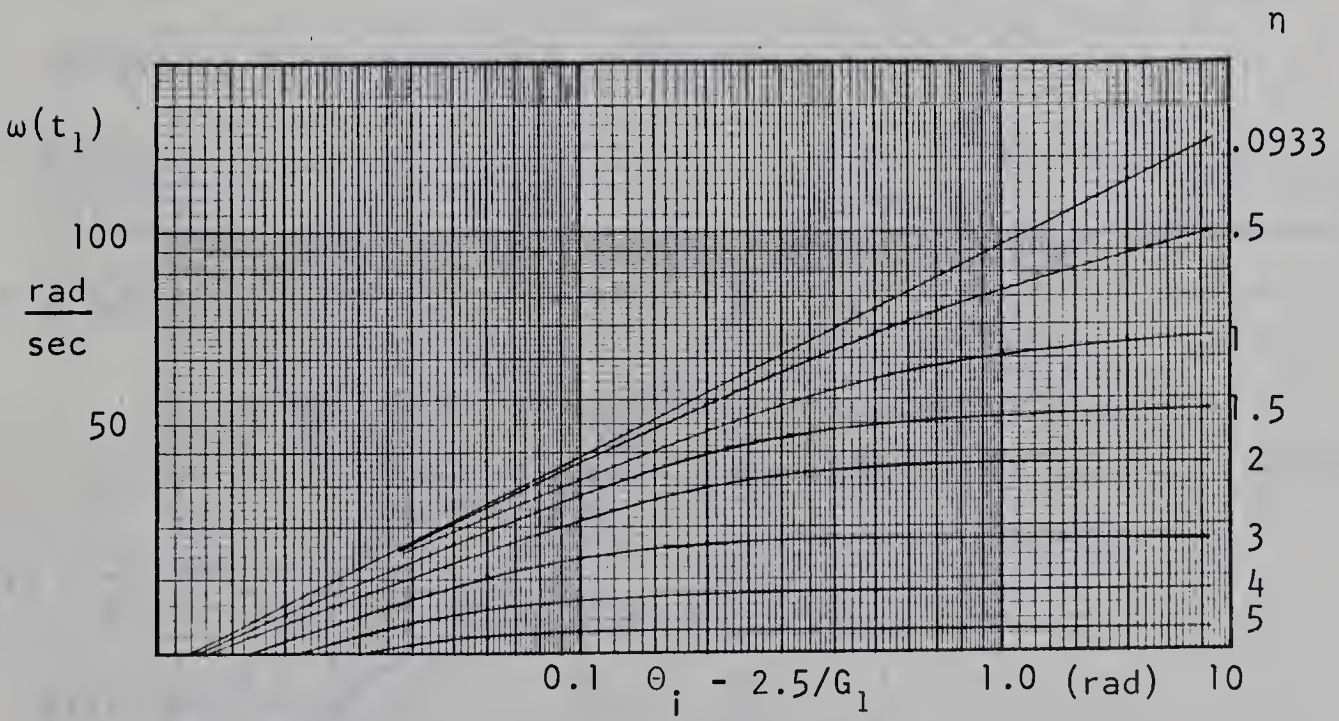

Figure 7.9 Velocity at Time of Exit From Limited Region - Modified Motor

Consider the response shown in figure 7.10. For cases in which the majority of the time spent in the limited region is undergone at the limiting velocity (i.e. very near ω_f), an approximation for t_1 may be obtained. Without introducing significant error, it may be assumed that $\omega \simeq \omega_f$ for $t > n\tau$, that is, the final velocity is essentially reached in n time constants.

$$t_1 \simeq n\tau + \frac{(\Theta_i - 2.5/G_1) - \Theta(n\tau)}{\omega_f} \tag{7.48}$$

$$\simeq n\tau + \frac{(\Theta_i - 2.5/G_1) - \omega_f\left((n-1)\tau + \tau e^{-n}\right)}{\omega_f} \tag{7.49}$$

$$\simeq \frac{\Theta_i - 2.5/G_1}{\omega_f} + \tau\left(1 - e^{-n}\right) \tag{7.50}$$

Providing n is sufficiently large such that $e^{-n} << 1$, then

$$t_1 = \tau + \frac{\Theta_i - 2.5/G_1}{\omega_f} \tag{7.51}$$

In figure 7.10, the value n = 3 is used.

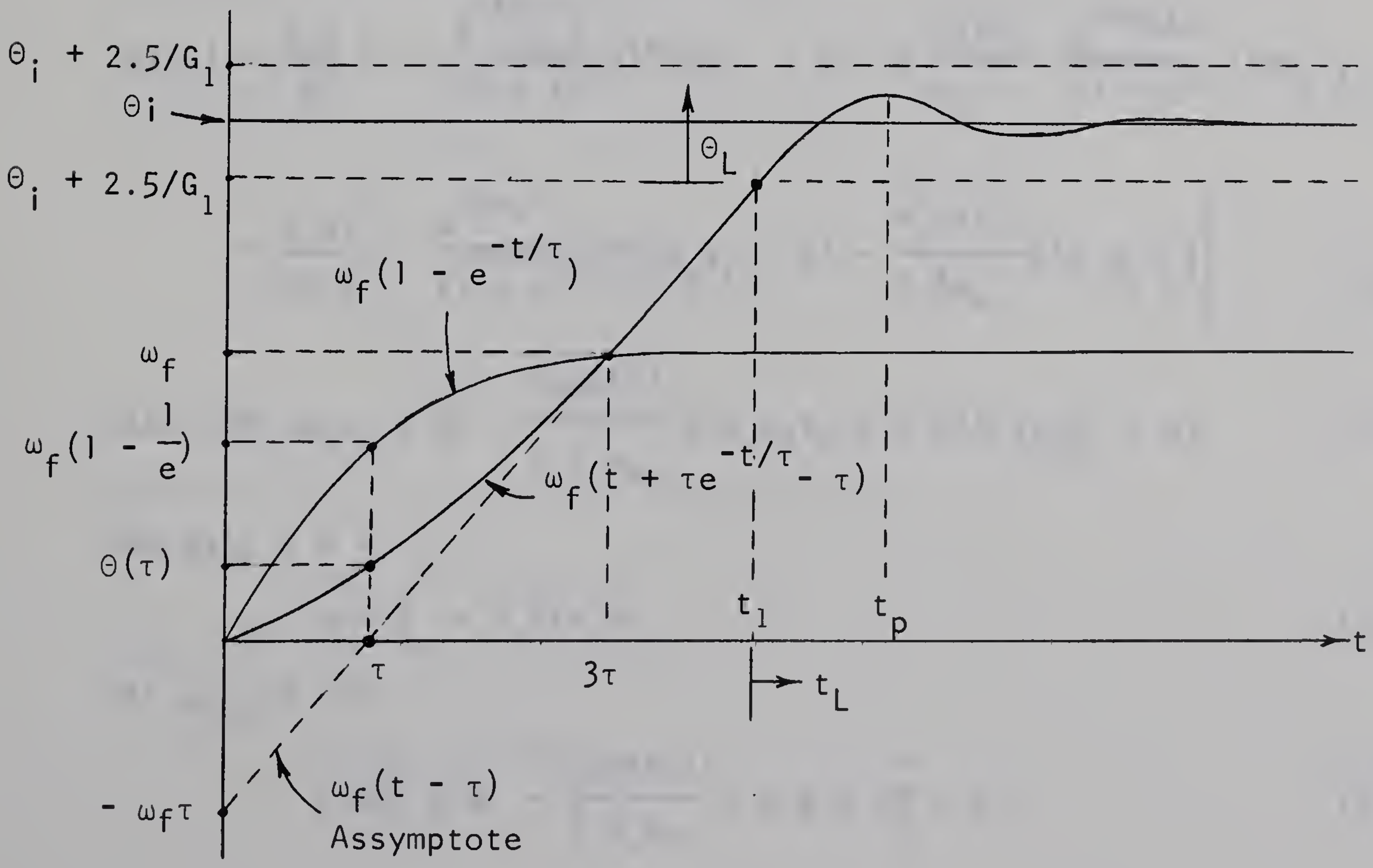

Figure 7.10 Approximation of Time Spent in Limited Region

To simplify analysis of the linear portion of the response,

let $$t_L = t - t_1 \qquad (7.52)$$

$$\Theta_L = \Theta - (\Theta_i - \frac{2.5}{G_1}) \qquad (7.53)$$

Then, on this new time basis

$$\Theta_L(0) = 0 \qquad (7.54)$$

$$\dot{\Theta}_L(0) = \omega(t_1) \qquad (7.55)$$

$$\Theta_{iL} = 2.5/G_1 \qquad (7.56)$$

$$t_{pL} = t_p - t_1 \qquad (7.57)$$

If $$F_L(s) = \mathcal{L}(f(t_L)) \qquad (7.58)$$

then $$\Theta_{iL}(s) = 2.5/sG_1 \qquad (7.59)$$

and $$\Theta_L(s) = \frac{\omega_n^2(2.5/G_1) + s\ \omega(t_1)}{s(s^2 + 2\xi\omega_n s + \omega_n^2)} \qquad (7.60)$$

From the inverse Laplace transform

$$\Theta(t_L) = \frac{2.5}{G_1}\left(1 - \frac{e^{-\xi\omega_n t_L}}{\sqrt{1-\xi^2}} \text{SIN}(\omega_d t_L + \phi)\right) + \frac{\omega(t_1)}{\omega_n} \frac{e^{-\xi\omega_n t_L}}{\sqrt{1-\xi^2}} \text{SIN}\omega_d t_L \qquad (7.61)$$

$$= \frac{2.5}{G_1}\left[1 - \frac{e^{-\xi\omega_n t}}{\sqrt{1-\xi^2}}\left(\text{SIN}(\omega_d t_L + \phi) - \frac{G_1\omega(t_1)}{2.5\omega_n}\text{SIN}\ \omega_d t_L\right)\right] \qquad (7.62)$$

Let $$\text{SIN}\ (\omega_d t_L + \phi) - \frac{G_1\omega(t_1)}{2.5\ \omega_n}\ \text{SIN}\ \omega_d t_L + A\ \text{SIN}\ (\omega_d t_L + \alpha) \qquad (7.63)$$

At $\omega_d t_L = 0$:

$$\text{SIN}\ \phi = A\ \text{SIN}\ \alpha \qquad (7.64)$$

At $\omega_d t_L = \pi/2$:

$$\text{SIN}(\frac{\pi}{2} + \phi) - \frac{G_1\omega(t_1)}{2.5\ \omega_n} = A\ \text{SIN}\ (\frac{\pi}{2} + \alpha) \qquad (7.65)$$

or

$$\cos\phi - \frac{G_1\omega(t_1)}{2.5\ \omega_n} = A \cos\alpha \tag{7.66}$$

thus

$$\tan\ \alpha = \frac{\sin\phi}{\cos\phi - \dfrac{G_1\omega(t_1)}{2.5\ \omega_n}} \tag{7.67}$$

$$= \frac{\sqrt{1-\xi^2}}{\xi - \dfrac{G_1\omega(t_1)}{2.5\ \omega_n}} \tag{7.68}$$

and

$$A = \frac{\sin\phi}{\sin\alpha} = \sqrt{1 - \frac{2\xi G_1\omega(t_1)}{2.5\ \omega_n} + \left(\frac{G_1\omega(t_1)}{2.5\ \omega_n}\right)^2} \tag{7.69}$$

The linear portion of the response is given by

$$\Theta(t_L) = \frac{2.5}{G_1}\left(1 - \frac{e^{-\xi\omega_n t_L}}{\sqrt{1-\xi^2}}\quad A \sin\ (\omega_d t_L + \alpha)\right) \tag{7.70}$$

And the velocity can be shown to be

$$\dot{\Theta}(t_L) = \frac{2.5}{G_1}\ \frac{A\ e^{-\xi\omega n t_L}}{\sqrt{1-\xi^2}} \sin\ (\omega_d t_L + \beta) \tag{7.71}$$

where

$$\tan\ \beta = \frac{\omega(t_1)\sqrt{1-\xi^2}}{\dfrac{2.5\omega_n}{\xi G_1} - \omega(t_1)} \tag{7.72}$$

$$= \frac{\omega(t_1)\ \sqrt{1-\xi^2}}{2\ \omega_f - \omega(t1)} \tag{7.73}$$

Setting $\dot{\Theta}(t_L) = 0$ to find the peak time

$$\omega_n\sqrt{1-\xi^2}\quad t_{Lp} + \beta = 0,\ \pi,\ 2\pi\ ,\cdots \tag{7.74}$$

thus the first peak occurs at

$$t_{Lp} = \frac{\pi - \beta}{\omega_n\sqrt{1-\xi^2}} \tag{7.75}$$

In cases where G_1 is large such that $\omega(t_1) \simeq \omega_f$, from equation 7.73

$$\text{TAN } \beta \simeq \sqrt{1 - \xi^2} \tag{7.76}$$

thus

$$\beta_{max} = \text{TAN}^{-1} \sqrt{1 - \xi^2} \tag{7.77}$$

For reasonable values of ξ, then $\beta << \pi$ and t_{Lp} is essentially independent of increment size. It is shown on the same graph as t_1 for the value of $\xi = .8$ in figure 7.11. The total time taken to reach the first peak is shown as the sum:

$$t_p = t_1 + t_{Lp} \tag{7.78}$$

Figure 7.11 now serves as an optimization chart for the unmodified motor (for this particular damping ratio). For example, for steps of up to π radians, the optimum value of G_1 would be in the order of 2 volts per radian whereas if increments of .5 radians or less were applied a gain of about 15 volts/rad. should be used. It should be noticed that the chart becomes increasingly inaccurate as G_1 is decreased since the dead zone effect which was neglected in the derivation becomes more significant. It is generally desireable to use values of G_1 somewhat larger than the optimum to improve system accuracy. The resulting increase in peak time is not too large due to the rather broad minima of the curves $t_p(G_1)$.

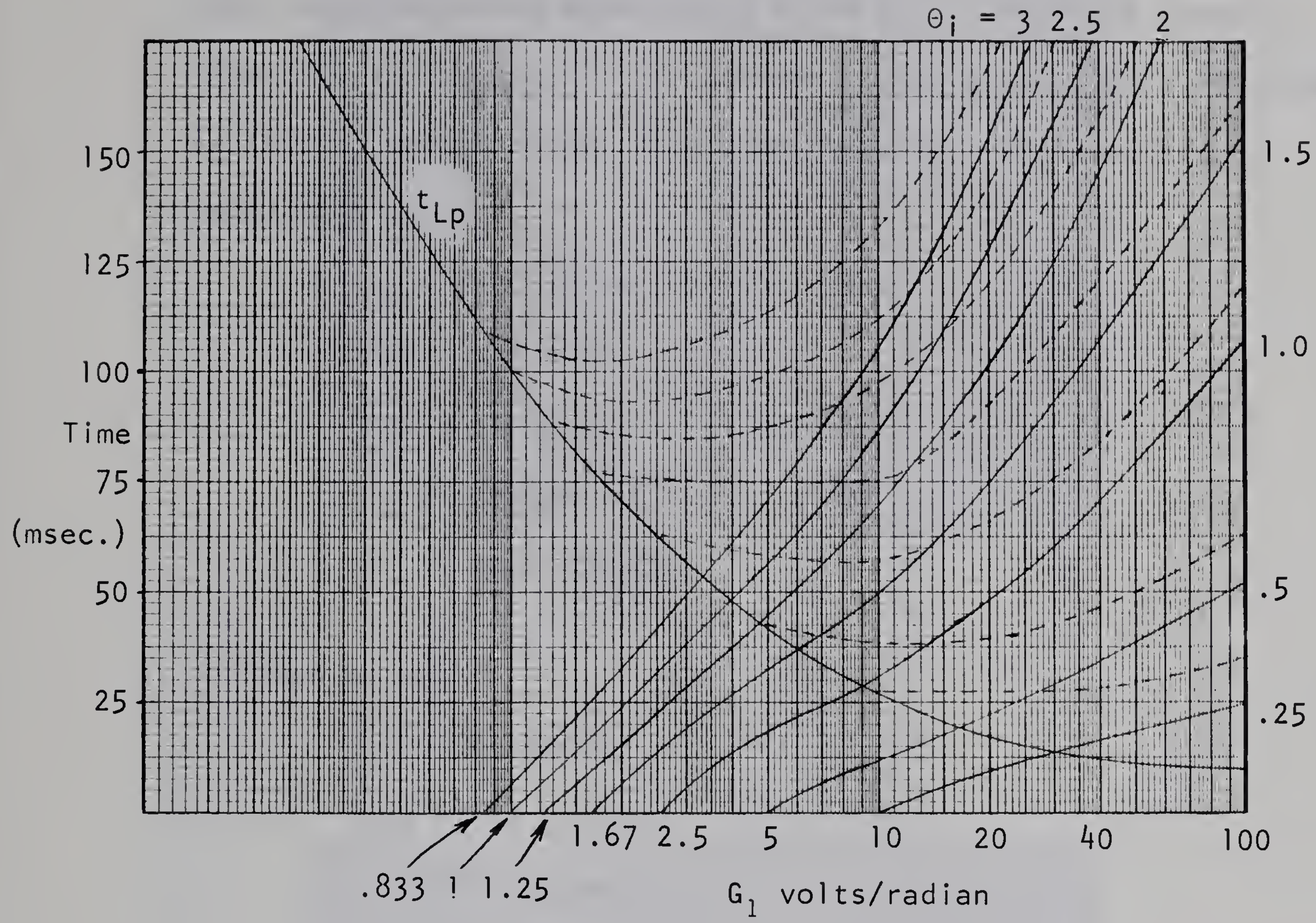

Figure 7.11 Optimization Chart for Minimizing Peak Times

——— t_1 and t_{Lp}

– – – – – t_p

7.4 EXPERIMENTAL RESULTS AND SUMMARY

The motor constants were first checked from the undamped step responses using equations 7.6 and 7.7. These are shown in figures 7.12 and 7.13. The increment size is about 20°. Vertical scales are uncalibrated. For both cases $G_1 = 4.34$ volts/rad.

Unmodified motor:

$\omega_d \simeq 113$ rad/sec

$\log A_1/A_2 \simeq .35$

$K \simeq 295$ rad/volt

$\tau_m \simeq .070$ sec

$K\tau_m \simeq 20.7 \frac{\text{rad/sec}}{\text{volt}}$

Modified motor:

$\omega_d \simeq 91$ rad/sec

$\log A_1/A_2 \simeq 0.25$

$K \simeq 191$ rad/volt

$\tau_m \simeq 0.135$ sec

$K\tau_m \simeq 25.8$ rad/sec

Agreement with the calculated values obtained (Section 3.8) and the measured values of τ_m (Sections 4.2 and 4.4) is seen to be quite good. The product $K\tau_m$ which is the D.C. value of the transfer function is also seen to closely agree with the measured slopes of the velocity transfer characteristics (Section 3.7).

Typical step responses are shown in figures 7.14 to 7.24 for various sizes of increment, gains and damping ratios. It was found that the subtraction method of tachometer feedback became difficult to use for gains greater than about 3 volts per radian.

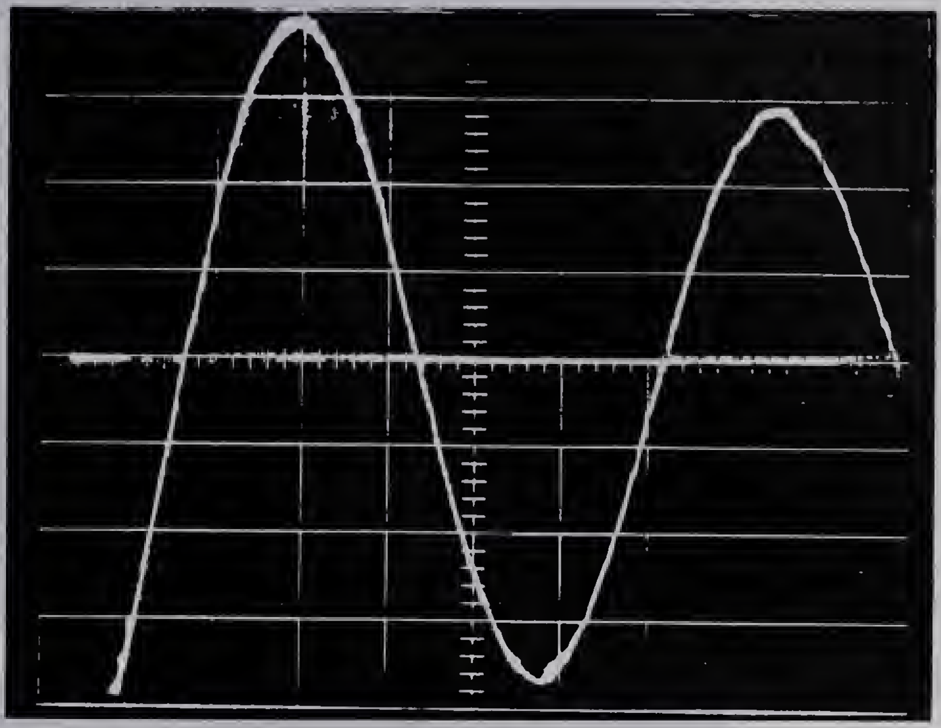

Figure 7.12

Undamped Response of Unmodified Motor

10 msec./div. horizontal

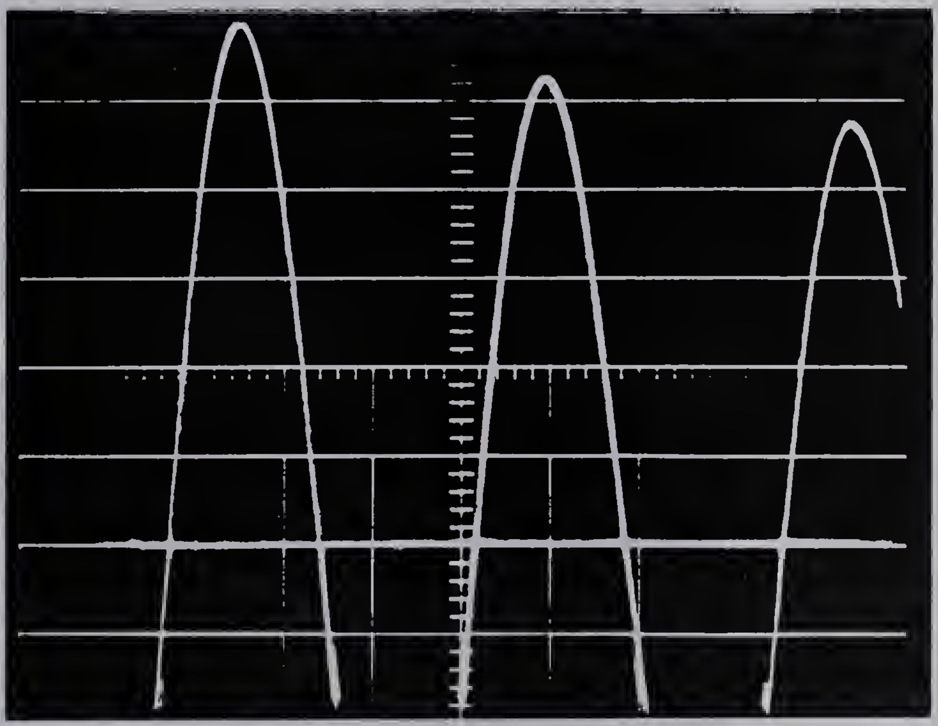

Figure 7.13

Undamped Response of Modified Motor

20 msec./div. horizontal

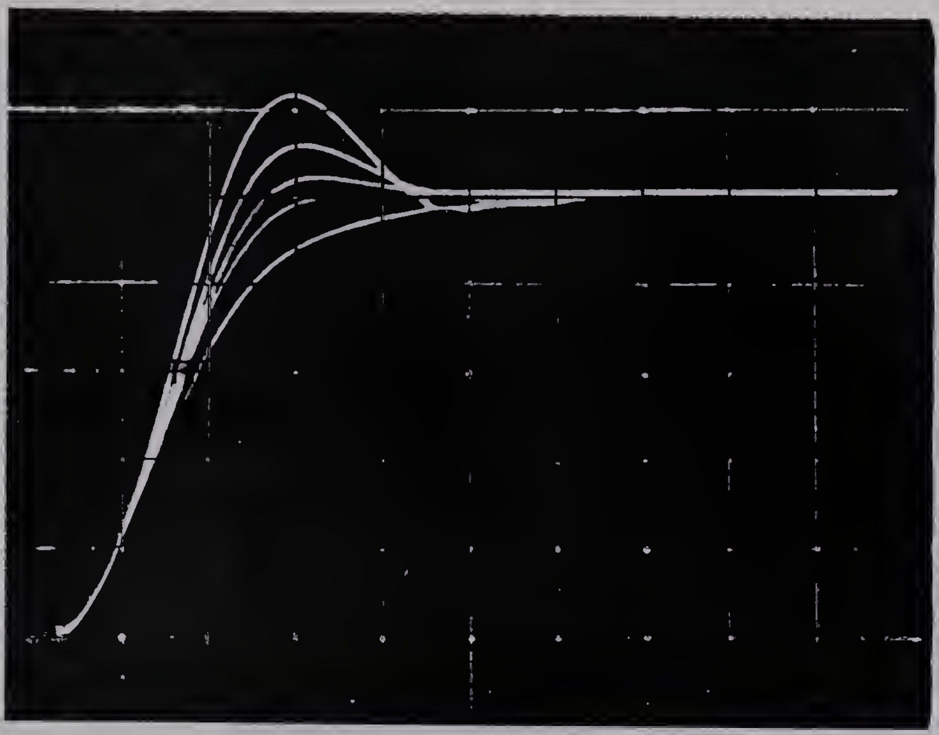

Figure 7.14

System 1, G_1 = 2.17

2 volts/div. vertical

20 msec./div. horiz.

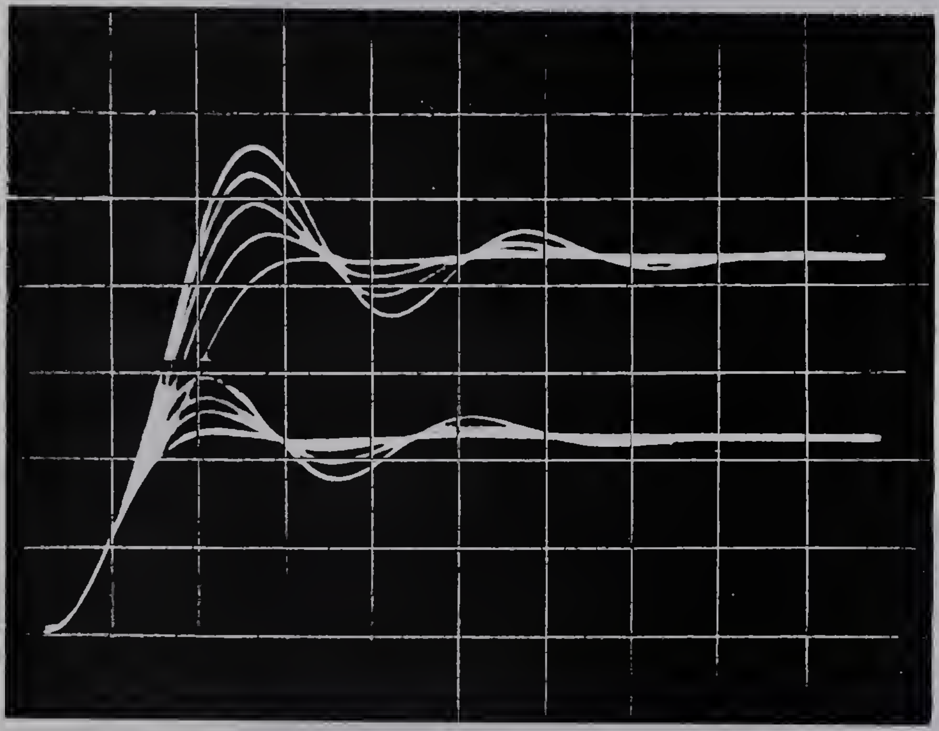

Figure 7.15

System 1, G_1 = 4.34

2 volts/div. vertical

20 msec./div. horiz.

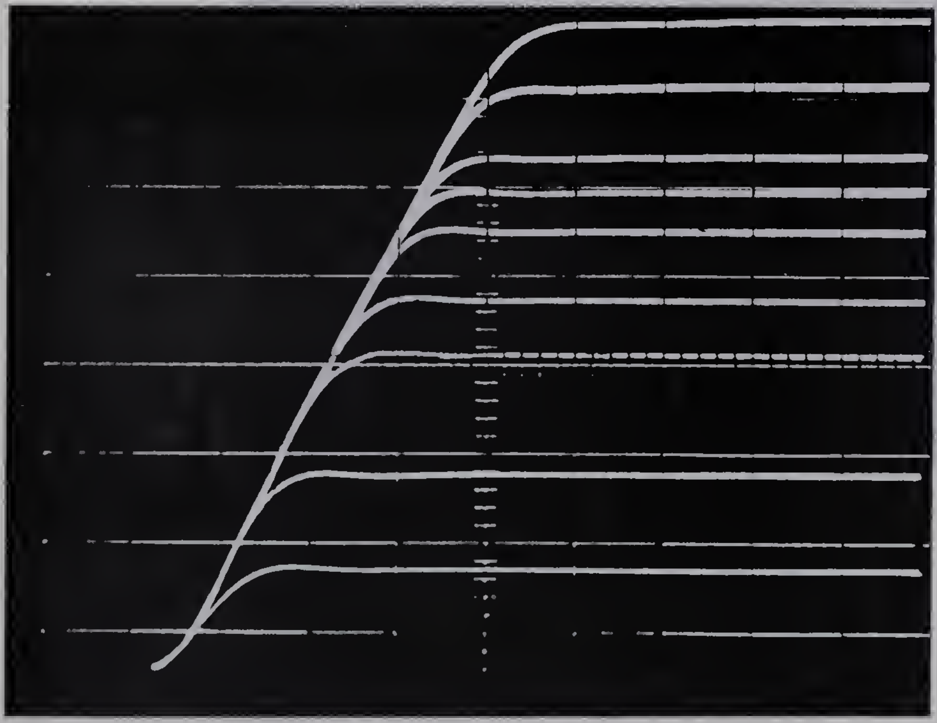

Figure 7.16

System 1, G_1 = 4.34

Constant Damping

2 volts/div. vertical

20 msec./div. horiz.

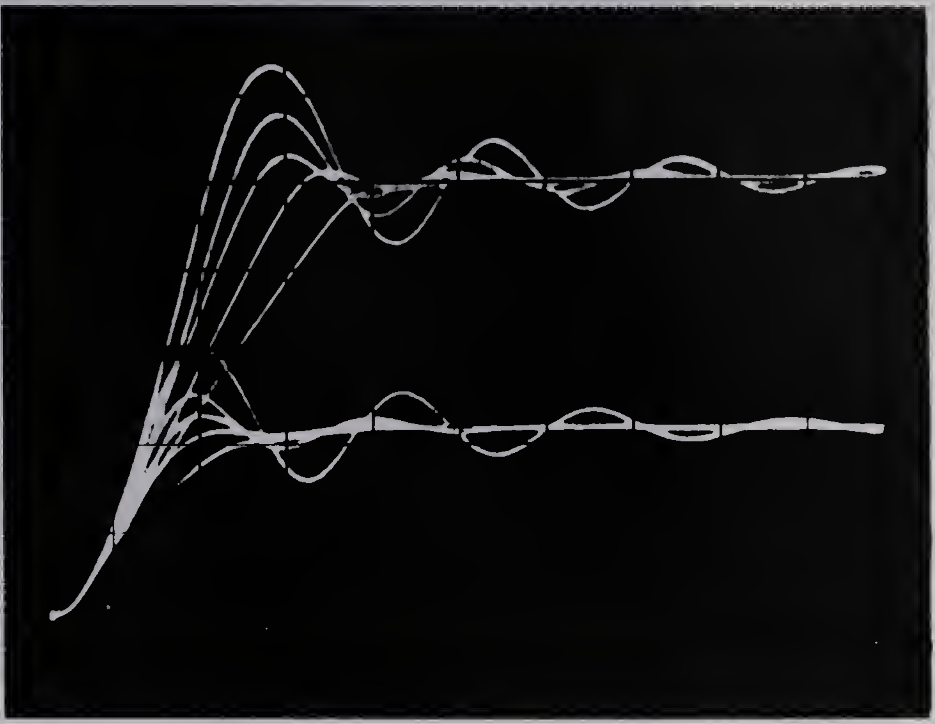

Figure 7.17 System 1, $G_1 = 8.68$

2 volts/div. vertical

20 msec./div. horiz.

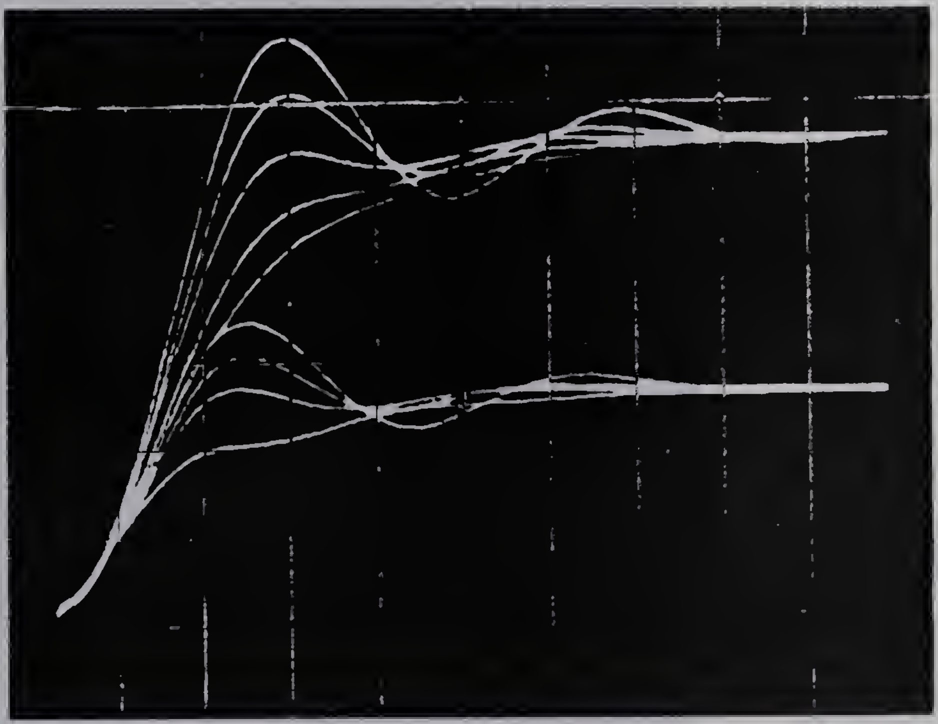

Figure 7.18 System 1, $G_1 = 8.68$

.5 volt/div. vertical

10 msec./div. horiz.

[illegible]

[illegible]

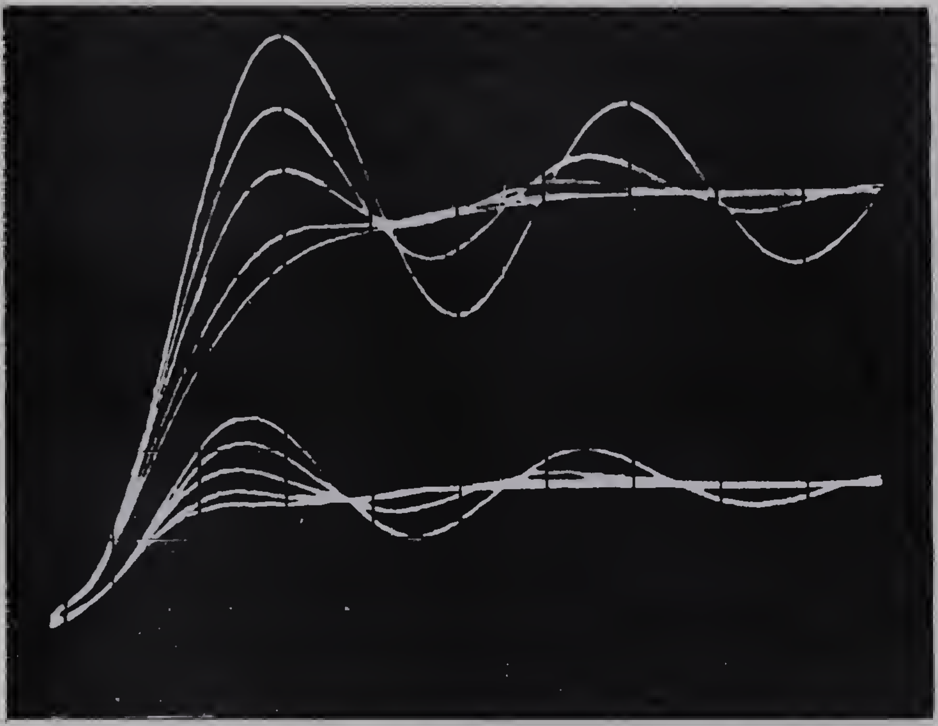

Figure 7.19
System 1, G_1 = 10.9

.5 volt/div. vertical
10 msec./div. horiz.

.5 volt/div. vertical
5 msec./div. horiz.

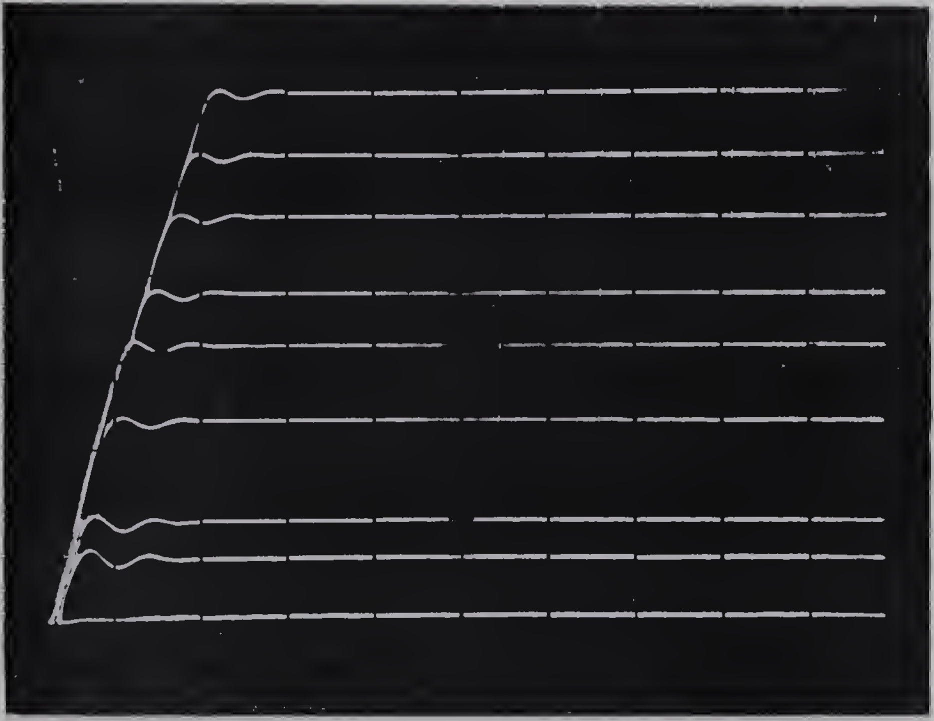

Figure 7.20

System 1, G_1 = 10.9

Constant damping

2 volts/div. vertical

50 msec./div. horiz.

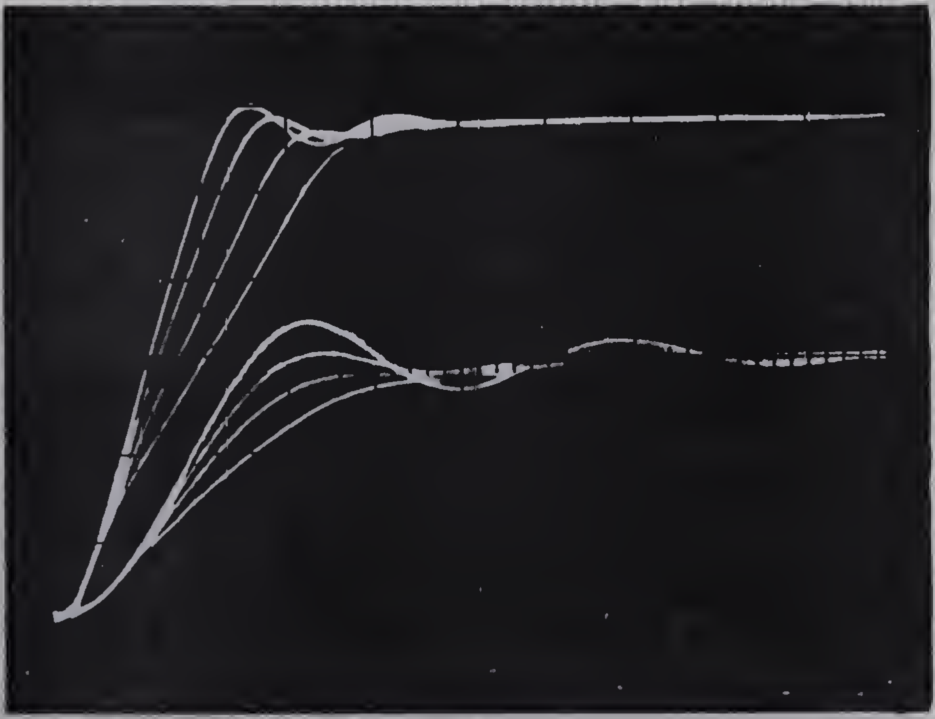

1 volt/div. vertical
20 msec./div. horiz.

1 volt/div. vertical
10 msec./div. horiz.

Figure 7.21
System 1, G_1 = 10.9

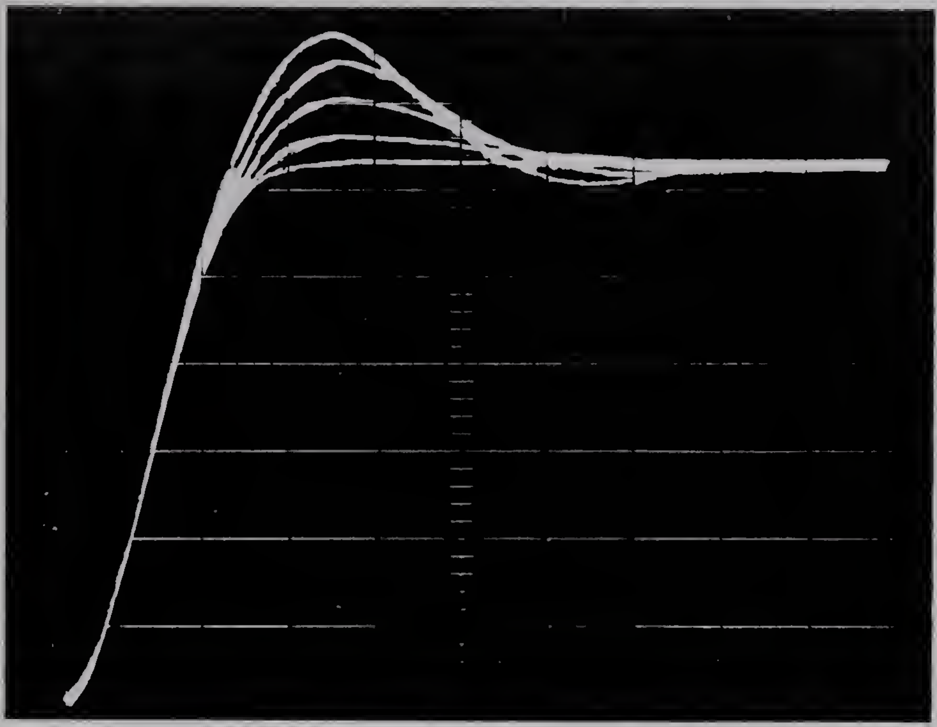

Figure 7.22

System 2, $G_1 = 2.17$

.5 volt/div. vertical

10 msec./div. horiz.

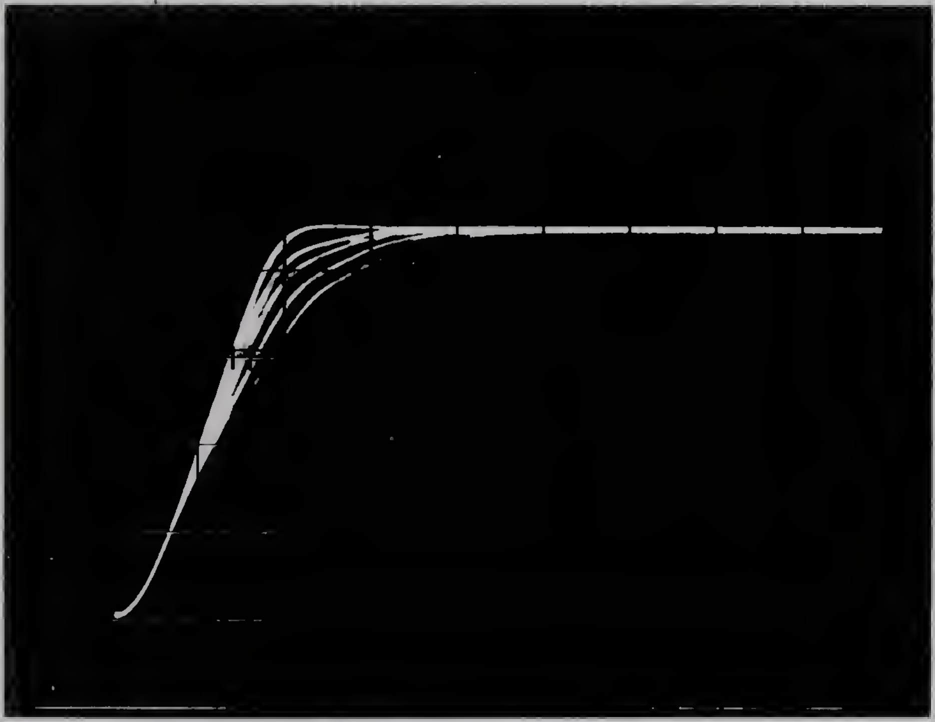

Figure 7.23

System 2, $G_1 = 2.17$

2 volts/div. vertical

20 msec./div. horiz.

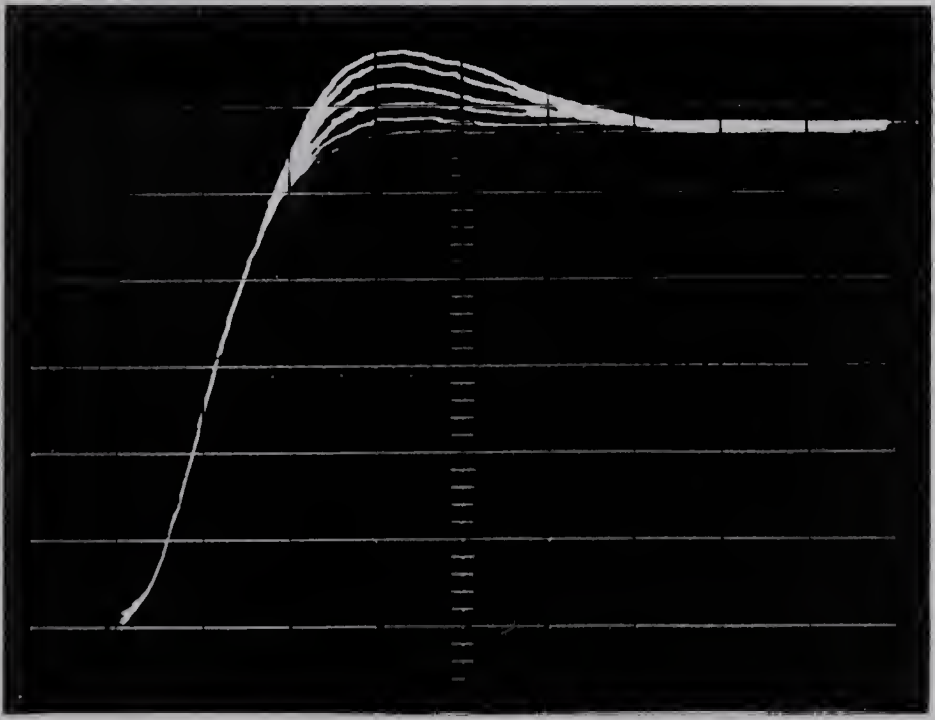

Figure 7.24

System 2, $G_1 = 2.17$

.2 volt/div. vertical

10 msec./div. horiz.

CHAPTER 8

DERIVATIVE OF ERROR CONTROL

8.1 INTRODUCTION

It has heretofore been assumed that rate damping is accomplished by the derivative of the output, that is, by a signal proportional to shaft velocity from the tachometer or subtraction method. It is equally reasonable to use the derivative of the error since $\omega_\varepsilon = -\omega$ for a step input. Such a system is shown in figure 8.1.

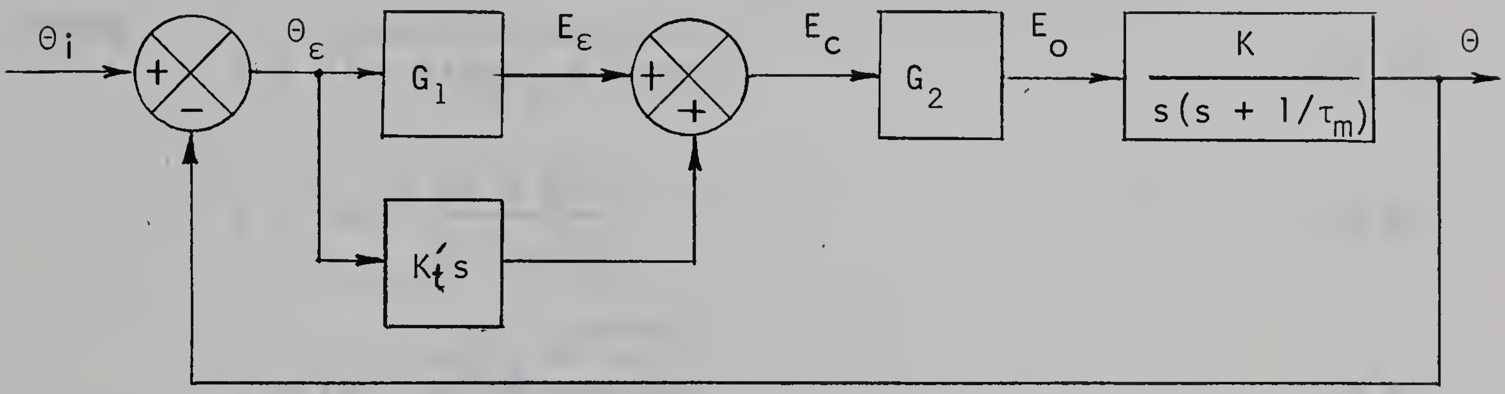

Figure 8.1 Derivative Of Error Control System

8.2 LINEAR ANALYSIS OF TRANSIENT RESPONSE

It can be shown that since derivative control is an anticipatory type, the response is slightly different from the tachometer feedback system.

The open-loop transfer function is given by

$$\frac{\Theta(s)}{\Theta_\varepsilon(s)} = \frac{\omega_n^2\left(1 + \frac{sK_t'}{G_1}\right)}{s(s + 1/\tau_m)} \tag{8.1}$$

It is seen to have a zero at $s = -\frac{G_1}{K_t'}$ which will be shown to give the derivative controlled system a slightly faster rise time than the tachometer feedback system.

The closed-loop transfer function is

$$\frac{\Theta(s)}{\Theta_i(s)} = \frac{\omega_n^2(1 + sK_t'/G_1)}{s^2 + 2\xi\omega_n s + \omega_n^2} \tag{8.2}$$

where $$2\xi\omega_n = 1/\tau_m + K_t' K G_2 \tag{8.3}$$

[illegible]

[illegible]

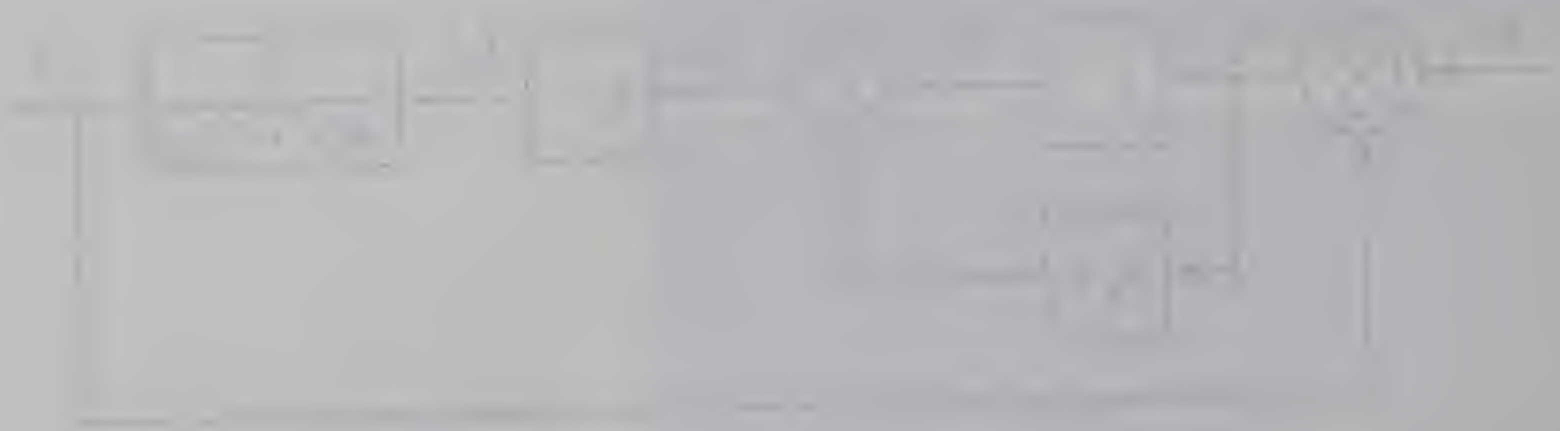

[illegible]

[illegible]

[illegible]

$$[illegible]$$

[illegible]

[illegible]

$$[illegible]$$

For a step input the form of $\Theta(s)$ is identical to that of equation 7.60. The derivation will not be repeated.

For convenience, let $\tau_d = K t'/G_1$ (8.4)

It can be shown that

$$\Theta(t) = \Theta_i \left(1 - \frac{e^{-\xi\omega_n t}}{\sqrt{1 - \xi^2}} C \ \mathrm{SIN}(\omega_n\sqrt{1 - \xi^2}t + \gamma)\right) \tag{8.5}$$

$$\omega(t) = \frac{\Theta_i C \omega_n e^{-\xi\omega_n t}}{\sqrt{1 - \xi^2}} \ \mathrm{SIN}(\omega_n\sqrt{1 - \xi^2}\ t + \delta) \tag{8.6}$$

where

$$C = \sqrt{1 - 2\xi\omega_n\tau_d + (\omega_n\tau_d)^2} \tag{8.7}$$

$$\gamma = \mathrm{TAN}^{-1}\left(\frac{\sqrt{1 - \xi^2}}{\xi - \omega_n\tau_d}\right) \tag{8.8}$$

$$\delta = \mathrm{TAN}^{-1}\left(\frac{\omega_n\tau_d\ \sqrt{1 - \xi^2}}{1 - \xi\omega_n\tau_d}\right) \tag{8.9}$$

Equating $\omega(t_p)$ to zero, it can then be shown that

$$t_p = \frac{\pi - \delta}{\omega_n\sqrt{1 - \xi^2}} \tag{8.10}$$

$$\Theta(t_p) = \Theta_i e^{-\xi(\pi - \delta)/\sqrt{1 - \xi^2}} \left(\frac{C^2 + 2\xi\omega_n\tau_d}{C}\right) \tag{8.11}$$

Thus the peak time is seen to be reduced by

$$\frac{\delta}{\omega_n\sqrt{1 - \xi^2}} \text{ seconds}$$

8.3 EXPERIMENTAL RESULTS

Experimental results were obtained using derivative control of the position error limited system with the unmodified printed motor. The differentiator was designed to limit high frequency noise and have very low D.C. gain. It is shown in figure A 4.8. The phase plane analysis is identical to that of Section 7 (equations 7.10 to 7.21). An additional unity-gain error-detector was added in the forward path in order to obtain access to the actual error signal. Typical responses are shown in figures 8.2 to 8.6 and are briefly discussed:

Figure 8.2: $G_1 = 4.34$ (linear region ≃ 33°). $C_i = .1\mu f$.
Response is nearly linear ($\Theta_i \simeq 36°$).
Peak times are approximately 23 msec.

Figure 8.3: $G_1 = 4.34$, response highly non-linear ($\Theta_i \simeq 140°$).
Slope of velocity-limited region is seen to increase with damping ratio. Peak time are about 40 msec.

Figure 8.4: $G_1 = 4.34$, damping is kept constant.
Largest increment is approximately 173°.
Longest peak time is about 60 msec.

Figure 8.5: $G_1 = 8.68$, damping is kept constant. $C_i = .013\mu f$.
Both positive and negative increments are shown.
Largest increment is approximately 170°.
Longest peak time is about 70 msec.

Figure 8.6: $G_1 = 8.68$, $C_i = .02\mu f$.
Very small increments are shown (largest is ≃ 7°).
Two different damping ratios used for each.
Note step-like nature due to potentiometer resolution.
Note finite steady-state error for smallest increment.
Response is entirely linear. Peak times are about 12 msec.

8.4 SUMMARY

Although the theoretical behaviour of the derivative-controlled system is somewhat better than that with tachometer feedback, reliable operation of the differentiator is not good in practice.

It was found that attempts to use gains of $G_1 > 8$ volts/rad. gave rise to a rather noisy system causing the motor to actually buzz in its final position.

It must be realized that the analysis given is based on use of an ideal differentiator, whereas the transfer function of that used was of the form

$$K_1 \frac{1 + as}{1 + bs} \tag{8.12}$$

where $a >> 1$ (8.13)

$b << 1$ (8.14)

A more detailed treatment of the system using a physically realizeable network will be given in Chapter 12.

The improvement in response time can be explained from equation 8.2. There is almost no velocity lag because of the term sK_t/G_1. That is, for a ramp (constant velocity) input, when the steady state is reached, $\theta \simeq \theta_i$, whereas this is not true for the velocity feedback system.

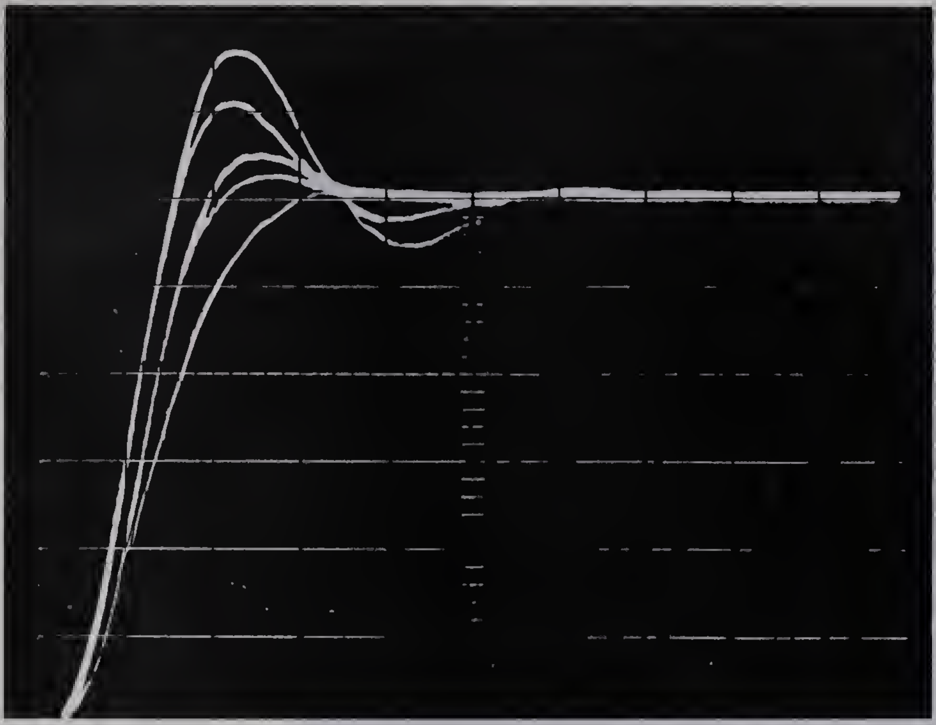

Figure 8.2

.5 volts/div. vertical

10 msec./div. horiz.

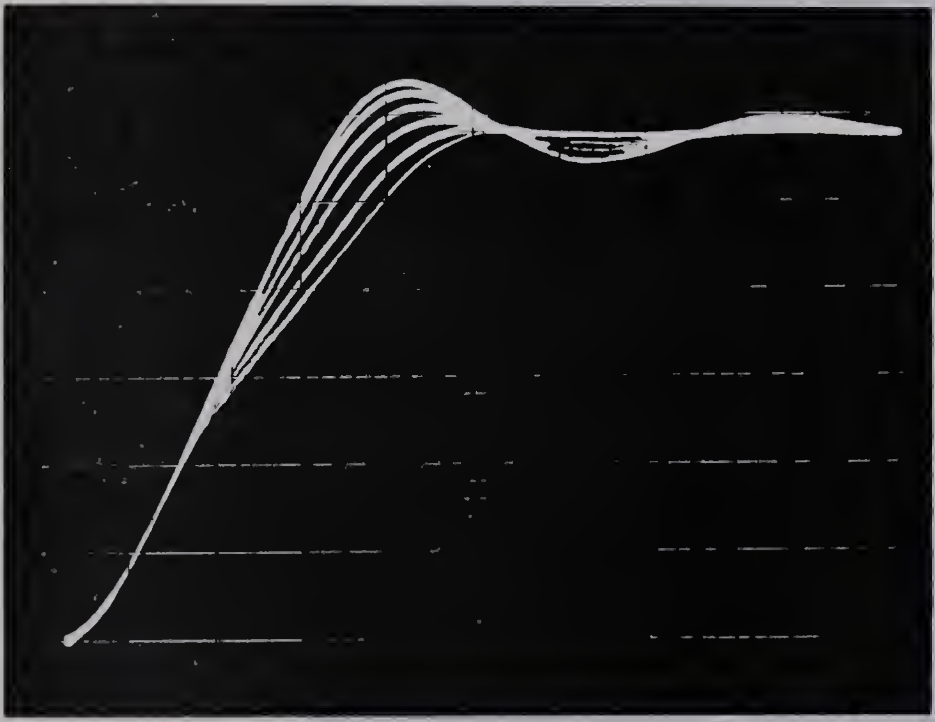

Figure 8.3

2 volts/div. vertical

10 msec./div. horiz.

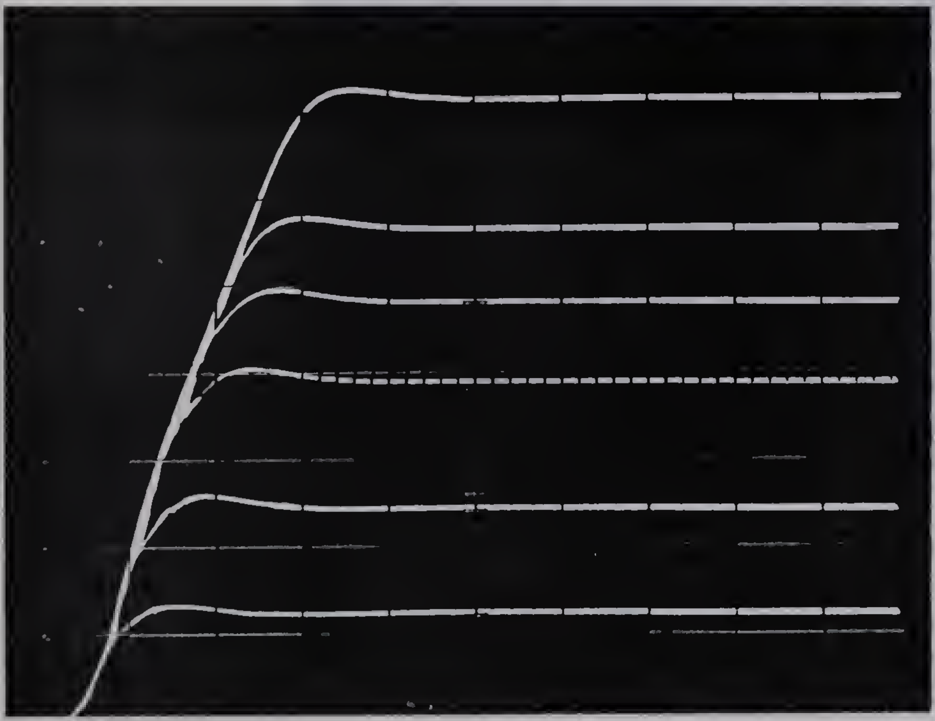

Figure 8.4

2 volts/div. vertical

20 msec./div. horiz.

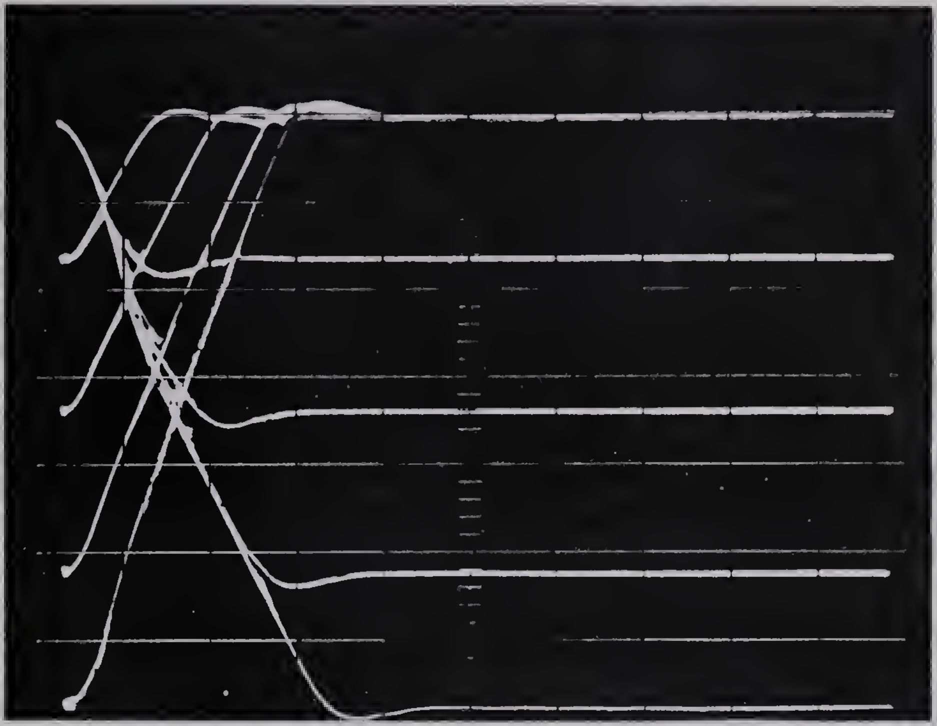

Figure 8.5

2 volts/div. vertical

20 msec./div. horiz.

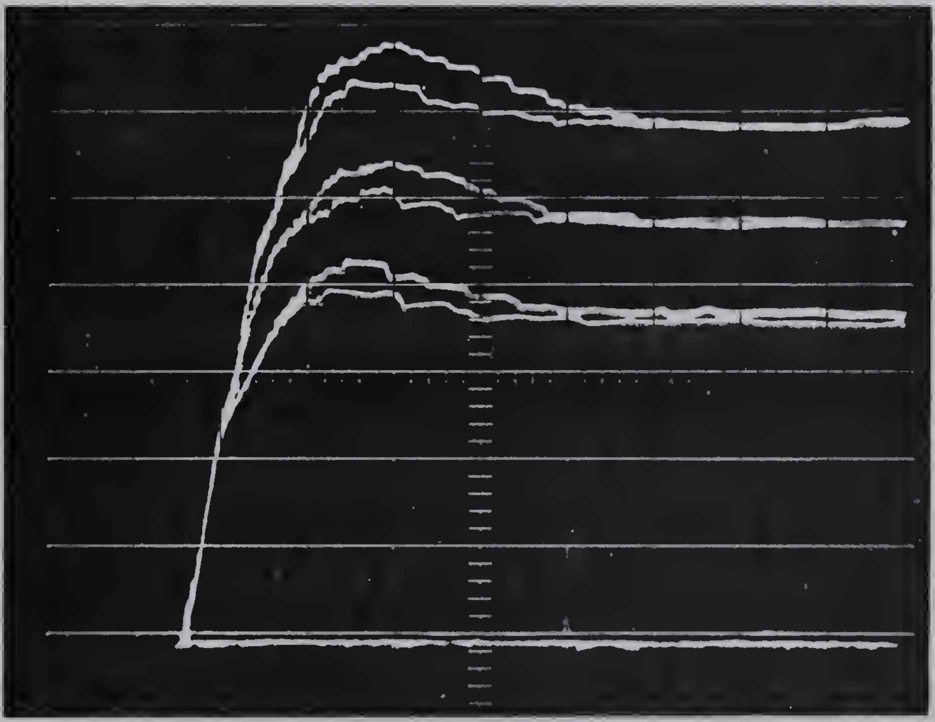

Figure 8.6

.1 volt/div. vertical

5 msec./div. horiz.

CHAPTER 9

USE OF CONDITIONAL DAMPING

9.1 INTRODUCTION

In Chapter 7, the limiting characteristic of the input amplifier was seen to often cause large response times for large increments because of the imposed upper velocity limit in the limited region. If damping could be applied only while the input amplifier was in its linear region (thus imposing no velocity limit) a considerable reduction in response time could be expected. For the case of tachometer feedback, this would require a "cutout switching circuit" to "gate" the rate signal to the power amplifier when $|E_\varepsilon| < 2.5$ volts as shown in figure 9.1. A circuit suggested to accomplish this is shown in figure A 4.9.

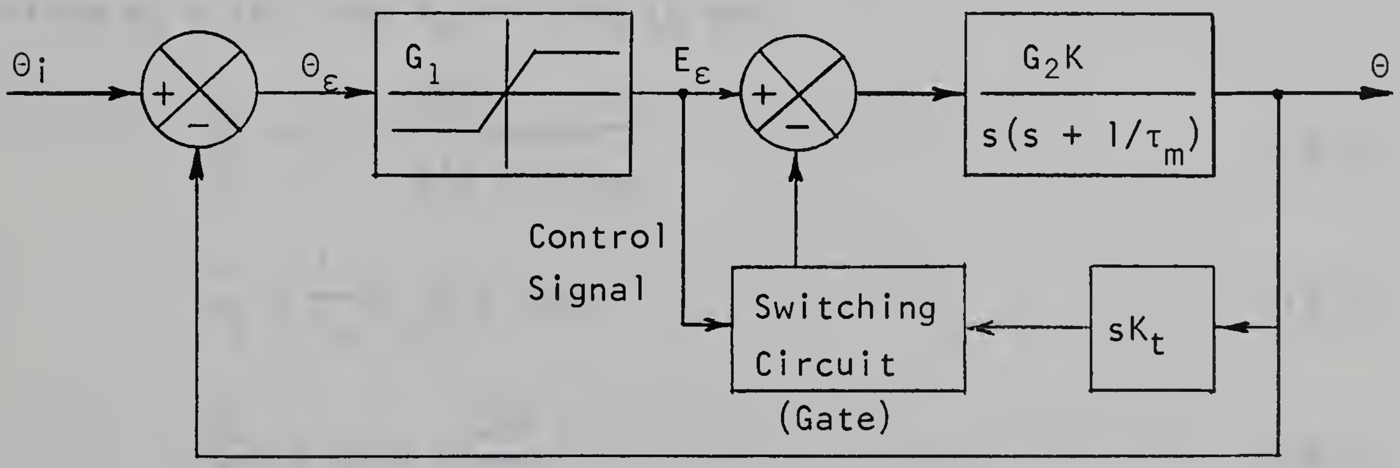

Figure 9.1 Conditional Tachometer Feedback

The system using derivative control provides a much simpler means of applying this conditional type of damping. If the output of the block containing the limiting characteristic is differentiated rather than the actual error signal, then in the limited region since $|E_\varepsilon| = 2.5$, $\dot{E}_\varepsilon = 0$ and no damping signal would be applied. The system is shown in figure 9.2.

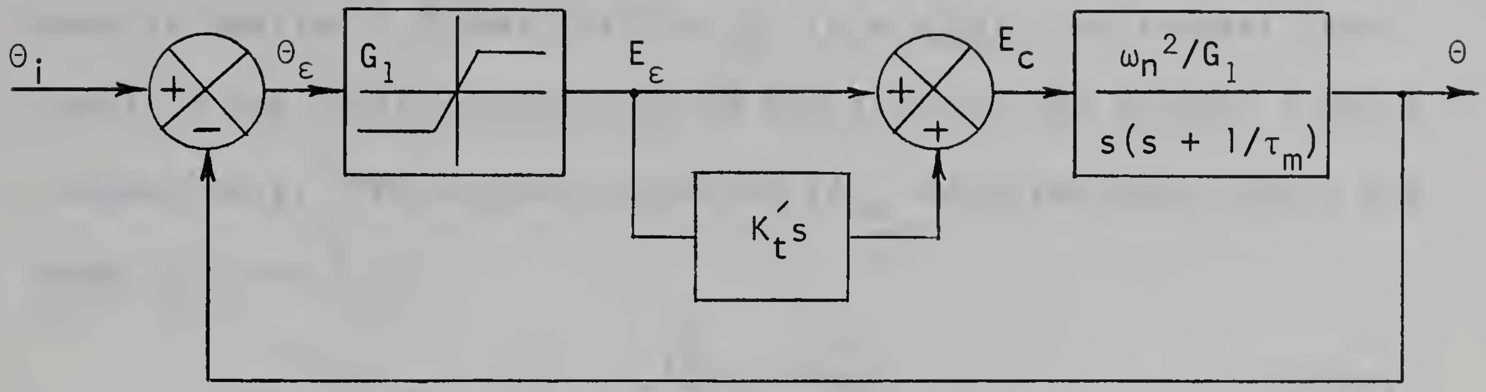

Figure 9.2 Conditional Derivative Damping

9.2 PHASE PLANE ANALYSIS

It will again be assumed that G_1 is sufficiently high that motor dead zone may be neglected in the analysis. For values of $\Theta_i > 2.5/G_1$, the system is initially an open-loop velocity system

where $$E_c(s) = 2.5/s \tag{9.1}$$

Since $G_2 = 10$, then $E_o = 25$ volts and

$$\Theta_\varepsilon = \Theta_i - \frac{25K}{s(s + 1/\tau_m)} \tag{9.2}$$

$$\ddot{\Theta}_\varepsilon + \frac{1}{\tau_m}\dot{\Theta}_\varepsilon = -\,25K \tag{9.3}$$

$$\frac{d\omega_\varepsilon}{d\Theta_\varepsilon} + \frac{1}{\tau_m} = -\,\frac{25K}{\omega_\varepsilon} \tag{9.4}$$

The isoclines are again horizontal straight lines. The velocity, however is given by

$$\omega(t) = -\,\omega_\varepsilon(t) = 25K\tau_m\ (1 - e^{-t/\tau_m}) \tag{9.5}$$

Thus, velocity is limited only by the motor parameters and the maximum achievable acceleration is utilized.

It is usually more convenient if the phase trajectory is described by an equation rather than by isoclines. Instead of the cumbersome exact form of equations 7.17 and 7.20, a reasonably good

approximate solution of equation 9.4 may be obtained here. It was seen in Section 7.3 that for $\tau = \tau_m$ ($\eta = \eta_{min}$), the longest time spent in the limited region was 38 and 31 msec. for Systems 1 and 2 respectively. The maximum values of t/τ_m which can occur then, are about 1/3 and 1/2.

$$e^{-t/\tau_m} = 1 - \frac{t}{\tau_m} + \frac{t^2}{2\tau_m{}^2} - \frac{t^3}{6\tau_m{}^3} + \cdots \tag{9.6}$$

Using the first two terms as an approximation, from equation 9.5

$$\omega_\varepsilon \simeq - 25Kt \tag{9.7}$$

$$\Theta_\varepsilon = \Theta_i - \int_0^t \omega(t)\ dt \tag{9.8}$$

$$= \Theta_i - 25K\tau_m \left(t + \tau_m e^{-t/\tau_m} - \tau_m\right) \tag{9.9}$$

$$= \Theta_i - 25K\tau_m{}^2 \left(\frac{t}{\tau_m} - 1 + e^{-t/\tau_m}\right) \tag{9.10}$$

Using the first three terms of the expression

$$\Theta_\varepsilon \simeq \Theta_i - 25K \frac{t^2}{2} \tag{9.11}$$

$$\simeq \Theta_i - \frac{\omega_\varepsilon{}^2}{50K} \tag{9.12}$$

Normalizing, as before, it is seen that the approximation for the phase trajectory is parabolic

$$\Theta_\varepsilon \simeq \Theta_i - \frac{G_1 G_2 \nu_\varepsilon{}^2}{50} \tag{9.13}$$

$$\simeq \Theta_i - \frac{G_1 \nu_\varepsilon{}^2}{5} \tag{9.14}$$

It should be mentioned that the approximation is equivalent to considering the motor as two integrators. Since its input (E_o = ± 25 volts) is constant, the acceleration is given by

$$|\ddot{\Theta}| \simeq 25K \frac{\text{rad}}{\text{sec}^2} \tag{9.15}$$

Thus constant acceleration is assumed whereas, from equation 9.5, the true acceleration is

$$|\ddot{\Theta}| = 25Ke^{-t/\tau_m} \tag{9.16}$$

Since the output of the power amplifier is limited to ± 25 volts, the system is seen to possess acceleration-limiting or torque-limiting.

When the value of $|\Theta_\varepsilon|$ becomes less than $\frac{2.5}{G_1}$, the input amplifier enters its linear region, damping is suddenly applied, and the linear response described by equations 7.60 to 7.78 ensues. Now, however, the values of $\omega(t_1)$ will be considerably larger and those of t_1 will be considerably smaller.

The angular distance travelled in time t_1 is given by

$$\Theta_i - \frac{2.5}{G_1} = \int_o^{t_1} \omega(t)dt \tag{9.17}$$

$$\simeq \int_o^{t_1} 25Ktdt \tag{9.18}$$

$$\simeq 12.5\ Kt_1^{\,2} \tag{9.19}$$

This parabolic function (based on the approximation of constant acceleration) is shown in figures 9.3 and 9.4 and is compared to the true function which was obtained in Section 7.3. The approximate velocity as the linear region is entered is also shown.

Unmodified motor:

$$t_1 \simeq \left(\frac{\Theta_i - 2.5/G_1}{12.5K}\right)^{\frac{1}{2}} = \left(\frac{\Theta_i - 2.5/G_1}{3750}\right)^{\frac{1}{2}} \tag{9.20}$$

$$\omega(t_1) \simeq 25\ Kt_1 = 7500t_1 \tag{9.21}$$

Modified motor:

$$t_1 \simeq \left(\frac{\Theta_i - 2.5/G_1}{2500}\right)^{\frac{1}{2}} \tag{9.22}$$

$$\omega(t_1) \simeq 5000\ t_1 \tag{9.23}$$

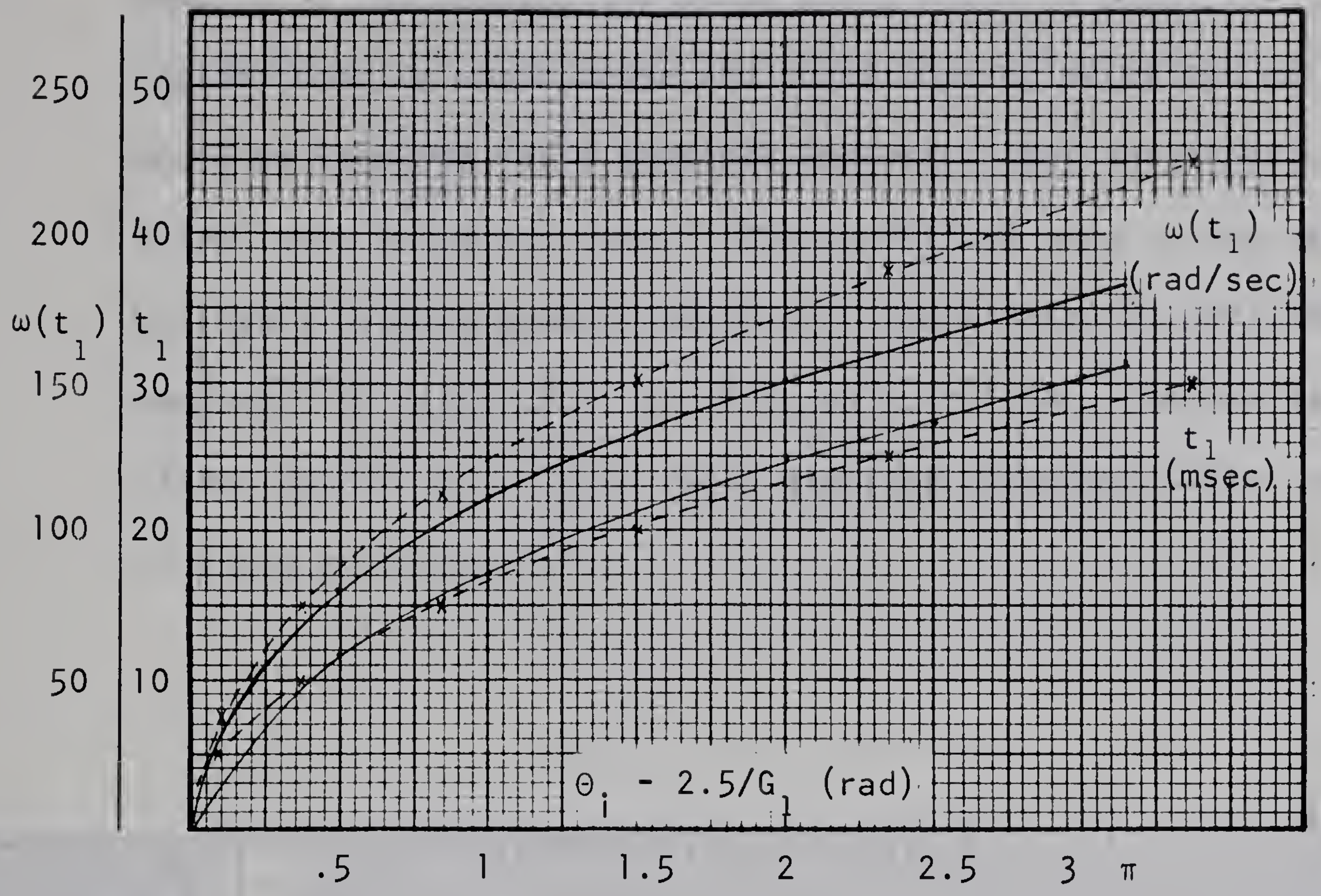

Figure 9.3 Initial Time Spent in Limited Region And Velocity at End of Limited Region - Unmodified Motor

——— Exact ----- Parabolic Approximation

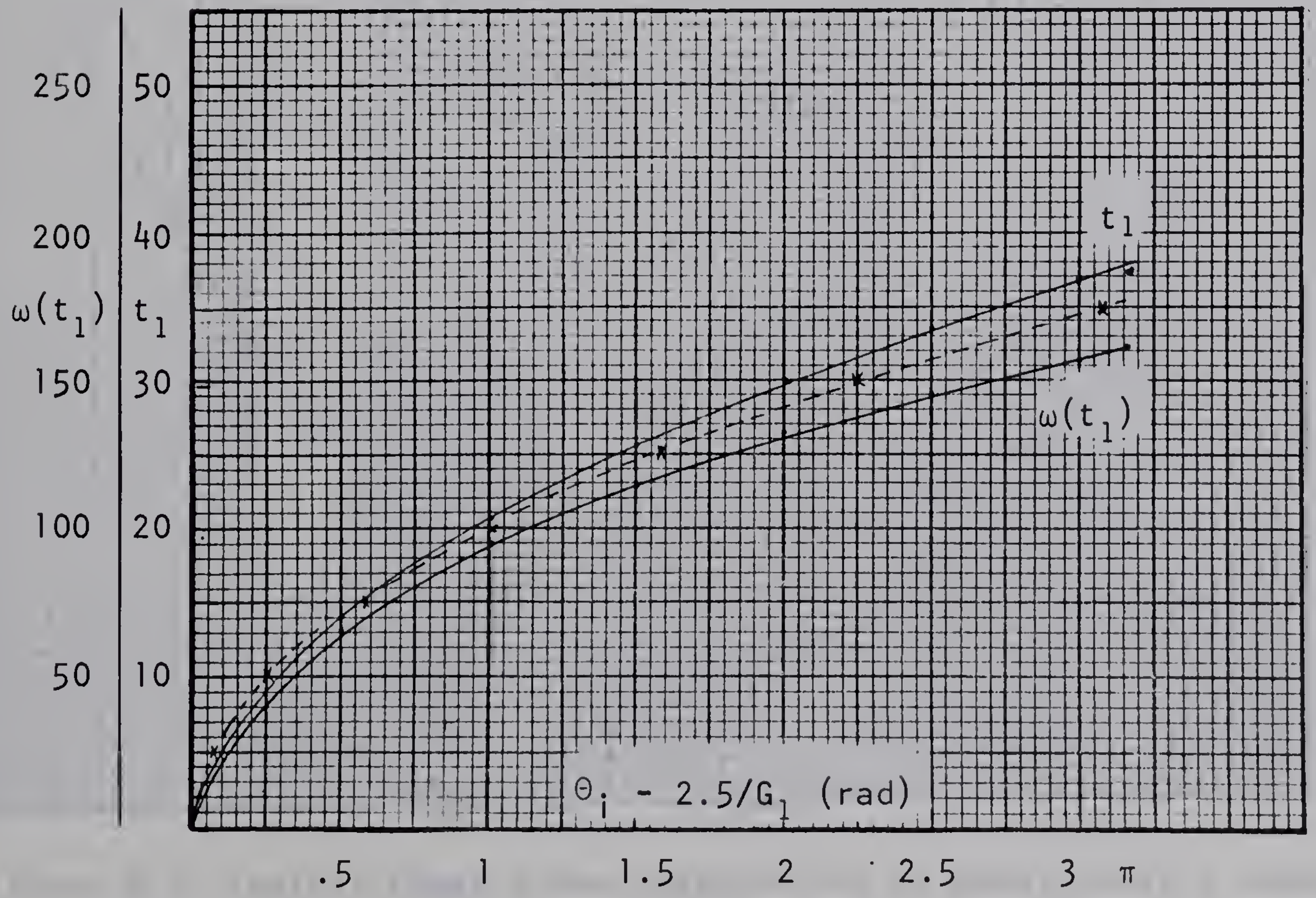

Figure 9.4 Initial Time Spent in Limited Region And Velocity at End of Limited Region - Modified Motor

If the width of the linear region is narrow enough and/or damping is low enough, the phase point would re-enter the limited region, damping would cease and conditions of exits and entries would be required for a complete analysis. For the practical situation, this would not occur. The conditions used in the example of figure 7.5 are again used to show the effect of conditional damping. In figure 9.5, $\xi = 0.8$ and $G_1 = 4.34$. The correspondingly higher values of $|\nu_\varepsilon(t_1)|$ which are seen to occur may be compared to those of figure 7.5.

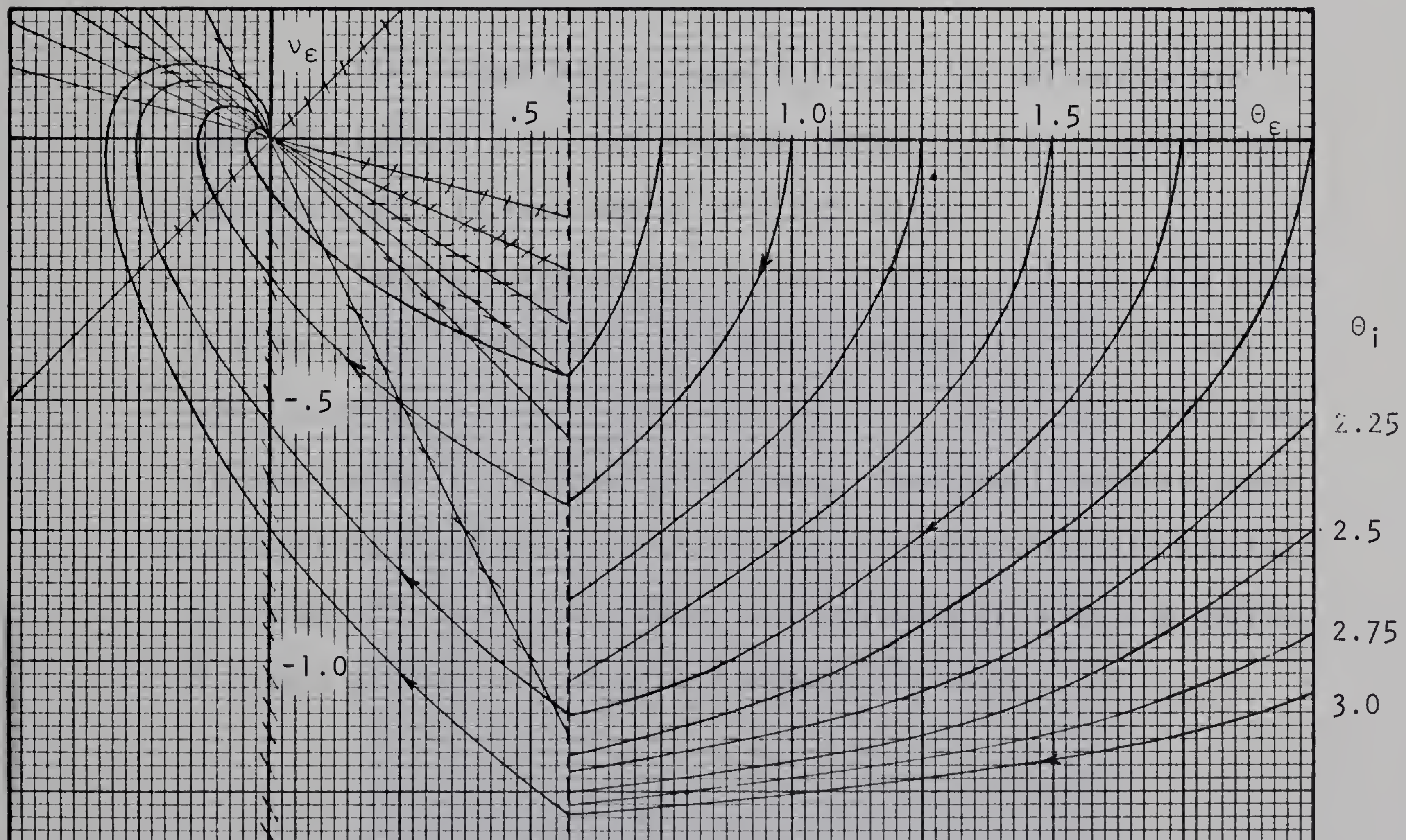

Figure 9.5 Typical Phase Plane Trajectories of Conditionally Damped System

9.3 EXPERIMENTAL RESULTS AND SUMMARY

The system of figure 9.2 was tested with $G_1 = 4.34$. It was necessary to isolate the two forward paths as shown in figure 9.6 (since the differentiator inverts).

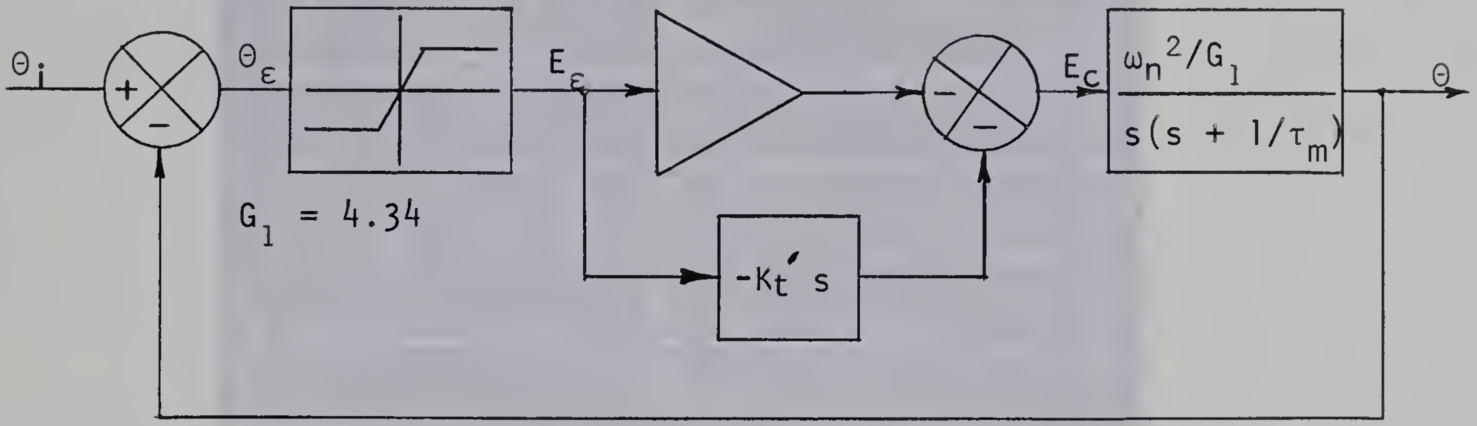

Figure 9.6 Physical System Using Conditional Derivative Control

The limited error signal $E_\varepsilon(t)$ and its derivative are shown in figure 9.7 for the undamped system ($K_t' = 0$). Notice that the rate signal is zero when $E_\varepsilon = \pm 2.5$ volts.

Typical responses for a step of about 1.08 rad. are shown in figure 9.8. The width of the linear region is $\frac{2.5}{G_1} \simeq .58$ rad. From figure 9.3 at $1.07 - .58 \simeq .5$ rad, $t_1 \simeq 11.5$ msec. Peak times are seen to be in the order of 30 msec. Overdamped responses were unattainable since the derivative signal caused noticeable buzzing of the motor. The problem would be alleviated by using the system of figure 9.1 but no attempt was made to try this.

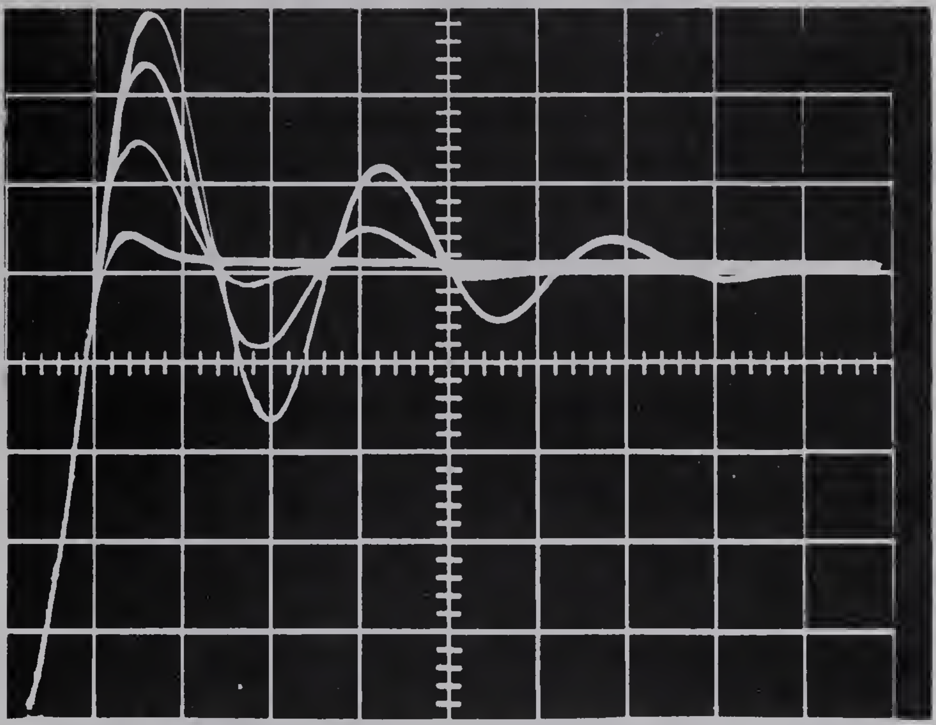

Figure 9.7 Response of System Using Conditional Derivative Damping

1 volt/div. vertical
20 msec./div. horiz.

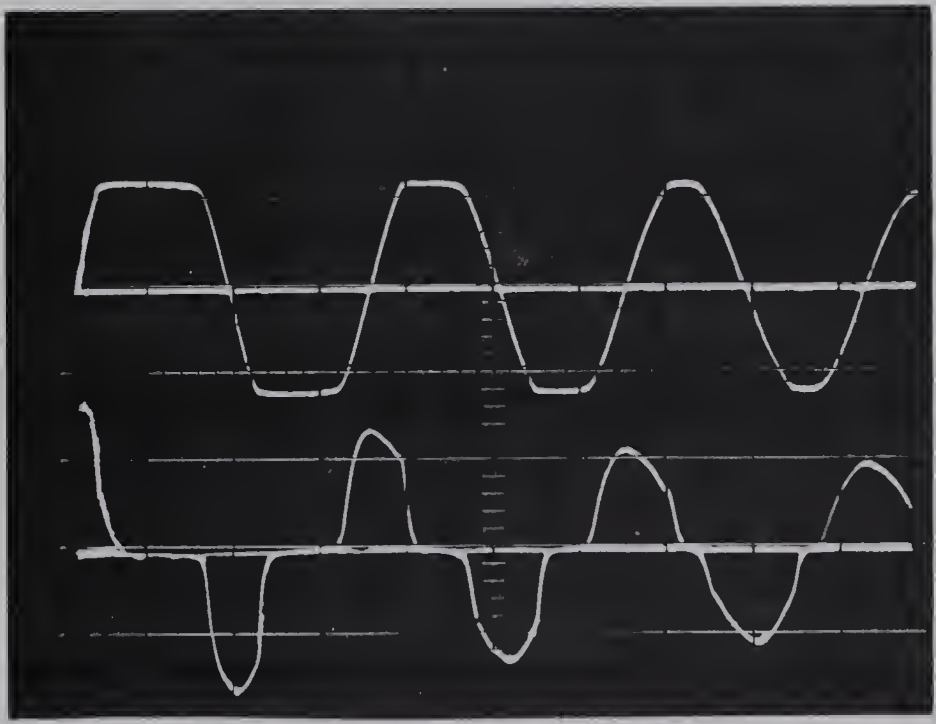

Figure 9.8 Limited Error and Derivative

$E_\varepsilon(t)$: 2 volts/div.; $\dot{E}_\varepsilon$: 5 volts/div.

20 msec./div. horiz.

CHAPTER 10

LIMITING OF CONTROL SIGNAL

10.1 INTRODUCTION

Due to the velocity limiting of a system with only positional error limiting, response times were generally high-valued. It is much more reasonable to have the maximum velocity possible in the limited region. This was accomplished in Chapter 9 by cutting out rate feedback in this region. A much more practical method is to limit the total error signal, that is, the control signal to the power amplifier.

Providing the gain of the error detector (G_1) is such that it never saturates, analysis is straightforward. The system to be investigated is shown in figure 10.1.

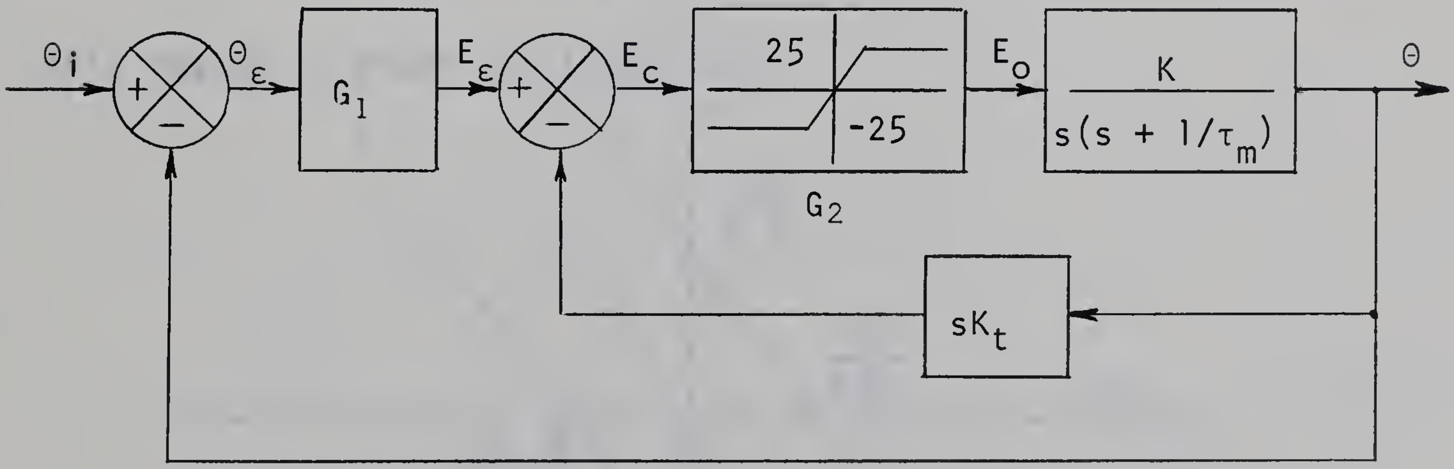

Figure 10.1 Control Signal Limiting

10.2 PHASE PLANE ANALYSIS

It can be seen that for any increment $|\Theta_i| > \frac{25}{G_1 G_2}$ the initial value of $|E_o|$ will be 25 volts causing the motor to accelerate as fast as possible. This utilization of maximum acceleration was described in Section 9.2. The same approximation will be

seen to be even more justified in the case at hand. The initial phase trajectory is thus described by equation 9.13.

The linear region is described by

$$-\frac{25}{G_2} < E_c < \frac{25}{G_2} \tag{10.1}$$

but

$$E_c = G_1\Theta_\varepsilon - K_t\dot{\Theta} \tag{10.2}$$

$$= G_1\Theta_\varepsilon + K_t\omega_\varepsilon \tag{10.3}$$

Thus the linear region is defined by

$$-\frac{25}{G_2} < G_1\Theta_\varepsilon + K_t\omega_\varepsilon < \frac{25}{G_2} \tag{10.4}$$

That is, it is enclosed by the two straight lines

$$G_1\Theta_\varepsilon + K_t\omega_\varepsilon = \frac{25}{G_2} \tag{10.5}$$

and

$$G_1\Theta_\varepsilon + K_t\omega_\varepsilon = -\frac{25}{G_2} \tag{10.6}$$

This region is shown in figure 10.2.

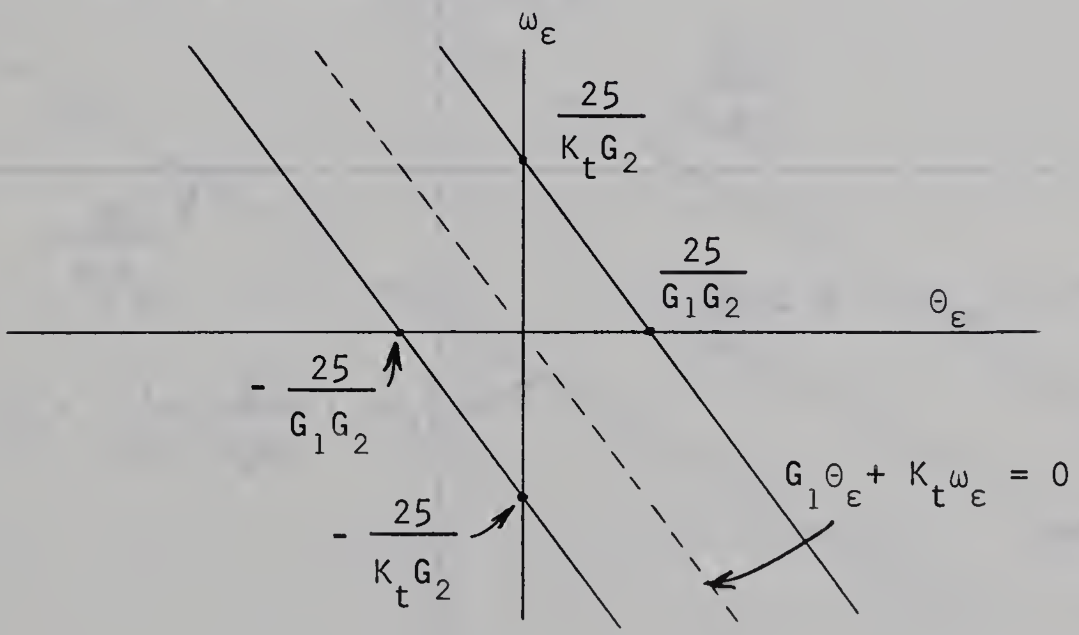
ω_ε
$\frac{25}{K_tG_2}$
$\frac{25}{G_1G_2}$
Θ_ε
$-\frac{25}{G_1G_2}$
$G_1\Theta_\varepsilon + K_t\omega_\varepsilon = 0$
$-\frac{25}{K_tG_2}$

Figure 10.2 Linear Region

The isoclinal equation 7.14 describes operation in the linear region

$$\nu_\varepsilon = -\frac{\Theta_\varepsilon}{2\xi + \frac{d\nu_\varepsilon}{d\Theta_\varepsilon}} \tag{10.7}$$

In order to facilitate analysis a further assumption must be made. For reasonable values of ξ, damping is almost entirely effected by the tachometer feedback (i.e. motor damping is assumed negligible). From equation 7.8

$$K_t = \frac{2\xi\sqrt{G_1}}{\sqrt{KG_2}} + \frac{1}{\tau_m KG_2} \tag{10.8}$$

$$\simeq \frac{2\xi\sqrt{G_1}}{\sqrt{KG_2}} \tag{10.9}$$

The linear region can therefore be defined in terms of damping ratio instead of tachometer constant. The resulting normalized phase plane is shown in figure 10.3.

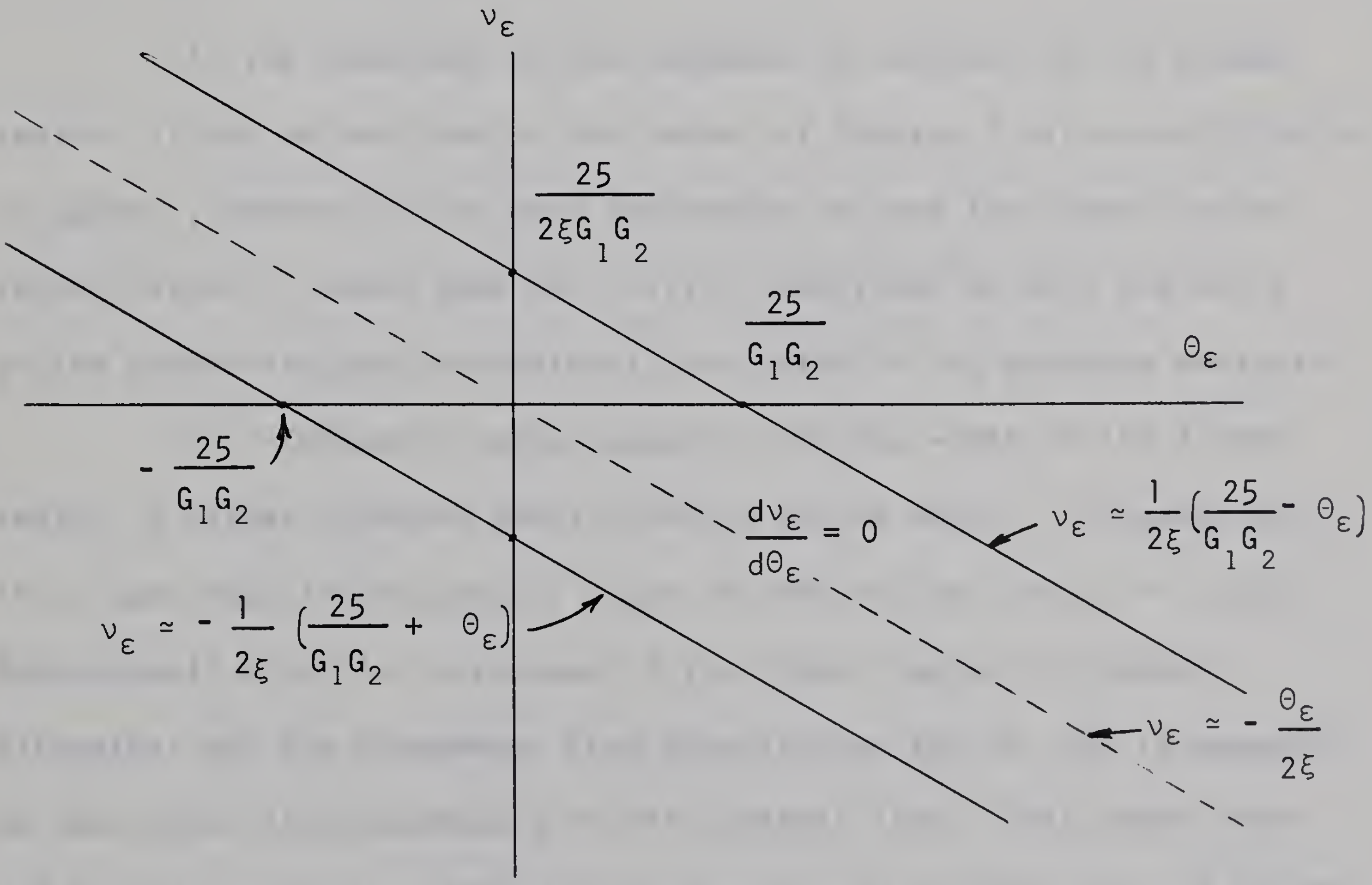
ν_ε
$\frac{25}{2\xi G_1 G_2}$
$\frac{25}{G_1 G_2}$
Θ_ε
$-\frac{25}{G_1 G_2}$
$\frac{d\nu_\varepsilon}{d\Theta_\varepsilon} = 0$
$\nu_\varepsilon \simeq \frac{1}{2\xi}(\frac{25}{G_1 G_2} - \Theta_\varepsilon)$
$\nu_\varepsilon \simeq -\frac{1}{2\xi}(\frac{25}{G_1 G_2} + \Theta_\varepsilon)$
$\nu_\varepsilon \simeq -\frac{\Theta_\varepsilon}{2\xi}$

Figure 10.3 Approximate Normalized Phase Plane Boundaries

It can be seen that for critical damping, the boundaries have a slope of $-\frac{1}{2}$ and for $\xi = 0.5$, the slopes are -1. For all practical values of ξ then, the initial distance traversed in the

limited region is much less than π radians, and less than $\pi/2$ radians for $\xi < 1$. Thus the time spent (t_1) is much less than the values of Chapter 9. This means that use of the expansion for e^{-t/τ_m} is very well justified here.

The phase point $\left(\Theta_\varepsilon(t_1),\ \nu_\varepsilon(t_1)\right)$ can be found by solving the simultaneous equations

$$\nu_\varepsilon = \frac{1}{2\xi}\left(\frac{25}{G_1G_2} - \Theta_\varepsilon\right) \tag{10.10}$$

$$\Theta_\varepsilon = \Theta_i - \frac{\nu_\varepsilon{}^2 G_1 G_2}{50} \tag{10.11}$$

The normalized value of the time when this point is reached is

$$\omega_n t_1 = -\frac{G_1}{2.5}\,\nu_\varepsilon(t_1) \tag{10.12}$$

If the remainder of the response is confined to the linear region, it may be analyzed in the manner of Chapter 7 with no difficulty. In general, however, it is more desireable to make the linear region rather narrow in which case the initial conditions of exit and entry at the boundaries must be tediously evaluated for an accurate analysis.

For increments large compared with the width of the linear region, a rather profound simplification can be made. In figure 10.3, it is seen that the trajectory slope is zero on the line $\nu_\varepsilon = -\Theta_\varepsilon/2\xi$. Only a small error is introduced if the linear region is ignored altogether and the changeover from acceleration 25K to -25K is assumed to take place instantaneously on this central line. This means, that for high forward gain, the system is very nearly identical to an on-off or "bang-bang" system except that the response finally enters the linear region and approaches the origin in a damped motion. With this assumption, the underdamped step response is now analyzed.

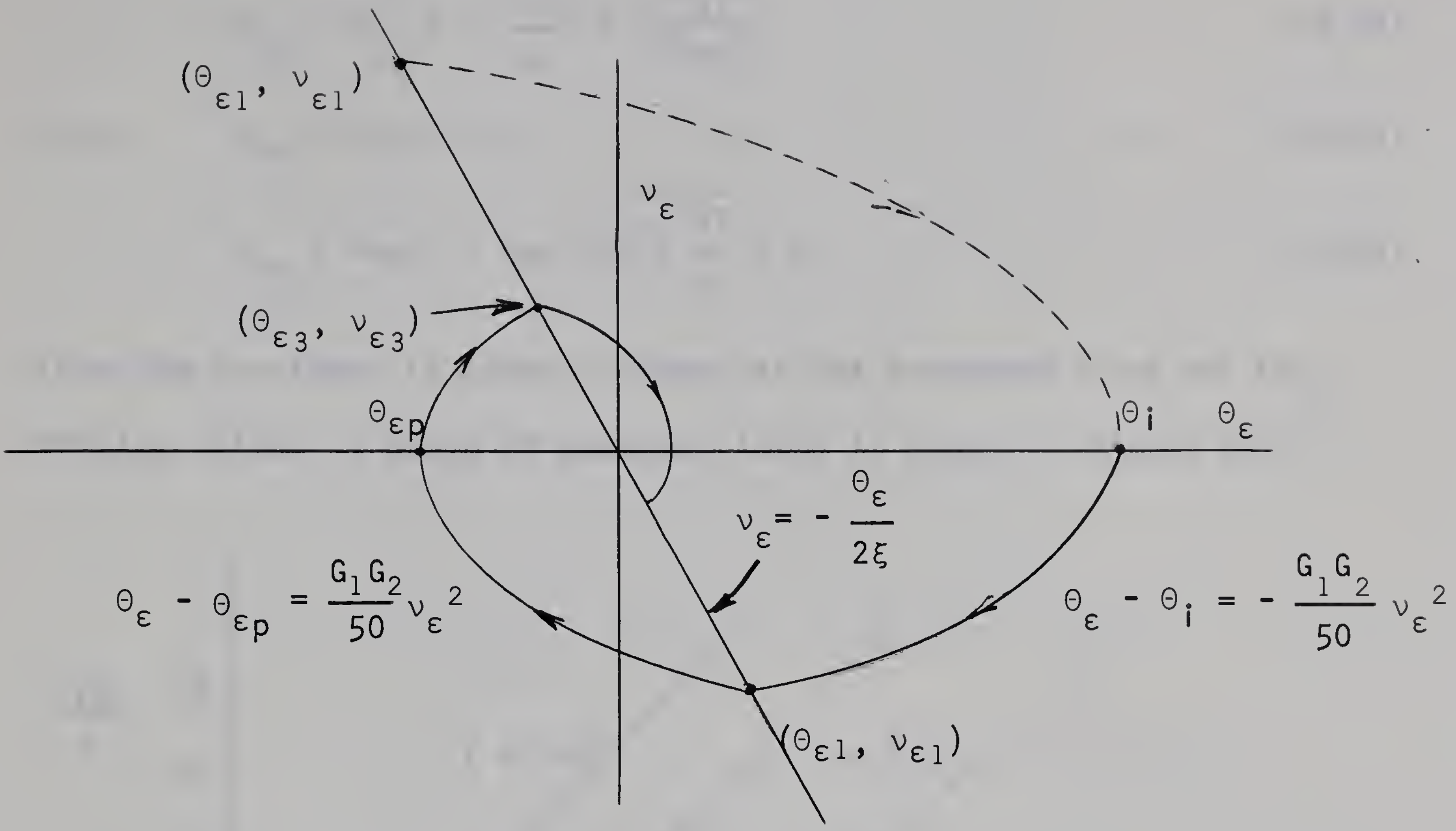
$(\Theta_{\varepsilon 1}, \nu_{\varepsilon 1})$
ν_ε
$(\Theta_{\varepsilon 3}, \nu_{\varepsilon 3})$
$\Theta_{\varepsilon p}$
Θ_i
Θ_ε
$\nu_\varepsilon = - \frac{\Theta_\varepsilon}{2\xi}$
$\Theta_\varepsilon - \Theta_{\varepsilon p} = \frac{G_1 G_2}{50} \nu_\varepsilon^2$
$\Theta_\varepsilon - \Theta_i = - \frac{G_1 G_2}{50} \nu_\varepsilon^2$
$(\Theta_{\varepsilon 1}, \nu_{\varepsilon 1})$

Figure 10.4 Phase Plane Trajectory of Underdamped "On-Off" System

The initial trajectory in the limited region is given by equation 10.11. In figure 10.4, this meets the central line at $(\Theta_{\varepsilon 1}, \nu_{\varepsilon 1})$. The width of the linear region will be defined:

$$w = \frac{50}{G_1 G_2} \tag{10.13}$$

$$\nu_{\varepsilon 1} = - \frac{\Theta_{\varepsilon 1}}{2\xi} \tag{10.14}$$

From equation 10.11

$$\Theta_{\varepsilon 1} - \Theta_i = - \frac{\nu_{\varepsilon 1}^2}{w} \tag{10.15}$$

$$= - \frac{\Theta_{\varepsilon 1}^2}{4w\xi^2} \tag{10.16}$$

Thus $$\Theta_{\varepsilon 1} = - 2w\xi^2 \pm 2w\, \xi\sqrt{\xi^2 + \frac{\Theta_i}{w}} \tag{10.17}$$

The incorrect (negative) solution is indicated by $(\Theta'_{\varepsilon 1}, \nu'_{\varepsilon 1})$.

At $(\Theta_{\varepsilon 1}, \nu_{\varepsilon 1})$ acceleration reverses direction and the peak point $(\Theta_{\varepsilon p}, 0)$ can be found.

$$\Theta_{\varepsilon p} - \Theta_{\varepsilon 1} = -\frac{\nu_{\varepsilon 1}^{2}}{w} = -\frac{\Theta_{\varepsilon 1}^{2}}{4w\xi^{2}} \qquad (10.18)$$

Thus $$\Theta_{\varepsilon p} = 2\Theta_{\varepsilon 1} - \Theta_i \qquad (10.19)$$

$$\Theta_{\varepsilon p} = -4w\xi^2 + 4w\xi\sqrt{\xi^2 + \frac{\Theta_i}{w}} - \Theta_i \qquad (10.20).$$

Thus the overshoot is found in terms of the increment size and the damping ratio. A graph of equation 10.20 is shown in figure 10.5(9).

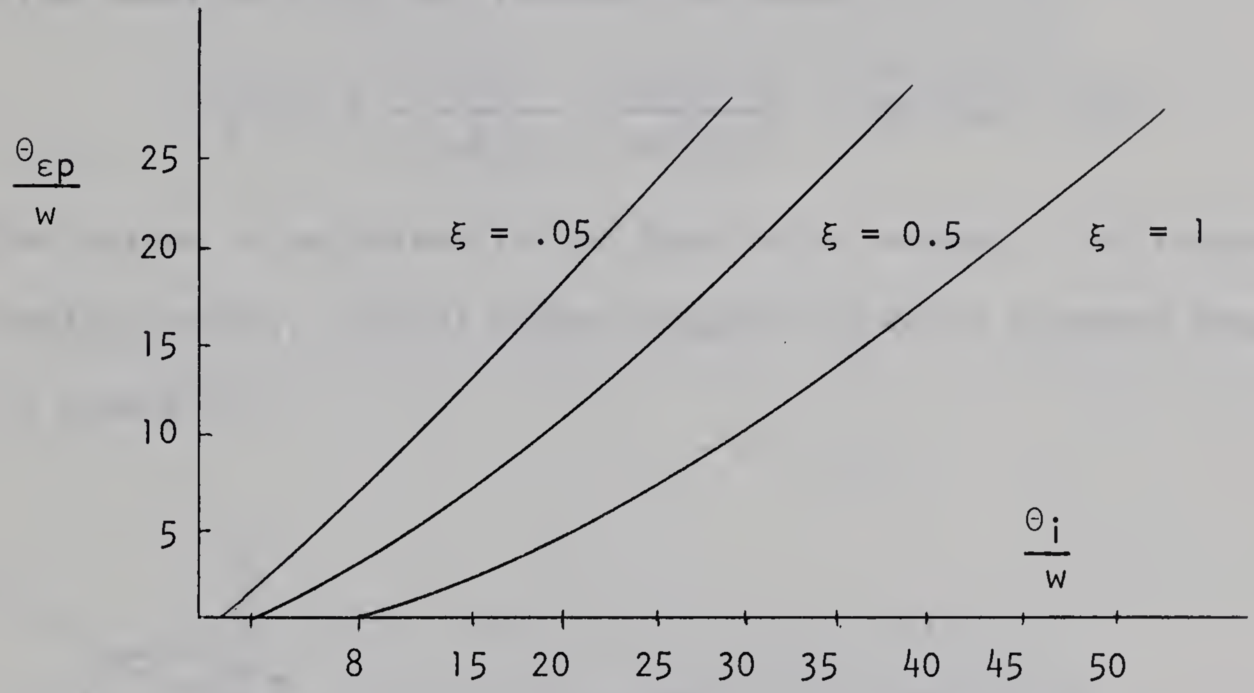

Figure 10.5 Chart for Determination of Overshoot

10.3 OPTIMIZING THE PHYSICAL SYSTEM

To find the condition for no overshoot, $\Theta_{\varepsilon p}$ is equated to zero.

$$\Theta_i + 4\xi^2 w = 4w\xi\sqrt{\xi^2 + \Theta_i/w} \qquad (10.21)$$

It can be seen that for $\xi = 1$, $\Theta_i = 8w$. This means that the critically damped system can have an input of eight times the width of the linear region without overshooting. This provides a means of finding an optimum value of forward gain.

For a maximum input of π radians, for the critically damped system to have no overshoot,

$$w = \frac{50}{G_1 G_2} = \frac{\pi}{8} = 22.5^\circ \qquad (10.22)$$

thus $$G_1G_2 = \frac{400}{\pi} = 127.5 \frac{\text{volts}}{\text{rad}} \tag{10.23}$$

Thus for an input of 11.25° or less, the response is entirely in the linear region, and for inputs up to sixteen times greater, the non-linear response still produces no overshoot. Using this as an optimum gain, the reduction in steady-state error over the basic (linear) system is 127.5/7.97 ≃ 16 times.

From equation 5.26, for the modified motor

$$\Theta_\varepsilon(\text{s.s.}) = \frac{T_cR_t}{K_TG_1G_2} \simeq \frac{165(1.1)}{360(127)} \simeq .004 \text{ rad} \simeq .23^\circ \tag{10.24}$$

The system is optimized for an input of π radians. For larger or smaller inputs, typical phase trajectories would resemble those shown in figure 10. 7.

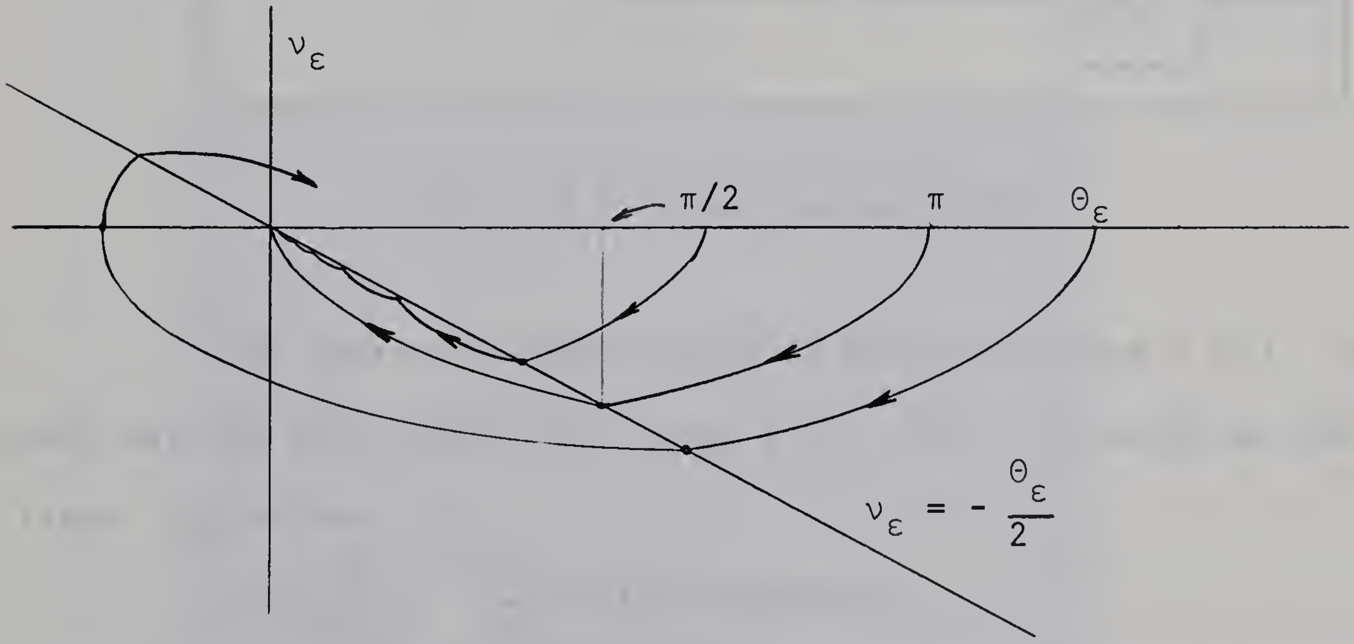

Figure 10.7 Non-Optimized Trajectories

For the system optimized for π radians, the time required for the phase point to reach the origin, for this input, is

$$t_p \simeq 2t_1 \tag{10.25}$$

$$\simeq 2\sqrt{2(\Theta_i - \Theta_{\varepsilon 1})/25K} \tag{10.26}$$

$$\simeq 2\sqrt{\pi/25K} \tag{10.27}$$

Unmodified motor:

$$t_p \simeq 2\sqrt{\pi/7500} \simeq 41 \text{ msec.} \tag{10.28}$$

Modified motor:

$$t_p \simeq 2\sqrt{\pi/5000} \simeq 50 \text{ msec.} \tag{10.29}$$

10.4 EXPERIMENTAL RESULTS AND SUMMARY

It has been seen that a considerable reduction in response times may be gained by limiting the total error signal and avoiding the effects of velocity limiting. The system which was tested experimentally is represented in figure 10.8.

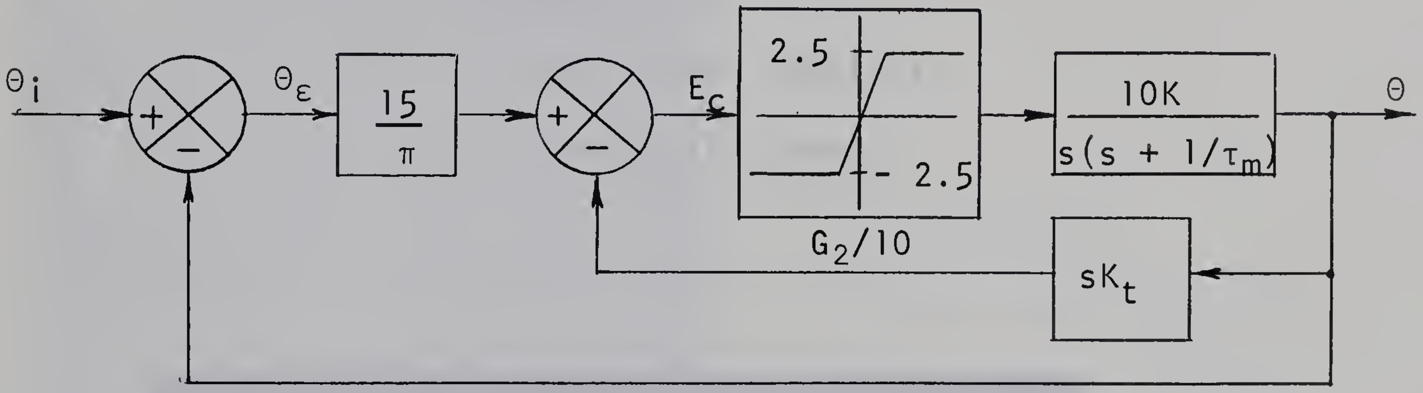

Figure 10.8 Experimental System

The control-signal limiter is shown in figure A 4.7. The gain was set with $R_f/R_i = 5.5$, thus $G_1G_2 \simeq 120$. The width of the linear region was

$$w = \frac{50}{G_1G_2} = \frac{50}{120} = .417 \text{ rad} \simeq 24^\circ$$

Typical responses for a constant damping ratio near unity are shown in figure 10.9. The largest increment is about 160°. Settling times are seen to be in the order of 60 to 70 msec. which are not quite as good as predicted. Smaller increments are shown in figure 10.10 for various settings of damping ratio. Typical phase trajectories for critically damped, underdamped, and overdamped cases are shown in figure 10.11, 10.12 and 10.13 respectively.

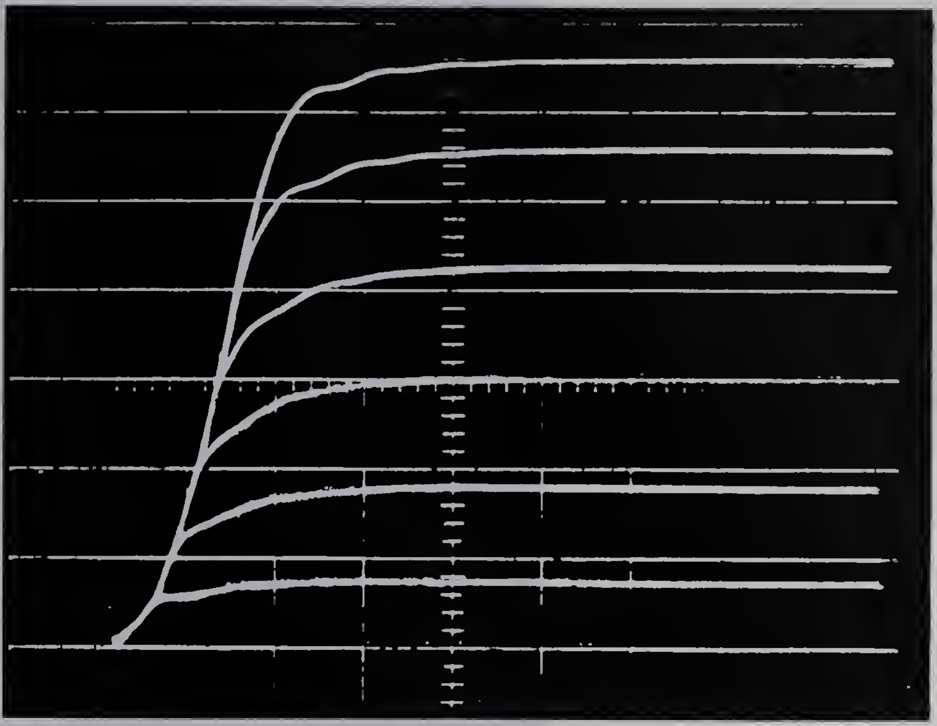

Figure 10.9

2 volts/div. vertical

20 msec./div. horiz.

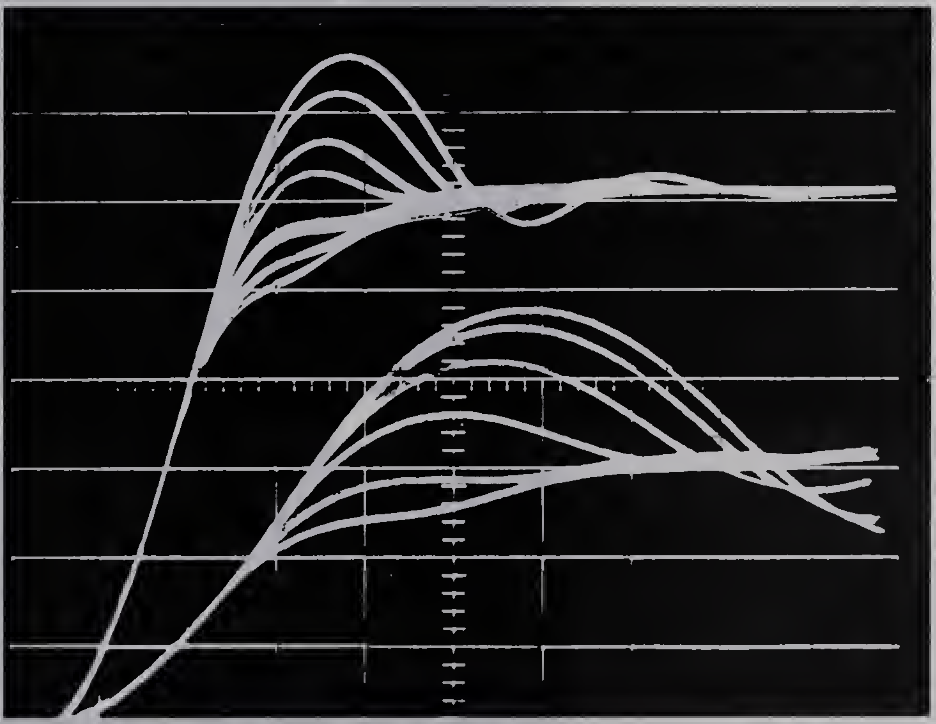

Figure 10.10

Upper traces : 10 msec./div. horiz.

Lower traces : 5 msec./div. horiz.

All traces : 1 volt/div. vertical

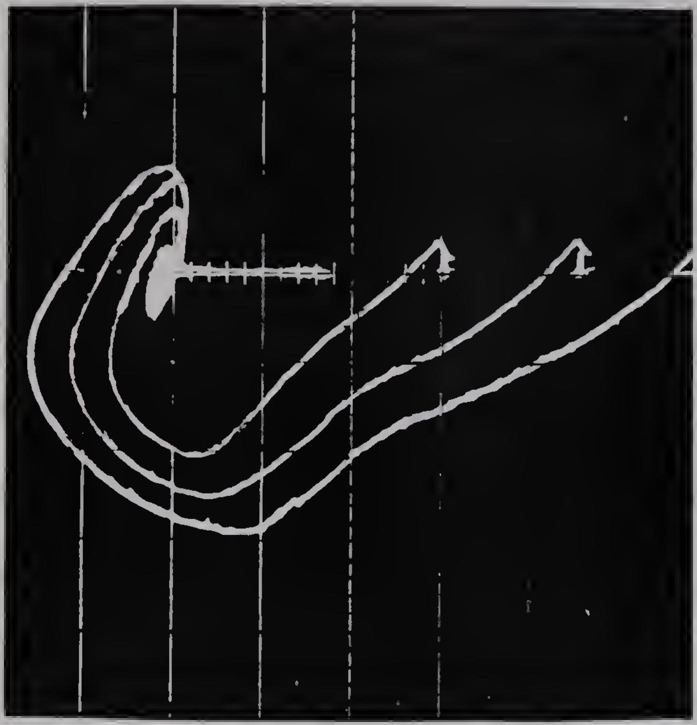

Figure 10.11

Phase Plane Trajectories

Of Underdamped System

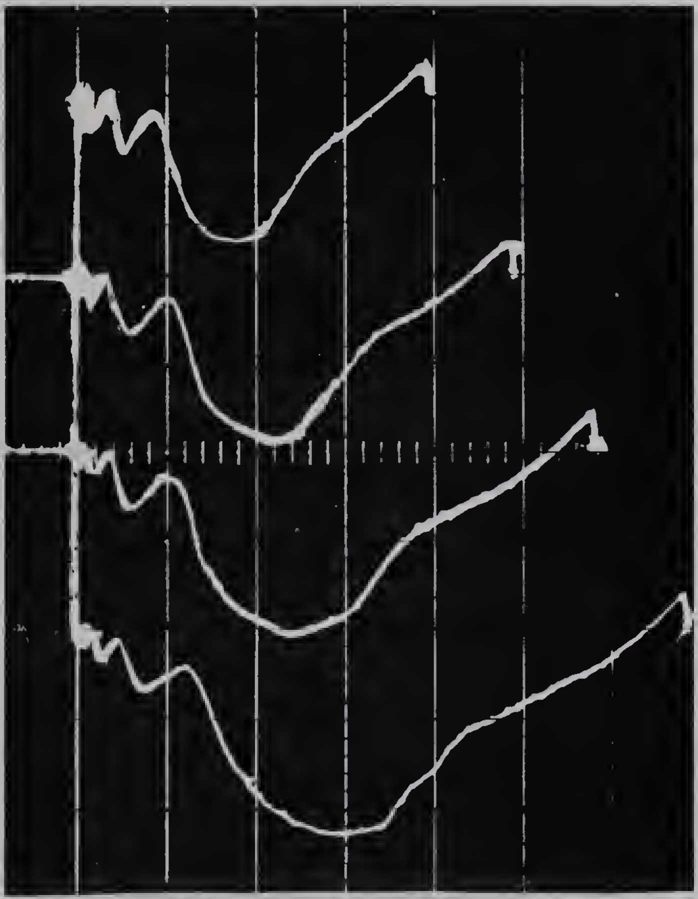

Figure 10.12

Phase Plane Trajectories

Of Overdamped System

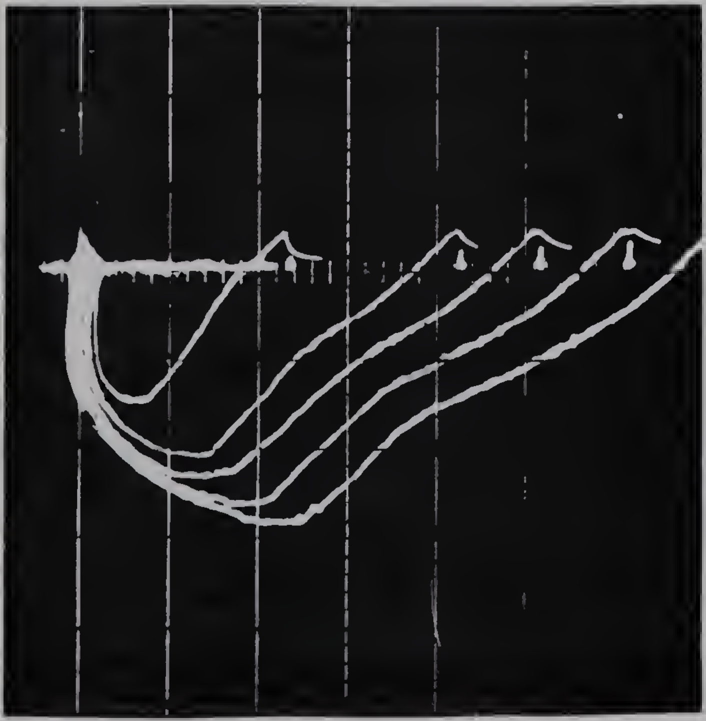

Figure 10.13

Phase Plane Trajectories

Of Correctly-damped System

CHAPTER 11

LIMITING OF POSITION ERROR PLUS CONTROL SIGNAL

11.1 INTRODUCTION

It was seen in Chapter 7 that positional error-limiting alone was unsatisfactory with regard to response times. A considerable improvement was achieved by the utilization of maximum acceleration in Chapter 10. For the sake of completeness now, the behavior of the system with both positional error and control signal limiting will be investigated. It will be shown that excellent response may be achieved if the velocity limit imposed by the error limiter is not less than the maximum velocity which would occur when maximum acceleration is utilized. The system is represented in figure 11.1.

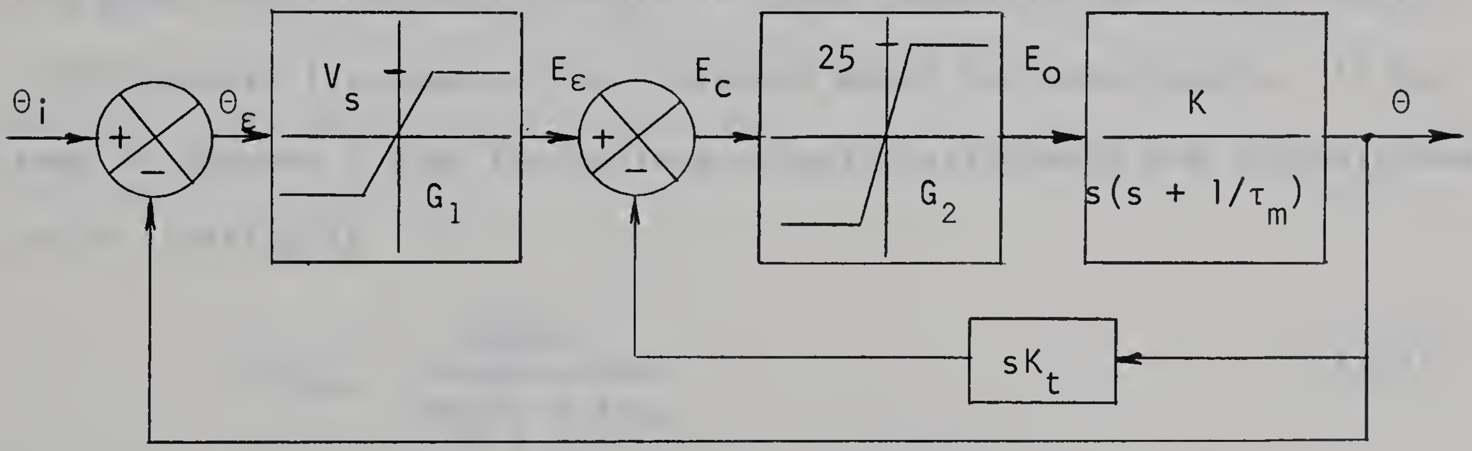

Figure 11.1 Limiting of Error and Control Signal

11.2 PHASE PLANE ANALYSIS

The linear region for the input amplifier (error detector) is

$$-\frac{V_s}{G_1} < \Theta_\varepsilon < \frac{V_s}{G_1} \qquad (11.1)$$

and for the power amplifier

$$-\frac{25}{G_2} < (E_\varepsilon - K_t\dot{\Theta}) < \frac{25}{G_2} \qquad (11.2)$$

If $|\Theta_\varepsilon| < \frac{V_s}{G_1}$, then the boundaries are as in equation 10.4

$$G_1\Theta_\varepsilon + K_t\omega_\varepsilon = \pm\frac{25}{G_2} \qquad (11.3)$$

If $\Theta_\varepsilon > \frac{V_s}{G_1}$, then the boundaries are

$$V_s + K_t\omega_\varepsilon = \pm \frac{25}{G_2} \tag{11.4}$$

or

$$\omega_\varepsilon = -\frac{1}{K_t}\left(V_s \pm \frac{25}{G_2}\right) \tag{11.5}$$

If $\Theta_\varepsilon < -\frac{V_s}{G_1}$, then the boundaries are

$$-V_s + K_t\omega_\varepsilon = \pm \frac{25}{G_2} \tag{11.6}$$

or

$$\omega_\varepsilon = \frac{1}{K_t}\left(V_s \pm \frac{25}{G_2}\right) \tag{11.7}$$

There are thus three possibilities for the shape of the regimes in the phase plane. For the cases where $V_s < \frac{25}{G_2}$ however, the power amplifier would remain in linear operation and the velocity limiting with its ensuing slow response would be undesireable. It was seen in Chapter 7 that the maximum velocity attainable due to positional error limiting is

$$|\omega_\varepsilon|_{max} = \frac{KG_2V_s}{KG_2K_t + 1/\tau_m} \tag{11.8}$$

The case for $V_s > \frac{25}{G_2}$ is shown in figure 11.2. The shaded region is that of linear operation of the power amplifier.

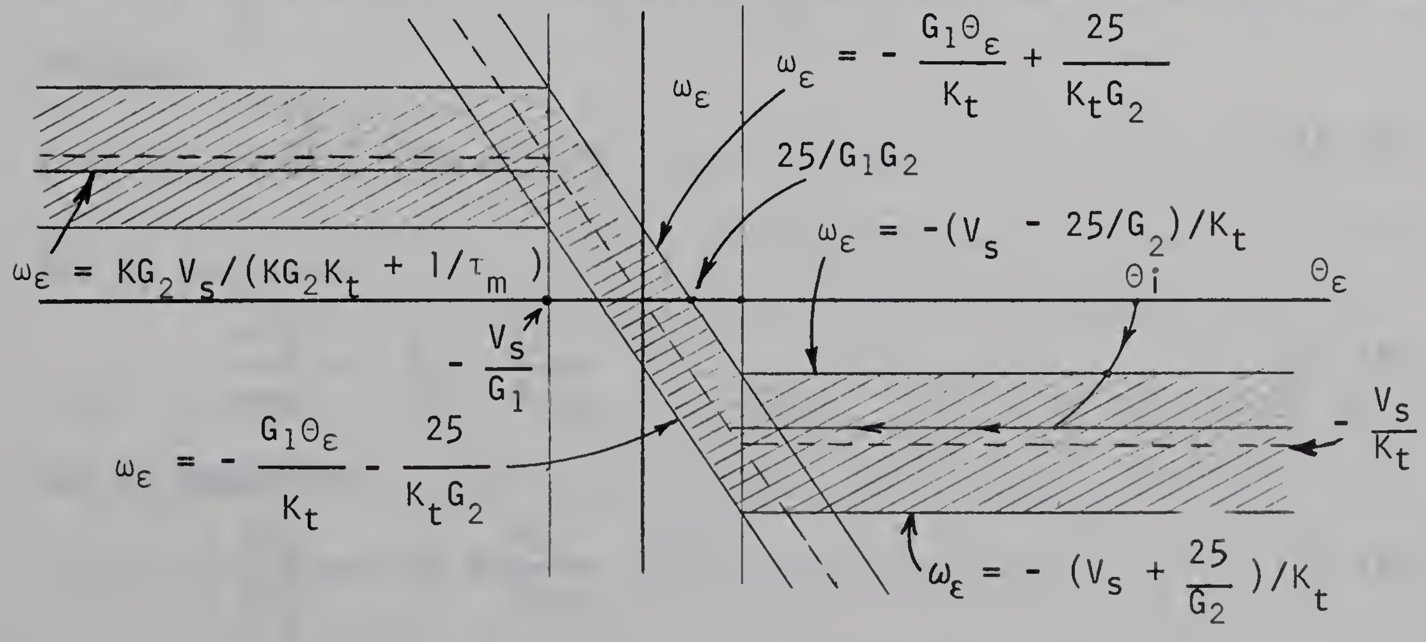
$\omega_\varepsilon = -\frac{G_1\Theta_\varepsilon}{K_t} + \frac{25}{K_tG_2}$
ω_ε
$25/G_1G_2$
$\omega_\varepsilon = -(V_s - 25/G_2)/K_t$
Θi
Θ_ε
$\omega_\varepsilon = KG_2V_s/(KG_2K_t + 1/\tau_m)$
$-\frac{V_s}{G_1}$
$\omega_\varepsilon = -\frac{G_1\Theta_\varepsilon}{K_t} - \frac{25}{K_tG_2}$
$-\frac{V_s}{K_t}$
$\omega_\varepsilon = -(V_s + \frac{25}{G_2})/K_t$

Figure 11.2 Boundaries of Linear Regions

If the assumption is again made that

$$\frac{1}{\tau_m} << KG_2K_t \tag{11.9}$$

then $$K_t \simeq \frac{2\xi G_1}{\omega_n} \tag{11.10}$$

and the parabolic trajectories of constant acceleration are encountered outside the shaded region. If t_2 is taken for G_2 to enter its linear region, then for a positive increment Θ_i,

$$\omega_\varepsilon(t_2) \simeq - 25\ Kt_2 \tag{11.11}$$

or $$\nu_\varepsilon(t_2) \simeq - \frac{25\omega_n t_2}{G_1G_2} \tag{11.12}$$

and $$\Theta_\varepsilon(t_2) \simeq \Theta_i - \frac{25\ Kt_2{}^2}{2} \tag{11.13}$$

In the horizontal shaded region, the maximum velocity now occurs midway between the boundaries.

That is $$|\omega_\varepsilon|_{max} = \frac{V_s}{K_t} \tag{11.14}$$

or $$|\nu_\varepsilon|_{max} = \frac{V_s}{2\xi G_1} \tag{11.15}$$

Motion in this region is described by the equation

$$KG_2\ (\pm\ V_s - K_t\dot{\Theta}) = \ddot{\Theta} \tag{11.16}$$

Normalizing and substituting for K_t, the isocline equations are now obtained

$$\pm \frac{V_s}{G_1} + 2\xi\nu_\varepsilon = - \dot{\nu}_\varepsilon \tag{11.17}$$

For Θ_ε positive

$$\frac{d\nu_\varepsilon}{d\Theta_\varepsilon} = - 2\xi - \frac{V_s}{G_1\nu_\varepsilon} \tag{11.18}$$

For Θ_ε negative

$$\frac{d\nu_\varepsilon}{d\Theta_\varepsilon} = - 2\xi + \frac{V_s}{G_1\nu_\varepsilon} \tag{11.19}$$

At time t_2, the velocity must lie on the horizontal boundary.

Thus

$$\omega_\varepsilon(t_2) = -\frac{V_s}{K_t} + \frac{25}{K_t G_2} \qquad (11.20)$$

or

$$\nu_\varepsilon(t_2) = \frac{1}{2\xi G_1}\left(-V_s + \frac{25}{G_2}\right) \qquad (11.21)$$

Equating to 11.12, the time can be found:

$$t_2 \simeq \frac{1}{2\xi\omega_n}\left(\frac{G_2}{25} V_s - 1\right) \qquad (11.22)$$

The positional error can then be found from equation 11.13.

The velocity in the horizontal region for $t > t_2$ is

$$\nu_\varepsilon(t) = -\frac{V_s}{2\xi G_1}\left(1 - e^{-(t - t_2)2\xi\omega_n}\right) + \nu_\varepsilon(t_2) \qquad (11.23)$$

The equation of the trajectory in this region is found from integration of equation 11.19.

$$\int_{\nu_\varepsilon(t_2)}^{\nu_\varepsilon} \frac{\nu_\varepsilon d\nu_\varepsilon}{V_s/G_1 - 2\xi\nu_\varepsilon} = \int_{\Theta_\varepsilon(t_2)}^{\Theta_\varepsilon} d\Theta_\varepsilon \qquad (11.24)$$

$$\frac{1}{4\xi^2}\left[\frac{V_s}{G_1} - 2\xi\nu_\varepsilon - \frac{V_s}{G_1}\log\left(V_s/G_1 - 2\xi\nu_\varepsilon\right)\right]_{\nu_\varepsilon(t_2)}^{\nu_\varepsilon} = \Theta_\varepsilon - \Theta_\varepsilon(t_2) \qquad (11.25)$$

$$\frac{1}{4\xi^2}\left[-2\xi\left(\nu_\varepsilon - \nu_\varepsilon(t_2)\right) - \frac{V_s}{G}\log\left(\frac{V_s/G_1 - 2\xi\nu_\varepsilon}{V_s/G_1 - 2\xi\nu_\varepsilon(t_2)}\right)\right] = \Theta_\varepsilon - \Theta_\varepsilon(t_2) \qquad (11.26)$$

Once Θ_ε reaches V_s/G_1, the response becomes linear until the power amplifier again becomes limited and the parabolic trajectory re-occurs.

From the form of equation 11.26, it can be seen that an exact solution of the transient response, including conditions at entry and exit from the linear regions would be very tedious. An approximate analysis may be used in the case where

$$V_s \gg \frac{25}{G_2} \qquad (11.27)$$

With this assumption the linear regions are reduced to straight lines as shown in figure 11.3. As in Chapter 10, the approximation is most valid for

$$\Theta_i \gg \frac{25}{G_1 G_2} \tag{11.28}$$

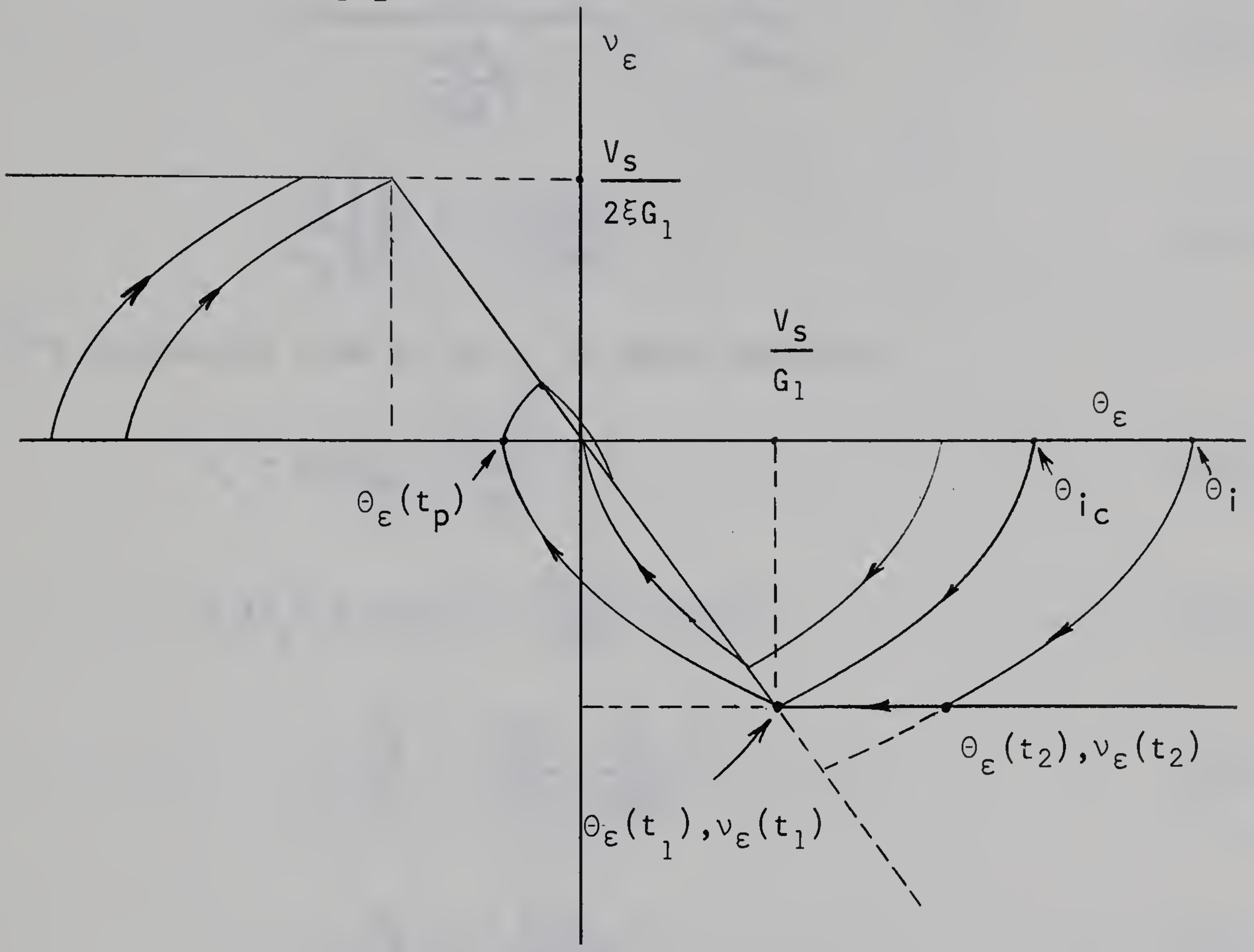
ν_ε
$\frac{V_s}{2\xi G_1}$
$\frac{V_s}{G_1}$
Θ_ε
$\Theta_\varepsilon(t_p)$
Θ_{i_c}
Θ_i
$\Theta_\varepsilon(t_2),\nu_\varepsilon(t_2)$
$\Theta_\varepsilon(t_1),\nu_\varepsilon(t_1)$

Figure 11.3 Approximate Phase Trajectories

For values of Θ_i greater than the critical value (Θ_{i_c} in figure 11.3), peak time is easily found.

$$\nu_\varepsilon(t_2) \simeq -\frac{25\omega_n t_2}{G_1 G_2} \simeq \frac{V_s}{2\xi G_1} \tag{11.29}$$

thus

$$t_2 \simeq \frac{G_2 V_s}{50\xi\omega_n} \tag{11.30}$$

and

$$\Theta_\varepsilon(t_2) \simeq \Theta_i - \frac{25K}{2}\left(\frac{G_2 V_s}{50\xi\omega_n}\right)^2 \tag{11.31}$$

$$\simeq \Theta_i - \frac{V_s^{\,2} G_2}{200\xi^2 G_1} \tag{11.32}$$

$$t_p \simeq \frac{\Theta_\varepsilon(t_1) - \Theta_\varepsilon(t_2)}{\omega_\varepsilon} + 2t_2 \tag{11.33}$$

$$\simeq \frac{\Theta_i - \dfrac{V_s{}^2 G_2}{200\xi^2 G_1} - \dfrac{V_s}{G_1}}{\left(\dfrac{\omega_n V_s}{2\xi G_1}\right)} + \frac{G_2 V_s}{25\xi\omega_n} \tag{11.34}$$

$$\simeq \frac{2\xi}{\omega_n}\left[\frac{G_1}{V_s}\,\Theta_i + \frac{3V_s G_2}{200\xi^2} - 1\right] \tag{11.35}$$

The trajectory from t_1 to t_p is again parabolic

$$\Theta_\varepsilon - \Theta_\varepsilon(t_p) = \frac{G_1 G_2}{50}\,\nu_\varepsilon{}^2 \tag{11.36}$$

$$\Theta_\varepsilon(t_p) = \Theta_\varepsilon(t_1) - \frac{G_1 G_2}{50}\,\nu_\varepsilon(t_1)^2 \tag{11.37}$$

$$= \frac{V_s}{G_1} - \frac{G_1 G_2}{50}\left(\frac{V_s}{2\xi G_1}\right)^2 \tag{11.38}$$

$$= \frac{V_s}{G_1}\left(1 - \frac{G_2 V_s}{200\xi^2}\right) \tag{11.39}$$

11.3 OPTIMIZING THE PHYSICAL SYSTEM

For the case at hand, that is limiting, or saturation of the input amplifier (error detector) optimizing is not quite as simple. The added variables G_1 and V_s must now be set. The condition for no overshoot is found by equating $\Theta_\varepsilon(t_p)$ to zero.

$$G_2 V_s = 200\xi^2 \tag{11.40}$$

For this condition then, the trajectory, from equation 11.36 is

$$\nu_\varepsilon{}^2 \simeq \pm\frac{50}{G_1 G_2}\,\Theta_\varepsilon \tag{11.41}$$

The trajectory is called the critical boundary. It is shown in figure 11.4 for different slopes.

and $$G_1 G_2 = 127.5 \text{ volts/rad} \tag{11.47}$$

which is identical to the value obtained in Section 10.3. The time required to reach the origin is found from equation 11.35.

$$t_p \simeq 2t_2 = \frac{G_2 V_s}{25\xi\omega_n} \tag{11.48}$$

For the optimized system then,

$$t_p \simeq \frac{3}{5} \sqrt{G_2/KG_1} \tag{11.49}$$

which yields the values of equations 10.28 and 10.29 for the two motors.

For an increment of π radians with this system, the error detector will be in saturation for half the response time.

11.4 EXPERIMENTAL RESULTS AND SUMMARY

The system of figure 11.1 was tested with $V_s = 15$ volts using the modified motor.

Figure 11.5 shows near-optimum responses ($G_1 = 9.1$ instead of 13.33). For steps of up to 155° no overshoot occurs. Damping is constant. Response times are less than 60 msec.

Figure 11.6 shows various damping ratios for two steps of smaller magnitude. The step of about 68° has peak times of about 35 msec. while the step of 32° has peak times of about 30 msec.

To show the effect of too high a gain, G_2 was increased to 22.75. In figure 11.7 it is seen that for constant damping, an overshoot occurs for larger increments. Peak times however are quite low: about 45 msec. for the largest step (155°).

Two smaller steps (60° and 24°) are again shown in figure 11.8 with the damping varied. The tachometer output and power amplifier output voltages are shown for this case in figure 11.9.

The gain G_1 was then increased to $60/\pi$ such that velocity limiting could occur. Forward gain $G_1 G_2 \simeq 435$ volts/rad is nearly four times its optimum value. Results are shown in figures 11.10, 11.11 and 11.12. As expected, overshooting begins to occur at a considerably lower increment magnitude.

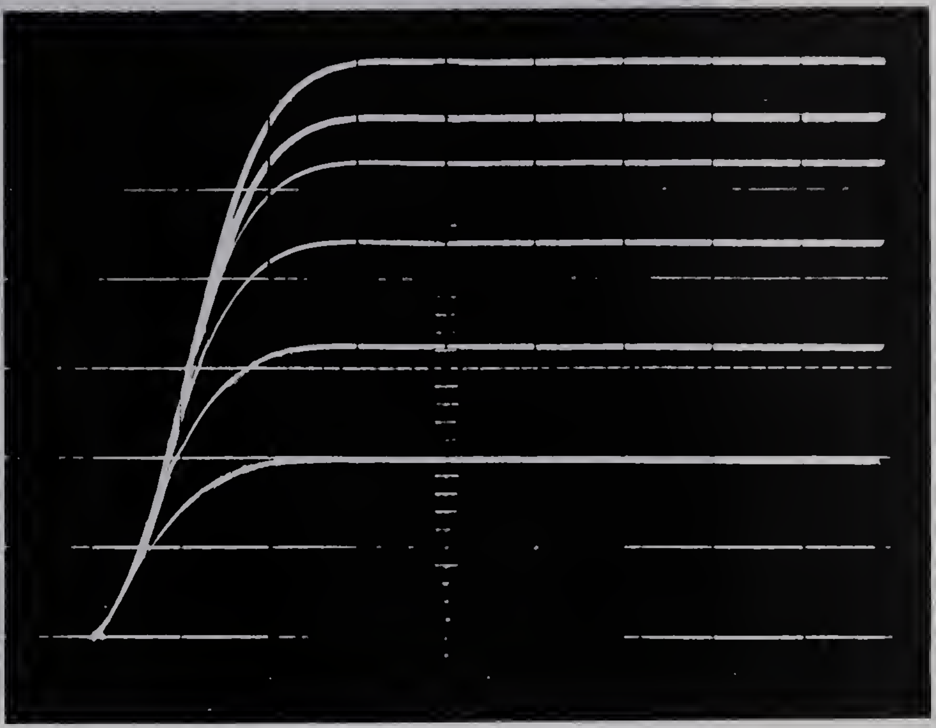

Figure 11.5 Near-Optimal Responses

2 volts/div. vertical

20 msec./div. horiz.

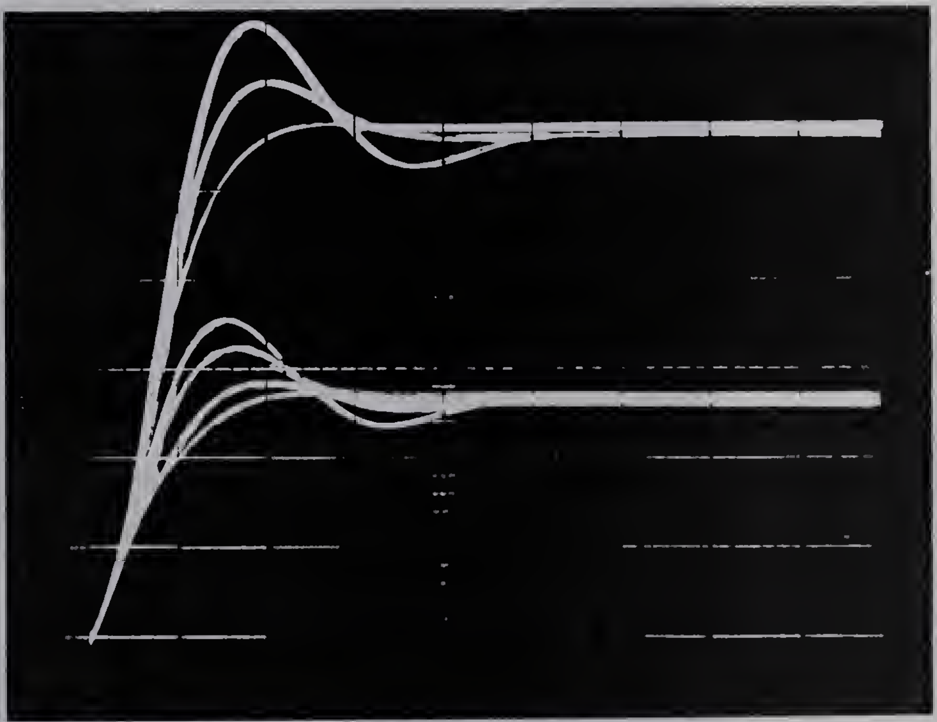

Figure 11.6 Underdamped Responses

1 volt/div. vertical

10 msec./div. horiz.

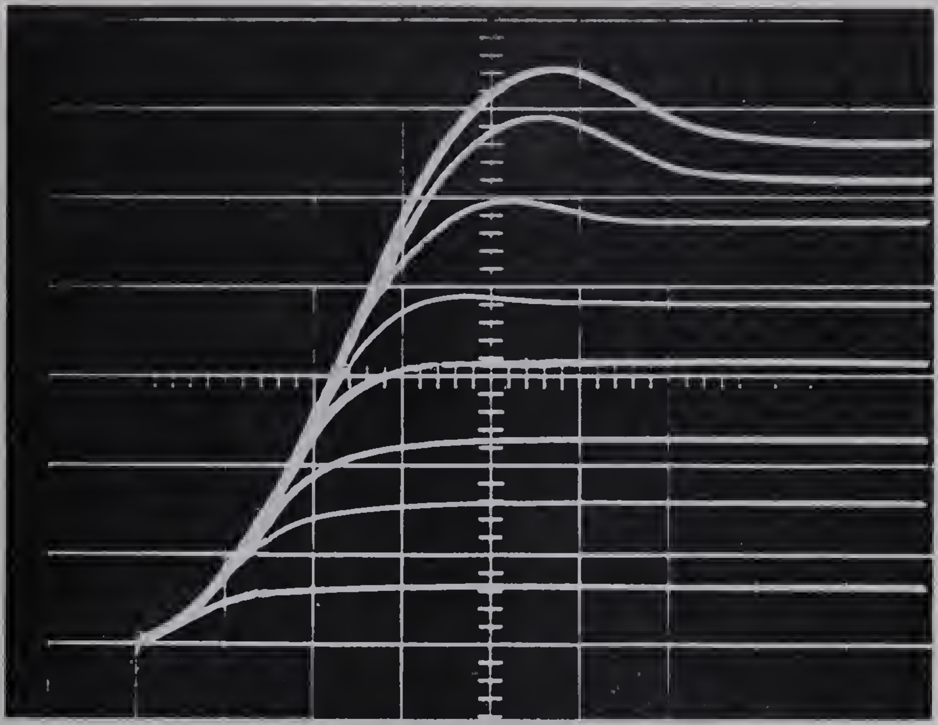

Figure 11.7

Effect of Gain Being Too High

2 volts/div. vertical

10 msec./div. horiz.

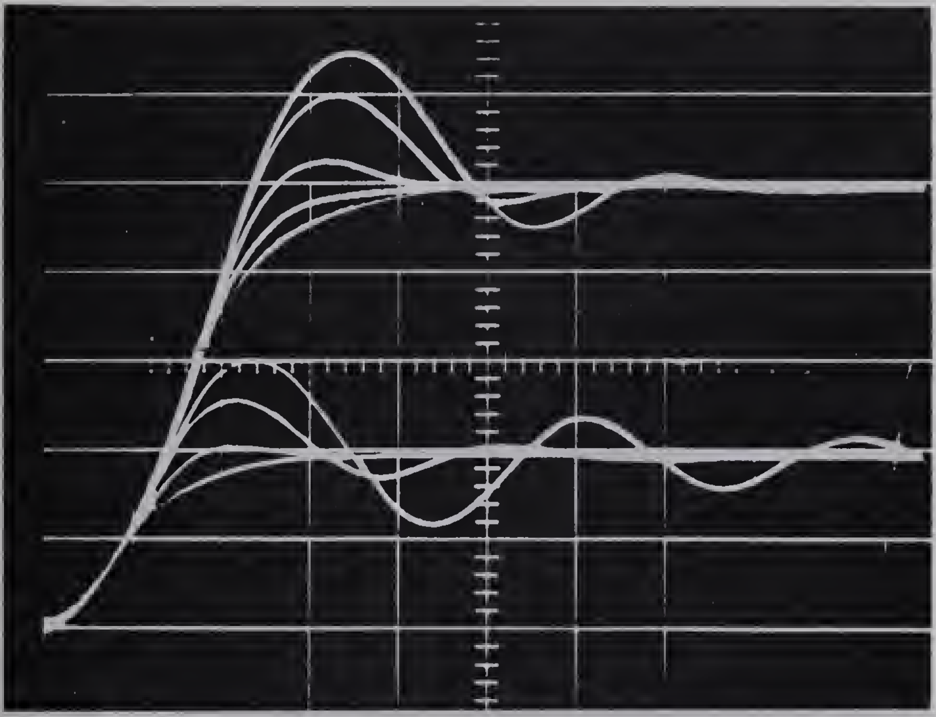

Figure 11.8

Underdamped Responses

1 volt/div. vertical

10 msec./div. horiz.

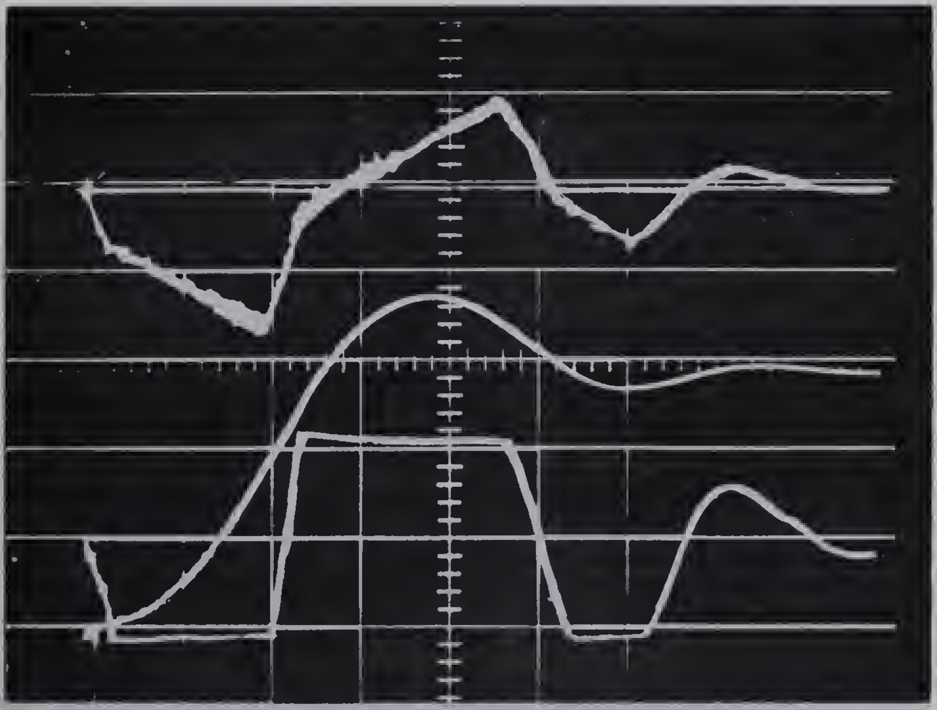

Figure 11.9

Tachometer Output
.2 volts/div.

Response
1 volt/div.

Amplifier Output
20 volts/div.

10 msec./div. horiz.

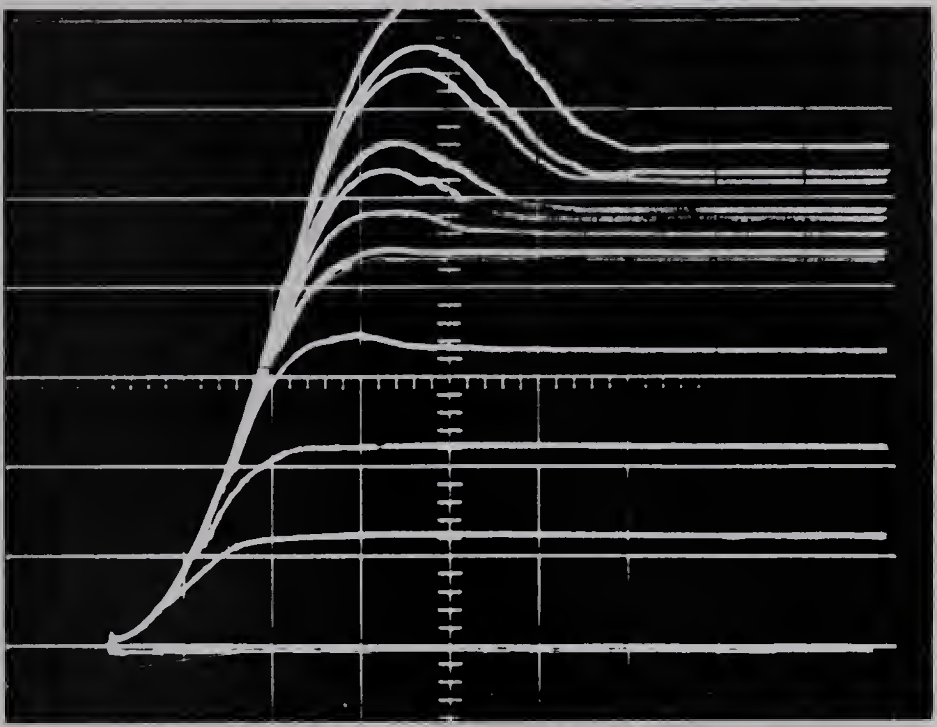

Figure 11.10

Effect of a Further Increase in Gain

1 volt/div. vertical

10 msec./div. horiz.

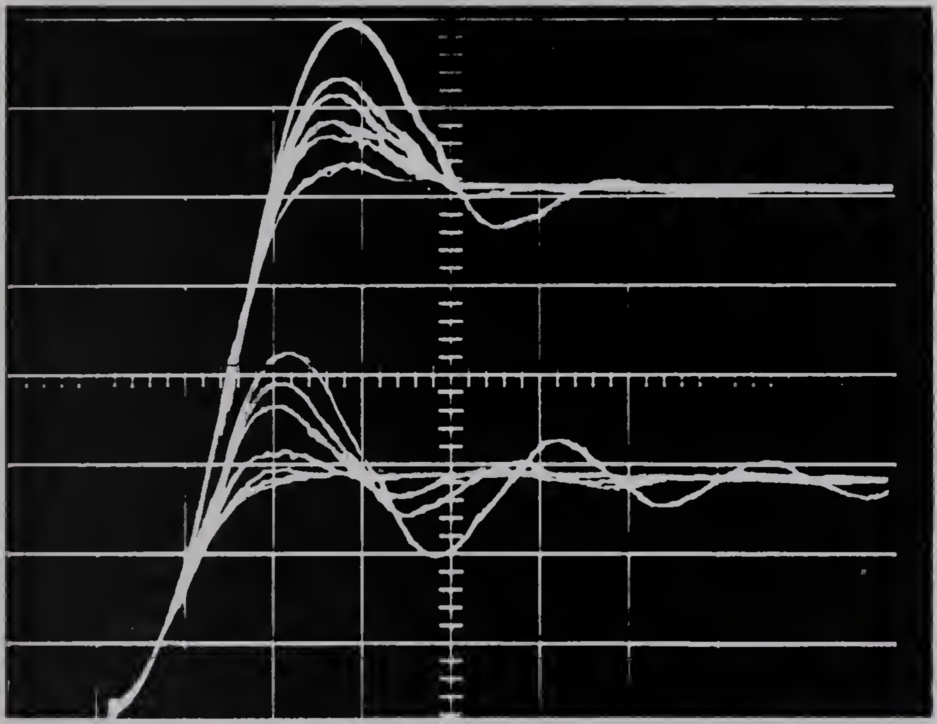

Figure 11.11

Underdamped Responses

.5 volts/div. vertical

10 msec./div. horiz.

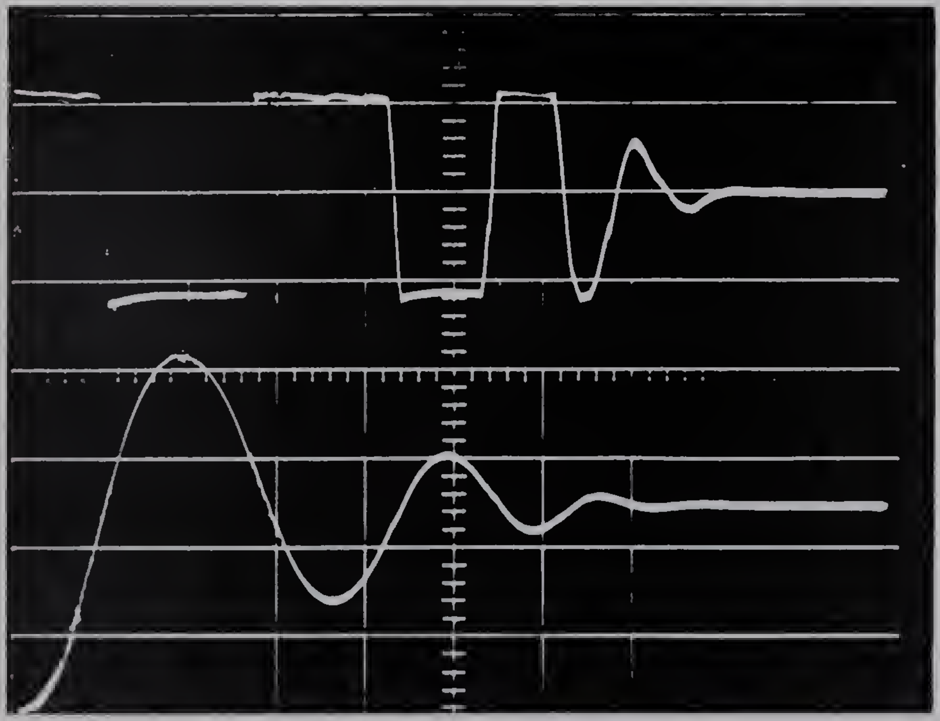

Figure 11.12

Amplifier Output
20 volts/div.

Response
2 volts/ div.

20 msec./div. horiz.

CHAPTER 12

PHASE ADVANCE STABILIZATION

12.1 INTRODUCTION

The use of derivative-of-error was found in Chapter 8 to be slightly unreliable in the cases of high input-amplifier gain. In order to avoid a "floating" input to the differentiator, the transfer function was necessarily of the form

$$G_d(s) = K_1(1 + as) \qquad (12.1)$$

where $a >> 1$ (12.2)

The differentiator was therefore an augmenting type. It is apparent then that the input amplifier and differentiator can well be replaced by a single block as shown in figure 12.1.

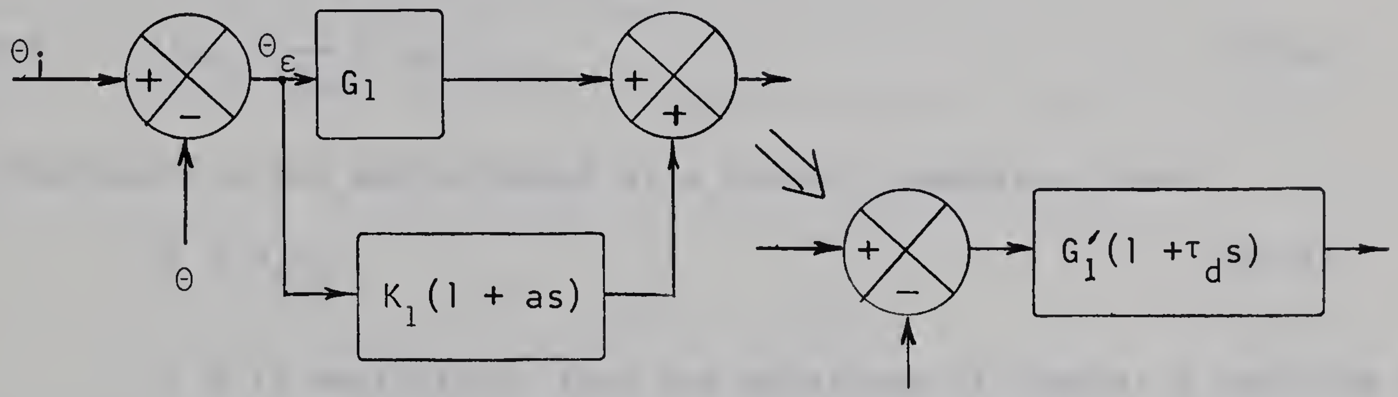

Figure 12.1 Derivative Controller and Ideal Lead Network

Due to the frequency limitations of physical components, the transfer function will also possess an upper cutoff frequency. A physically realizeable network will thus have a transfer function the form of equation 8.12.

The reason for the location of this chapter is that this phase-advance or phase-lead stabilization will be used in conjunction with the utilization of maximum acceleration. Velocity limiting will be avoided. The system is shown in figure 12.2.

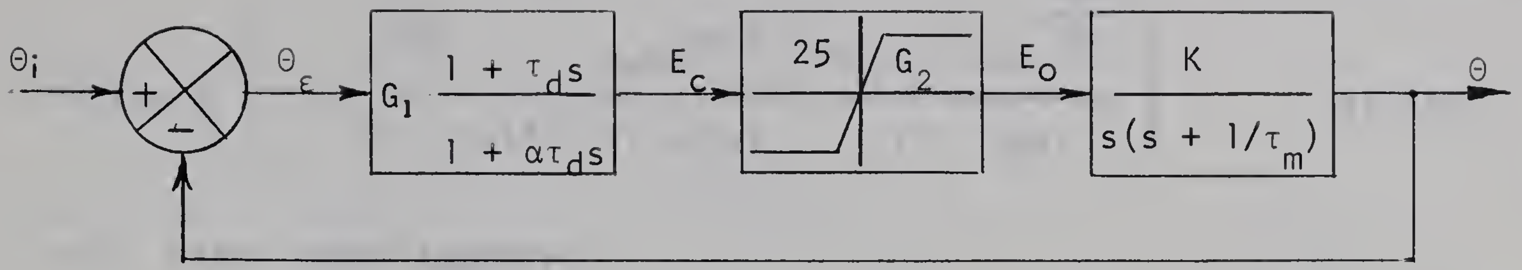

Figure 12.2 Phase Advance Stabilization

12.2 TRANSIENT ANALYSIS IN LINEAR REGION

The closed-loop transfer function is given by

$$\frac{\Theta(s)}{\Theta_i(s)} = \frac{\omega_n^2\ (1 + \tau_d\ s)}{\alpha\tau_d s^3 + s^2 + 2\xi\omega_n s + \omega_n^2} \tag{12.3}$$

where $$2\xi\omega_n = \frac{1}{\tau_m} + \omega_n^2\tau_d \tag{12.4}$$

If the motor is now approximated as a double integrator, then

$$2\xi \simeq \omega_n\tau_d \tag{12.5}$$

If α is negligible, then the equations of Chapter 8 describe the linear response. For very small values of α, critical damping occurs approximately at $\xi = 1$. It should be noted that critical damping here does not imply no overshoot, but simply a non-oscillatory solution. For this case, the denominator of equation 12.3 may be factored approximately$^{(9)}$. Again, for convenience, time is normalized.

$$F(p) = \mathcal{L}\left(f(t_n)\right) \tag{12.6}$$

$$\frac{\Theta(p)}{\Theta_i(p)} = \frac{1 + 2p}{2\alpha p^3 + p^2 + 2p + 1} \tag{12.7}$$

$$\simeq \frac{1 + 2p}{(p + 1)^2\ (2\alpha p + 1)} \tag{12.8}$$

$$\simeq \frac{2(1 - \alpha)}{(1 - 2\alpha)^2(p + 1)} - \frac{1}{(1 - 2\alpha)(p + 1)^2} - \frac{4\alpha(1 - \alpha)}{(1 - 2\alpha)^2(2\alpha p + 1)} \tag{12.9}$$

For an increment Θ_i, the inverse Laplace transform yields the response

$$\Theta(t) = \Theta_i \left[1 - \frac{e^{-\omega_n t}}{(1 - 2\alpha)^2} - \frac{\omega_n t e^{-\omega_n t}}{(1 - 2\alpha)} + \frac{4\alpha(1 - \alpha)e^{-\frac{\omega_n t}{2\alpha}}}{(1 - 2\alpha)^2} \right] \tag{12.10}$$

12.3 PHASE PLANE ANALYSIS

If the approximations of Chapter 10 are again made, behaviour in the limited region ($|E_c| > 25/G_2$) is described by equation 10.11. The boundaries of the linear region, however are slightly different. In the linear region, the system is of third-order and the isoclines cannot be defined on the ν_ε vs. Θ_ε plane. An approximation may be made when α is very small in which case the complex roots are dominant and the system behaves essentially as a second-order one with damping ratio specified by the ξ of the complex poles. For small α, the transfer function of the phase advance network is given approximately by

$$G_1 \frac{1 + \tau_d s}{1 + \alpha\tau_d s} \simeq G_1(1 + \tau_d s)(1 - \alpha\tau_d s) \tag{12.11}$$

$$\simeq G_1\left(1 + s\tau_d(1 - \alpha) - \alpha s^2\tau_d^2\right) \tag{12.12}$$

From equation 12.5, for reasonable values of ω_n, $\tau_d << 1$ and $\tau_d^2 << \tau_d$. It is reasonable then to neglect the last term. The boundaries of the linear region are therefore given approximately by

$$G_1\left(1 + s\tau_d\ (1 - \alpha)\right)\ \Theta_\varepsilon = \pm\ 25/G_2 \tag{12.13}$$

Substituting for τ_d from equation 12.5 and normalizing

$$\Theta_\varepsilon + 2\xi(1 - \alpha)\nu_\varepsilon = \pm\ 25/G_1G_2 \tag{12.14}$$

The resulting phase plane diagram is shown in figure 12.2. Comparing this to figure 10.3, the boundaries are seen to be rotated clockwise through an angle determined by the magnitude of α.

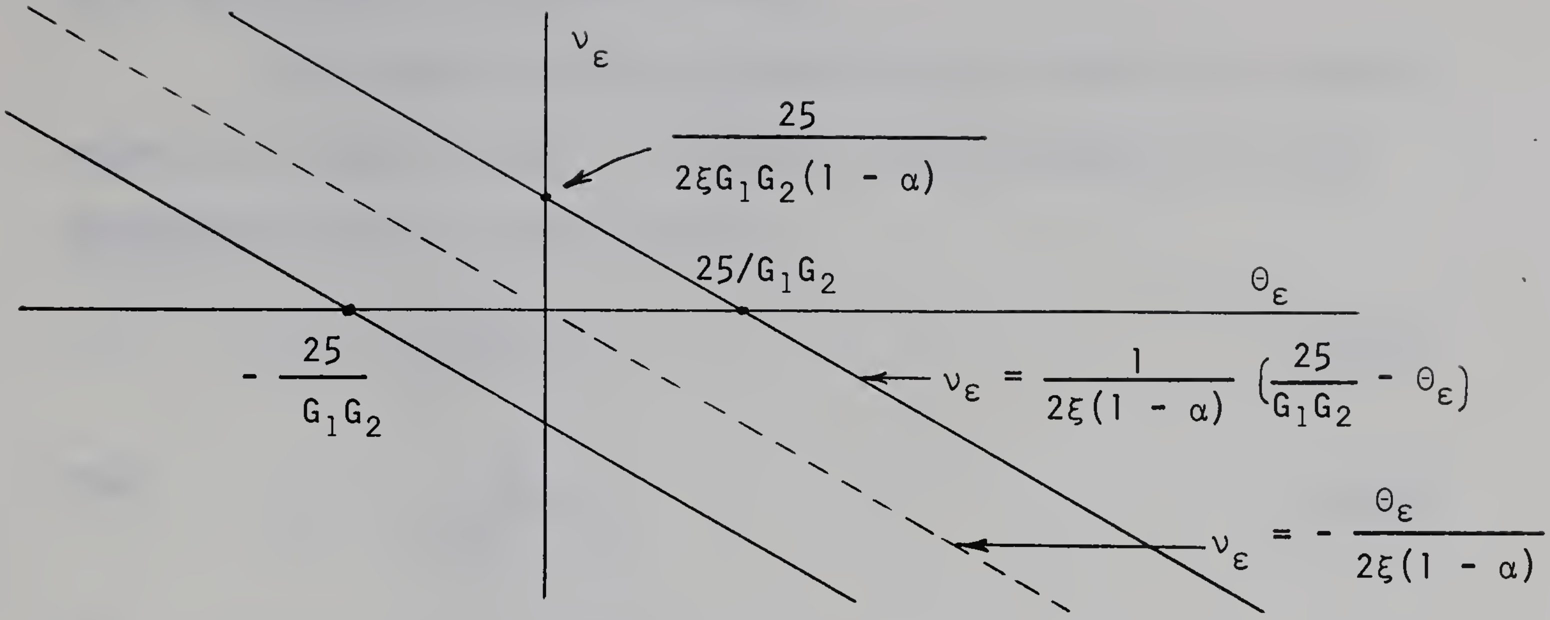
ν_ε
$\frac{25}{2\xi G_1 G_2 (1 - \alpha)}$
$25/G_1G_2$
Θ_ε
$-\frac{25}{G_1G_2}$
$\nu_\varepsilon = \frac{1}{2\xi(1 - \alpha)} \left(\frac{25}{G_1G_2} - \Theta_\varepsilon\right)$
$\nu_\varepsilon = -\frac{\Theta_\varepsilon}{2\xi(1 - \alpha)}$

Figure 12.3 Approximate Normalized Phase Plane Boundaries

Again using the approximation of equation 12.12, the isoclinal equation in the linear region may be obtained.

$$\Theta_\varepsilon = \Theta_i - \frac{\omega_n^2\left(1 + s\tau_d(1 - \alpha) - \alpha s^2 \tau_d^2\right)}{s(s + 1/\tau_m)} \Theta_\varepsilon \tag{12.15}$$

$$s^2\Theta_\varepsilon\left(1 - \alpha\tau_d^2\right) + s\Theta_\varepsilon\left[\frac{1}{\tau_m} + \omega_n^2\tau_d(1 - \alpha)\right] + \omega_n^2\Theta_\varepsilon \tag{12.16}$$

$$(1 - \alpha\tau_d^2\omega_n^2)\frac{d\omega_\varepsilon}{d\Theta_\varepsilon} + (2\xi\omega_n - \alpha\tau_d\omega_n^2) + \frac{\Theta_\varepsilon}{\omega_\varepsilon}\omega_n^2 = 0 \tag{12.17}$$

Normalizing,

$$(1 - \alpha\tau_d^2\omega_n^2)\frac{d\nu_\varepsilon}{d\Theta_\varepsilon} + (2\xi - \alpha\tau_d\omega_n) + \frac{\Theta_\varepsilon}{\nu_\varepsilon} = 0 \tag{12.18}$$

If the motor is again approximated as a double integrator,

$$\frac{d\nu_\varepsilon}{d\Theta_\varepsilon}(1 - 4\alpha\xi^2) + 2\xi(1 - \alpha) + \frac{\Theta_\varepsilon}{\nu_\varepsilon} \simeq 0 \tag{12.19}$$

Thus the isoclines are approximately given by

$$\nu_\varepsilon = -\frac{\Theta_\varepsilon}{2\xi(1 - \alpha) + \frac{d\nu_\varepsilon}{d\Theta_\varepsilon}(1 - 4\alpha\xi^2)} \tag{12.20}$$

which may be compared to equation 10.7.

12.4 OPTIMIZING THE PHYSICAL SYSTEM

The simplification of neglecting the width of the linear region will again be used. In figure 10.4, the equation of the changeover boundary is now given by

$$\nu_\varepsilon = - \frac{\Theta_\varepsilon}{2\xi\ (1 - \alpha)} \qquad (12.21)$$

Thus

$$\nu_{\varepsilon 1} = - \frac{\Theta_{\varepsilon 1}}{2\xi(1 - \alpha)} \qquad (12.22)$$

and

$$\Theta_{\varepsilon 1} - \Theta_i = - \frac{{\Theta_{\varepsilon 1}}^2}{4\omega\xi^2(1 - \alpha)^2} \qquad (12.23)$$

$$\Theta_{\varepsilon 1} = -2w\xi^2(1 - \alpha)^2 + 2w\xi(1 - \alpha)\ \sqrt{\xi^2(1 - \alpha)^2 + \frac{\Theta_i}{w}} \qquad (12.24)$$

$$\Theta_{\varepsilon p} = 2\Theta_{\varepsilon 1} - \Theta_i$$

$$= -4w\xi^2\ (1 - \alpha)^2 + 4w\xi(1 - \alpha)\sqrt{\xi^2(1 - \alpha)^2 + \frac{\Theta_i}{w}} - \Theta_i \qquad (12.25)$$

The condition for no overshoot is now given by

$$\frac{\Theta_i}{w} + 4\xi^2(1 - \alpha)^2 = 4\xi(1 - \alpha)\sqrt{\xi^2(1 - \alpha)^2 + \frac{\Theta_i}{w}} \qquad (12.26)$$

Thus, for $\xi = 1$,

$$w = \frac{\Theta_i}{8\ (1 - \alpha)^2} \qquad (12.27)$$

For no limiting of the positional error

$$G_1 = 1\ \frac{\text{volt}}{\text{volt}} = \frac{15}{\pi} = 4.34\ \frac{\text{volts}}{\text{rad}} \qquad (12.28)$$

For increments of up to π radians to have no overshoot

$$w \simeq \frac{\pi}{8\ (1 - \alpha)^2} \qquad (12.29)$$

Thus, from equation 10.22

$$G_2 = \frac{50}{wG_1} = \frac{80(1-\alpha)^2}{3} \qquad (12.30)$$

The upper corner frequency of the power amplifier (see Appendix 2) is about 1K Hz. Its transfer function is given by

$$G(s) \simeq \frac{10}{1 + s/6280} \qquad (12.31)$$

$$\simeq \frac{10}{1 + .00016s} \qquad (12.32)$$

that is

$$\alpha\tau_d \simeq .00016 \qquad (12.33)$$

Since $\xi = 1$ was used to obtain equation 12.30, it is reasonable to establish the last required equation on this basis, that is, from equation 12.5;

$$\tau_d \simeq 2/\omega_n \qquad (12.34)$$

This value, however, does not ensure critical damping (i.e. no oscillations). The required value may alternatively be found directly from the closed-loop transfer function using the approximation of equation 12.11.

$$\frac{\Theta(s)}{\Theta_i(s)} \simeq \frac{\omega_n^2\,(1+\tau_d s)\,(1-\alpha\tau_d s)}{s(s+1/\tau_m) + \omega_n^2(1+\tau_d s)(1-\alpha\tau_d s)} \qquad (12.35)$$

$$\simeq \frac{\omega_n^2\,\left(1+\tau_d(1-\alpha)s - \alpha\tau_d^2 s^2\right)}{s^2\left(1-\alpha\tau_d^2\omega_n^2\right) + s\left(1/\tau_m + \omega_n^2\tau_d\,(1-\alpha)\right) + \omega_n^2} \qquad (12.36)$$

For critical damping the roots of the denominator must be identical. The motor may again be approximated as a double integrator, hence

$$\left(\omega_n^2\tau_d(1-\alpha)\right)^2 \simeq 4(1-\alpha\tau_d^2\omega_n^2)\omega_n^2 \qquad (12.37)$$

$$\omega_n^2\tau_d^2(1-\alpha)^2 \simeq 4 - 4\alpha\tau_d^2\omega_n^2 \qquad (12.38)$$

$$(\tau_d \omega_n)^2 \simeq \frac{4}{(1+\alpha)^2} \qquad (12.39)$$

$$\tau_d \simeq \frac{2}{\omega_n(1+\alpha)} \qquad (12.40)$$

This is seen to yield a smaller value than equation 12.34. It is difficult to say which will render the system nearest to critically damped. Neither will ensure zero overshoot. Little difference is made however, since for the physical system, using the unmodified motor, the optimum values are:

$\alpha \simeq .016$

$\tau_d \simeq .01$

$G_2 \simeq 26$

12.5 EXPERIMENTAL RESULTS AND SUMMARY

The phase advance network used is shown in figure A 4.10. Typical responses are shown in figures 12.3 and 12.4. For the largest step of about 160°, the response is just beginning to overshoot. Peak time for this increment is about 40 msec. This is the best result obtained which is understandable since the unmodified motor was used (high gain), and optimal forward gain was used in conjunction with the anticipatory nature of the phase-lead network.

Responses to very small increments are shown in figure 12.4. The smallest is about 3.5°. The finite resolution of the potentiometer is noticeable.

A solution for the transient response is also possible from the approximate transfer function of equation 12.35. The result is somewhat different than equation 12.10. The necessity of making approximations to simplify the cubic form of the characteristic equation is probably the reason that phase-lead stabilized systems

are generally analyzed by the frequency response method.

In spite of the gross simplifications used in the optimization however, the value $\tau_d \simeq .01$ was seen to give almost the exact predicted results. This in itself is strong support for the validity of the approximations.

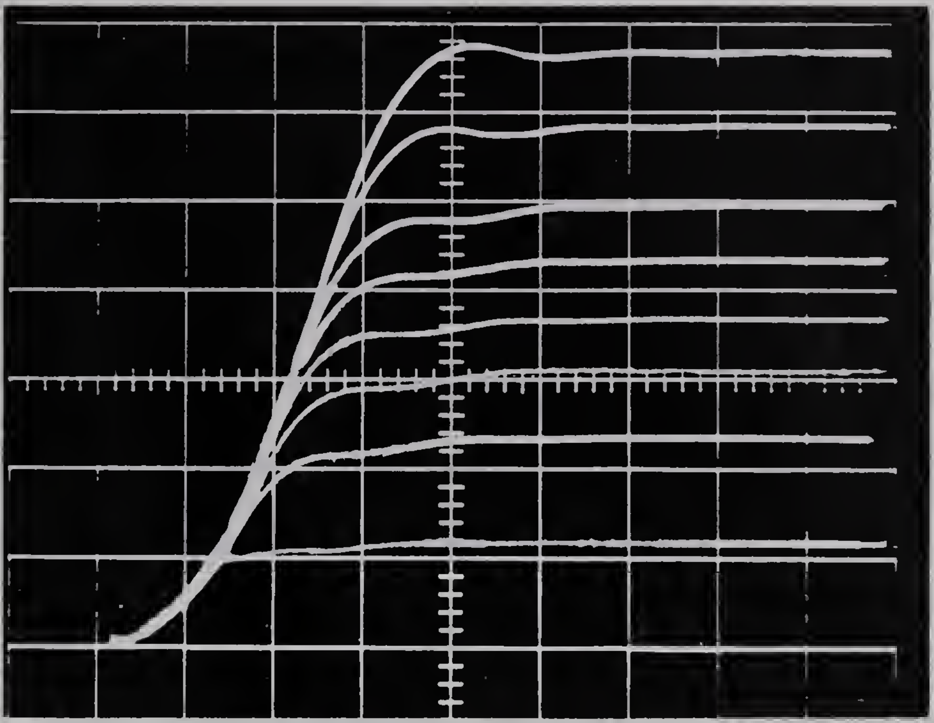

Figure 12.3

2 volts/div. vertical

10 msec./div. horiz.

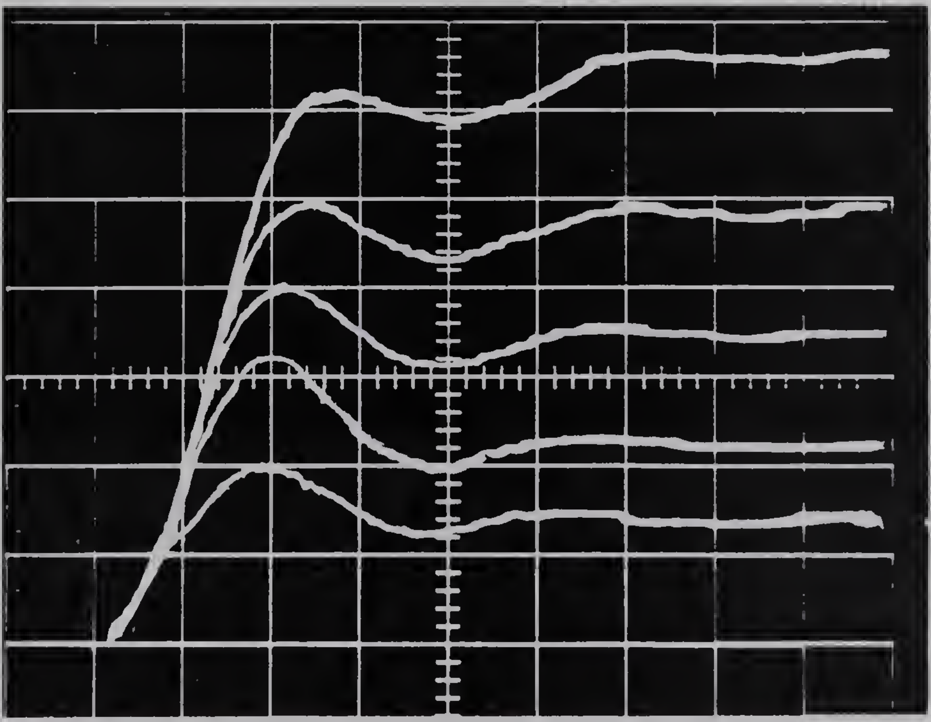

Figure 12.4

.2 volts/div. vertical

5 msec./div. horiz.

CHAPTER 13

REALIZATION OF OPTIMAL RESPONSE

13.1 INTRODUCTION

The assumptions used in the last three chapters may be summarized: (1) the system is an ideal second order system with negligible friction; (2) the motor is a double integrator; (3) the width of the linear region of the power amplifier may be considered negligible for large increments.

Thus, the analysis was that of an on-off or switched system. The critical boundary defined in Section 11.4 can be considered to be the ideal changeover or switching boundary.

It was possible to optimize the response for only one value of increment size. The largest occurring value of π radians was used to establish optimum values of gain. For increments other than π radians, responses were seen to be non-optimal as shown in figure 10.7.

The "chattering" trajectory for increments less than π radians was not really a significant problem (as it is in real switched systems) since the narrow linear region is entered as the origin is approached. The response, however, is far from ideal. If the system were optimized for a different increment size, say $\pi/2$, undesirably large overshoots would occur for larger increments. With this as a prelude, a system designed to achieve ideal, or optimal response for all magnitudes of step inputs will now be presented.

13.2 PHASE PLANE ANALYSIS OF OPTIMAL RESPONSE

The equation for the critical boundary may be written:

$$\omega_\varepsilon \, |\omega_\varepsilon| = -\, 50K \, \Theta_\varepsilon \tag{13.1}$$

Let the control signal be given by the general non-linear function:

$$E_c = f_1(\Theta_\varepsilon) + f_2(\omega_\varepsilon) \tag{13.2}$$

Since the linear region has been assumed negligible, then the changeover occurs when

$$E_c \simeq 0 \tag{13.3}$$

thus $$f_2(\omega_\varepsilon) = -\, f_1(\Theta_\varepsilon) \tag{13.4}$$

If the changeover is to occur on the critical boundary, then equations 13.1 and 13.4 must be identical. If f_1 and f_2 can be chosen to accomplish this then the initial trajectory will be given by

$$\omega_\varepsilon \, |\omega_\varepsilon| = 50K \, (\Theta_\varepsilon - \Theta_i) \tag{13.5}$$

which will intersect the critical boundary at

$$\left(\frac{\Theta_i}{2}, \; -\frac{\omega_n \Theta_i}{4\xi}\right)$$

from here the phase point will follow the critical boundary as a trajectory until, near the origin, the linear region is entered. Providing G_2 is sufficiently large, then phase trajectories for typical positive inputs of any magnitude will resemble those shown in figure 13.1.

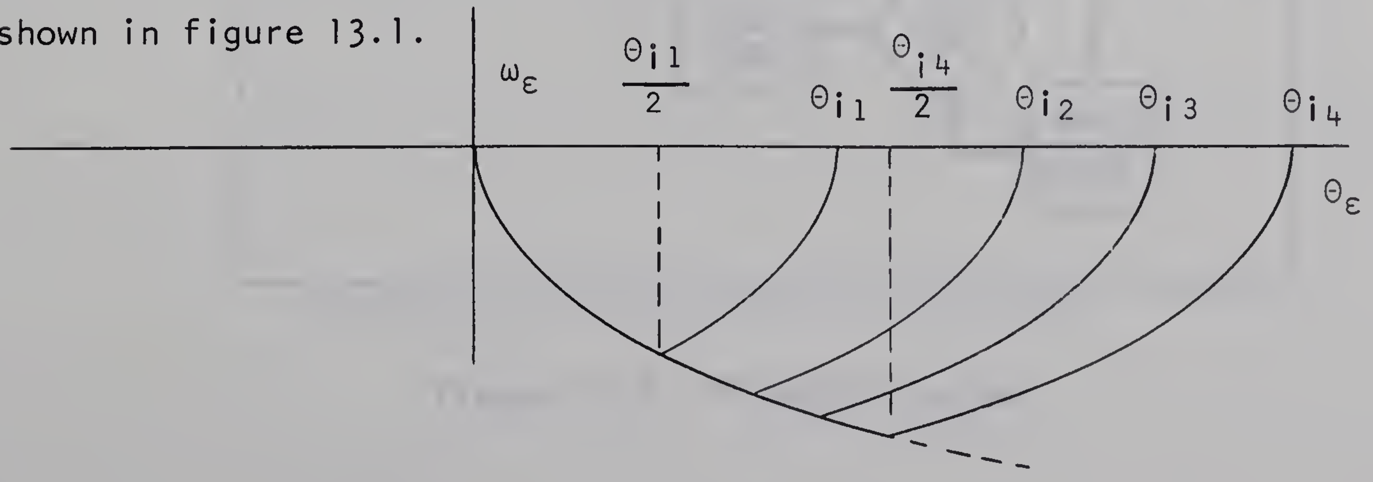

Figure 13.1 Optimal Trajectories

13.3 THE "V-MOD-V" SYSTEM

The simplest solution for a choice of f_1 and f_2 is to make use of the normal error signal, that is

$$f_1(\Theta_\varepsilon) = G_1\Theta_\varepsilon \tag{13.6}$$

then

$$f_2(\omega_\varepsilon) = - G_1\Theta_\varepsilon \tag{13.7}$$

$$= + \frac{G_1}{50K}\,\omega_\varepsilon\,|\omega_\varepsilon| \tag{13.8}$$

or, if the rate signal is to be derived from the output velocity (i.e., the tachometer output) then the control signal will be given by

$$E_c = G_1\left(\Theta_\varepsilon - \frac{\omega\,|\omega|}{50K}\right) \tag{13.9}$$

This form of "velocity squared" damping has been called "V-Mod-V". The system using this method is shown in figure 13.2.

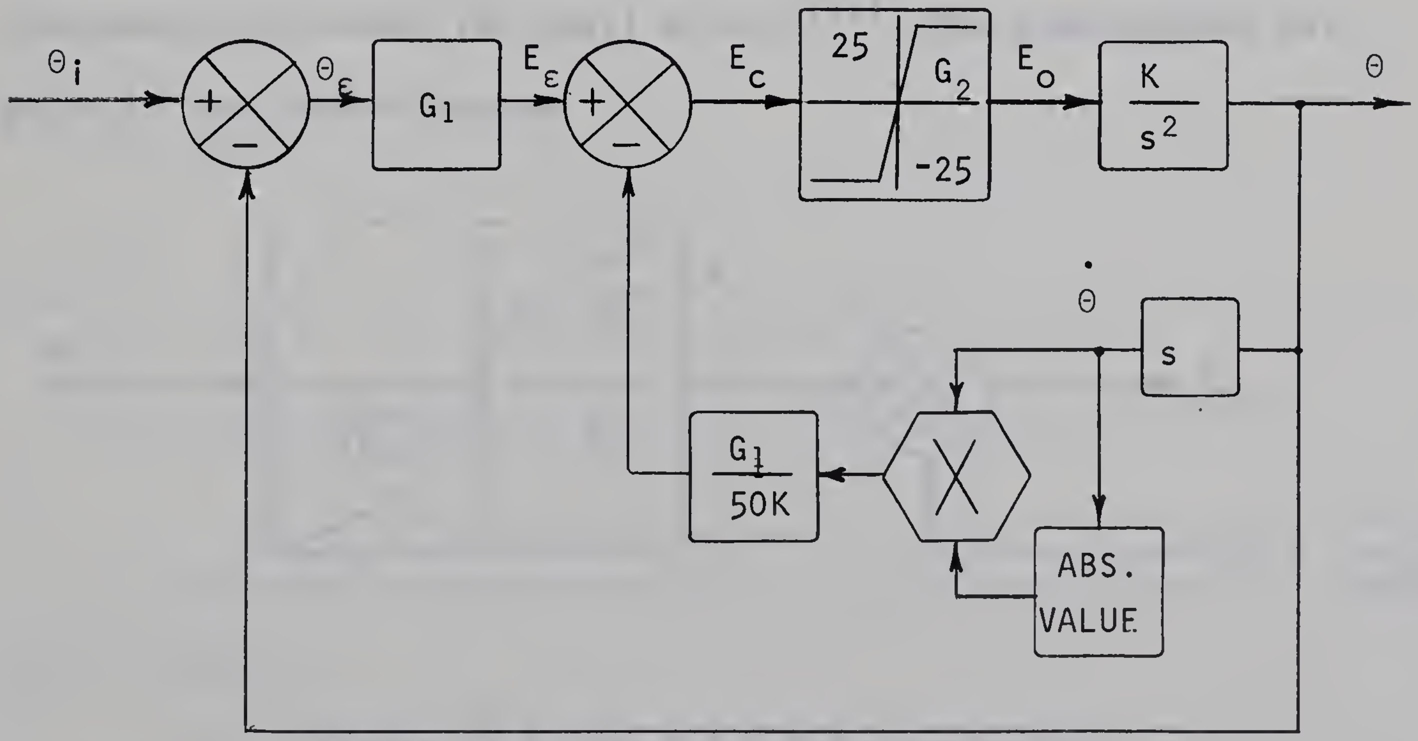

Θ_i
+
−
Θ_ε
G_1
E_ε
+
−
E_c
25
G_2
-25
E_o
$\frac{K}{s^2}$
Θ
$\dot{\Theta}$
s
$\frac{G_1}{50K}$
ABS. VALUE

Figure 13.2 "V-Mod-V" System

13.4 THE S.E.R.M.E. SYSTEM

Of the many choices of functions available to satisfy the conditions, one sometimes used(11) is

$$f(\omega_\varepsilon) = \frac{\omega\varepsilon}{\sqrt{50K}} \qquad (13.10)$$

that is, velocity damping is used in the normal manner to satisfy the condition of equation 12.1. It can then be shown that

$$f(\Theta_\varepsilon) = (\text{sign } \Theta_\varepsilon)\sqrt{|\Theta_\varepsilon|} \qquad (13.11)$$

Thus, the system takes its name from the initials of "Sign Error Root Modulus of Error". The characteristic is shown in figure 13.3.

A problem can be seen to occur: when the system is not in its limited region and the error is very small, the gain through the block generating $f(\Theta_\varepsilon)$ becomes extremely large and approaches infinity as Θ_ε approaches zero. This would result in instability causing a high-frequency, low-amplitude oscillation similar to the chattering of off-on systems. It may be avoided by making the characteristic linear for small errors.(10) The problem does not exist in the V-Mod-V system.

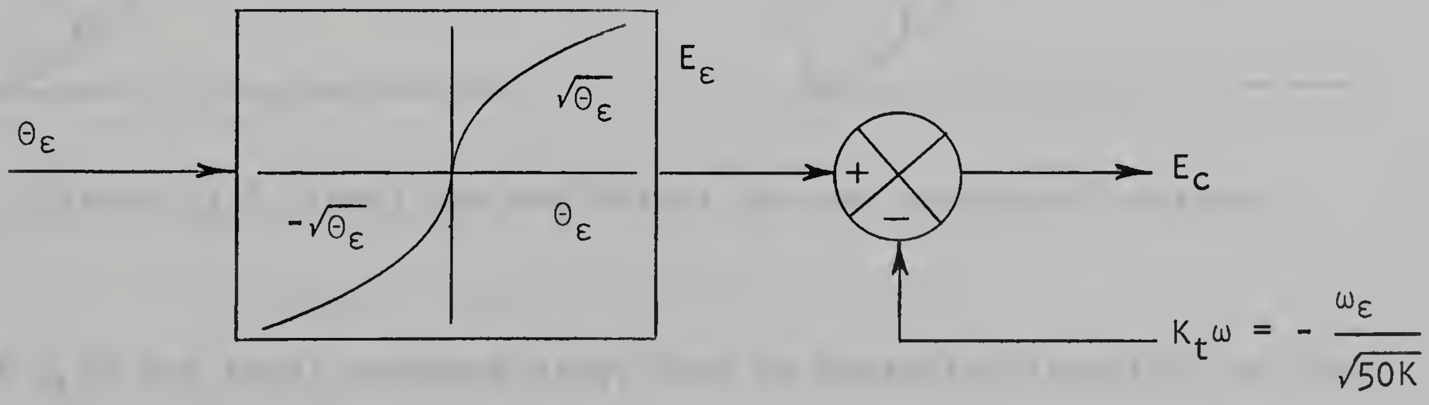
$\Theta\varepsilon$
$\sqrt{\Theta_\varepsilon}$
$-\sqrt{\Theta_\varepsilon}$
Θ_ε
E_ε
+
−
E_c
$K_t\omega = -\frac{\omega\varepsilon}{\sqrt{50K}}$

Figure 13.3 The S.E.R.M.E. Controller

13.5 OPTIMAL RESPONSE TIMES FOR THE PHYSICAL SYSTEMS

In order to determine how closely the objective of high speed was approached in this work, the minimum response times theoretically attainable will now be determined for the two physical systems. For the optimally switched systems, trajectories are as shown in figure 13.1. It should be recalled that these are based on the approximation of parabolic phase plane trajectories of Chapter 9. The corresponding functions $\ddot{\Theta}$, $\dot{\Theta}$ and Θ are shown in figure 13.4 for two different increments. The true functions are shown for comparison.

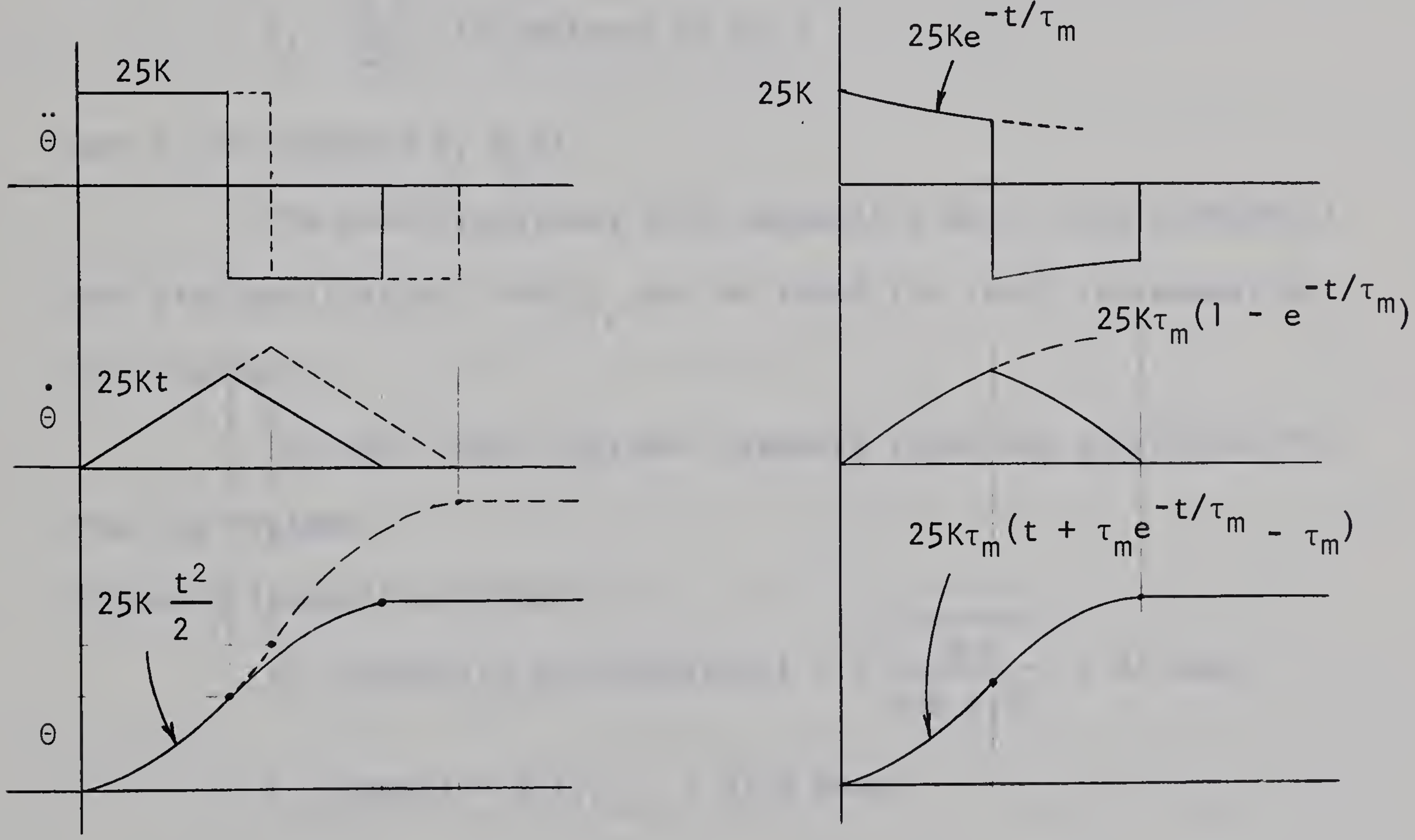

Figure 13.4 Idealized and Actual Optimal Response Functions

If t_p is the total response time, then by reasoning identical to that used in Chapter 9

$$\frac{\Theta_i}{2} = \int_0^{t_p/2} \omega(t)dt$$

$$= \int_0^{t_p/2} 25K(1 - e^{-t/\tau_m})dt$$

$$\approx \int_{0}^{t_p/2} 25Kt\,dt$$

$$\approx 25K \left.\frac{t^2}{2}\right|_{0}^{t_p/2}$$

$$\approx 25Kt_p^2/8$$

thus

$$t_p \approx \sqrt{4\Theta_i/25K}$$

The region of the graphs of figures 9.3 and 9.4 are applicable up to $\pi/2$ if

$$\Theta_i - \frac{2.5}{G_1} \text{ is replaced by } \Theta_i/2$$

and t_1 is replaced by $t_p/2$

The exact solutions (not neglecting motor time constants) are also applicable. Thus t_p can be found for input increments up to π radians.

For this input, optimal response times are calculated for the two systems.

System 2 (Unmodified Motor):

$$t_p \text{ (parabolic approximation) } \approx \sqrt{\frac{4\pi}{300 \times 25}} \approx 41 \text{ msec.}$$

$$t_p \text{ (exact) } = 2(t_1)_{\pi/2} \approx 43.6 \text{ msec.}$$

System 1 (Modified Motor):

$$t_p \text{ (parabolic approximation) } \approx 50 \text{ msec.}$$

$$t_p \text{ (exact) } \approx 52.2 \text{ msec.}$$

CONCLUSIONS

This report has described the use of a printed motor in a positional control system designed to achieve minimum response time and maximum accuracy. It is best suited for positioning low-inertia, low-friction loads since peak time increases with the square root of the total moment of inertia and steady state error is proportional to total non-viscous frictional torque.

Direct drive servos such as machine tool controllers and mechanisms used in business machines and data processing equipment are typical applications in which high speed and accuracy are demanded requirements. In such systems the printed motor, with its high torque to inertia ratio, offers decided advantages over conventional servo motors.

Using high gain and limiting, operation closely approached that of an on-off system. Steady state error was made almost negligible and response times of 56 and 42 msec. for an increment of about 175° were accomplished using the modified and unmodified motors respectively. Very little improvement could be achieved by use of an actual on-off system (49 and 40 msec.) and the relay chattering problem would have to be solved. A dual-mode system (two forward paths) would be a practical alternative.

The most significant improvement could be realized by elimination of the series resistor. The "stiffness", and therefore the accuracy of the system would be doubled (equations 7.3 and 7.4) and response times would be reduced by approximately 30%. The doubled current requirement of both the power amplifier and its supply, however, would likely double the system cost. Power supply regulation, which was only a minor drawback in this work, would become an expensive consideration.

The best improvement obtainable with the power amplifier used would be the accomplishment of optimal response for all magnitudes of inputs by using one of the systems recommended in Chapter 13.

BIBLIOGRAPHY

(1) Burr, R.P.: "The Printed Motor - A New Approach to Intermittent and Continuous Motion Devices in Data Processing Equipment"; Proc. Eastern Joint Computers Cont., Vol. 18, pp. 325-342; 1960.

(2) Burn, R.P. and Henry-Baudot, J.: "Printed-Circuit D.C. Motors for Electronic and Instrument Applications"; IRE National Convention Record, Part 9, pp. 102-112; 1959.

(3) Martin, V.C.: "Printed Circuit Motors for High Speed Incrementing of Inertial and Dissipative Loads"; IRE Transactions on Industrial Electronics, pp. 28-45; May, 1963.

(4) MacDonald, Gerald S.: "The S-1 Servo System - A General Description and Analysis"; Technical Articles and Papers, Printed Motors, Inc., Glen Cove, N.Y.

(5) Kuo, B.C.: "Automatic Control Systems"; pp. 27-134, 451-454, 144-145, 101-105.

(6) Brenneman, Kerchner and Kloeffler: "Direct Current Machinery"; The MacMillan Co., pp. 318-332; 1949.

(7) Langsdorf: "Principles of D.C. Machines"; McGraw-Hill; 1959.

(8) Pastel and Thaler: "Analysis and Design of NL FB Control Systems"; McGraw-Hill; 1962.

(9) West, J.C.: "Analytical Techniques for NL Control Systems"; The English Universities Press Ltd.; 1960.

(10) Douce, Taylor and West: "The Effects of the Addition of Some Non-Linear Elements on the Transient Response of a Simple RPC System Possessing Torque Limitation"; Proc. IEE, Vol. 101, Part II, p. 156.

(11) Dalton and West, J.C.: "The Step-Function Response of an RPC System Possessing Torque Limitation"; Proc. IEE, Vol. 101, Part II, p. 166; 1954.

(12) Printed Motor Servos, Photocircuits Corporation, Glen Cove, N.Y.

APPENDIX 1: PRINTED MOTOR SPECIFICATIONS

MODEL 488 MOTOR CHARACTERISTICS*

Rated Torque (continuous duty)	42.5 ounce-inches
Maximum Pulse Torque Capability (intermittent)	375 ounce-inches
Armature Inertia (including hub and shaft)	.018 oz-in-sec^2
Mechanical Time Constant	.030 seconds
Equivalent Series Mechanical Impedance (at constant terminal voltage)	15.37×10^{-3} krpm/oz-in.
Armature Inductance	Less than 100 micro-henries
Rated Speed (continuous duty)	3300 RPM
Rated Current for 70° C rise (continuous)	7.5 amps
Maximum Stall Current (continuous)	6 amps
Rated Voltage	24 volts D.C.
Power Output at 3300 rpm	105 Watts
Magnetic Field	8 pole Alnico
Number of commutation segments	121
Armature Resistance	.600 ohms
Maximum Friction Torque	2.0 ounce-inches
Back EMF per 1000 RPM	5.55 volts
Average Torque per ampere	7.5 ounce-inches
Weight	6.5 pounds

---

* Supplied with Printed Motor

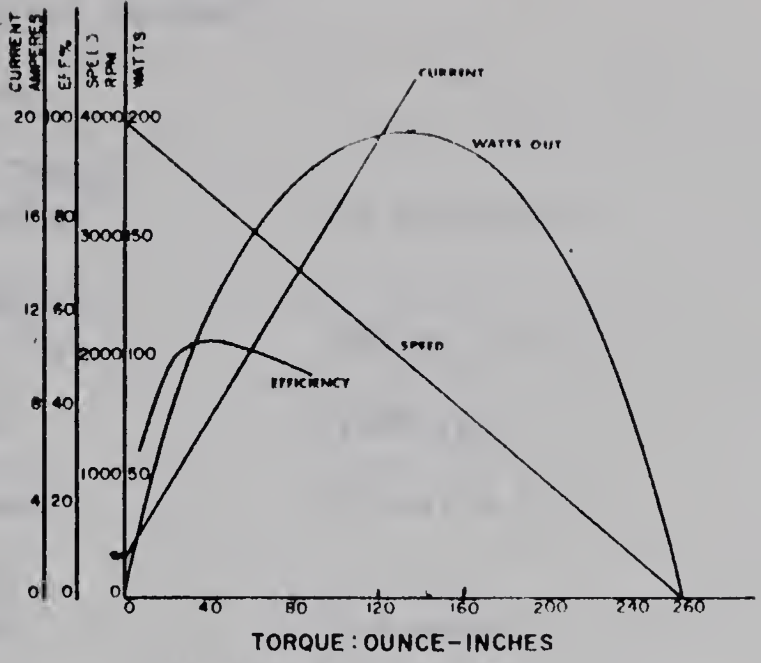

Figure A1.1 PERFORMANCE CURVES (24 V DC INPUT)

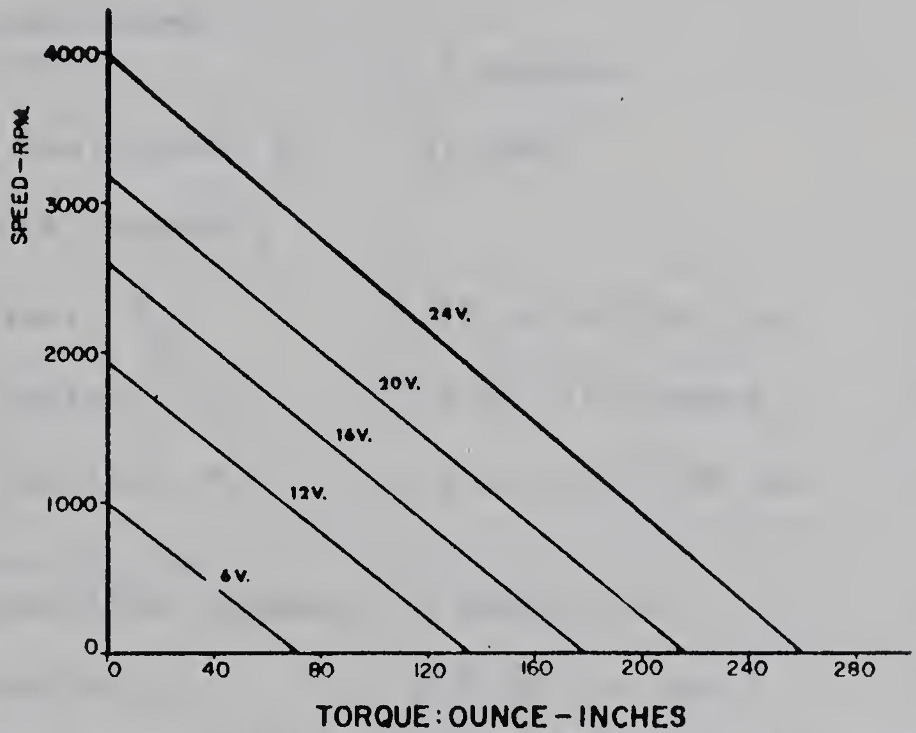

Figure A1.2 SPEED TORQUE CHARACTERISTICS

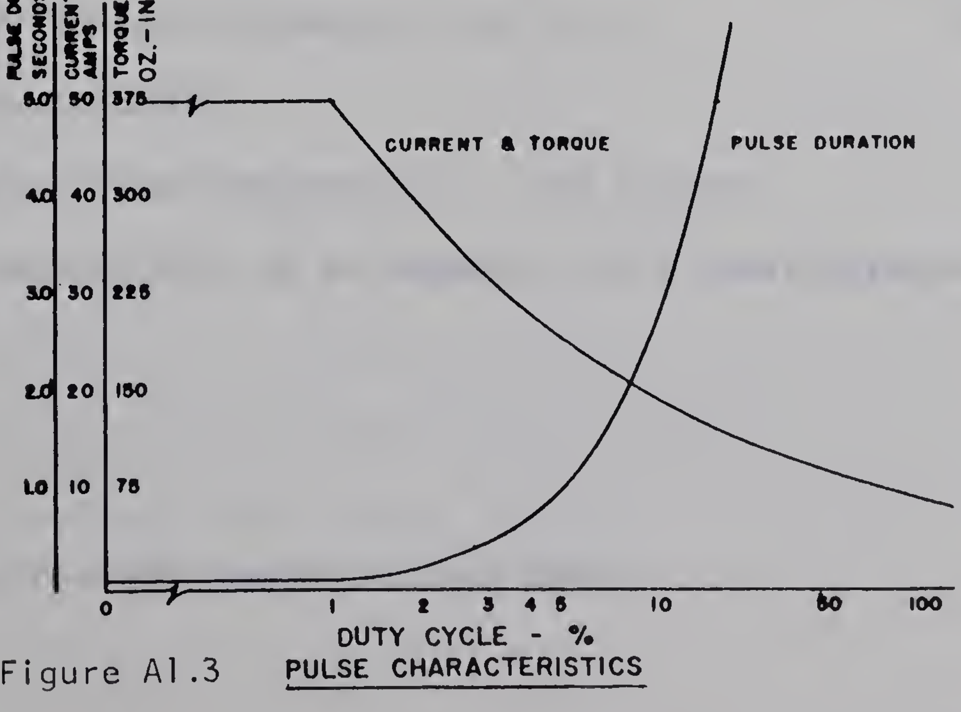

Figure A1.3 PULSE CHARACTERISTICS

[illegible]

[illegible]

[illegible]

MODEL PM-488 MOTOR CHARACTERISTICS *
(all values are nominal)

MOTOR RATINGS

Continuous Torque (rated speed):	42.5 oz.-in.	3.1 kg.-cm.
Pulse Torque at 60 amperes, T_p:	450 oz.-in.	32.4 kg.-cm.
Rated Speed:	3600 rpm.	377 rad./sec.
Rated Voltage:	24 volts D.C.	
Power Output at Rated Speed:	114 watts.	
Rated Current	7.5 amperes.	
Maximum Continuous Stall Current:	7.0 amperes.	
Terminal Resistance, R_a	.53 ohms.	

BASIC MOTOR CONSTANTS

EMF Constant, K_g	5.55 volts/1000 rpm.	.0529 volts/rad.-sec^{-1}
Torque Constant, K_T	7.5 oz.-in./ampere	540 gr.-cm./ampere
Damping Constant, K_d	3.2 oz.-in./1000 rpm.	2.2 gr.-cm./rad/sec.
Regulation, K_m, at constant applied voltage:	13 rpm/oz.-in.	.019 rad/sec/gr.-cm.
Rotor Inertia, J_a	.018 oz.-in. sec.^{2}	1.29 gm.-cm. sec.^{2}
Armature Inductance	Less than 100 microhenries	
Average Friction Torque, T_f	3 oz.-in.	216 gm.-cm.

DERIVED CONSTANTS

Mechanical Time Constant, τ_m: .023 seconds

Power Rate (T_p^2/J) at 60 amperes: 78 kilowatts/second

---

* Taken from PMI Technical Data Sheet

APPENDIX 2: POWER AMPLIFIER

The power amplifier which was used in this work is a solid state D.C. amplifier, Model 1833-AN-06R1 made by Dynatran Electronics Corporation. It is wired as an operational amplifier with single-ended input and output connections. Linear non-switching circuitry results in wide range frequency responses and eliminates the RFI problems inherent with high power switching circuitry. The amplifier is phase inverting and has feedback that provides good linearity under both no load and full load conditions. The Class B output stage provides high efficiency and low power consumption under no load conditions. The amplifier is convection cooled. The following list of detailed specifications is taken from the amplifier instruction manual.

A. Maximum power output: 600 watts (25 volts at 24 amperes).

B. Frequency response at full D.C. and peak A.C. output power: -3 db at 1KC minimum.

C. Voltage gain: 10 (same for all three inputs).

D. Input impedance: 25K (resistive); three summing inputs are provided.

E. Equivalent input drift and noise: 100 millivolts maximum.

F. Linearity: 1% typical.

G. Ambient temperature: 0° - 55°C, i.e., temperature of ambient air and mounting frame.

H. Power supply requirements: ±30 volts D.C. at 4.5 to 28.5 amps. The sum of the positive and negative supply currents, however, will not exceed 33 amps simultaneously.

I. Recommended power supply regulation and ripple: 1 to 2%.

J. Load: Output load should not be less than 1.04 ohms under any conditions.

K. Short circuit protection: If the load current or current in the output stage exceeds approximately 25 amps for 1 millisecond or longer, the short circuit protection will operate to blow the fuses in the power supply line.

L. Size: 7'' x 19'' rack panel mounted, 16 3/4'' behind panel.

M. Weight: 28 lbs.

A simplified schematic diagram of the amplifier is shown in figure A2.1.

The amplifier frequency response and phase shift were measured experimentally and are shown in figures A2.2 and A2.3.

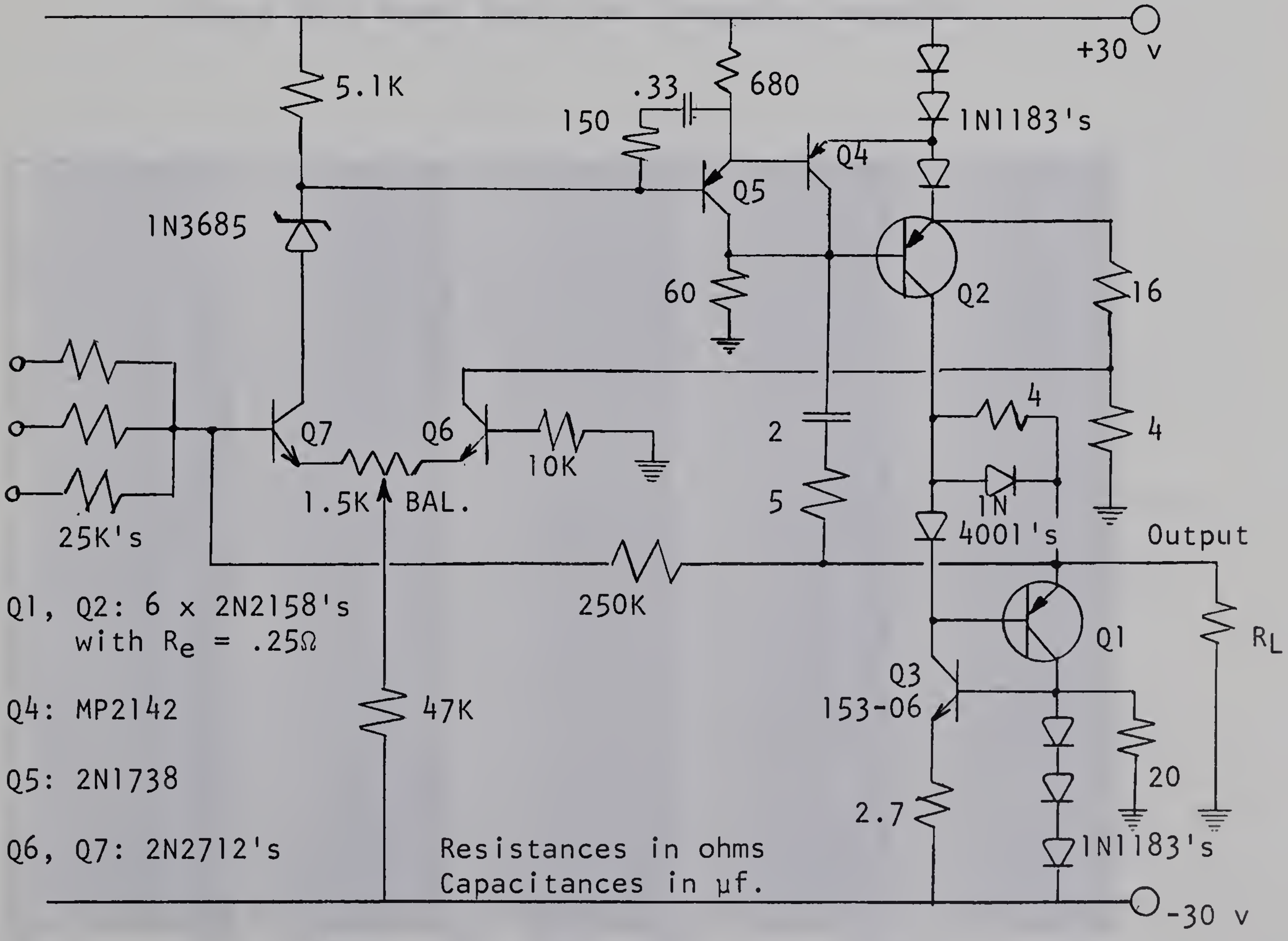
+30 v
5.1K
.33
680
150
1N1183's
Q4
Q5
1N3685
60
Q2
16
25K's
Q7
Q6
10K
1.5K
BAL.
2
5
4
4
1N 4001's
Output
250K
Q1, Q2: 6 x 2N2158's with R_e = .25Ω
Q1
R_L
Q3 153-06
47K
Q4: MP2142
Q5: 2N1738
20
2.7
1N1183's
Q6, Q7: 2N2712's
Resistances in ohms
Capacitances in µf.
-30 v

Figure A2.1 Power Amplifier Simplified Schematic

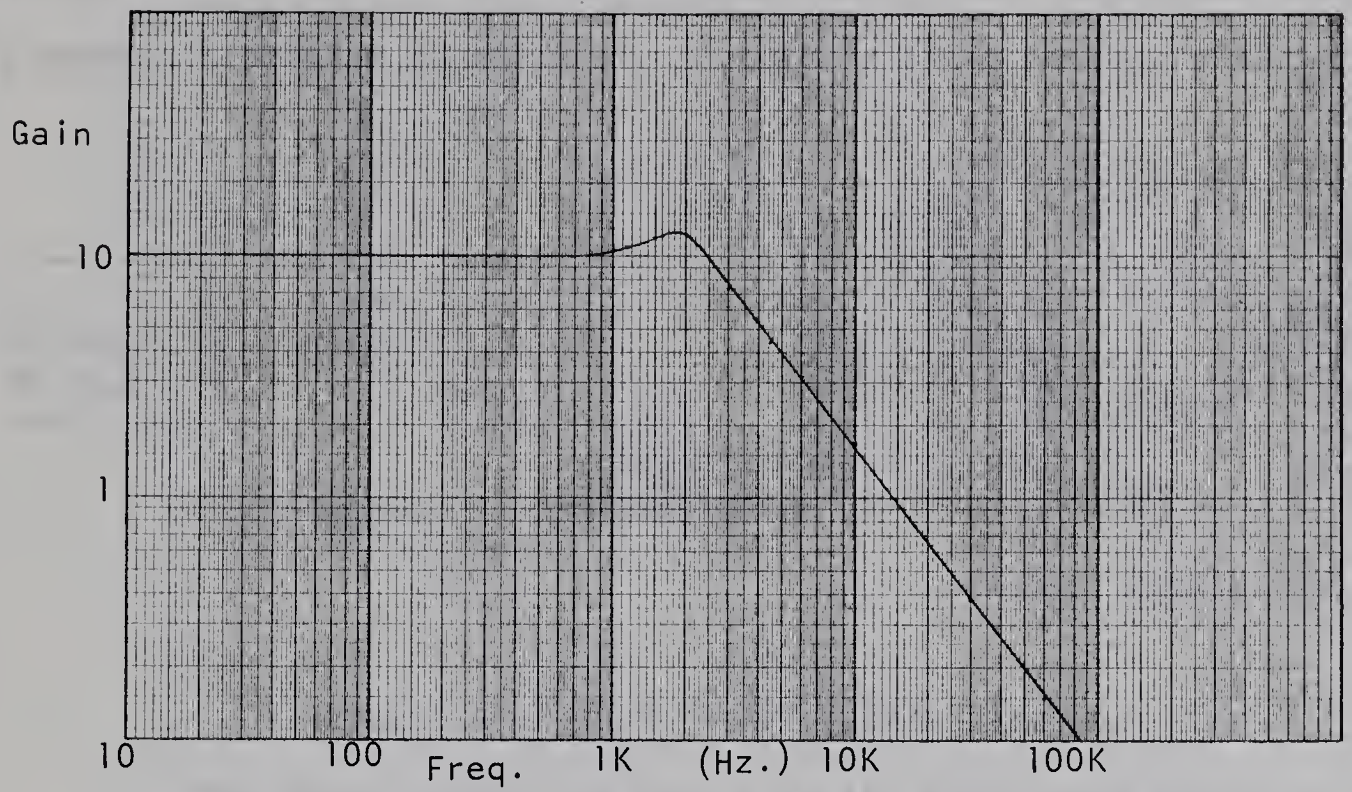

Figure A2.2 Power Amplifier Frequency Response

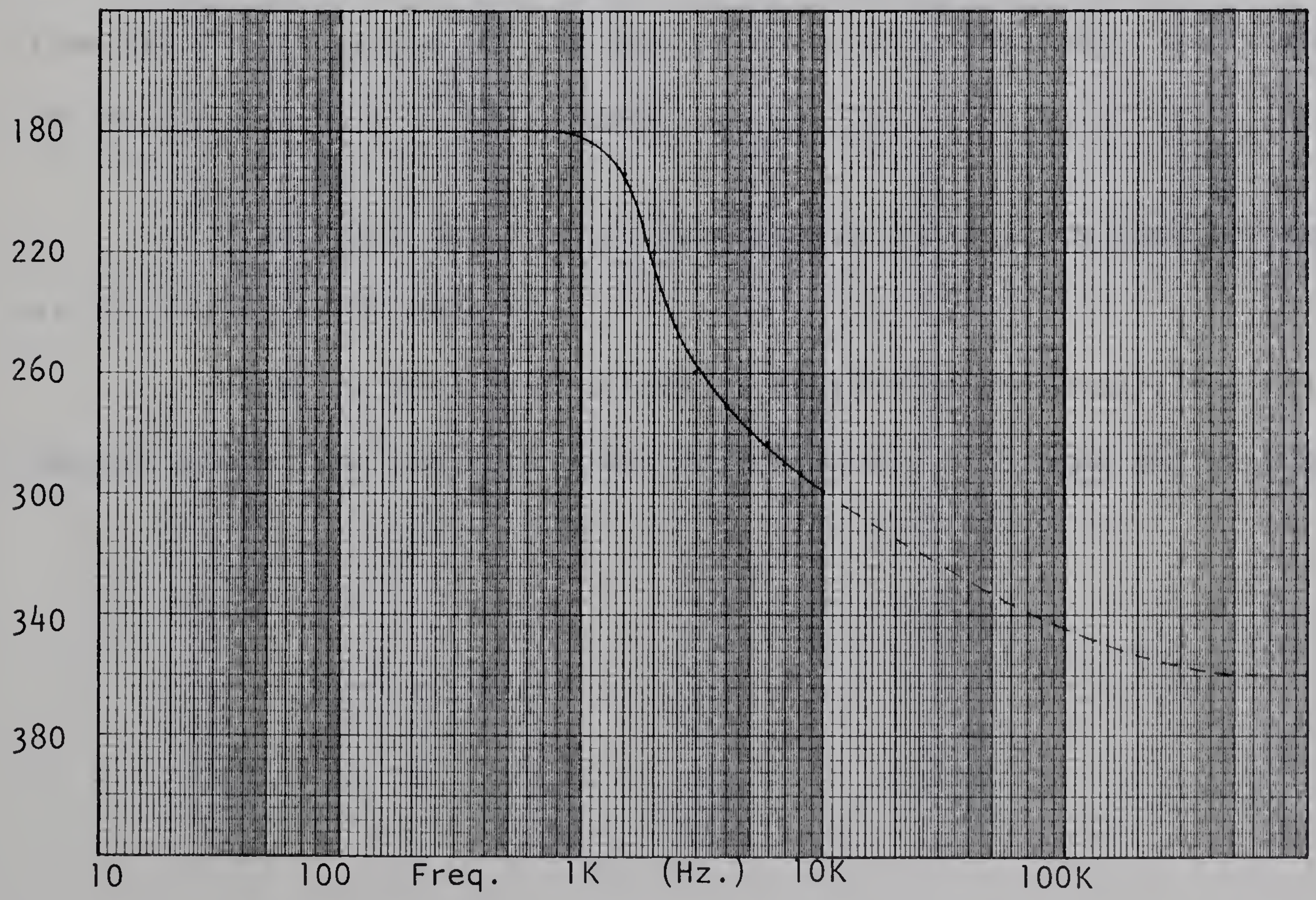

Figure A2.3 Power Amplifier Phase Shift

APPENDIX 3: DUAL POWER SUPPLY

The power supply used to provide the nominal ±30 volts D.C. at ±25 amps for the 600 watt power amplifier is of the "brute force" type. A schematic diagram of the basic circuit is shown in figure A3.1.

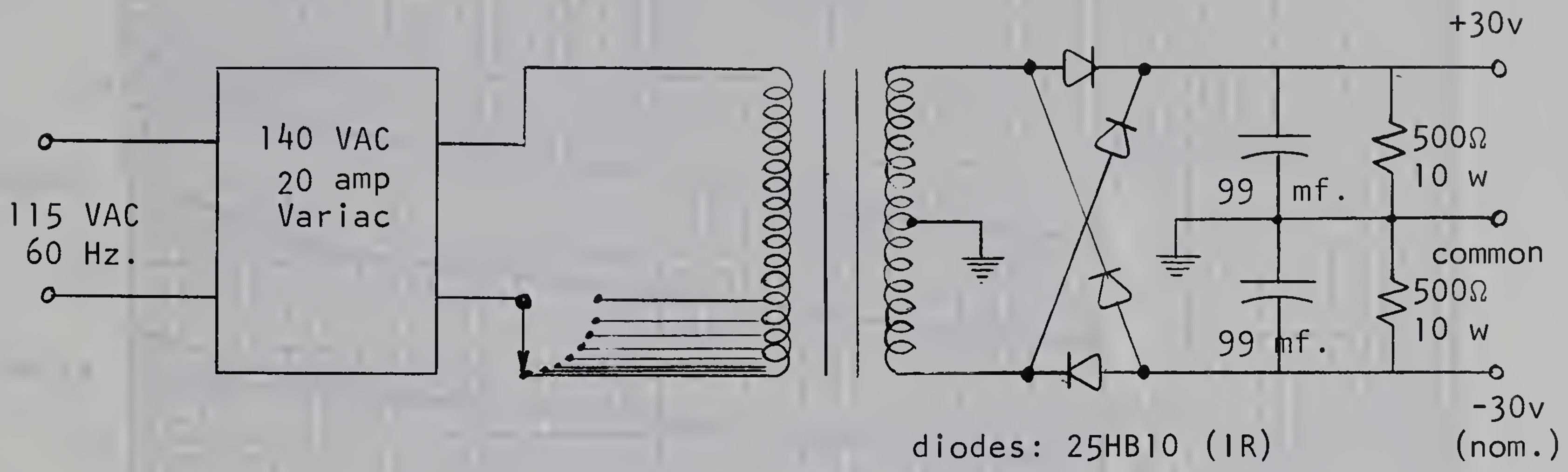
+30v
140 VAC
20 amp
Variac
115 VAC
60 Hz.
99 mf.
500Ω
10 w
common
99 mf.
500Ω
10 w
-30v
(nom.)
diodes: 25HB10 (IR)

Figure A3.1 Dual Power Supply Circuit

The power supply was used with the eight-pole switch on the primary winding in its maximum position. The voltage regulation which was measured for this case is shown in curve A in figure A3.2. From the linear region of the regulation curves, the output resistance of the power supply is calculated: $R_o = \frac{\Delta V}{\Delta I} \simeq 0.125\ \Omega$.

Ripple was measured as approximately 0.7 volts peak-to-peak at at current of 30 amperes.

With the amplifier unloaded, at zero volts output, the quiescent current drawn from the supply was approximately -2.5 amps and +3.0 amps.

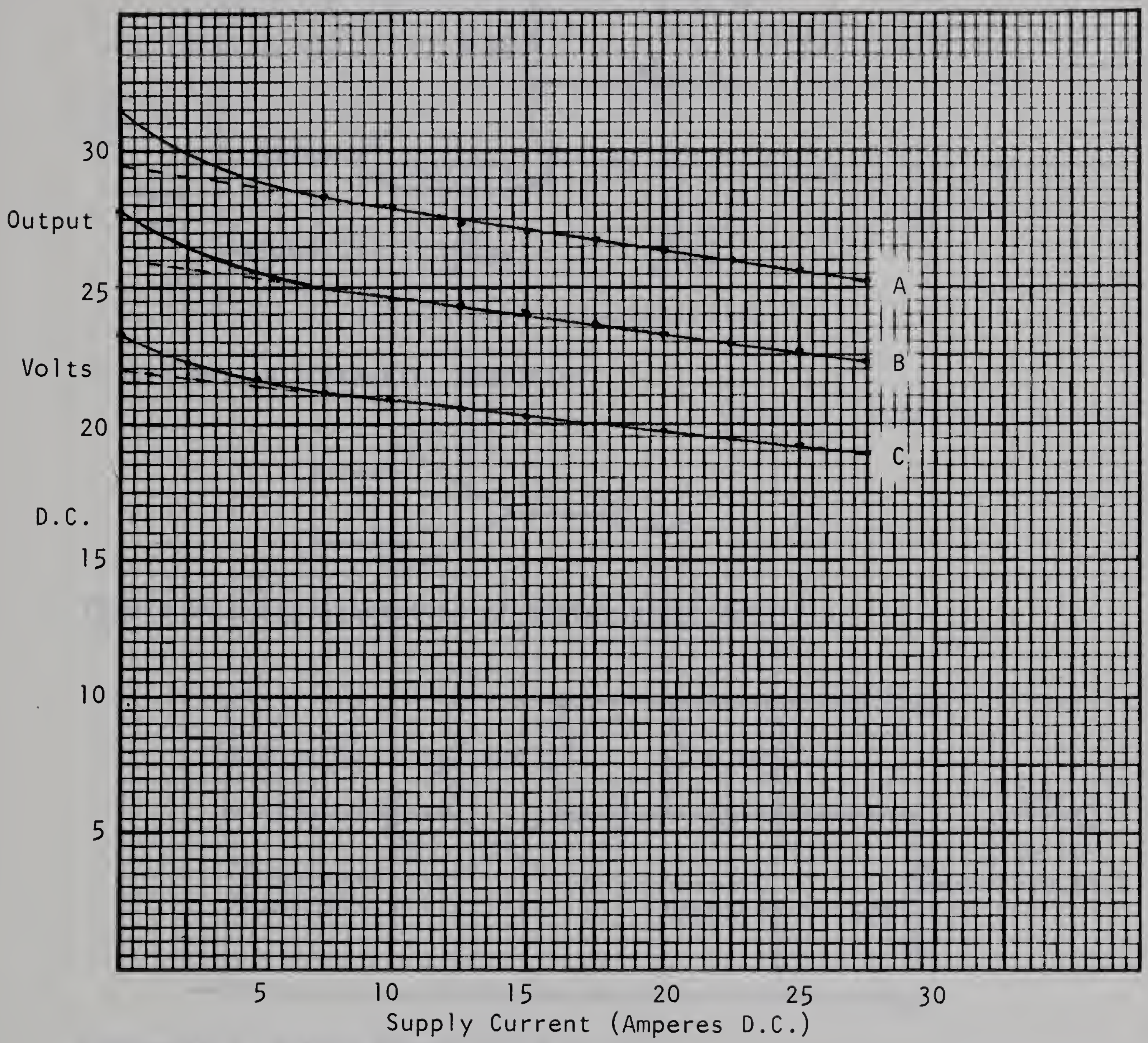

Figure A3.2 Dual Power Supply Voltage Regulation Curves

A : 140 VAC Variac feed; switch in maximum position

B : 115 VAC (line) " " " minimum "

C : 140 VAC Variac " " " maximum "

APPENDIX 4 : SCHEMATIC DIAGRAMS OF CIRCUITS USED

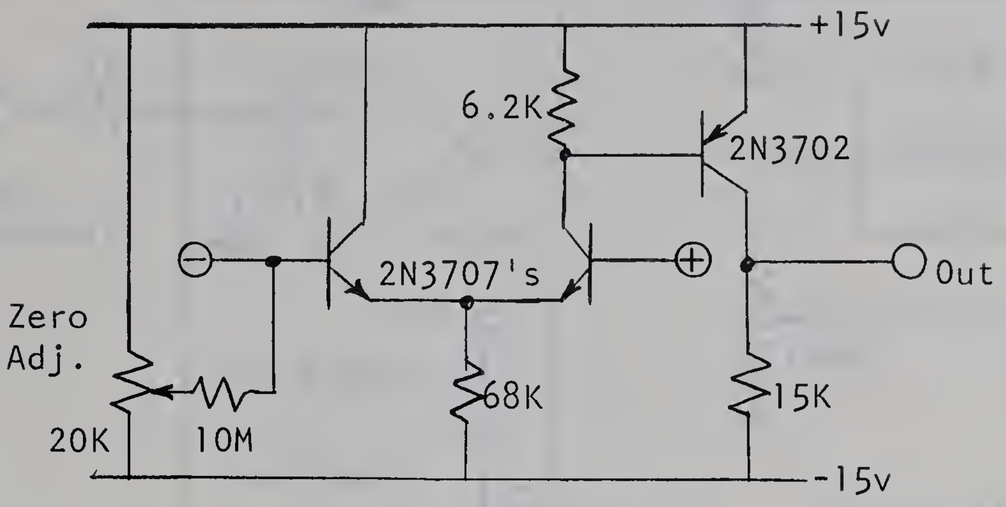
+15v
6.2K
2N3702
2N3707's
Out
Zero
Adj.
20K
10M
68K
15K
-15v

Figure A4.1 Differential Amplifier

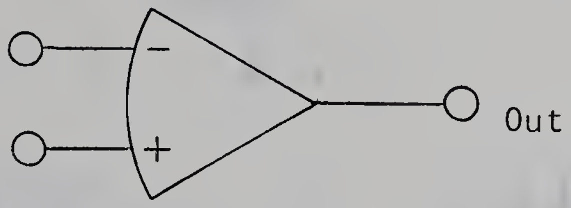

Figure A4.2 Representation of Differential Amplifier

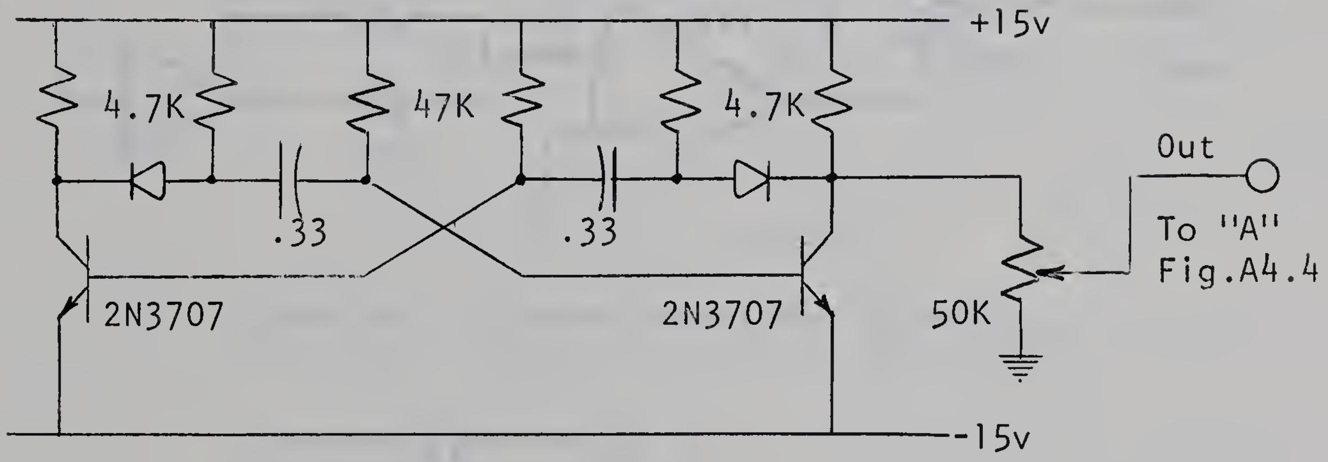
+15v
4.7K
47K
4.7K
Out
.33
.33
To "A"
Fig.A4.4
2N3707
2N3707
50K
-15v

Figure A4.3 Dither Generating Circuit

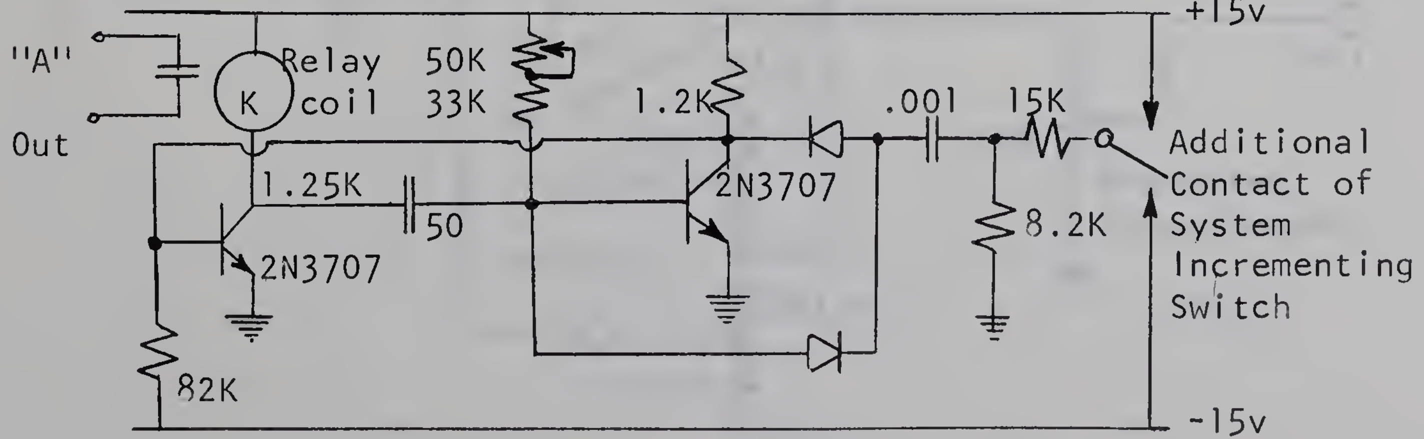
"A"
Out
+15v
Relay
coil
K
50K
33K
1.2K
.001
15K
1.25K
50
2N3707
2N3707
8.2K
82K
Additional
Contact of
System
Incrementing
Switch
-15v

Figure A4.4 Dither Duration Circuit

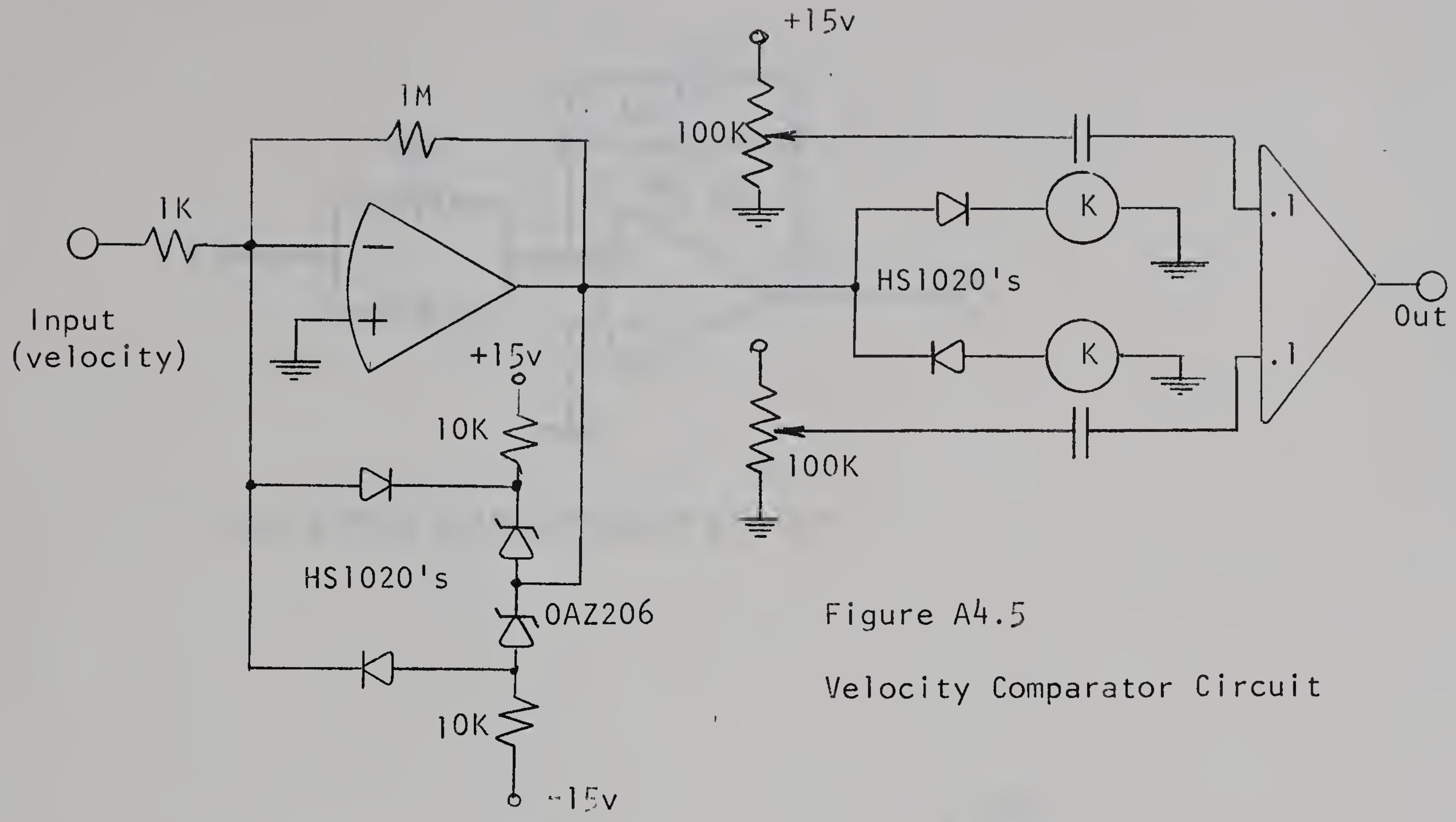
+15v
1M
100K
1K
Input
(velocity)
HS1020's
K
K
.1
.1
Out
+15v
10K
100K
HS1020's
0AZ206
10K
-15v

Figure A4.5

Velocity Comparator Circuit

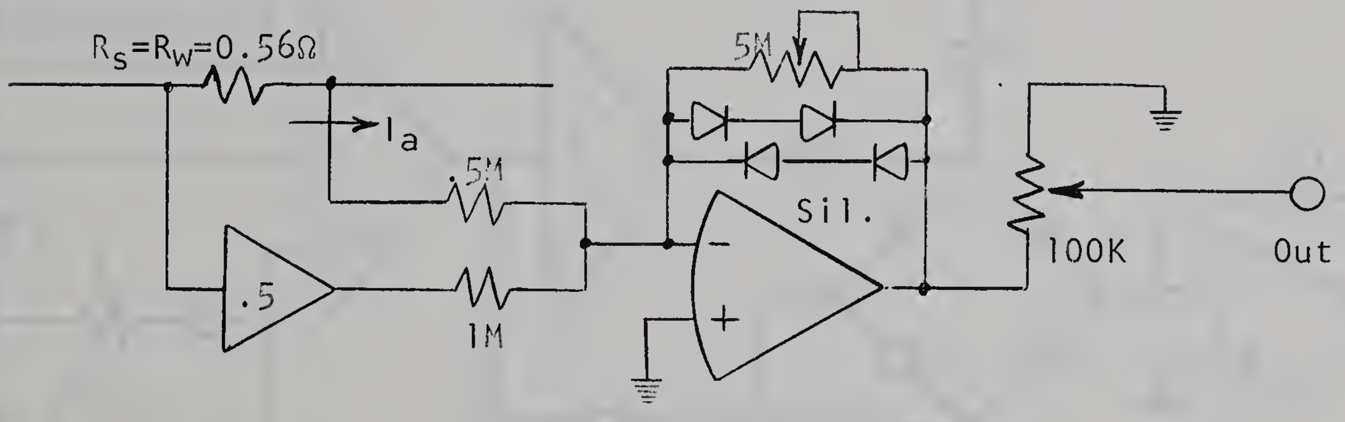
$R_s=R_W=0.56\Omega$
I_a
5M
.5M
Sil.
.5
1M
100K
Out

Figure A4.6 Current Comparator Circuit

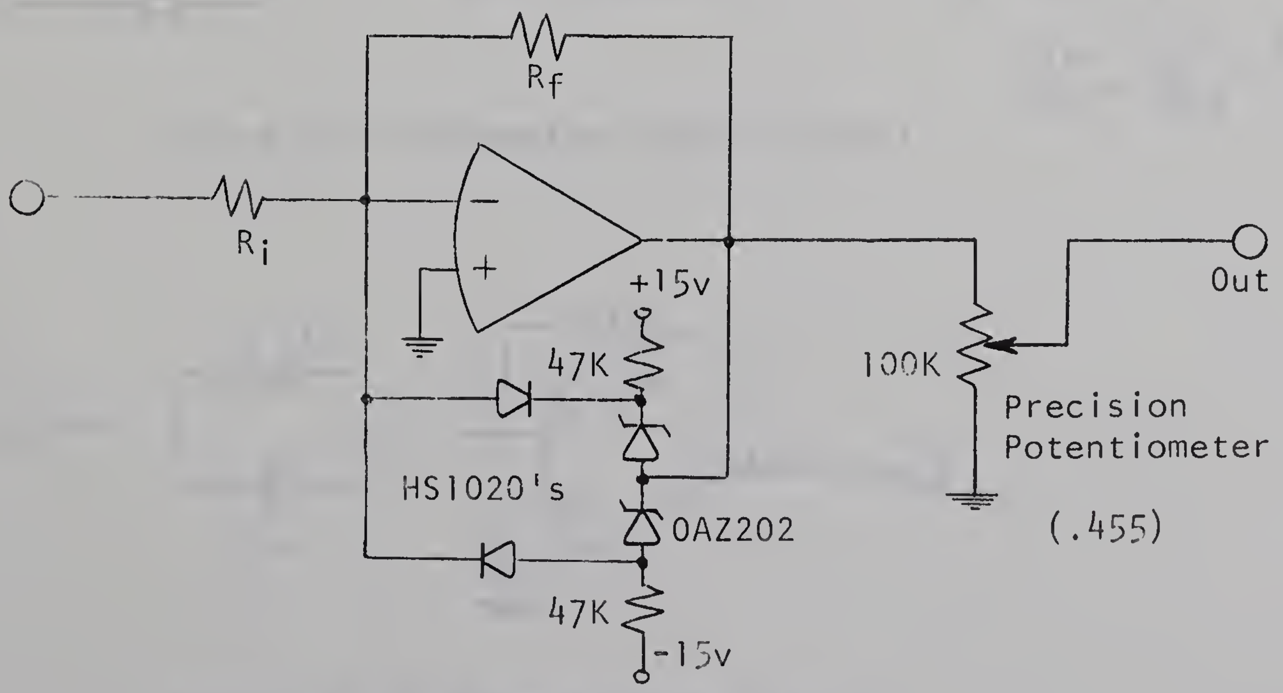
R_f
R_i
+15v
47K
100K
Out
Precision
Potentiometer
HS1020's
0AZ202
(.455)
47K
-15v

Figure A4.7 Voltage Limiter Circuit

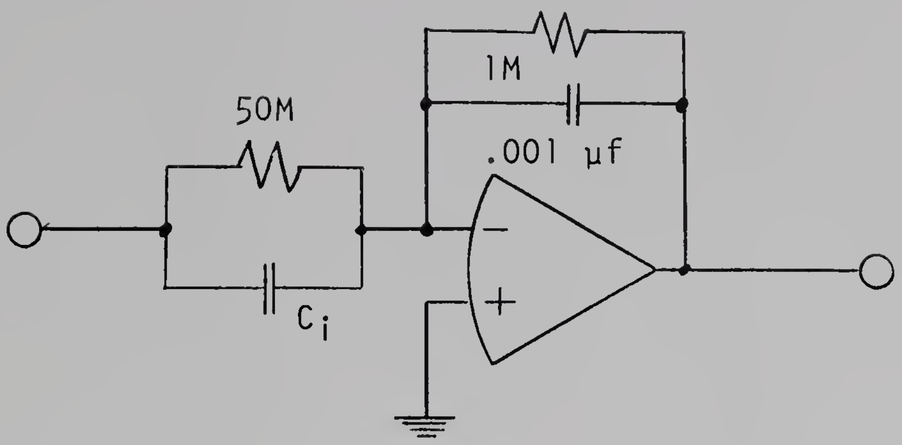
1M
50M
.001 µf
C_i
−
+

Figure A4.8 Differentiator Circuit

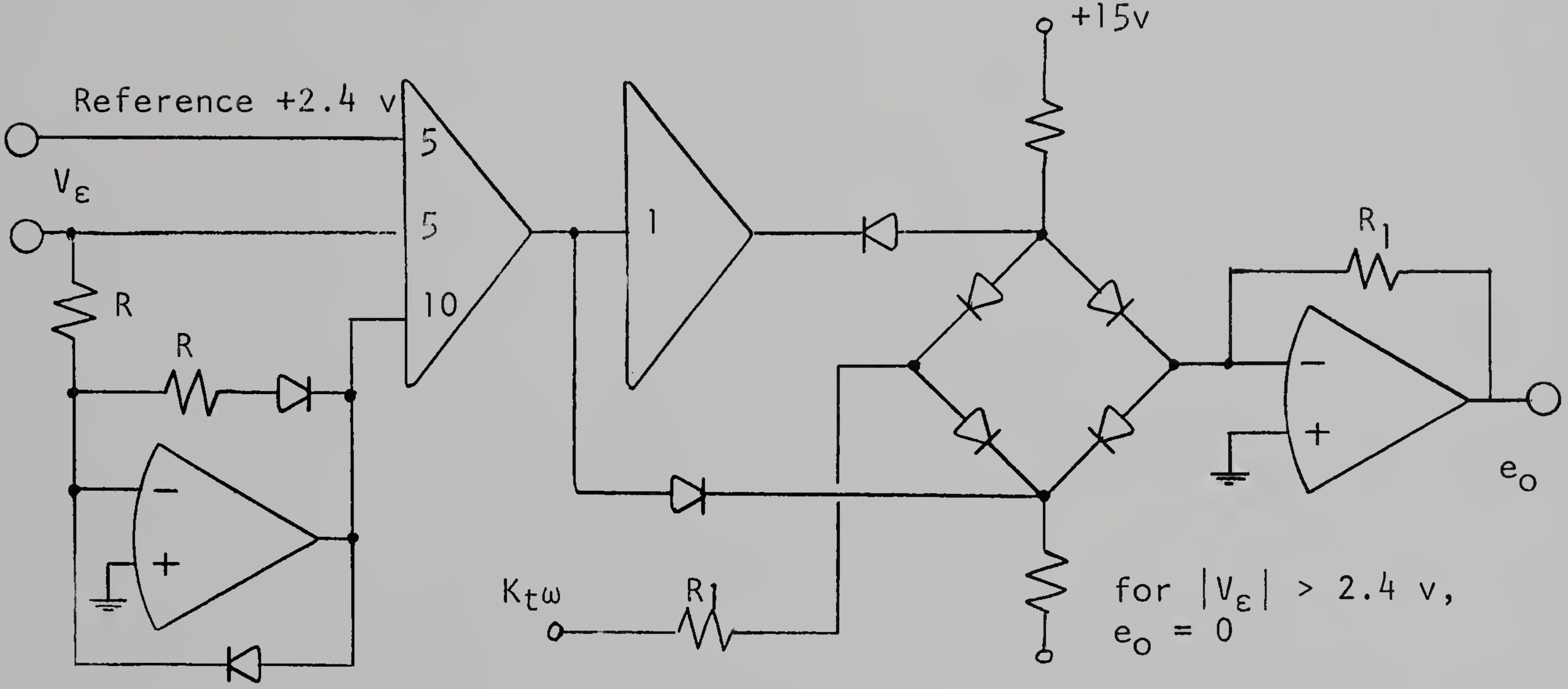
+15v
Reference +2.4 v
5
V_ε
5
10
1
R
R
R_1
−
+
−
+
e_o
$K_t\omega$
R

for $|V_\varepsilon| > 2.4$ v,
$e_o = 0$

for $|V_\varepsilon| < 2.4$ v,
$e_o = -K_t\omega$

Figure A4.9 Tachometer Cutout Circuit

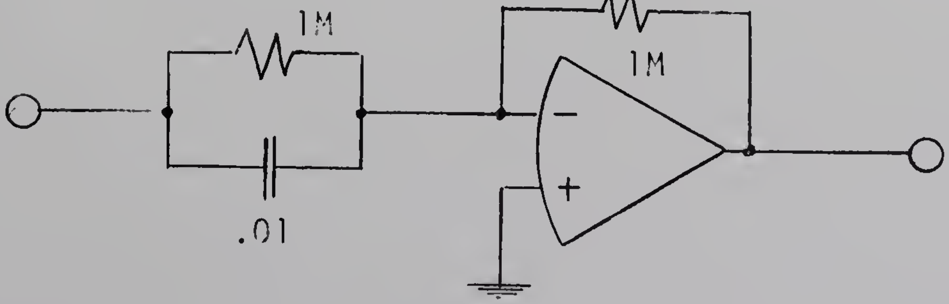

Figure A4.10 Phase Advance Circuit

B29870